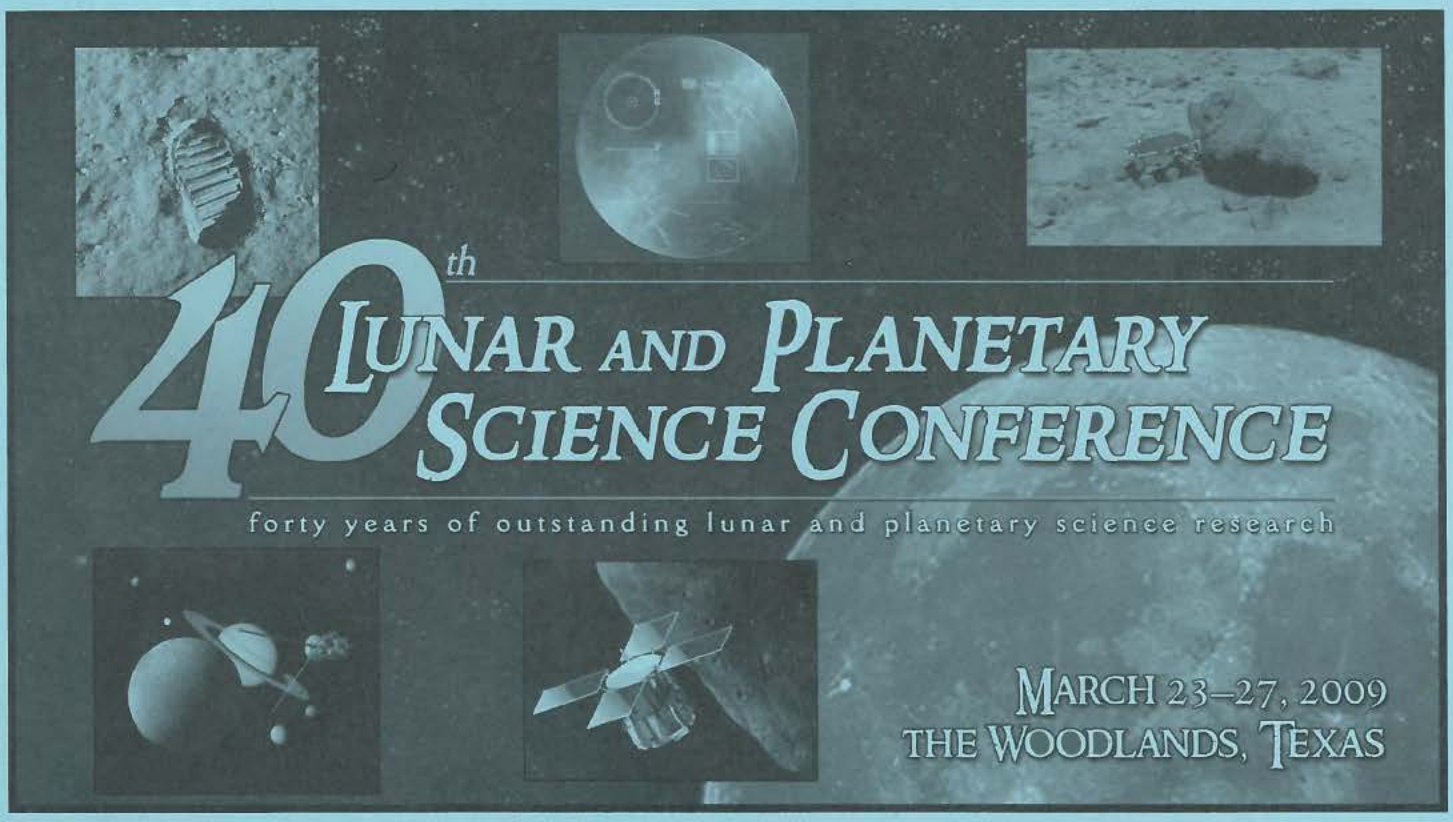

40TH LUNAR AND PLANETARY SCIENCE CONFERENCE
PROGRAM OF TECHNICAL SESSIONS

SPONSORED BY
LUNAR AND PLANETARY INSTITUTE
NASA JOHNSON SPACE CENTER

LUNAR AND PLANETARY INSTITUTE

FORTIETH LUNAR AND PLANETARY SCIENCE CONFERENCE

Program of Technical Sessions

March 23–27, 2009

The Woodlands Waterway Marriott Hotel
and Convention Center
The Woodlands, Texas

Sponsored by

Lunar and Planetary Institute
NASA Johnson Space Center

Conference Co-Chairs

Stephen Mackwell, Lunar and Planetary Institute
Eileen Stansbery, NASA Johnson Space Center

Woodlands Waterway Convention Center Map

UPPER LEVEL

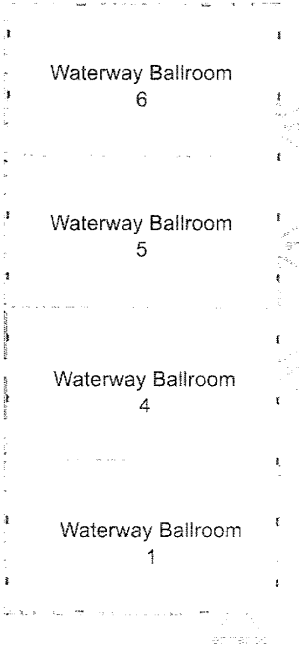

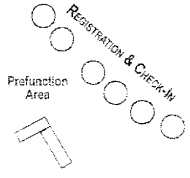

LOWER LEVEL

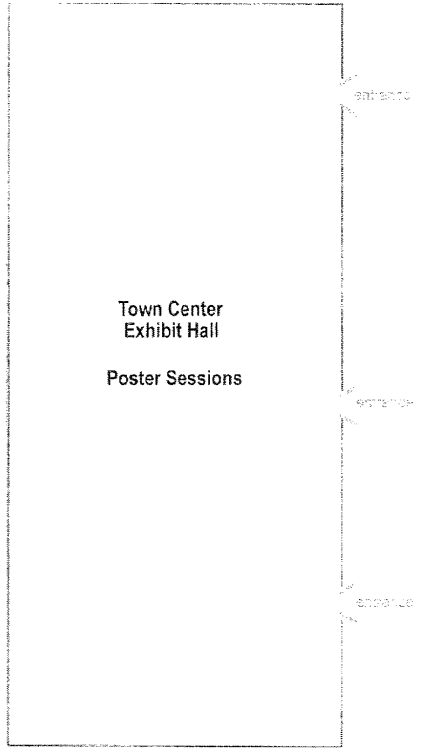

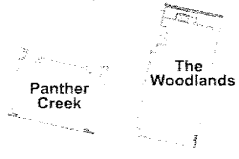

GUIDE TO TECHNICAL SESSIONS AND ACTIVITIES

Wednesday Morning, March 25, 8:30 a.m.

** Denotes speaker*

PHOENIX: EXPLORATION OF THE MARTIAN ARCTIC
Monday, 8:30 a.m. Waterway Ballroom 1

Chairs: **Raymond Arvidson and Peter Smith**

8:30 a.m. Smith P. H. *
Water at the Phoenix Landing Site **[#1329]**
The Phoenix mission found a water ice layer 5 cm beneath a dry soil overburden. The presence of Ca-carbonate and other aqueous minerals suggests that the soil has been modified through the action of liquid water in the recent past.

8:45 a.m. Hudson T. L. * Zent A. Hecht M. H. Wood S. Cobos D.
Near-Surface Humidity at the Phoenix Landing Site as Measured by the Thermal and Electrical Conductivity Probe (TECP) **[#1804]**
Atmospheric humidity data from the Thermal and Electrical Conductivity Probe (TECP) on the Phoenix Mars lander is analyzed. Trends in diurnal and seasonal humidity are presented and hypotheses for the mechanisms controlling near-surface humidity are discussed.

9:00 a.m. Sizemore H. G. * Mellon M. T. Searls M. L. Zent A. P. Heet T. L. Arvidson R. E.
In Situ Analysis of Ice Table Depth Variability Under a Rock at the Phoenix Landing Site, Mars **[#1940]**
We examine ice table depth variability under a rock at the Mars Phoenix landing site and compare our observations to predictions from heterogeneous ice-stability simulations. We discuss implications for the current climate and the history of water in the northern plains.

9:15 a.m. Mellon M. T. * Arvidson R. E. Malin M. C. Heet T. L. Sizemore H. G. Searls M. L. Lemmon M. T. Keller H. U. Phoenix Science Team
Permafrost and Polygons at the Phoenix Landing Site **[#1904]**
We examine the ground ice and periglacial landforms at the Phoenix landing site and relate observations to the history of the martian climate.

9:30 a.m. Arvidson R. E. * Phoenix Science Team
Geologic Setting and Surface Properties of the Mars Phoenix Landing Site **[#1067]**
Analyses of trenches excavated by the Phoenix lander and coordinated orbital observations provide a self-consistent model of grain size distribution and mineralogy of surface deposits, along with the presence of water adsorbed onto surface grains.

9:45 a.m. Blaney D. L. * Archer D. Arvidson R. Cull S. Ellehoj M. Fisher D. Hecht M. Lemmon M. Mellon M. Morris R. Pike T. Smith P. Stoker C. Phoenix Science Team
Multi-Spectral Imaging of the Phoenix Landing Site: Characteristics of Surface and Subsurface Ice, Rocks, and Soils **[#2047]**
The Phoenix landing site had two types of ice soil mixtures with variable purity. No spectral evidence for high concentration perchlorate brines was found from analysis of trench (e.g. no layering) and sublimation lag deposits.

10:00 a.m. Goetz W. * Hviid S. F. Keller H. U. Markiewicz W. J. Madsen M. B. Leer K. Drube L. Pike T. W. Hecht M. H. Parrat D. Sykulska H. Vijendran S. Marshall J. Morris R. V. Arvidson R. E. Smith P. H.
Microscopic Views of Soil and Dust at the Phoenix Landing Site, and How that Relates to Other Landing Sites **[#2425]**
Images from the Phoenix Optical Microscope show different types of soil particles. Based on spectral and magnetic data and by comparison with MER, it is inferred which particles are global and which ones are specific to the Phoenix landing site.

10:15 a.m. Poulet F. * Langevin Y. Bibring J.-P. Arvidson R. E. Boubin G. Gondet B.
Mineralogy of the High Latitudes of Mars Including the Phoenix Landing Site **[#1551]**
We report the surface distribution of some minerals in the high latitude (>50° North and South) regions of Mars from the analysis of the OMEGA/MEx observations in the visible and near-infrared wavelength domains (0.4–4 μm).

10:30 a.m. Boynton W. V. * Ming D. W. Sutter B. Arvidson R. E. Hoffman J. Niles P. B. Smith P. Phoenix Science Team
Evidence for Calcium Carbonate at the Phoenix Landing Site **[#2434]**
Using differential scanning calorimetry and mass spectrometry, the TEGA instrument on the Phoenix lander has found evidence for calcium carbonate.

10:45 a.m. Hecht M. H. * Catling D. C. Clark B. C. DeFlores L. Gospodinova K. Kapit J. Kounaves S. P. Ming D. W. Quinn R. C. West S. J. Young S. M. M.
Perchlorate in Martian Soil: Evidence and Implications **[#2420]**
The Phoenix mission found approximately 1% perchlorate salts in the surface soil of Mars. Depending on the cation, properties of these salts may include the capability to form brines at temperatures comparable to the mean martian frostpoint.

11:00 a.m. Holstein-Rathlou C. * Gunnlaugsson H. P. Merrison J. Taylor P. Lange C. Davis J. Lemmon M. Phoenix Science Team
Winds at the Mars Phoenix Landing Site **[#1548]**
The Telltale is a mechanical anemometer mounted atop the meteorological mast on the Mars Phoenix lander. Images taken with the Surface Stereo Imager allow local wind speeds and directions to be quantified and the data is used to study local weather.

11:15 a.m. Whiteway J. * Komguem L. Dickinson C. Cook C. Duck T. Taylor P. Davy R. Seabrook J. Fisher D. Carswell A. Daly M. Popovici V. Phoenix Science Team
Phoenix Lidar Observations of Dust, Clouds, and Precipitation on Mars **[#2202]**
The Phoenix Mars Lidar instrument observed that atmospheric dust is well mixed up to a height of 4 km. The lidar also observed that water ice clouds form within the PBL each night in late summer and that ice crystals precipitate toward the surface.

11:30 a.m. Tamppari L. K. * Bass D. S. Cantor B. Daubar I. Fisher D . Fujii K. Gunnlaugsson H. P. Hudson T. L. Kass D. Kleinboehl A. Lemmon M. Mellon M. Pankine A. Searls M. Seelos F. Smrekar S. Taylor P. von Holstein-Rathlou C. Whiteway J. Wolff M.
Phoenix and MRO Coordinated Atmospheric Science **[#2000]**
The Phoenix and MRO spacecraft performed coordinated/simultaneous observations of the martian atmosphere to capture seasonal and diurnal variability.

ORIGIN AND EARLY EVOLUTION OF THE MOON
Monday, 8:30 a.m. Waterway Ballroom 4

Chairs: **David Kring and David Draper**

8:30 a.m. Jacobsen S. B. * Remo J. L. Petaev M. I. Sasselov D. D.
Hf-W Chronometry and the Timing of the Giant Moon-forming Impact on Earth **[#2054]**
For Hf-W chronometry of the Earth-Moon system (EMS) there are currently two end member options: (i) the formation of the EMS at ~32 Myr or (ii) formation of 90% of the Earth in the first six Myr followed by a very late (~100 Myr) formation of the Moon.

8:45 a.m. Touboul M. * Kleine T. Bourdon B. Nyquist L. Shih C.-Y.
New ^{142}Nd Evidence for a Non-Chondritic Composition of the Moon **[#2269]**
Here we present new Sm-Nd data for lunar rocks that are used to evaluate the significance of the ^{146}Sm-^{142}Nd systematics for constraining the timescale of lunar differentiation and the bulk Nd isotope composition of the Moon.

9:00 a.m. Elardo S. M. * Draper D. S.
Crystallization of a Lunar Magma Ocean: Preliminary Experimental Results **[#1181]**
Though widely accepted, the lunar magma ocean hypothesis has never been fully tested experimentally. Presented here are the preliminary results of experiments conducted on a bulk Moon composition to simulate lunar magma ocean crystallization.

9:15 a.m. Pahlevan K. * Stevenson D. J.
Chemical Fractionation after the Moon-forming Giant Impact **[#2392]**
We test the hypothesis that the lunar mantle is derived from the terrestrial mantle via liquid-vapor fractionation during the afterglow of the giant impact.

9:30 a.m. Zindler A. * Jacobsen S. B.
Isotopic Equilibration of Earth's Mantle and the Moon Subsequent to the Giant Impact? **[#2542]**
The striking oxygen, chromium, and tungsten isotopic similarities between the Earth's mantle and the Moon are discussed and modeled with a 3-box model.

9:45 a.m. Parmentier E. M. *
On the Scale of Lunar Mantle Overturn Following Magma Ocean Fractional Solidification: The Role for Multiple Scales of Convective Motion **[#1781]**
Multiple scales of mantle overturn following magma ocean fractional solidification reconciles the magmatic evolution of the Moon many of its important geological and geophysical characteristics.

10:00 a.m. Longhi J. *
Origin of the Magnesian Suite Cumulates **[#2356]**
Melting calculations on various combinations of rock types formed in the lunar magma ocean suggest that highly magnesian olivine characteristic of magnesian suite cumulates ultimately derives from the earliest dunite cumulates of the magma ocean.

10:15 a.m. Grange M. L. * Nemchin A. A. Pidgeon R. T. Meyer C.
Early History of the Moon: Zircon Perspective **[#1473]**
U-Pb ages of lunar zircons highlight new details in the early history of the Moon, providing a younger limit for the LMO crystallization and indicating that the impact history of the Moon is more complex than the accepted late period of bombardment.

10:30 a.m. Frey H. V. *
Crustal Thickness Evidence for More Previously Unrecognized Large Lunar Basins **[#1687]**
Crustal thickness model data reveal the presence of even more large lunar basins that were previously unrecognized. The total number of lunar basins >300 km diameter may exceed 150, more than three times that determined by photogeologic mapping alone.

10:45 a.m. Wieczorek M. A. Le Feuvre M. *
Did a Large Impact Reorient the Moon? **[#1554]**
More impacts should occur on the Moon's western hemisphere as a result of this body's synchronous rotation. We show that there are more old basins located on the Moon's eastern hemisphere, suggesting that a large impact reoriented the Moon by 180°.

11:00 a.m. Jolliff B. L. * Korotev R. L. Zeigler R. A. Prettyman T. H.
Connecting Lunar Meteorite Dhofar 961 to the South Pole-Aitken Basin Through Lunar Prospector Gamma-Ray Data **[#2555]**
Lunar meteorite Dhofar 961, which contains mafic impact-melt components, is matched to locations within South Pole-Aitken Basin through the 5-degree Lunar Prospector gamma-ray data. Implications for a lower crustal provenance are discussed.

11:15 a.m. Cahill J. T. S. * Lucey P. G. Wieczorek M. A.
The Composition of Lunar Central Peaks Relative to Lunar Samples **[#1222]**
Here we place the modeled mineralogy of lunar impact crater central peaks in the context of the lunar sample collection.

11:30 a.m. Wingo D. R. Cowing K. L.
Recovering High Resolution Lunar Orbiter Images from Analog Tape **[#2517]**
Original FR-900 tape recorders have been refurbished to play, digitize, and store, the original highest resolution images of the Moon. This paper outlines the process and the initial results of our efforts.

COMET WILD 2: MINERALOGY AND MORE
Monday, 8:30 a.m. Waterway Ballroom 5

Chairs: **Anton Kearsley and Andrew Westphal**

8:30 a.m. Messenger S. * Joswiak D. Ito M. Matrajt G. Brownlee D. E.
Discovery of Presolar SiC from Comet Wild-2 **[#1790]**
We report isotopic measurements of a SiC grain identified in a Stardust mission sample. The C isotopic composition and crystallography of the grain is consistent with mainstream SiC grains from meteorites. This is the first presolar grain identified in a Stardust track.

8:45 a.m. Brownlee D. E. * Joswiak D. Matrajt G. Messenger S. Ito M.
Silicon Carbide in Comet Wild 2 and the Abundance of Pre-Solar Grains in the Kuiper Belt **[#2195]**
Pre-solar SiC has been found in comet dust collected by the Stardust mission. SiC is robust, survives aerogel capture and it is identified by TEM + nanoSIMS. SiC provides a new means to estimate the pre-solar content of Wild 2, a Kuiper belt comet.

9:00 a.m. Stadermann F. J. * Floss C. Gavinsky A. Kearsley A. T. Burchell M. J.
Calibrating the Abundance Determinations of Presolar Grains in Wild 2 Cometary Matter **[#1188]**
We have performed test shots of powdered Acfer 094 material into Al foils under Stardust-like conditions for calibration purposes. Early results indicate that the true abundances of presolar grains in Wild 2 may be higher than previously estimated.

9:15 a.m. Kearsley A. T. * Burchell M. J. Price M. C. Graham G. A. Cole M. J.
Porous Aggregates in Comet 81P/Wild 2? Stardust Al Foil Craters Compared to Experimental Impacts from Artificial Aggregates and Meteorite Powders **[#1517]**
Stardust Al foil craters show that comet Wild 2 doesn't contain much very fine, low density, high porosity dust. Experimental shots of artificial aggregate projectiles give realistic simulation of these impacts, and create bulbous tracks in aerogel.

9:30 a.m. Greenberg M. * Ebel D. S.
Nondestructive 3D Confocal Laser Imaging with Deconvolution of Seven Whole Stardust Tracks with Complementary XRF and Quantitative Analysis **[#2124]**
We present a nondestructive 3D system for analysis of whole Stardust tracks, using a combination of Laser Confocal Scanning Microscopy and synchrotron XRF. 3D deconvolution is used for optical corrections, and results of quantitative analyses of several tracks are presented.

9:45 a.m. Clemett S. J. * Nakamura-Messenger K. McKay D. S.
Origin and Evolution of Organic Matter Preserved in Stardust Cometary Aerogel Tracks **[#2395]**
The nature and spatial distribution of aromatic and conjugated organic species has been investigated along individual cometary tracks in Stardust aerogel.

10:00 a.m. Wirick S. * Flynn G. J. Keller L. Nakamura Messenger K. Sandfrod S. A. Zolensky M. E. Peltzer C. Jacobsen C.
Evidence for Changes in 81P/Wild 2 Organic Matter Since Collection and Comparison of 81P/Wild 2 and IDP Organic Matter to Assess the Thermal Effects of Aerogel Capture **[#1366]**
Carbon XANES spectra from two 81P/Wild 2 particles are compared to C XANES spectra from two IDPs. One set of particles shows there is a change in the organics over time. The other set shows that some organic matter can survive temperatures of 1000°C.

10:15 a.m. Nakamura-Messenger K. * Keller L. P. Clemett S. J. Messenger S.
NM-Scale Anatomy of an Entire Stardust Carrot Track **[#1989]**
All the fine grains along the track wall were examined to determine if they are small fragments of the same material as the terminal particle shed during the capture event, or whether they represent discrete materials.

10:30 a.m. van der Bogert C. H. * Stephan T. Jessberger E. K.
Separation of Primary Amorphous Silicates and Capture-related Glasses in Stardust Cometary Samples **[#2404]**
We identified a partially amorphous anorthite grain, which raises questions about the possibility of primary amorphous silicates in Stardust.

10:45 a.m. Bridges J. C. * Changela H. C. Carpenter J. D. Gurman S. J.
Oxide Minerals in Comet Wild 2: TEM and Synchrotron Characterisation **[#1889]**
We describe oxide minerals in Wild 2 samples. They have various origins including high and low temperature and possibly space weathering. The assemblages are reminiscent of C-chondrites. Oxidation during capture also occurred.

11:00 a.m. Berger E. L. * Keller L. P. Joswiak D. J. Lauretta D. S.
Low Temperature Sulfides in CI Chondrites and Stardust **[#1892]**
TEM analyses of Stardust sulfides (cubanite, pyrrhotite, pentlandite) reveal similarities with CI-chondrite sulfides. The presence of orthorhombic cubanite, in the Stardust collection, has implications for the thermal history of Comet Wild 2.

11:15 a.m. Flynn G. J. * Lanzirotti A. Sutton S. R.
Elemental and Mineralogical Compositions of Cluster IDPs: A Possible Analog to the Wild 2 Particles Collected by Stardust **[#1166]**
Cluster IDPs, consisting of ~30% CP-IDP material and ~70% larger silicate and sulfide grains, have a CI-like element pattern. They seem to be analogs to Wild 2 particles, suggesting larger particles must be analyzed to determine Wild 2's composition.

11:30 a.m. Westphal A. J. * Fakra S. Gainsforth Z. Marcus M. A. Ogliore R. C. Butterworth A. L.
Mixing Fraction of Inner Solar-System Material in Comet 81P/Wild2 **[#1819]**
Using synchrotron-based x-ray microprobe measurements of the fraction of iron in sulfides and in crystalline materials in Stardust cometary samples, we estimate the fraction of inner nebular material in comet 81P/Wild 2 to be 0.6 ± 0.1.

ASTROBIOLOGY: METEORITES, MICROBES, HYDROUS HABITATS, AND IRRADIATED ICES
Monday, 8:30 a.m. Waterway Ballroom 6

Chairs: **Inge ten Kate and Elisabeth Hausrath**

8:30 a.m. Gibson E. K. * McKay D. S. Thomas-Keprta K. L. Clemett S. J. Wentworth S. J.
Development of Life on Early Mars **[#1175]**
For life to exist on a planet there must be water, carbon and energy sources along with a dynamic geologic past. Mars meets all of these requirements. Life is probably present beneath the surface of Mars today in regions associated with water.

8:45 a.m. Vítek P. * Jehlička J. Edwards H. G. M. Osterrothová K.
β-Carotene as a Potential Biomarker in Martian Evaporitic Rocks: Evaluation of Raman Microspectrometric Analysis **[#1729]**
In this study, Raman microspectrometry was tested as a nondestructive method of determining the lowest detectable beta-carotene content in experimentally prepared evaporitic matrices (with respect to martian geology)– namely, gypsum, halite and epsomite.

9:00 a.m. Nittler L. R. * Alexander C. M. O'D. Cody G. D. De Gregorio B. T. Kilcoyne A. L. D. Stroud R. M. Tiwari A.
Micro-Scale Characteristics of Insoluble Organic Matter in Chondrites: A Coordinated TEM, STXM and SIMS Study **[#1145]**
A coordinated study of meteoritic insoluble organic matter reveals that hollow organic globules are chemically similar to other IOM, but abundances and sizes of globules vary between meteorites. IOM is sensitive to electron and X-ray induced beam damage.

9:15 a.m. Berkley J. L. * Dykstra K.
Mars Sediment Analog? Dark Biomineralized Mn-Oxide/Hydroxide Cemented Sandstone of Low-T Spring Origin **[#1963]**
A dark colored sandstone permeated by paleo-aqueous spring flow contains Ba-rich, Mn oxide/hydroxide mineralization of probably biogenic origin. On a wetter and warmer Mars, similar processes may have acted to produce dark, biomineralized sediments.

9:30 a.m. Fernández-Remolar D. C. * Sánchez-Román M. Rodríguez N. Amils R. Romanek C.
The Association of Carbonate Minerals to Acidic Environments: A Possible Biosignature for Mars **[#1214]**
Carbonate minerals are associated to extremely acidic environments of Río Tinto. Microbes mediate carbonate in acidic sediments and subsurface. Under these circumstances, same carbonate phases could be used as potential biosignatures to detect life on Mars.

9:45 a.m. Johnson S. S. * Carr C. E. Amils R. Zuber M. Ruvkun G.
Extensive Sequencing Approaches to the Search for Life: Initial Results from the Rio Tinto **[#2532]**
We present the SETG instrument and consider this new life detection strategy vis-à-vis a training set of phylotypes detected in the Mars-like chemistry of the Rio Tinto.

10:00 a.m. Cabrol N. A. * Grin E. A. Bebout L. Chong G. Demergasso C. Fleming E. Gaete V. Gibson J. Häder D. P. Mack J. Minkley E. Pinto E. Rose K. Ukstins Peate I. Tambley C. Williamson C. Wynne J. J.
High Lakes Project — Impact of Climate Variability and High UV Flux on Lake Habitat: Implications for Early Mars and Present-Day Earth **[#1141]**
HLP studies lakes between 4,200–6,000 m elevation in the Central Andes. Its primary objective is to understand the impact of increased environmental stress on lake habitats and their evolution during rapid climate change as an analogy to early Mars.

10:15 a.m. Abramov O. * Mojzsis S. J.
Microbial Habitability of the Hadean Earth During the Late Heavy Bombardment **[#2379]**
We explored the thermal state and habitability of Hadean Earth during the late heavy bombardment using several thermal models of the lithosphere. Our analysis shows that there is no plausible scenario in which the habitable zone was fully sterilized.

10:30 a.m. Bao H. *
How to Make Otherworldly Oxygen Isotope Signatures on Earth and to Preserve Them in Rocks **[#2174]**
I identify here two major pathways by which ^{17}O-anomalous sulfate oxygen isotope compositions can be generated with ^{17}O enrichment and ^{17}O depletion, respectively.

10:45 a.m. Fu Q. * Seyfried W. E. Jr.
Experimental Study of Abiotic Synthesis Processes in a Hydrothermal Flow System: Implications for Organic Matter Formation in Extraterrestrial Environments **[#2504]**
Carboxylic acids were observed in carbon reduction experiments using a hydrothermal flow reactor. Controlling factors for hydrocarbon formation were identified. It provides evidence for evaluating abiogenic synthesis on Mars and other planets.

11:00 a.m. Vance S. *
Habitability of Icy Worlds Electrochemical Capacitance of Serpentinizing Hydrothermal Systems **[#1994]**
Deeply fractured rock,slow steady serpentine springs,renewed by heat flash.

11:15 a.m. Nna-Mvondo D. * Khare B. N. McKay C. P.
Experimental Simulation of Chemistry Induced by Hypervelocity Impacts on Icy Moons Surfaces: Laser-induced Shocks in Ices **[#2507]**
We have conducted laboratory experiments to study the possible chemical production induced by meteoritic impact shocks on planetary ices. A pulsed Nd-YAG laser was used to reproduce the shock phenomena during hypervelocity impacts into the ice.

11:30 a.m. Milam S. N. * Nuevo M. Sandford S. A. Elsila J. E. Dworkin J. P.
Photo-Irradiation of Pyrimidine in Interstellar Ice Analogs: Searching for Nucleobases **[#2330]**
Nucleobases have been detected in meteorites and possibly form in space. The functionalization of PAHs from UV photons in mixed ices has proven effective in the lab. Here we investigate how irradiation affects pyrimidine in interstellar ice analogs.

PLENARY SESSION: MASURSKY LECTURE AND DWORNIK AWARD PRESENTATIONS
Monday, 1:30 p.m. Waterway Ballroom 4

Chairs: **Stephen Mackwell and Eileen Stansbery**

Presentation of the 2008 GSA Stephen E. Dwornik U.S. Citizen Student Award Winners

Presentation of the 2009 LPI Career Development Award Winners

Masursky Lecture:

Masursky Lecture by Dr. Alan Stern

Planet Categorization and Planetary Science: Coming of Age in the 21st Century

Most planetary scientists and astronomers grew up and were educated in a universe with nine planets. Today, however, hundreds of planets are known and thousands soon will be. Moreover, the variety of planetary types has exploded from "terrestrials," "gas giants," and "misfit Pluto" to include pulsar planets, ice giants, super-Earths, icy and rocky dwarfs, hot Jupiters, and still more; and like the known population, this variety can be confidently expected to only increase. I will briefly review this transformation in perspective and speak to a few of the categorization challenges facing us as both researchers and educators of science in the midst of this ongoing revolution.

PHOENIX: SOIL, CHEMISTRY, AND HABITABILITY
Monday, 2:30 p.m. Waterway Ballroom 1

Chairs: **Suzanne Young and Aaron Zent**

2:30 p.m. Keller H. U. * El Maarry M. R. Goetz W. Hviid S. F. Markiewicz W. J. Hecht M. Madson M. Mellon M. Ming D. Pike W. T. Smith P. Staufer U. Zent A.
Physical Properties of the Icy Soil at the Phoenix Landing Site **[#1671]**
The physical properties of the icy martian soil documented by the robotic arm camera of the Phoenix lander are discussed. The soil is friable and porous. Its cohesiveness changes when separated from the ground, most probable due to sublimation of its spurious water content.

2:45 p.m. Zent A. P. * Hudson T. L. Hecht M. H. Cobos D. Wood S. E.
Mars Regolith Thermal and Electrical Properties: Initial Results of the Phoenix Thermal and Electrical Conductivity Probe (TECP) **[#1125]**
Initial results from the Phoenix Thermal and Electrical Conductivity Probe suggest the landing event disturbed the thermal properties of the regolith surface. H_2O is exchanged between the atmosphere and regolith, and observed both in RH and dielectric measurements.

3:00 p.m. Renno N. O. * Bos B. J. Catling D. Clark B. C. Drube L. Fisher D. Goetz W. Hviid S. F. Keller H. U. Kok J. F. Kounaves S. P. Leer K. Lemmon M. Madsen M. B. Markiewicz W. Marshall J. McKay C. Mehta M. Smith M. Smith P. H. Stoker C. Young S. M. M. Zent A.
Physical and Thermodynamical Evidence for Liquid Water on Mars **[#1440]**
We show independent physical and thermodynamical evidence that liquid saline-water exists in areas disturbed by the Phoenix lander and that the thermodynamics of freeze-thaw cycles leads to the formation brine layers. Thus, liquid saline-water might be common on Mars.

3:15 p.m. Kounaves S. P. * Catling D. Clark B. C. DeFlores L. Gospodinova K. Hecht M. H. Kapit J. Ming D. W. Quinn R. C. Phoenix Science Team
Aqueous Carbonate Chemistry of the Martian Soil at the Phoenix Landing Site **[#2489]**
The Wet Chemistry Labs on Phoenix gave pH, conductivity, ions, and evidence that the salts have previously interacted with water and contain high levels of carbonates. Carbonate results show the need for more extensive laboratory work and equilibrium modeling.

3:30 p.m. Hanley J. * Chevrier V. F. Altheide T. S.
Low Temperature Aqueous Perchlorate Solutions on the Surface of Mars **[#1380]**
Perchlorates may hold the key to finding liquid water on Mars. We demonstrate that Mg- and Na-perchlorate solutions can have low evaporation rates and high stability on the martian polar surface.

3:45 p.m. Davis B. L. * Chevrier V. F. Altheide T. S. Swaffar C.
Reflectance Spectra of Low-Temperature Chloride and Perchlorate Hydrates and their Relevance to the Martian Surface **[#1387]**
Reflectance spectra of chloride and perchlorate hydrates were measured, since they are thermodynamically more stable than their anhydrous counterpart under Mars low-temperatures. Results show that these hydrates show specific spectral features.

4:00 p.m. Archer P. D. Jr.* Imanaka H. Smith M. A. Ming D. W. Boynton W. V. Smith P. H.
UV Photolysis of Mellitic Acid — A Possible Organic at the Mars Phoenix Landing Site **[#2077]**
The Phoenix lander is the first mission since Viking that could detect organics. Mellitic acid is a possible decay product of meteoritic organics. We irradiate mellitic acid with UV, producing a residue to analyze and compare to Phoenix results.

4:15 p.m. Young S. M. M. * Stoker C. R. Hecht M. H.
Polar Mars Biohabitability Assessment of the Wet Chemistry Analysis on the 2007 Phoenix Mars Scout Mission **[#1178]**
The Phoenix Mars mission included ions analysis by the Wet Chemistry Lab. One mission objective was to address biohabitability through water, energy sources, and subsurface bio-hostility. WCL experiments contribute much to these discussions.

4:30 p.m. Stoker C. R. * Archer P. D. Jr. Catling D. Clark B. Marshall J. Smith P. Young S. Phoenix Science Team
The Habitability of the Phoenix Landing Site: A Comparative Assessment **[#2082]**
We evaluate the habitability north polar region of Mars based on the results of the Phoenix mission and show that the region has greater habitability and potential for detecting life than other sites visited by Mars landers.

PLANETARY DIFFERENTIATION
Monday, 2:30 p.m. Waterway Ballroom 4

Chairs: **Rajdeep Dasgupta and William McDonough**

2:30 p.m. Brown S. * Elkins-Tanton L. T.
Earliest Planetary Crusts: Constraints on the Formation of Mercury and Implications for Bodies of Different Sizes **[#1334]**
We discuss the mechanisms for the production of the earliest crusts on terrestrial bodies and their implications for the crustal composition of Mercury.

2:45 p.m. Dauphas N. * Craddock P. R. Bennett V. Ohnenstetter D.
The Iron Isotopic Composition of the Silicate Earth: Clues from Chondrites, Peridotites, and Eoarchean Magmas **[#1769]**
While phanerozoic MORBs and OIBs have fractionated iron isotopic compositions relative to chondrites (+0.1 ‰), >3.7 Ga terrestrial magmas seem to have near chondritic iron isotopic compositions.

3:00 p.m. Shahar A. * Ziegler K. Young E. D. Ricolleau A. Macris C. A. Schauble E. A. Fei Y.
Experimental Evidence for Isotope Fractionation During Planetary Differentiation **[#1640]**
We provide experimental evidence suggesting that isotope fractionation of major elements at high pressure and temperature can be significant and are essential in interpreting stable isotope data on the planetary scale.

3:15 p.m. Armytage R. M. G. * Georg R. B. Halliday A. N.
The Non-Chondritic Silicon Isotope Composition of the Bulk Silicate Earth **[#1167]**
New results confirm a resolvable difference in Si isotopes between chondrites and terrestrial samples. As fractionation during core formation is the likeliest cause, Si is a strong contender for one of the light elements in the Earth's core.

3:30 p.m. Ziegler K. * Young E. D. Wasson J. T.
High-Precision Silicon Isotope Ratio Measurements of Earth and Enstatitic Meteorites and Implications for Si Isotope Fractionation During Core Formation **[#2446]**
Planetary core formation may impart stable isotope signatures on bulk silicate Earth due to partitioning between core and silicate. Si isotope data from silicate from E-chondritic meteorite and Earth suggest that there is no substantial difference.

3:45 p.m. Chabot N. L. * Safko T. M. McDonough W. F.
Exploring the Effect of Si in Metal on Element Partitioning Behavior **[#1112]**
Silicon is considered a potential light element in Earth's core, but data are lacking regarding the behavior of elements in systems with Si-bearing metals. Here we present new results of an experimental study examining the effects of Si.

4:00 p.m. Li J. * Chen B.
Melting Behavior of the Iron-Sulfur System and Chemical Convection in Iron-rich Planetary Cores **[#2091]**
We present experimental data on the high-pressure melting behavior of the Fe-S system from a synchrotron x-ray radiography study using the large volume press, with implications for the role of chemical convection in sulfur-bearing planetary cores.

4:15 p.m. Dasgupta R. * Buono A. Whelan G. Walker D.
High Pressure, Near-Liquidus Phase Relations in Fe-C-S Systems and Implications for Composition, Structure, and Process of Formation of Metallic Cores in Planetary Bodies **[#2008]**
We present new high pressure, near-liquidus phase relation experiments in Fe-C-S systems. Our experiments shed light on to the evolution and formation of metallic cores in differentiated planetary bodies in the presence of both carbon and sulfur.

4:30 p.m. McDonough W. F. * Brenan J. M.
Core Formation, HSE Partitioning and Non-Equilibrium Processes **[#1371]**
Os + Au metal-silicate partitioning experiments at ~core-forming conditions reveal D-Os of >107 and relative Os to Au partitioning of >104. Results are incompatible w/ equilibrium formation models requiring mantle addition of HSE post-core formation.

PRESOLAR GRAINS: STRUCTURES AND ORIGINS
Monday, 2:30 p.m. Waterway Ballroom 5

Chairs: **Manavi Jadhav and Tom Zega**

2:30 p.m. Vollmer C. * Brenker F. E. Hoppe P. Stroud R. M.
Transmission Electron Microscopy of Silicate Stardust Detected by NanoSIMS Imaging in Acfer 094 **[#1262]**
We report on combined NanoSIMS/TEM results of eight presolar silicates from the Acfer 094 meteorite. The mineralogical information will be compared to silicate dust properties obtained from infrared spectra and formation mechanisms in circumstellar outflows.

2:45 p.m. Stroud R. M. * Floss C. Stadermann F. J.
Structure, Elemental Composition and Isotopic Composition of Presolar Silicates in MET 00426 **[#1063]**
We investigated two presolar silicates from MET 00426 by TEM, Auger and NanoSIMS. The finely nanocrystalline microstructures and the non-stoichiometric compositions together indicate that these grains condensed under complex, non-equilibrium conditions.

3:00 p.m. Zega T. J. * Alexander C. M. O'D. Nittler L. R. Stroud R. M.
Transmission Electron Microscopy Analysis of a Presolar Spinel Grain **[#1342]**
We report the first microstructural analysis of a presolar spinel. The data are consistent with equilibrium condensation and show that O-rich AGB stars can condense single-crystal spinel grains.

3:15 p.m. Gyngard F. * Morgand A. Nittler L. R. Stadermann F. J. Zinner E.
Extreme Oxygen and Magnesium Isotopic Anomalies in Presolar Spinel Grains from the Murray Carbonaceous Meteorite **[#1386]**
We report here the extremely anomalous O and Mg isotopic compositions of some newly discovered presolar spinel grains from the Murray meteorite.

3:30 p.m. Hynes K. M. * Amari S. Croat T. K. Mertz A. F. Bernatowicz T. J.
An Analysis of Presolar SiC X Grains and Mainstream Grains Using Transmission Electron Microscopy **[#1398]**
We report the results of a coordinated NanoSIMS and TEM study of seven SiC X grains and two mainstream grains from the same size fraction in order to compare the isotopic and microstructural results of formation in two very different stellar environments.

3:45 p.m. Jadhav M. * Amari S. Zinner E. Maruoka T.
Continued Isotopic Studies of Low-Density Graphite Grains from Orgueil **[#2394]**
We report C, N, O, Si, Al-Mg, K and Ca isotopic ratios in low-density presolar graphite grains from Orgueil. Some inferred $^{26}Al/^{27}Al$ ratios are as high as those seen in SiC-X grains - much larger than those previously observed in low-density graphites.

4:00 p.m. Croat T. K. * Jadhav M. Lebsack E. Bernatowicz T. J.
Low-Density Presolar Graphite Spherules from the Orgueil Meteorite **[#2175]**
TEM studies of two Orgueil low-density SN graphites reveal internal SiCs and TiAl-rich grains, phases not seen in Murchison SN graphites. Metallic RuOs-rich grains in a ^{13}C-rich graphite indicate that the source of ^{13}C-rich graphites is s-process enriched.

4:15 p.m. Daulton T. L. * Bernatowicz T. J. Croat T. K.
Alteration of TiC in Supernovae Outflows: Transmission Electron Microscopy Study of TiC Subgrains in Supernovae Graphite **[#1996]**
TiC and metal subgrains within supernovae graphites often exhibit rims suggesting alteration prior to encapsulation in the graphite. Detailed TEM microcharacterizations of the rimmed grains are performed to determine the mechanism of rim formation.

4:30 p.m. Fedkin A. V. * Meyer B. S. Grossman L. Desch S. J.
Condensation in Supernova Ejecta at High Spatial Resolution **[#1699]**
^{44}Ti-rich TiC condenses before graphite in SN ejecta only if thin sub-layers of the main burning zones mix together; such mixing is also needed to form Fe-olivine. High-T phases change from carbides to oxides along composition gradients within the He/N zone.

4:45 p.m. Levine J. * Savina M. R. Dauphas N. Davis A. M. Isselhardt B. H. Knight K. B. Lewis R. S. Pellin M. J. Stephan T.
First Four-Isotope Measurements of Chromium in Presolar SiC Grains **[#1982]**
We report measured abundances of all four chromium isotopes in presolar SiC grains, obtained by resonance ionization mass spectrometry.

SPECIAL SESSION: VENUS ATMOSPHERE: VENUS EXPRESS AND FUTURE MISSIONS
Monday, 2:30 p.m. Waterway Ballroom 6

Chairs: **Kevin Baines and Jorn Helbert**

2:30 p.m. Russell C. T. * Luhmann J. G. Wei H. Y. Ma Y. J. Daniels J. T. M. Barabash S. Zhang T. L.
Venus Express: Atmospheric Loss and Electrodynamics **[#1408]**
The solar wind interaction with Venus is eroding the Venus atmosphere in several different ways so that Venus is losing about 10^{25} ions per second. The Venus atmosphere is a strong generator of electromagnetic signals expected from lightning.

3:00 p.m. Piccioni G. * Drossart P. VIRTIS-Venus Express Team
A Review of the Main Results about Venus' Atmosphere from VIRTIS on Venus Express **[#2569]**
A review of results about the Venus atmosphere achieved by the VIRTIS instrument on board the ESA Venus Express mission. The VIRTIS imaging spectrometer in the range of 0.25 to 5 μm provide a powerful means to study Venus in depth from the surface up to the upper atmosphere.

3:30 p.m. Migliorini A. * Grassi D. Piccioni G. Drossart P. Cardesin-Moinelo A. VIRTIS-Venus Express Team
Thermal Structure in the Venusian Atmosphere: Results after More than Two Years in Orbit of Venus-Express Mission **[#1937]**
Atmospheric structure of Venus in the southern hemisphere, retrieved from the data of VIRTIS instrument on board of Venus Express mission is discussed. The results are compared with the findings from previous missions about the northern hemisphere.

3:45 p.m. Limaye S. S. *
Vortex Circulation of Venus **[#2564]**
Venus Express mission is providing us with new insights into the vortex circulation of the atmosphere of Venus. First discovered from the Mariner 10 observations, the vortex circulation centered over each pole shows many similarities with terrestrial tropical cyclones.

4:00 p.m. Yung Y. L. * Yang D. Lee C. Liang M. C. Chen P.
The Sulfur Cycle on Venus: New Insights from Venus Express **[#2559]**
Sulfur chemistry is critical to the composition of the Venus atmosphere.

4:15 p.m. Grinspoon D. H. * Taylor F. W.
Evolution of Climate on Venus: Knowledge, Uncertainty and Prospects **[#1375]**
A summary of recent progress in understanding climate evolution on Venus with an emphasis on Venus Express results.

4:30 p.m. Helbert J. * Müller N. Maturilli A. Piccioni G. Drossart P.
The Long and Hot Way from Brightness Anomalies to Compositional Information — High Temperature Laboratory Spectroscopy for VIRTIS on Venus Express **[#1678]**
To support the analysis of VIRTIS on VEX surface data the PEL will provide a database of emissivity spectra in the 1–1.2 micron range at Venus temperatures.

4:45 p.m. Stofan E. R. * Smrekar S. E. Helbert J. Martin P. Mueller N.
Coronae and Large Volcanoes on Venus with Unusual Emissivity Signatures in VIRTIS-Venus Express Data **[#1033]**
Recent Visual and Infrared Thermal Imaging Spectrometer (VIRTIS) images from the Venus Express mission found emissivity variations that correlate with some volcanic edifices and coronae, including Shiwanokia and Shulamite Coronae in Themis Regio.

5:00 p.m. Baines K. H. * Atreya S. K. Crisp D. Hall J. L. Kerzhanovich V. V. Limaye S. S. Zahnle K.
In-Situ Exploration of Venus by Balloon — Science Objectives and Mission Architecture **[#1238]**
High-altitude balloon missions to Venus address numerous high-priority science issues including origin/evolution, chemical cycles, and the roles of waves, convection, and cloud-level solar energy deposition in driving circulation and super-rotation.

5:15 p.m. Bullock M. A. * Senske D. A. Balint T. S. Benz A. Campbell B. A. Chassefiere E. Colaprete A. Cutts J. A. Glaze L. Gorevan S. Grinspoon D. H. Hall J. Hashimoto G. L. Head J. W. Hunter G. Johnson N. Kerzhanovich V. V. Kiefer W. S. Kolawa E. A. Kremic T. Kwok J. Limaye S. S. Mackwell S. J. Marov M. Y. Ocampo A. Schubert G. Stofan E. R. Svedhem H. Titov D. V. Treiman A. H.
A Venus Flagship Mission: Report of the Venus Science and Technology Definition Team **[#2410]**
The Venus STDT has defined the goals, objectives, mission architecture, science investigations and payload for a Flagship-class mission to Venus. The mission puts advanced exploration capabilities in orbit, in the atmosphere, and on the surface.

MARS POLAR CAPS: PAST AND PRESENT
Tuesday, 8:30 a.m. Waterway Ballroom 1

Chairs: **Kathryn Fishbaugh and Timothy Titus**

8:30 a.m. Phillips R. J. * Putzig N. E. Head J. W. Egan A. F. Plaut J. J. Safaeinili A. Smrekar S. E. Milkovich S. M. Nunes D. C. Campbell B. A. Carter L. M. Holt J. W. Seu R. Orosei R.
Subsurface Structure of the South Polar Layered Deposits, Mars **[#2007]**
SHARAD radar sounding of the south polar layered deposits on Mars reveals similarities and differences in subsurface structure when compared to the north polar layered deposits.

8:45 a.m. Fishbaugh K. E. * Hvidberg C. Byrne S. Herkenhoff K. Fortezzo C. Kirk R. Winstrup M.
The Stratigraphic Record in the Martian North Polar Layered Deposits as Measured by High Resolution Stereo Topography **[#1998]**
We present the most detailed stratigraphic column of the martian north polar layers produced to date and will discuss the preliminary results of a unique inverse model used to extract a connection with the insolation curve over the last 5 Myrs.

9:00 a.m. Smith I. B. * Holt J. W. Christian S. W. Safaeinili A.
Evidence for Spiral Trough Migration and Evolution from SHARAD Radar Observations of Stratigraphy within the Northern Polar Layered Deposits, Mars **[#1423]**
Unconformities found in the NPLD of Mars resemble slopes and V shapes that we interpret as former trough locations. Evidence supports the idea that the troughs have migrated both northward and upward as deposition took place.

9:15 a.m. Holt J. W. * Safaeinili A.
Northern Polar Layered Deposits, Mars: Structural Relationships Between Gemina Lingula, the Main Lobe, and Chasma Boreale from SHARAD Radar Stratigraphy **[#1721]**
SHARAD radar stratigraphy reveals structure within the northern polar layered deposits that sheds light on the linked histories of Gemina Lingula and Chasma Boreale, major deposition and erosional episodes, and possible flow.

9:30 a.m. Winebrenner D. P. * Koutnik M. R. Waddington E. D. Pathare A. V. Byrne S. Murray B. C.
Spatially Resolved Glacial History on Gemina Lingula from Analysis of Topography Between Troughs **[#2384]**
We derive spatially resolved information on surface mass balance in the recent past on the martian north polar layered deposits, from analysis of topography between troughs on Gemina Lingula.

9:45 a.m. Tanaka K. L. * Rodriguez J. A. P. Fortezzo C. M. Seelos F.
Obliquity-driven Periods of Extended Erosion and Deposition in the Geologic Record of Planum Boreum, Mars **[#2476]**
Two major unconformities mapped in north polar deposits define the Olympia and Tenuis Hiatuses. We propose that they coincide with epochs of lower obliquity.

10:00 a.m. Banks M. E. * Galla K. G. Bryne S. Murray B. C. McEwen A. S. HiRISE Team
Crater Population and Resurfacing of the Martian North Polar Cap **[#2441]**
Over 100 impact craters have been identified in CTX images of the north polar layered deposits (NPLD) and residual cap (NRC). Using NRC cratering data we will use landscape evolution modeling to investigate the recent mass-balance history of the NRC.

10:15 a.m. Herkenhoff K. E. * Byrne S. Fishbaugh K. Hansen C. Milazzo M. Rosiek M. Russell P. HiRISE Team
HiRISE Observations of Recent Phenomena in the North Polar Region of Mars **[#2231]**
A summary of preliminary analyses of HiRISE north polar data from MRO's primary science phase, focusing on active and recent processes including evolution of the seasonal caps, frost streaks, and the residual caps.

10:30 a.m. Kolb E. J. * Tanaka K. L.
Bed Structures of Polar Layered Deposit Outcrops in Australe Mensa: Implications for the Formational History of Planum Australe, Mars **[#2230]**
We've characterized bedding structures and correlated unconformities identified in Australe Mensa with those seen previously in other parts of Planum Australe. Using this stratigraphic framework, we discuss Planum Australe's geologic history.

10:45 a.m. Brown A. J. * Calvin W. M. Murchie S. L.
MRO (CRISM/MARCI) Mapping of the South Pole — First Mars Year of Observations **[#1860]**
We have used MARCI and CRISM observations of the south pole over the first Mars year of MRO operations. We observed cloud dynamics from L_s=160–200, found a seasonal peak in CO_2 grain sizes and mapped the springtime recession of the south polar cap.

11:00 a.m. Calvin W. M. * Thomas P. C. Titus T. N. Brown A. J. James P. B.
Composition of the Residual South Polar Cap of Mars from CRISM **[#1984]**
Analysis of high resolution CRISM data shows that water ice is a small component of the residual south ice deposits and is spatially variable in extent and amount. CO_2 features are often observed suggesting mobile frost patches throughout the summer.

11:15 a.m. Titus T. N. * Michaels T. I.
Comparisons of MRO-Odyssey Observations of the South Polar Cryptic Region Giza to Mesoscale Models **[#1933]**
Every southern spring, a dark CO_2 ice region forms within the seasonal cap. This region, called the Cryptic region, has been actively monitored by many spacecraft. Observations of Giza, within the Cryptic region, are compared to mesoscale models.

11:30 a.m. Thomas P. C. * James P. B. Calvin W. Haberle R. M. Malin M. C.
Residual South Polar Cap of Mars: MRO Results, Interpretations, and Puzzles **[#1267]**
MRO data from CTX, CRISM, and HiRISE are used to inventory units and study changes and compositions in the residual south polar cap.

SPECIAL SESSION: LUNAR MISSIONS: RESULTS FROM KAGUYA, CHANG'E-1, AND CHANDRAYAAN-1, PART I
Tuesday, 8:30 a.m. Waterway Ballroom 4

Chairs: **Clive Neal and Alian Wang**

8:30 a.m. Goswami J. N. * Annadurai M.
Chandrayaan-1: India's First Planetary Science Mission to the Moon **[#2571]**
The first Indian planetary exploration mission, Chandrayaan-1, was launched on 22 October, 2008. We will present a brief summary of the science objectives, various payloads, mission details and observational plans.

9:00 a.m. Gopala Krishna B. * Amitabh Sanjay S. Srivastava P. K. Kiran Kumar A. S.
Digital Elevation Models of the Lunar Surface from Chandrayaan-1 Terrain Mapping Camera (TMC) Imagery — Initial Results **[#1694]**
Initial results of digital elevation model obtained from the stereo triplet images acquired by the Terrain Mapping Camera onboard the Chandrayaan-1 spacecraft are discussed.

9:15 a.m. Kiran Kumar A. S. * Roy Chowdhury A. Murali K. R. Sarkar S. S. Joshi S. R. Patel V. D. Dave A. B. Shah K. J. Banerjee A. Arya A. S. Chauhan P. Mathew K. Sharma B. N.
The Terrain Mapping Camera on Chandrayaan-1 and Initial Results **[#1584]**
The Terrain Mapping Camera on Chandrayaan-1, acquires stereo triplet images of Moon in visible band. With the successful launch, spacecraft reached the 100 kilometer polar orbit around the moon and has since been returning images of Moon.

9:30 a.m. Dachev Ts. P. * Tomov B. T. Matviichuk Yu. N. Dimitrov Pl. S. Angelis G. De. Spurny F. Vadawale S.
Monitoring of the Earth and Moon Radiation Environment by the RADOM Instrument on Indian Chandrayyan-1 Satellite. Preliminary Results **[#1274]**
This paper describes preliminary scientific results from the measurements of the Earth and Moon radiation environment by RADOM instrument since 22nd October 2008.

9:45 a.m. De Angelis G. * Dachev Ts. P. Tomov B. Matviichuk Yu. Dimitrov Pl. Spurny F. Vadawale S.
Modeling of the Moon Radiation Environment at the Altitude of the Indian Chandrayaan-1 Satellite and a Comparison with the RADOM Experiment Data **[#1310]**
These results for the moon radiation environment as well as for the cruise phase have been obtained in the framework of the Radom investigation that is on-board the Chandrayaan-1 mission by the Indian Space Agency ISRO.

10:00 a.m. Spudis P. D. * Bussey D. B. J. Butler B. Carter L. Gillis-Davis J. Goswami J. Heggy E. Kirk R. Misra T. Nozette S. Robinson M. Raney R. K. Thomson B. Ustinov E.
The Mini-SAR Imaging Radar on the Chandrayaan-1 Mission to the Moon **[#1098]**
The Mini-SAR is an imaging radar instrument on the Indian Chandrayaan-1 mission to the Moon. It will map both lunar poles, revealing terrain in permanently dark areas and characterizing the backscattering properties of these areas, looking for evidence of ice.

10:15 a.m. Senthil Kumar A. Kiran Kumar A. S. * Goswami J. N. Pieters C. M. Krishna B. G. Chauhan P.
Lunar Orientale Basin: Topology and Morphology of Impact Melt Region from Chandrayaan-1 TMC and HYSI **[#1505]**
Initial results of Chandrayaan-1 Terrain Mapping Camera and Hyperspectral Imager data acquired the Orientale Basin of lunar surface are presented.

10:30 a.m. Kamalakar J. A. * Laxmi Prasad A. S. Bhaskar K. V. S. Selvaraj P. Sridhar Raja V. L. N. Goswami A. Kalyani K. Ravikumar K. Jain Y. K. Daniel D. A. Gopinath N. S.
Laser Ranging Experiment Aboard Chandrayaan-I: Instrumentation and Preliminary Results **[#1487]**
This paper presents the instrumentation details, end-to-end testing of the Lunar Laser Range Instrument (LLRI) aboard Indian lunar mission Chandrayaan-1 and focus on the present status and preliminary results obtained by the instrument.

10:45 a.m. Grande M. * Kellett B. J. Maddison B. J. Sreekumar P. Huovelin J. Howe C. J. Crawford I. A. Narendranath S.
Initial Results from the C1XS X-Ray Spectrometer on Chandrayaan-1 **[#1840]**
C1XS in flight calibration shows the instrument is performing well. C1XS observed the Moon during an A class flare on 12-12-2008; characteristic x-ray lines at Mg, Al and Si are clearly resolved. Analysis shows that C1XS easily meets spec.

11:00 a.m. Pieters C. M. * Moon Mineralogy Mapper Team
Mineralogy of the Lunar Crust in Spatial Context: First Results from the Moon Mineralogy Mapper (M^3) **[#2052]**
Mineralogy across the Orientale Basin measured with initial M^3 data indicate the peak ring exposed a massive crustal layer of almost pure anorthosite. This is underlain by noritic materials. More mineralogy data of the lunar crust is being acquired.

11:15 a.m. Green R. O. * Pieters C. M. Boardman J. Barr D. Bruce C. Bousman J. Chatterjee A. Eastwood M. Essandoh V. Geier S. Glavich T. Green R. Haemmerle V. Hyman S. Hovland L. Koch T. Lee K. Lundeen S. Motts E. Mouroulis P. Paulson S. Plourde K. Racho C. Robison D. Rodriguez J. Rothman P. Sellar G. Smith C. Sobel H. Stamp J. Tseng H. Varanasi P. Wilson D. White M.
The Moon Mineralogy Mapper (M^3) Imaging Spectrometer: Early Assessment of the Spectral, Radiometric, Spatial, and Uniformity Characteristics **[#2307]**
The Moon Mineralogy Mapper is a high uniformity and high signal-to-noise ratio NASA imaging spectrometer that is a guest instrument on the Indian Chandrayaan-1 Moon Mission. We present an early assessment of the M^3 science measurement performance.

11:30 a.m. Li C. L. * Liu J. J. Mu L. L. Ren X. Zou Y. L. Zhang H. B. Lu C. Liu J. Z. Zuo W. Su Y. Wen W. B. Bian W. Zou X. D. Ouyang Z. Y.
A New Global Image of the Moon by Chinese Chang'E Probe **[#2568]**
Mapping procedure of the global image of the Moon is described, including introduction of data, data processing and map-making. The results shows that the Chinese global image map provides new and highly precise data for lunar topographic demonstration and research.

11:45 a.m. Liu J. J. * Ren X. Mu L. L. Zhao B. C. Xiangli B. Yang J. F. Zou Y. L. Zhang H. B. Lu C. Liu J. Z. Zuo W. Su Y. Wen W. B. Bian W. Zou X. D. Li C. L.
Automatic DEM Generation from CE-1's CCD Stereo Camera Images **[#2570]**
The goal of the CCD Stereo Camera is to acquire 3D-images of lunar surface bewteen 70S and 70N. We describe the process of the images acquired, configuration of imaging system, camera sensor model, camera trajectory model and EFP photogrammetric triangulation algorithm.

EARLY NEBULA PROCESSES AND MODELS
Tuesday, 8:30 a.m. Waterway Ballroom 5

Chairs: **James Lyons and Rachel Smith**

8:30 a.m. Ciesla F. J. *
A New Approach to Nebular Transport Models: Particle Trajectories **[#1099]**
A new method to nebular transport modeling is explored where particle trajectories are calculated, allowing the physical and chemical alteration that would occur to individual particles to be determined.

8:45 a.m. Keller L. P. * Messenger S.
Equilibrated Aggregates in Cometary IDPs: Insights into the Crystallization Process in Protoplanetary Disks **[#2121]**
The presence of equilibrated aggregates in cometary IDPs provides evidence for grain coagulation and annealing in the protoplanetary disk. Compositional data indicate that GEMS grains are the likely precursors to equilibrated aggregates.

9:00 a.m. Hughes A. L. H. * Armitage P. J.
Tracking Dust at the Disk Midplane: Implications for Stardust **[#1884]**
We present simulations of dust particle transport at the midplane of a protoplanetary disk, including gas drag and turbulent diffusion effects. Our model takes into account dust particle size and the viscous evolution of the disk.

9:15 a.m. Boss A. P. * Ipatov S. I. Keiser S. A. Myhill E. A. Vanhala H. A. T.
Simultaneous Triggered Presolar Cloud Collapse and Injection of Short-lived Radioisotopes by a Supernova Shock Wave **[#1002]**
We use the FLASH hydrodynamics code to show that supernova shock waves with speeds in the range from 5 to 70 km/sec can simultaneously trigger collapse of the presolar cloud and inject radioisotopes from the shock wave.

9:30 a.m. Gounelle M. * Meibom A. Hennebelle P. Inutsuka S.-I.
Supernova Propagation and Cloud Enrichment: A New Model for the Origin of ^{60}Fe in the Early Solar System **[#1624]**
We quantitatively evaluate a scenario proposing that ^{60}Fe was inherited in the progenitor molecular cloud from several supernovae belonging to previous episodes of star formation rather than injected in the protoplanetary disk by a single supernova.

9:45 a.m. Estrada P. R. * Cuzzi J. N.
A Faster Model for Coagulative Growth in Nebular and Subnebular Environments **[#1241]**
We report on the development of global nebula evolution models utilizing a mathematical scheme that makes the full-scale solution to the problem of dust coagulation less prohibitive.

10:00 a.m. Gilmour J. D. * Filtness M.
Does Late Processing of Primitive Chondrites Record the Dissipation of a Solar System Debris Disk? **[#1607]**
We discuss whether the range of I-Xe ages of chondrules from a primitive meteorite might record collisions during the dissipation of a debris disk.

10:15 a.m. Weidenschilling S. J. *
How Big Were the First Planetesimals? Does Size Matter? **[#1760]**
Accretion of ~10 km bodies yields the best match for the size distribution of the early asteroid belt. If initial planetesimals had a single size, bodies of 1 km or larger than a few tens of km are excluded.

10:30 a.m. Smith R. L. * Pontoppidan K. M. Young E. D. Morris M. R. van Dishoeck E. F.
High-Precision $C^{17}O$, $C^{18}O$ and $C^{16}O$ Measurements in Young Stellar Objects: Analogues for CO Self-shielding in the Early Solar System **[#1471]**
We report precise CO isotopologue ratios obtained with high-resolution IR observations, and find a mass-independent oxygen isotope trend in a T Tauri circumstellar disk. We explain our results by CO self-shielding in this early solar system analogue.

10:45 a.m. Chakraborty S. * Ahmed M. Dominguez G. Thiemens M. H.
Oxygen Isotopic Fractionation in Vacuum Ultraviolet Photodissociation of CO: Lack of Self-shielding and Relevance to the Early Solar System **[#2075]**
VUV photodissociation at shielding and non-shielding wavelengths yield same slope value in three isotope oxygen plot. These results do not indicate self-shielding rather dissociation through leaky isotope selective channels may be more important.

11:00 a.m. Lyons J. R. *
The Predominance of Self-shielding in Laboratory CO Photolysis Experiments **[#2377]**
I argue here that the laboratory CO photolysis results of Chakraborty et al. (2008) are, in fact, a result of CO self-shielding, and I present model simulations of several of their experiments as support.

11:15 a.m. Berg T. * Marosits E. Maul J. Schönhense G. Hoppe P. Ott U. Palme H.
Evidence for Nebular Condensation of Sub-Micron Refractory Metal Alloys **[#1585]**
Analysis of sub-micron refractory metal alloys provide direct evidence for condensation in the early solar system. Comparison of compositions with condensation calculations allows to estimate maximum cooling rates of the parental nebula.

11:30 a.m. Nagahara H. * Ozawa K.
Condensation Kinetics of Forsterite and Metal and Chemical Fractionation in the Proto Solar Nebula **[#2158]**
Condensation sequence and their grain size distribution in a cooling gas system including heterogeneous condensation of metallic iron onto forsterite were investigated. Heterogeneous condensation results in Fo-core and Fe-mantle grains.

SPECIAL SESSION:
ICY SATELLITES OF JUPITER AND SATURN: COSMIC GYMNASTS
Tuesday, 8:30 a.m. Waterway Ballroom 6

Chairs: **Michael Bland and Steve Vance**

8:30 a.m. Rudolph M. L. * Manga M.
Ocean Pressurization, Stress Evolution, and Tensile Fracture Within Icy Moons **[#2436]**
Thickening of an ice shell overlying an ocean pressurizes the ocean and tangential stresses of several MPa are produced in the overlying ice shell. These stresses drive tensile fractures which may facilitate cryovolcanism.

8:45 a.m. Han L. * Showman A. P.
Tidal Dissipation in Europa's Ice Shell with a Heterogeneous Temperature Distribution **[#2279]**
We present numerical simulations of the tidal oscillation process to studythe temperature and spatial dependence of tidal dissipation in a ice shell with heterogeneous temperature distribution.

9:00 a.m. Sarid-Rhoden A. R. * Militzer B. Huff E. M. Hurford T. A. Manga M. Richards M.
Implications for Europa's Obliquity from Cycloid Modeling **[#1891]**
We will present improved fits to Europan cycloids in the southern hemisphere and the first fits to equatorial cycloids, which we obtained using a tidal model that includes the effects of obliquity.

9:15 a.m. Matson D. L. * Castillo-Rogez J. C. Johnson T. V. Turner N. Lee M. H. Lunine J. I.
^{26}Al Decay: Heat Production and Revised Age for Iapetus **[#2191]**
We revisit the decay energies that have been used for computing the heat produced by the decay of ^{26}Al in geophysical models. Using the most recent nuclear constants, we recommend a heat production value of 3.12 MeV per decay and a half-life of 0.717 My.

9:30 a.m. Roberts J. H. * Nimmo F.
Tidal Dissipation Due to Despinning and the Equatorial Ridge on Iapetus **[#1927]**
The equatorial ridge on Iapetus cannot be formed by despinning stresses alone. However, heat dissipated by despinning may promote the formation of a degree-2 convective upwelling and positive dynamic topography at the equator.

9:45 a.m. Melosh H. J. * Nimmo F.
An Intrusive Dike Origin for Iapetus' Enigmatic Ridge? **[#2478]**
The symmetry and linearity of Iapetus' equatorial ridge suggest an extensional dike origin. Tidal despinning may provide both the heat and stress necessary to guide fluid intrusion from its interior.

10:00 a.m. Schenk P. M. * Moore J. M.
Eruptive Volcanism on Saturn's Icy Moon Dione **[#2465]**
Volcanic plains on Dione include unusual crater-like landforms indicative of eruptive volcanism. Although older than resurfacing on Enceladus, these features confirm that Saturn's icy moons have diverse and complex geologic histories.

10:15 a.m. Johnson T. V. * Castillo-Rogez J. C. Matson D. L. Thomas P. C.
Phoebe's Shape: Possible Constraints on Internal Structure and Origin **[#2334]**
We address the origin of Phoebe's shape and discuss the potential constraints on the internal structure and thermal evolution of Phoebe that can be inferred from Cassini observations.

10:30 a.m. Asmar S. W. * Nimmo F. Thomas P. C. Bills B. G.
A Shape Model For Rhea and Implications for its Gravity Coefficients and Internal Structure **[#2219]**
We have determined the shape of Rhea in the form of a spherical harmonic expansion to degree 10 from limb profiles and investigated the implication to gravity coefficients.

10:45 a.m. Zhang K. * Nimmo F.
Internal Structure of Enceladus and Dione from Orbital Constraints **[#2199]**
Based on orbital constraints, we find that Enceladus is likely to have a liquid ocean beneath its conductive ice shell. Dione probably has a similar internal structure.

11:00 a.m. Kieffer S. W. * Lu X. McFarquhar G. Wohletz K. H.
Ice/Vapor Ratio of Enceladus' Plume: Implications for Sublimation **[#2261]**
The ice/vapor ratio for the Enceladus' plume, using the originally reported data ISS and UVIS data should be 0.2, not 0.4. The corrected data are compatible with sublimation. Conclusions about the need for a liquid reservoir need to be reexamined.

11:15 a.m. Mitri G. * Iess L. Rappaport N. J.
Interior Structure of Titan **[#2019]**
Cassini radio science data indicates that Titan is nearly in hydrostatic equilibrium. We have used thermal models and hydrostatic equilibrium theory to derive interior models of Titan.

11:30 a.m. Bills B. G. * Nimmo F.
Titan's Spin, Gravity, and Moments of Inertia **[#1462]**
The gravitational field and spin state of Titan yield separate estimates of the polar moment of inertia, and they differ as would be expected for a body with a decoupled shell floating on a subsurface ocean.

MARS: GROUND ICE AND CLIMATE CHANGE
Tuesday, 1:30 p.m. Waterway Ballroom 1

Chairs: **Richard Soare and Norbert Schorghofer**

1:30 p.m. Safaeinili A. * Holt J. Plaut J. Posiolova L. Philips R. Head J. W. Seu R.
New Radar Evidence for Glaciers in Mars Phlegra Montes Region **[#1988]**
There is new radar evidence for the presence of debris-covered glacier at 36°N latitude in the Phlegra Montes region of Mars. The depth of the glacier is estimated at about 180 m. This is the closest glacier to the equator found by SHARAD to date.

1:45 p.m. Head J. W. * Marchant D. R. Forget F. Laskar J. Madeleine J.-B. Fastook J. L.
Deciphering the Late Amazonian Climate History of Mars: Assessing Obliquity Predictions with Geological Observations and Atmospheric General Circulation Models **[#1349]**
We use the geological record of non-polar ice deposits to distinguish between predicted obliquity scenarios for the Late Amazonian climate history of Mars; extended periods of consistently high or low obliquity are unlikely during the last 250 My.

2:00 p.m. Marchant D. R. * Head J. W.
The Glacial Deposits of the Northern Mid-Latitudes: Remnants of Large-Scale Plateau Glaciation **[#2355]**
Glaciers in Antarctica provide insight into the origin of debris-covered glaciers on Mars. The Antarctic analogs suggest that the dichotomy boundary was largely covered with plateau ice fields during parts of the Amazonian.

2:15 p.m. Fastook J. L. * Head J. W. Madeleine J.-B. Forget F. Marchant D. R.
Modeling Northern Mid-Latitude Glaciation with GCM-driven Climate: Focus on Deuteronilus-Protonilus Mensae Valleys **[#1144]**
Model investigations of paleo-ice sheets on Mars help identify and interpret glacial deposits observed from orbit and aid in explaining the mechanisms responsible for formation of the ice-rich mantling seen north of ~50N latitude by Mars Odyssey.

2:30 p.m. Kadish S. J. * Head J. W. Barlow N. G.
Mid-Latitude Pedestal Crater Heights: A Proxy for the Thickness of a Past Climate-related, Ice-rich Substrate **[#1313]**
The armored surfaces of mid-latitude pedestal craters (Pd) on Mars preserve a past climate-related, ice-rich substrate deposited during periods of higher obliquity. The Pd heights thus provide insight into the regional thicknesses of the substrate.

2:45 p.m. Dundas C. M. * Byrne S. McEwen A. S.
Modeling Sublimation of Ice Exposed by Recent Impacts in the Martian Mid-Latitudes **[#2168]**
Very recent impacts in the martian mid-latitudes have exposed ground ice at shallow depths. We describe modeling of the sublimation of this ice and discuss implications for the ground ice. Modeled rates of sublimation suggest that this ice is more pure than pore-filling.

3:00 p.m. Schörghofer N. *
Mars: Response of Ice-rich Permafrost to Milankovitch Forcing and the Origin of the Polar Layered Deposits **[#1429]**
A subsurface-atmosphere climate model of Mars is used to estimate the volume of ice released from ice-rich permafrost as a result of Milankovitch cycles; the polar layered deposits may result from periodic retreat of mid-latitude subsurface ice.

3:15 p.m. Levy J. S. * Head J. W. III Marchant D. R.
Thermal Contraction Crack Polygons on Mars: Classification, Distribution, and Context for Phoenix from North and South Polar HiRISE Observations **[#1616]**
Thermal contraction crack polygon morphology is used to understand the deposition and modification of young, ice-rich mantling units across martian mid-high latitudes and at the Phoenix landing site. Signatures of excess ice and sublimation dominate.

3:30 p.m. Osinski G. R. * Soare R. J. Pearce G.
Impact Craters in Utopia Planitia, Mars: Windows into an Ice-rich Subsurface **[#1215]**
We demonstrate that impacts have occurred into ice-rich periglacial terrains in Utopia Planitia and show that the impact stratigraphy can be used to build up a clearer picture of the geological history of this region of Mars.

3:45 p.m. Soare R. J. * Osinski G. R. Thomson L.
Perennial mounds in Utopia Planitia: (HiRISE) Evidence of a Glacial Origin **[#1278]**
Here, we use HiRISE and high-resolution MOC images to discuss sub-kilometer pingo-like mounds in Utopia Planita. The mounds show geological characteristics consistent with formation by glacial accumulation, and ablation by sublimation.

4:00 p.m. Séjourné A. * Costard F. Gargani J. Marmo C. Forget F. Madeleine J.-B. Soare R. J.
Periglacial Processes In Utopia Planitia, Evolution of Scalloped Terrains: New Insights from HiRISE Observations **[#1733]**
We produced a geomorphologic study of scalloped terrains and polygonal networks in western Utopia Planitia with HiRISE images and MOLA altimetry.

4:15 p.m. Wood S. E. * Griffiths S. D.
Mars Subsurface Warming Due to Atmospheric Collapse at Low Obliquity **[#2490]**
We present a modeling study of a subsurface warming mechanism that has not previously been considered but is expected to operate during the periodicintervals when Mars' obliquity was lower than 25°.

4:30 p.m. Clifford S. M. * Heggy E. Boisson J. McGovern P. Max M. D.
The Occurrence and Depth of Subpermafrost Groundwater on Present-Day Mars: Implications of Revised Estimates of Crustal Heat Flow, Thermal Conductivity, and Freezing-Point Depression **[#2557]**
We conclude that the present day cryosphere may be up to twice as deep as previously believed, raising questions about the continued survival of subpermafrost groundwater.

SPECIAL SESSION: LUNAR MISSIONS: RESULTS FROM KAGUYA, CHANG'E-1, AND CHANDRAYAAN-1, PART II
Tuesday, 1:30 p.m. Waterway Ballroom 4

Chairs: Lisa Gaddis and Jeff Taylor

1:30 p.m. Sobue S. S. * Sasaki S. S. Kato M. K. Maejima H. M. Minamino H. M. Nakazawa S. N. Ootake H. O. Konishi H. K. Tateno N. T. Yonekura K. Y. Hoshino H. H. Kimura J. K.
The Project Highlight of Japan's Lunar Explorer Kaguya (SELENE) **[#1224]**
Kaguya (SELENE) was successful launched on September 14, 2007 at Tanegashima Space Center of JAXA. This paper describes the overview of Kaguya system, highlight of operation, public promotion result and future expected operation plan.

1:45 p.m. Kato M. * Takizawa Y. Sasaki S. SELENE Project Team
The Kaguya (SELENE) Mission and its Lunar Science **[#1226]**
The lunar orbiter Kaguya has completed steady observation for ten month. We would like to talk on science results and mission summary.

2:00 p.m. Ohtake M. * Matsunaga T. Yokota Y. Haruyama J. Miyamoto H. Arai T. Hirata N. Takeda H. Nakamura R. Morota T. Honda C. Ogawa Y. Kitazato K. LISM Team
Anorthosite with 100% Plagioclase on the Moon Detected by the SELENE Multiband Imager **[#1557]**
We find exceptionally feldspathic rock with ~100% Fe-bearing plagioclase at the base of central peak of Tycho by using Multiband Imager data on board SELENE. We are conducting similar analyses at other locations.

2:15 p.m. Matsunaga T. * Ohtake M. Haruyama J. Ogawa Y. Nakamura R. Yokota Y. Morota T. Honda C. Torii M. Abe M. Nimura T. Hiroi T. Arai T. Saiki K. Takeda H. Hirata N. Kodama S. Sugihara T. Demura H. Asada N. Terazono J. Otake H.
Current Status and First Scientific Results of SELENE Spectral Profiler **[#2133]**
Spectral Profiler (SP) is a visible — near infrared spectrometer onboard Japanese SELENE spacecraft. Its spectral specifications are optimized for lunar surface mineral survey. In this paper, SP's status and first scientific results are presented.

2:30 p.m. Yamashita N. * Hasebe N. Shibamura E. Kobayashi M.-N. Karouji Y. Hareyama M. Kobayashi S. Okudaira O. Takashima T. d'Uston C. Maurice S. Gasnault O. Forni O. Diez B. Reedy R. C. Kim K. J. Arai T. Ebihara M. Sugihara T. Takeda H. Hayatsu K. Iwabuchi K. Nemoto S. Takeda Y. Tsukada K. Nagaoka H. Hihara T. Maejima H. Nakazawa S. Otake H.
Precise Observation of Uranium, Thorium, and Potassium on the Moon by the SELENE GRS **[#1855]**
The SELENE GRS revealed the global distribution of U on the lunar surface for the first time. The U distribution and its trend with K and Th are discussed to help understand thermal history of the Moon.

2:45 p.m. Gasnault O. * Forni O. Diez B. d'Uston C. Maurice S. Hasebe N. Okudaira O. Yamashita N. Kobayashi S. Karouji Y. Hareyama M. Shibamura E. Kobayashi M. N. Reedy R. C. SELENA GRS Team
Preliminary Analysis of SELENE GRS Data — The Iron Case **[#2253]**
The lunar compositional poles can be seen in the SELENE gamma-ray data through statistical processing of the spectra. Independent component analysis leads to a map of Th and a preliminary map of Fe, which can be normalized with Lunar Prospector data.

3:00 p.m. Namiki N. * Sugita S. Matsumoto K. Goossens S. Ishihara Y. Noda H. Sasaki S. Iwata T. Hanada H. Araki H. Kurosawa K. Matsumura M. Yokoyama M. Kamata S. Kubo N. Mori A. Sato M.
Comparative Study of Compensation Mechanism of Lunar Impact Basins from New Gravity Field Model of SELENE (Kaguya) **[#1519]**
Based on the gravity model of the Moon by SELENE, we propose new classification and compensation mechanism of lunar impact basins. Impact basins on lunar far side are classified into two types depending on free-air and Bouguer gravity anomalies.

3:15 p.m. Ishihara Y. * Namiki N. Sugita S. Matsumoto K. Goossens S. Araki H. Noda H. Sasaki S. Iwata T. Hanada H.
Localized Gravity/Topography Correlation and Admittance Spectra on the Moon **[#1623]**
We show the results of localized correlation and admittance analysis using new lunar gravity and topography models from Kaguya mission.

3:30 p.m. Araki H. * Tazawa S. Noda H. Ishihara Y. Goossens S. Kawano N. Sasaki S. Kamiya I. Otake H. Oberst J. Shum C. K.
The Lunar Global Topography by the Laser Altimeter (LALT) Onboard Kaguya (SELENE): Results from the One Year Observation **[#1432]**
A global and precise topographic map of the Moon has been derived by the laser altimeter (LALT) onboard the Japanese lunar explorer Kaguya (SELENE). Results of the one year observation and implications from the LALT topography will be presented.

3:45 p.m. Antonenko I. * Cooper B. L. Yamaguchi Y. Ono T. Kumamoto A. Osinski G.
Preliminary Regional Analysis of the Kaguya Lunar Radar Sounder (LRS) Data Through Eastern Mare Imbrium **[#2406]**
We processed preliminary Kaguya Lunar Radar Sounder data to form a coarse 3D voxel grid model. This model shows topography, a regional boundary at ~3.8 km depth (but dipping to ~4.4 km in SE Mare Imbrium), and the probable detection limits of the instrument at ~6.3 km depth.

4:00 p.m. Honda R. * Yamazaki J. Mitsuhashi S. Tachino J. Yamauchi M. Shirao M.
Results of High-Definition Television System (HDTV) On Board SELENE (Kaguya) **[#2540]**
The current status of the HDTV, recent data obtained, and ongoing data analysis of HDTV images such as the creation of digital elevation model (DEM) from the moving images are reported.

4:15 p.m. Haruyama J. * Ohtake M. Matsunaga T. Morota T. Honda C. Yokota Y. Ogawa Y. LISM Working Group
SELENE (Kaguya) Terrain Camera Observation Results of Nominal Mission Period **[#1553]**
We will overview observation results of the 10 m-resolution stereo-camera, Terrain Camera, aboard SELENE (Kaguya) during its nominal mission period of about one-year.

4:30 p.m. Hirata N. * Haruyama J. Ohtake M. Matsunaga T. Yokota Y. Morota T. Honda C. Ogawa Y. Sugihara T. Miyamoto H. Demura H. Asada N.
Morphological Analyses of Tycho Crater with Kaguya Data **[#1514]**
We investigated a large lunar crater Tycho with Kaguya/LISM data to reconstruct the impact event forming the crater from distributions of its ejecta and other associated features.

CHONDRITE PARENT-BODY PROCESSES
Tuesday, 1:30 p.m. Waterway Ballroom 5

Chairs: Adrian Brearley and Molly McCanta

1:30 p.m. Grossman J. N. * Rubin A. E. Sears D. W. G.
The Mineral Compositions and Classification of High Type-3 and Type-4 Ordinary Chondrites **[#1679]**
The type 3/4 and 4/5 boundaries in ordinary chondrites are poorly defined; literature classifications may be inaccurate. Mineralogical trends across type 4 will permit better classification and improved understanding of asteroidal thermal histories.

1:45 p.m. Ragland C. * Bretzius S. A. Naranjo A. M. Thomas T. Grossman J. N. Rubin A. E. Sears D. W. G.
Metamorphism of Ordinary Chondrites at the Type-3/Type-4 Boundary **[#1122]**
A multidisciplinary study of ordinary chondrites at the type 3.7 to type 3/type 4 boundary is being undertaken to understand metamorphism in this little-studied range. Results for the first 11 samples will be discussed.

2:00 p.m. Brearley A. J. *
Matrix Olivines in the Metamorphosed CK Chondrite NWA 1628: Possible Affinities to Olivines in the Matrices of Oxidized CV3 Chondrites and Dark Inclusions **[#1791]**
Matrix olivines in NWA 1628 contain voids and inclusions of sulfides and are similar to matrix olivines in the Allende CV3 chondrite. Rare phyllosilicate phases are also present, indicating fluids played a role in the formation of the olivine grains.

2:15 p.m. McCanta M. C. * Beckett J. R. Stolper E. M.
Phosphorus Zonation in H Chondrite Olivines: The Effects of Increasing Petrologic Grade **[#2048]**
Olivines in type IIA chondrules in H chondrites were mapped to study the effects of thermal processing on phosphorus zonation. While zoned grains were found in meteorites of all petrologic grades, changes in their spatial distribution were observed.

2:30 p.m. Sharp T. G. * Trickey R. Xie Z. De Carli P. S.
Ringwoodite Microstructures in L-Chondrites RC 106 and Acfer 040: Implications for Transformation Mechanisms **[#2541]**
The transformation of olivine to ringwoodite is important because the transformation kinetics can be used to constrain shock duration. Here we examine the microstructures in ringwoodites from L chondrites RC106 and Acfer040 to better understand transformation mechanisms.

2:45 p.m. Abreu N. M. * Stanek G. L.
Chemical and Petrologic Evidence of Extensive and Complex Aqueous Alteration of the CR GRA 06100 **[#2393]**
GRA 06100 is a CR chondrite containing partially to completely oxidized kamacite and taenite. However, its alteration style differs significantly from CR1 GRO 95577.

3:00 p.m. Alexander C. M. O'D. * Newsome S. N. Fogel M. L. Cody G. D.
Deuterium Enrichments -- Parent Body Products or a Question of Preservation? **[#2546]**
Large D and ^{15}N in OC and CM IOM correlate with parent body metamorphism/alteration conditions suggesting there may have been previously unrecognized fractionation processes at work.

3:15 p.m. Tyra M. A. * Brearley A. J. Hutcheon I. D. Ramon E. Matzel J. Weber P.
Carbonate Formation Timescales Vary Between CM1 Chondrites ALH84051 and ALH84034 **[#2474]**
We use nanoSIMS to examine ^{53}Mn in carbonates of chondrites ALH 84051 and ALH 84034. Values obtained support early and prolonged aqueous alteration within their parent body.

3:30 p.m. de Leuw S. * Rubin A. E. Schmitt A. K. Wasson J. T.
Mn-Cr Systematics for the CM2.1 Chondrites QUE 93005 and ALH 83100: Implications for the Timing of Aqueous Alteration **[#1794]**
Little is known about the timescale of alteration processes on the CM parent body. We studied two CM2.1 chondrites, QUE 93005 and ALH 83100, and compared the data with previous studies. The results imply that alteration lasted at least 4 Ma.

3:45 p.m. Petitat M. * McKeegan K. Gounelle M. Mostefaoui S. Marrocchi Y. Meibom A. Leshin L. A.
Duration and Sequence of Carbonate Crystallization on the Orgueil Protolith: ^{53}Mn-^{53}Cr Systematics of their Evolution in O and C Isotopic Evolution **[#1657]**
We present a NanoSims ^{53}Mn-^{53}Cr systematics of eight breunnerites and three dolomites previously studied for $\delta^{18}O$ and $\delta^{13}C$ to constrain the duration and sequence of carbonate crystallization on the Orgueil protolith.

4:00 p.m. Cody G. D. * Heying E. Alexander C. M. O'D.
A Post Accretionary Origin for Meteoritic and Cometary Organic Solids? **[#2325]**
Recent molecular analyses of meteoritic and cometary organics and supporting experiments suggest a common origin for both being derived from a formaldehyde sourced sugar-like precursor. Extraterrestrial organic solids may have formed post accretion.

4:15 p.m. Herd C. D. K. * Nittler L. R. Alexander C. M. O'D.
Isotopically Heterogeneous Organic Matter in the Tagish Lake Meteorite **[#1818]**
NanoSIMS analysis of fragments from two lithologies within the Tagish Lake carbonaceous chondrite shows significant nanoscale N, H and C isotopic variation, providing possible new insights into the source and processing of primitive organic matter.

4:30 p.m. Remusat L. * Guan Y. Eiler J. M.
Organic Constituents in Carbonaceous Chondrites; Evidence for Preservation of Pristine Particles of Mixed Origins **[#1294]**
Organic matter in carbonaceous chondrites occurs as sub-micron particles. Some of these particles have been subjected to intense irradiation in the early solar system. This indicates important mixing processes during this time.

SPECIAL SESSION:
ICY SATELLITES OF JUPITER AND SATURN: SALUBRIOUS SURFACES
Tuesday, 1:30 p.m. Waterway Ballroom 6

Chairs: **Amanda Hendrix and Jani Radebaugh**

1:30 p.m. Buratti B. J. * Mosher J. A. Abramson L. Akhter N. Clark R. N. Brown R. H. Baines K. H. Nicholson P. D. DeWet S.
Opposition Surges of the Satellites of Saturn from the Cassini Visual Infrared Mapping Spectrometer (VIMS) **[#1738]**
The Cassini Visual Infrared Mapping Spectrometer returned observations of the opposition surge for Enceladus, Tethys, Dione, Rhea, and Iapetus. Each body shows a surge at phase angles of 1–12 degrees, and three exhibit a larger surge under 1 degree.

1:45 p.m. McCord T. B. * Hansen G. B. Combe J-Ph. Hayne P.
Hydrated Minerals on Europa's Surface **[#1736]**
Heavily hydrated materials on Europa's surface shows more evidence of salts and locations consistent with endogenic processes.

2:00 p.m. Dalton J. B. * Shirley J. H. Prockter L. M. Kamp L. W.
Compositional Gradients of Anti-Jovian Surface Units on Europa from Despiked Galileo NIMS Observations **[#2511]**
We have detected compositional gradients of hydrated sulfuric acid and hydrated salts on Europa.

2:15 p.m. Hendrix A. R. * Johnson R. E.
Europa: A New Look at Galileo UVS Data **[#2526]**
Europa observations from the Galileo UVS are studied to investigate the distribution of the 280 nm absorption feature. The absorber is more abundant on the trailing hemisphere; a correlation exists between absorption strength and dark features (linea and chaos regions).

2:30 p.m. Kirk R. L. * Howington-Kraus E. Redding B. L. Becker T. L. Lee E. M. Stiles B. W. Hensley S. Hayes A. G. Lopes R. M. C. Lorenz R. D. Mitchell K. L. Radebaugh J. Paganelli F. Soderblom L. A. Stofan E. R. Wood C. A. Wall S. D. Cassini RADAR Team
Three-Dimensional Views of Titan's Diverse Surface Features from Cassini RADAR Stereogrammetry **[#1413]**
Cassini RADAR has returned high resolution stereo images of dozens of areas on Titan. Digital topography extracted from the images provides new insight into lakes, dunes, mountains, flows, and other features including the enigmatic Ganesa Macula.

2:45 p.m. Nelson R. M. * Kamp L. W. Lopes R. M. C. Matson D. L. Kirk R. L. Hapke B. W. Boryta M. D. Leader F. E. Smythe W. D. Mitchell K. L. Baines K. H. Jaumann R. Sotin C. Clark R. N. Cruikshank D. P. Drossart P. Lunine J. I. Combes M. Bellucci G. Bibring J.-P. Capaccioni F. Cerroni P. Coradini A. Formisano V. Filacchione G. Langevin Y. McCord T. B. Mennella V. Nicholson P. D. Sicardy B. Irwin P. G. J. Pearl J. C.
Cassini Evidence for Active Cryovolcanism on Saturn's Moon Titan **[#2262]**
We report evidence for surface morphology changes on the surface of Saturn's satellite Titan from information returned by the Visual and Infrared Mapping Spectrometer (VIMS) aboard the Cassini Orbiter spacecraft. This is strong evidence for active cryovolcanism on Titan.

3:00 p.m. Davies A. G. * Matson D. L. Sotin C. Castillo-Rogez J. C. Johnson T. V.
Assessing Cryovolcanic Resurfacing on Titan **[#1906]**
We estimate the significance of cryovolcanism as a Titan resurfacing mechanism. To resurface Titan in this way over geological time (~0.5 Ga) requires only a very low effusion rate, so detection of active cryolava flows may be difficult.

3:15 p.m. Radebaugh J. * Valora P. Lorenz R. D. Wall S. D. Kirk R. L. Wood C. A. Lunine J. I. Stofan E. R. Lopes R. M. Farr T. G. Mitri G. Cassini Radar Team
Evidence of Extensional and Compressional Tectonism and Erosion in Titan's Xanadu Province **[#1037]**
Titan's Xanadu province, bright to all instruments and extending over 1000 km, is one of the oldest terrains on Titan. We suggest its origin and evolution have been controlled and shaped by compressional and extensional tectonism in its icy crust.

3:30 p.m. Jaumann R. * Stephan K. Sotin C. Brown R. H. Langhans M. Soderblom J. Soderblom L. A. LeMouélic S. Clark R. N. Buratti B. J. Baines K. H. Cruikshank D. P. Nicholson P. D. Filacchione G. Wagner R. Barnes J. Nelson R. M.
Erosion and Stratigraphic Relations on Titan **[#1599]**
Bohai Sinus is one of the most prominent disintegration areas between bright and dark materials and exhibit similar spectral signatures as the Huygens landing site. Thus morphological and compositional information can be brought into context.

3:45 p.m. Sotin C. * Mielke R. Choukroun M. Neish C. Barmatz M. Castillo J. Lunine J. Mitchell K.
Ice-Hydrocarbon Interactions Under Titan-like Conditions: Implications for the Carbon Cycle on Titan **[#2088]**
A Titan chamber has been set up in order to investigate the physical and chemical behavior of drops of liquid methane and ethane with substrates of water ice. They imply that Titan's subsurface must be saturated with liquid hydrocarbons.

4:00 p.m. Mitchell K. L. * Stiles B. Zebker H. A. Kirk R. L. Lunine J. I. Hayes A. Wood C. A. Lorenz R. D. Stofan E. R. Lopes R. M. C. Vance S. Cassini RADAR Team
A Global Subsurface Alkanofer System on Titan? **[#1966]**
Hydrocarbon sea, under Titan's icy wastes flows from pole to pole.

4:15 p.m. Furfaro R. * Kargel J. S. Candelaria P.
Modeling the Thermal State of Titan Volatiles and Shallow Melting Involving Hydrocarbons, Organics and Ice **[#1828]**
This paper is about modeling the thermal environment within, beneath and adjacent to hydrocarbon sand dunes overlying a water-ice crust on Titan. Finite element modeling provides a key basis for the analysis.

4:30 p.m. Wood C. A. * Kirk R. Lorenz R. D.
Numbers, Distribution and Morphologies of Impact Craters on Titan **[#2242]**
Cassini Radar reveals seven certain impact craters on Titan and 50 more possible ones. The craters have two distinct rim morphologies, normal lunar-like and jagged. Excess craters are on the leading hemisphere and a deficiency is in the north polar region.

SNC METEORITES
Tuesday, 1:30 p.m. Montgomery Ballroom

Chairs: **Richard Walker and Penny King**

1:30 p.m. Walker R. J. * Puchtel I. S. Brandon A. D. Day J. M. D. Irving A. J.
^{187}Re-^{187}Os and Highly Siderophile Element Systematics of Shergottites: New Puzzles Regarding the Martian Mantle **[#1263]**
Highly siderophile element and Os isotope data for shergottites may reveal both long-term enriched and depleted mantle sources. Osmium isotopic source characteristics, however, are decoupled from lithophile isotope systems for some meteorites.

1:45 p.m. Shih C.-Y. * Nyquist L. E. Reese Y.
Rb-Sr and Sm-Nd Studies of Olivine-Phyric Shergottites RBT 04262 and LAR 06319: Isotopic Evidence for Relationship to Enriched Basaltic Shergottites **[#1360]**
Rb-Sr and Sm-Nd data for olivine-phyric shergottites RBT 04262 and LAR 06319 show that they are similar to NWA 1068 and all are consistent with the derivation from enriched basaltic shergottite sources.

2:00 p.m. Lapen T. J. * Righter M. Brandon A. D. Beard B. L. Shafer J. Irving A. J.
Lu-Hf Isotope Systematics of NWA4468 and NWA2990: Implications for the Sources of Shergottites **[#2376]**
Lu-Hf age and isotope data for olivine basaltic shergottite NWA 4468 with discussion of the source of enriched shergottites.

2:15 p.m. Basu Sarbadhikari A. Day J. M. D. Liu Y. * Taylor L. A.
Olivine-Phyric Shergottite LAR 06319: Its Relation to the Enriched Components in Martian Basalts **[#1171]**
Detailed petrology of Larkman Nunatak (LAR) 06319 are discussed for its olivine megacryst population in olivine-phyric shergottites, as well as the nature of the incompatible-element enriched component in martian basaltic magmas.

2:30 p.m. Rao M. N. * Nyquist L. E. Bogard D. D. Garrison D. H. Sutton S.
Isotopic Evidence for a Martian Regolith Component in Martian Meteorites **[#1361]**
Neutron capture isotopes ^{80}Kr and ^{149}Sm in GRIM glasses reveal the presence of martian regolith component in shergottites.

2:45 p.m. Rumble D. III* Irving A. J.
Dispersion of Oxygen Isotopic Compositions Among 42 Martian Meteorites Determined by Laser Fluorination: Evidence for Assimilation of (Ancient) Altered Crust **[#2293]**
Oxygen isotope data support models of variable contamination of martian magmas by ancient altered crust.

3:00 p.m. McSween H. Y. * Taylor G. J.
Diagnostic Geochemical and Mineralogical Fingerprints for Mars: A Critical Reassessment **[#1269]**
Bulk geochemistry of martian meteorites does not consistently discriminate samples from Mars, but mineral composition discriminants appear to be valid.

3:15 p.m. Taylor G. J. * Boynton W. V.
Global Concentrations of Thorium, Potassium, and Chlorine: Implications for Martian Bulk Composition **[#1411]**
Global measurements by the Mars Odyssey GRS suggest that bulk silicate Mars has chondritic K/Cl, reinforcing the idea that Mars is enriched in moderately-volatile elements compared to Earth, and possibly in water and other volatiles.

3:30 p.m. McCubbin F. M. * Smirnov A. Nekvasil H. Wang J. Hauri E. Lindsley D. H.
Hydrous Magmatism on Mars: A Source for Water on the Ancient Martian Surface and the Current Martian Subsurface? **[#2207]**
Water was analyzed in amphibole and biotite from melt inclusions in the Chassigny meteorite. The measured values are much higher than previous analyses and may allow for a much wetter martian interior than has been previously postulated.

3:45 p.m. King P. L. * Guan Y. Vennemann T. W. Leshin L. A. Sharp Z. D.
The Role of Dehydrogenation on the Hydrogen Contents and δD Values of Kaersutites **[#2322]**
SIMS analyses, conventional analyses and Rayleigh fractionation models of natural and heat-treated amphiboles are used to show that dehydrogenation may explain much of the δD and H variations in natural and martian kaersutites.

4:00 p.m. Filiberto J. * Treiman A. H.
Martian Magmas: Water-poor but Chlorine-rich **[#1449]**
This study shows mineralological, cosmochemical, and experimental results that suggest that parental magmas of martian meteorites were chlorine-rich and water-poor.

4:15 p.m. Cartwright J. A. * Gilmour J. D. Burgess R.
Halogens in Martian Shergottite RBT 04262 **[#1686]**
Analysis of minerals in RBT 04262 reveals considerable variation in halogen abundances and ratios. Martian halogen components may include magmatic (in melt inclusions), shock implanted crustal sources (in maskelynite), and in alteration products.

4:30 p.m. Righter K. * Pando K. M. Danielson L.
Solubility of Sulfur in Shergottitic Silicate Melts up to 0.8 GPa: Implications for S Contents of Shergottites **[#1428]**
Our new experimental results show that existing models under-predict S contents of sulfide saturated sherottitic liquids by a factor of two.

POSTER SESSION I
Tuesday, 6:30 p.m. Town Center Exhibit Area

LUNAR MISSIONS: RESULTS FROM KAGUYA, CHANG'E-1, AND CHANDRAYAAN-1

Arai T. Yamamoto Y. Okada T. Kato M.
Lessons Learned in Onboard Software Processing of XRS-Kaguya **[#2212]**
We introduce the functional control, data reduction and observation control by the software processing of X-ray spectrometers onboard Kaguya, and we discuss the lessons-learned from the lunar X-ray observation.

Terazono J. Asada N. Demura H. Hirata N. Saiki K. Iwasaki A. Oka R. Hayashi T. Suzuki T. Miyamoto H. Haruyama J. Ohtake M. Matsunaga T. Sobue S. Okumura H. Fujita T. Yamamoto A.
Integrated Lunar Web-GIS Environment Using Data Obtained by Lunar Exploration **[#1232]**
The report of current implementation and development status about integrated GIS infrastructure using lunar exploration data including Kaguya, Japanese lunar explorer.

Okumura H. Sobue S. Hoshino H. Yamamoto A. Fujita T.
Data Archive and Visualization for Lunar Orbiter Kaguya (SELENE) **[#1518]**
Kaguya Data Archive (L2DB) and Kaguya Web Map Server(WMS) are being developed in JAXA Sagamihara Campus and will be open to the public from Nov. 2009. Also World Wind for Kaguya and KML data set will be prepared for the purpose of research and EPO.

Shibata Y. Hirata N. Demura H. Asada N. Yokota Y. Morota T. Honda C. Matsunaga T. Ohtake M. Haruyama J.
Semi-Automatic Recognition of Lunar Geologic Units Based on Texture and Spectral Features Using Image Data Observed by Kaguya, LISM TC/MI **[#1615]**
This research shows first step for semi-automatic recognition by means of ongoing Kaguya data. We especially focus on recognition of geologic units by combining texture and spectral features extracted from image data observed by LISM TC/MI.

Hodokuma T. Kuriki K. Asada N. Demura H. Terazono J. Hirata H. Haruyama J. Ohtake M. Matsunaga T. Araki H.
Integration of Multi-Instrumental Data Sets of Kaguya, LISM and LALT **[#1637]**
We report current status on integration of multi-instrumental data sets of Kaguya, LISM and LALT, such as digital terrain model, altitude profiles, multiband images, and spectral data.

Yokota Y. Matsunaga T. Ohtake M. Haruyama J. Ogawa Y. Nakamura R. Honda C. Morota T. Saiki K. Kawabe S. Nagasawa K. Kitazato K. LISM Working Group
Lunar Phase Curve at Vis/NIR Wavelength Observed by SELENE Spectral Profiler **[#2525]**
We report preliminary results of Disk-resolved lunar phase curve at highland in Vis/NIR wavelength range by SELENE Spectral Profiler data.

Ogawa Y. Matsunaga T. Nakamura R. Takeda H. Ohtake M. Morota T. Hiroi T. Arai T. Saiki K. Sugihara T. Haruyama J. Yokota Y. Honda C. Nimura T. Hirata N. Demura H. Asada T. Terazono J.
Mineral Compositions of the Bright Rayed Craters and Lunar Far-Side Crust Revealed by the Continuous VIS-NIR Spectrum by SP (Spectral Profiler) on SELENE/Kaguya **[#1650]**
SP is a visible and near infrared spectrometer onboard SELENE/Kaguya satellite. Based on the SP spectral data we are conducting a preliminary survey to collect compositional information of the lunar highland crust on the far-side.

Migita E. Araki H. Noda H. Tazawa S. Ishihara Y. Iwata T.
Laser Altimeter Lunar Crater Measurement by SELENE (Kaguya) **[#1981]**
Laser Altimeter (LALT) on board SELENE (Kaguya) can determine anew crater diameter. LALT data is accurate as compared with Clementine LIDAR data. Especially, central peaks seen in LALT data are clearer than those seen in LIDAR data.

Honda C. Morota T. Yokota Y. Ogawa Y. Demura H. Hirata N. Matsunaga T. Ohtake M. Haruyama J.
Morphologic Characteristics of the Vallis Schröteri **[#1524]**
Using our DTM derived from TC stereo pair images of Kaguya, we measured the morphologic characteristics of the Vallis Schröteri as a function of distance from vent-like feature.

Morota T. Haruyama J. Honda C. Ohtake M. Yokota Y. Kimura J. Matsunaga T. Ogawa Y. Hirata N. Demura H. Iwasaki A. Miyamoto H. Nakamura R. Ishihara Y. Sasaki S.
Ages and Thicknesses of Mare Basalts in Mare Moscoviense: Results from SELENE (Kaguya) Terrain Camera Data **[#1280]**
We investigate ages and thicknesses of mare basalts in Mare Moscoviense, which is in the northern hemisphere of the lunar farside, using high-resolution images and digital terrain models (DTMs) obtained by SELENE Terrain Camera (TC).

Kobayashi M. Hasebe N. Shibamura E. Miyachi T. Takashima T. Okudaira O. Yamashita N. Kobayashi S. Hareyama M. Karouji Y. Ebihara M. Arai T. Sugihara T. Takeda H. Iwabuchi K. Hayatsu K. Nemoto S. Hihara T. Nakazawa S. Otake H. d'Uston C. Maurice S. Gasnault O. Diez B. Reedy R. C.
Status and Performance of the Gamma-Ray Spectrometer on the Kaguya (SELENE) **[#1735]**
The Kaguya main orbiter carries a GRS, which is providing elemental information on lunar surface. In this presentation, the status and performance of the Kaguya GRS observations in the primary mission and early extended mission are given.

Hareyama M. Hasebe N. Shibamura E. Kobayhashi M.-N. Yamashita N. Karouji Y. Kobayashi S. Okudaira O. Takashima T. d'Uston C. Maurice S. Gasnault O. Forni O. Diez B. Reedy R. C. Kim K. J. Arai T. Ebihara M. Sugihara T. Takeda H. Hayatsu K. Iwabuchi K. Nemoto S. Takeda Y. Tsukada K. Nagaoka H. Hihara T. Maejima H. Nakazawa S.
High Energy Gamma Rays from the Lunar Surface Observed by GRS Onboard SELENE **[#1734]**
The distribution map of lunar gamma-rays in the energy range of 8–13 MeV observed by SELENE-GRS is presented and discussed about area dependencies.

Reedy R. C. Hasebe N. Yamashita N. Karouji Y. Hareyama M. Kobayashi S. Okudaira O. Shibamura E. Kobayashi M. N. Kim K. J. d'Uston C. Diez B. Gasnault O. Forni O. Kaguya GRS Team
Gamma Rays in Spectra Measured by the Kaguya Gamma-Ray Spectrometer **[#1788]**
Of 200 peaks observed in spectra measured by the Kaguya Gamma Ray Spectrometer, the sources of 80% have been identified. Most are from the Ge detector, structural Al, and other local matter. Some gamma rays are from several elements in the Moon.

Okada T. Shiraishi H. Shirai K. Yamamoto Y. Arai T. Ogawa K. Kato M. Grande M. SELENE XRS Team
X-Ray Fluorescence Spectrometer (XRS) on Kaguya: Current Status and Results **[#1897]**
X-ray fluorescence spectrometer (XRS) for major elemental composition mapping of lunar surface is carried on Kaguya, but some difficulties of its observations are found due to degradation of CCD detectors and due to historically quiescent solar activity.

Clark R. Pieters C. M. Green R. O. M3 Science Team
Thermal Removal from Moon Mineralogy Mapper (M^3) Data **[#2136]**
Near-infrared spectra of the Moon contain a mixture of reflectedsunlight and thermal emission caused by heating of the surface fromthe sun at wavelengths beyond about 2 microns. Thermal emission is a factor in analyzing data from M^3.

Taylor L. A. Liu Y. Pieters C. Tompkins S. Isaacson P. Cheek L. Thaisen K.
Lunar Magma Ocean Crust: Implications of FeO Contents in Plagioclase **[#1304]**
The FeO and MgO compositions of the highland plagioclase, particularly that in the FANs, do not represent those from the original LMO. The re-equilibrated values are due to slow cooling of the proto-crust, similar to anorthosites on Earth (Phinney, 1991).

Pieters C. Kumar S. Head J. W. Goswami J. N. Kumar K. Green R. Boardman J. Staid M. Petro N. Isaacson P.
Lunar Orientale Basin: Nature of Impact Melt and Volcanic Flooding from Chandrayaan-1 (M3, TMC, HySI) **[#2157]**
A subset of data observed by M3, TMC, and HySI is used to evaluate the relation of the Maunder Formation and neighboring basalts. The MF is shown to be highly feldspathic and the basalts exhibit features suggestive of magma movement during cooling.

Kiran Kumar A. S. Roy Chowdhury A. Murali K. R. Sarkar S. S. Joshi S. R. Mehta S. Dave A. B. Shah K. J. Banerjee A. Mathew K. Sharma B. N.
The Hyper Spectral Imager Instrument on Chandrayaan-1 **[#1589]**
The Hyperspectral imager on Chandrayaan-1 provides images of lunar surface with a spatial resolution of 80 meters in 64 contiguous spectral bands in visible and near infrared regions for mineralogical mapping.

Sreekumar P. Umapathy C. N. Ramakrishna Sharma M. Sreekantha C. V. Tyagi A. Kumar A. B. Sudhakar M. Abraham L. Kulkani R. Premlatha R. L. Srivastava A. K. Neeraj Kumar S. Bug M. Acharya Y. B. Vadawale S. Shanmugam M. Banerjee D. Purohit S. Patel H. Goswami J. N.
High-Energy X-Ray Spectrometer (HEX) on Chandrayaan-1: Studies of Volatile Transport on Moon and Mapping of U, Th-rich Terrain **[#2572]**
In situ measurements, remote sensing technique and laboratory analysis of returned samples provide information on the elemental composition of a planetary body.

LRO AND LCROSS

Mazarico E. Neumann G. A. Rowlands D. D. Lemoine F. G. Smith D. E. Zuber M. T.
Multi-Beam Altimetric Crossovers for the Precision Orbit Determination of the Lunar Reconnaissance Orbiter **[#2244]**
We study a new type of altimetric crossovers enabled by LOLA multi-beam configuration. Those use the cross-track information and can help the LRO goal of creating a new lunar reference frame by providing stronger constraints on the orbit.

Greenhagen B. T. Paige D. A.
Overview of the 2009 LRO Diviner Lunar Radiometer Compositional Investigation **[#2255]**
The Compositional Investigation will analyze data from Diviner's nine spectral channels (0.3–300 μm). Diviner's channels are sensitive to different aspects of composition and have the potential to enhance our understanding of the lunar surface.

Thomas I. R. Bowles N. E. Greenhagen B. T.
Reflectance and Emission Measurements of Lunar Analogues for Interpretation of Returning Data from the Diviner Lunar Radiometer on NASA's Lunar Reconnaissance Orbiter (LRO) **[#2110]**
In support of the Diviner Compositional Investigation, spectra of many lunar analogues were measured from UV/VIS to FIR. Reflectance and emission spectra were found for samples with differing mineralogy and grain size, in various atmospheric pressures.

Sanin A. B. Boynton W. Evans L. Harshman K. Kozyrev A. Litvak M. Malakhov A. McClanahan T. Milikh G. Mitrofanov I. Mokrousov M. Sagdeev R. Shevchenko V. Schvetsov V. Starr R. Trombka J. Vostrukhin A.
Lunar Exploration Neutron Detector (LEND) for NASA Lunar Reconnaissance Orbiter: Searching for the Water Ice **[#1249]**
The LEND instrument is orbital neutron telescope for orbital mapping of the Moon's neutron albedo. The LEND instrument on board the NASA LRO spacecraft will measure neutron emission from the lunar surface and the local neutron background in orbit.

Lawrence S. J. Robinson M. S. Jolliff B. L. Bowman-Cisneros E. Tranh T. Stopar J. D. Hawke B. R. Thompson S. D. Koeber S. LROC Targeting Action Team
Preparing to Scout the Next Frontier: Hardware and Operational Constraints Encountered During Targeting of the Lunar Reconnaissance Orbiter Camera Narrow Angle Cameras **[#2316]**
The two Lunar Reconnaissance Orbiter Camera Narrow Angle Cameras (LROC-NAC) will take 0.5m/pixel images of the lunar surface. This abstract details the important hardware and operational constraints on LROC-NAC observations.

Jolliff B. L. Lawrence S. J. Stopar J. D. Robinson M. R. Gaddis L. R. Hawke B. R.
Targeting the Lunar Reconnaissance Orbiter Narrow Angle Cameras: Target Sources and Selection Strategy **[#2343]**
Strategies and resources used by the LRO Camera Team in developing its exploration/science target list are presented.

Tschimmel M. Robinson M. S. Humm D. C. Denevi B. W. Lawrence S. J. Brylow S. Ravine M. Ghaemi T.
Lunar Reconnaissance Orbiter Camera (LROC): Ready for Rocks **[#2475]**
The Lunar Reconnaissance Orbiter Camera (LROC) consists of three cameras: the Wide-Angle Camera and two identical Narrow Angle Cameras. This abstract describes the properties of the instruments and the results of the laboratory calibration efforts.

Heldmann J. L. Colaprete A. Wooden D. Asphaug E. Schultz P. Plesko C. S. Ong L. Korycansky D. Galal K. Briggs G.
Lunar Crater Observation and Sensing Satellite (LCROSS) Mission: Opportunities for Observations of the Impact Plumes from Ground-based and Space-based Telescopes **[#1898]**
The primary objective of the LCROSS mission is to investigate the presence or absence of water on the Moon. Ground-based and orbital observatories can observe the dust and water vapor plume caused by the two impacts into the lunar surface.

Ennico K. Colaprete A. Heldmann J. Kojima G. Lynch D. Shirley M. Wooden D.
Lunar Crater Observation and Sensing Satellite (LCROSS) Science Payload Ground Development, Test, and Calibration **[#1878]**
The Lunar CRater Observation and Sensing Satellite (LCROSS) is an impactor mission designed to target and impact a permanently shadowed region at a lunar polar latitude. This paper describes the payload, testing, and calibration.

Bart G. D. Colaprete A.
Shadow Depths and Other Characteristics of Potential LCROSS Impact Sites **[#2151]**
LCROSS impact site selection is critical to mission success. We discuss the critical constraints site selection, the ongoing work to characterize potential sites, and the most recent work of determining shadow depths at potential impact sites.

Summy D. Goldstein D. B. Colaprete A. Varghese P. L. Trafton L. M.
LCROSS Impact: Dust and Gas Dynamics **[#2267]**
We present results from simulations of the plume resulting from the impact of the LCROSS vehicle(s) into a shadowed lunar polar cold trap. Results may be of particular interest to those planning observations of the H_2O, OH and dust plumes.

Hermalyn B. Schultz P. H. Heineck J. T.
LCROSS Early-Time Ejecta Distribution: Predictions from Experiments **[#2416]**
Experimental results of the early-time ejecta distribution from impacts of projectiles with a range of relative densities are presented, with implications and predictions for the upcoming LCROSS mission.

GEOPHYSICAL ANALYSIS OF THE LUNAR SURFACE AND INTERIOR

Reiff P. H. Freeman J. W. Vondrak R.
Apollo ALSEP Results — 40 Years Later **[#2363]**
This paper will discuss the main results from the Apollo/ALSEP SIDE and CPLEE experiments.

Lawrence K. P. Johnson C. L.
Magnetic Characterization of Lunar Samples: Back to Basics **[#1433]**
We present preliminary results of low and high temperature hysteresis, low and high temperature magnetic susceptibility, and Curie temperature analyses of multiple lunar samples.

Chi P. J. Russell C. T. Walker R. J. Williams D. Hills H. K. Mehlman R.
Restoration of Apollo Magnetic Field Data: A Progress Report **[#1894]**
Under the support by NASA's LASER Program we are restoring the Apollo data from Lunar Surface Magnetometer and Subsatellite Biaxial Magnetometer. These restored data will be accessible through a dedicated online server, PDS, and NSSDC.

Halekas J. S. Lillis R. J. Purucker M. E. Louzada K. L. Stewart S. T. Manga M.
Interpreting Lunar Impact Demagnetization Signatures Using Lunar Prospector Magnetometer/Electron Reflectometer Data **[#1354]**
We investigate impact demagnetization signatures observed by Lunar Prospector. We construct crater demagnetization models and compare to observations in order to constrain the strength and coherence scale of lunar crustal magnetization.

Williams J. G. Boggs D. H. Ratcliff J. T.
A Larger Lunar Core? **[#1452]**
New data improves lunar science results. A fluid core and tidal dissipation are inferred from dissipation effects on orientation. Detection of core-mantle boundary flattening and fluid core moment are additional evidence for a fluid core.

de Vries J. van den Berg A. P. van Westrenen W.
The Formation and Evolution of a Lunar Core from Ilmenite-rich Magma Ocean Cumulates **[#1244]**
The possibility of forming an ilmenite-rich core in the moon is studied, using numerical models. It is shown that core density and sharpness of the core-mantle boundary depend on the heat production in and the density of the ilmenite-rich material.

Sakai R. Kushiro I. Nagahara H. Ozawa K. Tachibana S.
Experimental Constraints on Composition of Lunar Magma Ocean from Physical Properties of Magma **[#1839]**
We performed high-pressure experiments to determine density and viscosity of magma with chemical compositions plausible to the anorthosite crust formation in order to put physical and chemical constraints on differentiation of the lunar magma ocean.

Tronche E. J. van Westrenen W.
Experimental Petrology of a Lunar Bulk Composition Constrained by Geophysical Data **[#1782]**
The crystallization sequence and phase chemistry of a cooling lunar magma ocean is experimentally investigated for a new lunar bulk composition relatively Al-poor and Fe-rich derived from inversion of seismic and gravity data.

Bauch K. E. Hiesinger H. Helbert J.
Estimation of Lunar Surface Temperatures: A Numerical Model **[#1789]**
We present global temperature estimates for sunrise, noontime and sunset. This work provides new and updated research on the temperature variations by taking into account the surface and subsurface bulk thermophysical properties.

Weber R. C. Bills B. G. Johnson C. L.
A Simple Physical Model for Deep Moonquakes **[#1870]**
Tidal stress is widely believed to influence the occurrence times of deep moonquakes. We explore several simple models of stress buildup and release that can be used to create moonquake-like time sequences of events.

Kawamura T. Tanaka S. Saito Y. Kobayashi Y. Horai K. Hagermann A.
Re-Determination of Deep Moonquake Sources Using the Apollo 17 Lunar Surface Gravimeter **[#1653]**
We performed the first seismic analysis of deep moonquakes using the Apollo 17 Lunar Surface Gravimeter. We re-determined the seismic source of the deep moonquakes and evaluated the contribution of the LSG.

Mazarico E. Han S.-C. Lemoine F. G. Smith D. E.
A New Solution of the Lunar Gravity Field Using Localized Spectral Constraint **[#2248]**
We use localized spherical harmonics to create a lunar gravity field solution with the Kaula constraint applied only to the far side. The differences with a globally constrained solution are correlated with the topography, suggesting an improvement.

de Meijer R. J. van Westrenen W.
An Alternative Hypothesis for the Formation of the Moon **[#1847]**
We propose an alternative explanation for the compositional correspondence between Moon and silicate Earth: the Moon formed from the ejection of terrestrial mantle material, triggered by a run-away natural georeactor at Earth's core-mantle boundary.

Bussey D. B. J. Sorensen S.-A. Spudis P. D.
Illumination and Temperature Modelling of the Lunar Polar Regions **[#2027]**
We have produced a model for determining the illumination and thermal conditions inside the permanently shadowed regions near the lunar poles.

Remote Observation and Geologic Mapping of the Lunar Surface

Campbell B. A. Campbell D. B. Carter L. M. Chandler J. Ghent R. R. Nolan M. Anderson R. F.
Earth-Based Radar Mapping of the Lunar Nearside at 12.6-cm Wavelength **[#1275]**
We are collecting a dual-polarization radar backscatter map of the lunar nearside at 12.6-cm (S-band) wavelength and 40-m single-look horizontal spatial resolution.

Wells K. S. Campbell D. B. Campbell B. A. Carter L. M.
Radar Circular Polarization Ratio Determination of Tycho Secondary Craters **[#1778]**
We identify 128 small lunar craters in the Newton-A Crater basin within the furthest extent of a Tycho Crater ray and classify secondary craters within the population by their elongated CPR ejecta blankets parallel to the Tycho ray.

Thompson T. W. Campbell B. A. Ghent R. R. Hawke B. R.
Differences in the Mega-Regolith Depth Across the Moon's Southern Highlands **[#1240]**
Differences in the frequencies of small (1–16 km diameter) radar-bright craters is not uniform across the southeastern nearside lunar highlands indicating a deeper megaregolith depth of 1 km associated with the South Pole Aitken Basin ejecta.

Chevrel S. D. Pinet P. C. Daydou Y. Le Mouélic S. Langevin Y. Costard F. Erard S.
The Aristarchus Plateau on the Moon: Nature and Stratigraphy of the Substratum **[#1234]**
From Clementine UVVIS and NIR spectral data, a statistical analysis and a mixture modeling, we present the mineralogy and the stratigraphy of the materials forming the substratum and volcanic deposits of the Aristarchus Plateau on the Moon.

Souchon A. L. Chevrel S. D. Pinet P. C. Daydou Y. H. Shevchenko V. V. Grieger B. Josset J. L. Beauvivre S. Shkuratov Y. Kaydash V. G. AMIE Team
Characterization of the Optical Properties of J. Herschel Pyroclastic Deposit Using SMART-1/AMIE Photometric Data **[#1237]**
SMART-1 data have been processed to estimate Hapke's photometric parameters on the dark deposit located on the floor of Herschel Crater. The comparison with natural and synthetic terrestrial materials strengthens the case for a pyroclastic origin.

Hawke B. R. Giguere T. A. Lawrence S. J. Campbell B. A. Blewett D. T. Carter L. M. Gaddis L. R. Hagerty J. J. Lucey P. G. Peterson C. A. Smith G. A.
Remote Sensing Studies of Pyroclastic Deposits in the Mare Humorum Region **[#1146]**
The two large regional pyroclastic deposits are dominated by Fe^{2+}-bearing pyroclastic glasses. Portions of the deposits are relatively thick and exhibit smooth, rock-poor surfaces that would be well suited for resource exploitation.

Weider S. Z. Crawford I. A. Joy K. H.
Investigating Oceanus Procellarum Basalt Flows Using Integrated Clementine UV-VIS and NIR Data **[#1573]**
We use UV-VIS and NIR data from Clementine to investigate the basaltic stratigraphy in a region of Oceanus Procellarum. This enables us to study the FeO and TiO_2 compositions, major mafic mineralogy, and extent of space weathering of these deposits.

Srivastava N.
Spectral Reflectance Studies for Maturation Trends in a Mare and Highland Swirl **[#1577]**
Regions shielded by maximum magnetic field intensity in the proto type swirl Reiner Gamma and the one near Airy Crater, have been investigated for maturity trends. Both the cases show differences (though of reversed nature) from the trend seen in nearby unshielded areas.

FuPing G. YanMei Y.
Geological Features Study of the Lunar Surface Using the Lunar Remote Sensing Data **[#1457]**
Taking typical craters of lunar surface as the test areas, using the Clementine UVVIS, NIR and lidar data, we study the relationship between the geological features and physiognomy, analyze the rule of lithology or mineral distribution of the lunar.

Ambrose W. A.
Distribution and Chronostratigraphy of Asymmetric Secondary Craters in the Nectaris Basin **[#1015]**
The Nectaris Basin contains well-preserved examples of radially distributed, asymmetric secondary craters, scours, and crater chains. They are unique morphological features that constrain estimated ages of overlapped landforms in the basin.

Dominov E. Mest S. C.
Geology of Antoniadi Crater, South Pole Aitken Basin, Moon **[#1460]**
Antoniadi crater is unique for three reasons: 1) unique impact crater shape; 2) deep impact depth; and 3) smooth crater floor material. Research was done by utilizing ArcGIS program in mapping the ejecta blanket of Antoniadi and crater counting.

LUNAR SPECTROSCOPY

Cheek L. C. Pieters C. M. Dyar M. D. Milam K. A.
Revisiting Plagioclase Optical Properties for Lunar Exploration **[#1928]**
Preliminary NIR analyses of a suite of terrestrial plagioclase identify the 1.3 μm CF absorption and highlight the importance of constraining compositional controls on spectral features and effects of minor absorbing phases in transparent mediums.

Aarthy R. S. Sanjeevi S. Vijayan S. Krishnamurthy J.
Spectral Studies of Anorthosite and Meteorite **[#2216]**
The aim of this study is for the better understanding of the lunar highland surface. Thus for the study anorthosite and meteorite (not yet being approve) spectral studies were carried out.

Foote E. J. Paige D. A. Johnson J. R. Grundy W. M. Shepard M. T.
The Bidirectional Reflectance of Apollo 11 Soil Sample 10084 **[#2500]**
We measured the bidirectional reflectance of Apollo 11 soil sample 10084 using the Bloomsburg University Goniometer (BUG) and fit the measured reflectances using Hapke's photometric model that includes the effects of large-scale roughness.

Li L. Lucey P. G.
Quantifying TiO_2 Abundance of Mare Soils: A Stratified Partial Least Squares Approach to Qualitative Interpretation **[#2226]**
A stratified partial least squares approach is used for the estimation of mare soil samples and qualitative interpretation of the result is achieved using stepwise multivariate regression analysis.

Li L. Lucey P. G.
Use of Multiple Endmember Spectral Mixture Analysis and Radiative Transfer Model to Derive Lunar Mineral Abundance Maps **[#1934]**
A new approach combining multiple endmemeber spectral mixture analysis (MESMA) and radiative transfer model (RTM) is proposed to generate lunar global mineral abundance maps from Clementine 1 km UVVIS data.

Hiroi T. Isaacson P. J. Klima R. L. Pieters C. M. Sarbadhikari A. B. Liu Y. Taylor L. A.
Reproducing Visible and Near-Infrared Reflectance Spectra of Lunar Rocks Directly from Their End-Member Spectra: Importance of Ilmenite in Estimating the Lunar Surface Composition **[#1723]**
Spectral mixing calculations have been performed on the bulk samples and major mineral separates of four Apollo basalts. The results demonstrate the importance of considering coexisting ilmenite in remotely estimating the lunar silicate composition.

Dhingra D.
Lithological Mapping of Lunar Terranes using Hybrid Classification Approach **[#1456]**
A new classification approach integrating mineralogy, elemental composition and maturity for lithological mapping on the lunar surface is discussed.

Donaldson Hanna K. L. Wyatt M. B. Helbert J. Maturilli A. Pieters C. M.
Constraining Lunar Surface Mineralogy with Combined Thermal- and Near-Infrared Spectral Data **[#2286]**
We examine the extent to which combined thermal- and near-infared anayses can be used to constrain the mineralogy of immature lunar surface lithologies using thermal infrared laboratory spectral measurements of minerals, a mineral mixture, and lunar highlands and mare soils.

Stockstill-Cahill K. R. Cahill J. T. S. Lucey P. G. Hawke B. R.
Radiative Transfer Modeling of Lunar Hyperspectral Data **[#1629]**
We have previously developed multispectral methods for deriving minerals from spectra. We are now extending these methods to continuous (hyperspectral) telescopic data for various locations on the nearside of the Moon.

VENUS GEOLOGY, GEOPHYSICS, MAPPING, AND SAMPLING

Peters G. H. Mungas G. S. Murray S. D. Polk J. E. Lindeman R. Beegle L.
Venus Analog Testbed for RASP and Sample Collection Testing **[#2518]**
Describes a testbed and method for simulating the fluid conditions of Venus in order to test RASP systems to provide samples during *in situ* missions to Venus.

Sharma S. K. Misra A. K. Clegg S. M. Barefield J. E. Wiens R. C. Quick C. R. Dyar M. D. McCanta M. C. Elkins-Tanton L.
Venus Geochemical Analysis by Remote Raman–Laser Induced Breakdown Spectroscopy (Raman-LIBS) **[#2548]**
The goal of this presentation is to demonstrate that remote Raman – LIBS spectra can be acquired under Venus conditions to yield quantitative geochemistry on Venus-analog rocks.

Treiman A. H.
Canali-forming Magmas: Generation of Carbonate-Sulfate Melts on Venus **[#1347]**
Venus' canali, long meandering channels, may have carried carbonate-sulfate (carbonatite) melts. Such liquids may arise by melting weathered basalt, which requires geotherms much hotter than Venus' average, or another heat source (intrusion, impact).

Orth C. P. Solomatov V. S.
The Effects of Dynamic Topography and Thermal Isostasy on the Topography and Geoid of Venus **[#1811]**
The magnitude of the dynamic topography on Venus is small. Long wavelength global geoid and topography anomalies can be explained by thermal thinning of a thick lithosphere with only a limited contribution from crustal thickness variations.

Guseva E. N.
Spacing of Structures in the Rift- and Groove Belt-related Coronae on Venus **[#1152]**
The spacing values of structures in the rims of the rift- and groove belt-related coronae on Venus appear to be almost identical.

Martin P. Stofan E. R. Smrekar S. E.
Volcano-Tectonics on Venus: A Comparison of Parga and Hecate Chasmata and Perunitsa and Khosedem Fossae **[#1041]**
In this study, we are undertaking comparative analysis of chasmata and fracture belt systems on Venus over a range of scales, to help constrain models of the formation and evolution of rift systems and associated volcanic processes on Venus.

Hansen V. L. López I.
Implications of Venus Evolution Based on Ribbon Tessera Terrain Relations Within Five Large Regional Areas **[#2306]**
We examine ribbon tessera terrain outcrop and structural relations within five large regional areas: A) lowland environment, B) lowland-volcanic rise transition, C) volcanic rise environment, D) mesoland environment, and E) a single planitia basin.

Gleason A. L. Glaze L. S. Herrick R. R. Garvin J. B.
Stereo-derived Topography from the Venus Magellan Dataset: An Assessment of the Quantitative Scientific Value of Sub-km DEM Products **[#1253]**
Quantitative information is difficult to extract from sub-km DEMs (derived from stereo SAR images) on surface properties and processes for a range of different landforms on Venus, including tesserae, coronae, lava flows, and lava channels.

Ivanov M. A.
Embayed Craters on Venus: How do They Correspond to the Catastrophic and Equilibrium Resurfacing Models? **[#1150]**
The style of resurfacing on Venus changed significantly during the observable portion of the geologic history from the catastrophic resurfacing to the equilibrium resurfacing.

Ivanov M. A. Head J. W.
Geological Mapping of the Fortuna Tessera Quadrangle (V-2), Venus: Preliminary Results **[#1151]**
Preliminary results of the geological mapping in the V-2 quadrangle on Venus are presented.

Hurwitz D. M. Head J. W.
Geologic Map of the Snegurochka Planitia Quadrangle (V1): Implications for Tectonic and Volcanic History of the North Polar Region of Venus **[#1174]**
We present our progress in mapping the spatial and stratigraphic relationships of material units of Snegurochka Planitia (V1) and our initial interpretations of the tectonic and volcanic history of the region surrounding the north pole of Venus.

PLANETARY DIFFERENTIATION

Kegler Ph. Holzheid A. McCannon C. Rubie D. C. Palme H.
Pressure and Temperature Dependent Partitioning of Copper: Implications for Terrestrial Core Formation **[#1685]**
To better understand the abundance of Cu in the Earth's mantle we studied the metal - silicate partitioning of Cu as function of P, T, silicate composition, and alloy composition (Cu, Fe, Ni, and C contents). The first results are presented here.

Yu G. Jacbosen S. B.
Core Formation and the Fe/FeO Ratio of the Earth, Mars and Vesta: Constraints from the ^{182}Hf-^{182}W System **[#2123]**
A dynamic core-formation model with a deep magma ocean for the Hf-W system, which can match the partitioning of Ni, Co and W in mantles of Earth, Mars and Vesta and yield mean age of formation of these planets of 12, 8 and 3 Myr respectively.

Prissel T. Colson R. O.
Additional Experiments Suggesting that Neutral Nickel is Soluble in Silicate Melts at Low Concentration **[#1172]**
Metal nuggets occur in experiments run at low fO_2 in silicate systems. We find a correlation between quench rate and nugget size, suggesting nuggets form during quench and neutral nickel may be an important species during differentiation at low fO_2.

Sharp Z. D. Draper D. S. Agee C. B.
Core/Mantle Partitioning of Chlorine and a New Estimate for the Hydrogen Abundance of Earth **[#1209]**
The core/mantle D value for chlorine was determined experimentally to be less than 0.01 at high P-T. Using mantle and crustal Cl abundances, and the H/Cl ratio of chondrites, the H content of Earth is estimated to be 2.8×10^{24} g or less.

Khan A. Connolly J. A. D.
A Geophysical Perspective on the Major Element Composition of Mars' Mantle **[#1013]**
We have inverted a set of areophysical data for Mars' mantle compostion andcore state, size and composition. We find an overall SNC-like mantle composition, with no transition to a lower mantle taking place as on Earth. Core radius and density are ~1680 km and ~6.7 g/ccm.

Elkins-Tanton L. T.
Early Planetary Evolution: The Crust and Mantle Before Plate Tectonics **[#1298]**
Magma ocean models that include small water contents predict a potentially important redistribution of mantle water, a "water catastrophe," after solidification. This event introduces fluid to the upper mantle and may speed onset of plate tectonics.

Gelman S. E. Elkins-Tanton L. T. Seager S.
Mantle Thermal Evolution in Tidally-locked Super-Earths **[#1338]**
We present a preliminary model of the mantle thermal evolution for tidally locked Super Earths and investigate the presence of magma ponds and liquid water/the habitable zone.

Duncan M. S. Agee C. B.
Partial Molar Volume of CO_2 in Peridotite Partial Melt at High Pressure **[#1406]**
Using the sink/float method with carbonated and non-carbonated peridotite partial melts, the partial molar volume of CO_2 is calculated at high pressure.

Riches A. J. V. Rogers N. W. Charlier B. L. A. Bodinier J.-L.
The Earth as a Planet: The Re-Os Isotope Evolution of Bulk Silicate Earth **[#1726]**
Re-Os isotopes provide pertinent age information in the Lherz peridotite (the type locality of terrestrial mantle lherzolite), and are used to constrain the composition and evolution of bulk silicate Earth.

Luo Y. Yin Q. Z. Ayers J. C. Ryerson F. Hutcheon I.
Experimental Measurements of Zircon/Melt Trace Element Partition Coefficients: Key Issues and Possible Solutions with Nano-SIMS **[#2516]**
We highlight the current problems with obtaining zircon/melt trace-element partition coefficient data and point out that Nano-SIMS *in situ* analysis at the zircon/melt interface (< submicron scale) may solve the long standing problem.

Ricolleau A. Fei Y. Castro V.
Oxygen Partitioning Between Metallic Alloy and Silicate Melts **[#2340]**
We investigated the solubility of oxygen in metallic alloy, such as Fe, Fe-Ni, Fe-Ni-S, Fe-Ni-S-C, in the presence of silicates melts, at 2 and 8 GPa, and at 2000° and 2600°C.

Larson A. L. Colson R. O.
Reintepretation of Observed Effects of CO on Crystallization in Silicate Melts at 1-Atmosphere Pressure **[#1343]**
We observe an effect of CO at 1-atm pressure on crystal growth in silicate melts, concluding that at least some of the observed effect is related to an effect of CO on melt quenchability.

Gupta G. Sahijpal S.
Planetary Differentiation of Vesta with ^{26}Al and ^{60}Fe as Heat Sources **[#1530]**
Numerical simulations have been performed for the planetary differentiation of Vesta and other differentiated meteorite parent bodies with ^{26}Al and ^{60}Fe as heat sources.

BUNBURRA AND BUZZARD COULEE: RECENT METEORITE FALLS

Hutson M. L. Ruzicka A. M. Milley E. P. Hildebrand A. R.
A First Look at the Petrography of the Buzzard Coulee (H4) Chondrite, a Recently Observed Fall from Saskatchewan **[#1893]**
Buzzard Coulee is a recent (November 20, 2008) fall from Saskatchewan, Canada. Here we discuss the classification of this meteorite and point out some unusual features, including abundant cryptocrystalline chondrules and igneously-textured light-colored inclusions.

Walton E. L. Herd C. D. K. Duke M. J. M.
Mineralogy, Petrology and Cosmogenic Radionuclide Chemistry of the Buzzard Coulee H4 Chondrite **[#2072]**
The Buzzard Coulee H4 chondrite was collected as fragments from a fireball witnessed at 5:23.46 MST on November 20, 2008 by thousands of residents across the Canadian prairies.

Spurny P. Bland P. A. Borovička J. Shrbený L. McClafferty T. Singelton A. Bevan A. W. R. Vaughan D. Towner M. C. Deacon G.
The Bunburra Rockhole Meteorite Fall in SW Australia: Determination of the Fireball Trajectory, Luminosity and Impact Position from Photographic Records **[#1498]**
We present basic data of the Bunburra Rockhole, the new photographically recorded meteorite fall by the Desert Fireball Network in SW Australia. It is the first achondrite with known orbit and the first such meteorite fall in the southern hemisphere.

METEORITES: TERRESTRIAL HISTORY

Jourdan F. Maier W. Andreoli M. A. G. McDonald I.
$^{40}Ar/^{39}Ar$ Thermochronology of a Fossil LL Chondrite from Morokweng Crater, South Africa **[#1221]**
$^{40}Ar/^{39}Ar$ thermochronology applied to plagioclase from the Morokweng LL chondrite possibly suggests large asteroid collisional (breakup?) events at ~2Ga and ~0.7 Ga and records the age of the impact on Earth at ~145 Ma.

Welten K. C. Nishiizumi K. Caffee M. W. Leclerc M. D. Jull A. J. T.
Cosmogenic Radionuclides in Chondrite Shower from Otway Massif, Antarctica **[#1488]**
Cosmogenic radionuclides in ordinary chondrites from the first strewnfield identified in Antarctica indicate that the strewnfield was preserved since its fall ~15 kyr ago, while cautioning that not all meteorites in the strewnfield area represent the same fall.

Heck P. R. Ushikubo T. Schmitz B. Kita N. T. Spicuzza M. J. Valley J. W.
High-Precision Oxygen Three-Isotope SIMS Analyses of Ordovician Extraterrestrial Chromite Grains from Sweden and China: Debris of the L Chondrite Parent Asteroid Breakup **[#1119]**
High-precision 3-O isotope SIMS data provide strong evidence chromite grains from 470 Ma fossil meteorites from Sweden and fossil micrometeorites from Sweden and China are genetically related to each other and to the L chondrite parent body breakup.

Losiak A. Velbel M. A.
Geographic Influences on Evaporite Formation During Weathering of Antarctic Meteorites **[#1394]**
The aim of this paper is to research influence of geographic location of meteorite-bearing ice fields on evaporite occurrence.

Makide K. Nagashima K. Krot A. N. Huss G. R.
Oxygen Isotopic Compositions of Solar, Micrometer-sized Corundum, Hibonite and Spinel Grains in Acid-resistant Residues from Ordinary and Carbonaceous Chondrites **[#2079]**
We report O-isotope compositions of refractory oxide grains in acid-resistant residues from primitive chondrites using the UH ims-1280 ion microprobe. They are consistent with $\Delta^{17}O$ values of the solar nebular and the Sun, ~−25‰, inferred from CAIs.

Craig J. Sears D. W. G.
Induced Thermoluminescence Properties of Forsterite and Implications for the History of Primitive Solar System Materials **[#1169]**
A study of micrometeorites and Semarkona matrix indicated forsterite is responsible for the TL. We examined forsterite from several terrestrial environments. Results indicated the forsterite in these materials may have an igneous origin, possibly from chondrule formation.

Ma C. Beckett J. R. Rossman G. R. Connolly H. C. Jr. Guan Y. Eiler J. M. Hofmann A. E.
In-Situ Discovery of a Cluster of Refractory Grains in an Allende Ferromagnesian Chondrule **[#2138]**
A unique corundum-rich cluster of irregular micrometer-sized refractory grains has been discovered in a type IA chondrule from Allende. The cluster also contains refractory phases of rutile, khamrabaevite, and a new mineral Ti_2O_3.

Boesenberg J. S. Ebel D. S.
Experiments to Confirm Condensed Phase Assemblages Predicted by Equilibrium Thermodynamic Calculation in Dust-Enriched Systems: Preliminary Results **[#2125]**
Experiments were run to investigate Cr-bearing, Mg-, Al-spinel assemblages that are predicted to form during condensation in dust-enriched systems. The spinels are compared to natural Cr-rich spinels found in the carbonaceous chondrite, Allende.

Hood L. L. Ciesla F. J. Artemieva N. A. Marzari F. Weidenschilling S. J.
Chondrule Formation in Nebular Shock Waves Generated by Planetesimals Passing Through Jovian Resonances: Relative Importance of Bow Shocks and Impact Shocks **[#1775]**
We investigate (a) the relative importance for chondrule formation of planetesimal bow shocks and impact shocks; and (b) whether these shocks were numerous and widespread enough to explain the observed abundance of chondrules in chondrites.

Morris M. A. Desch S. J. Ciesla F. J.
Tying Up Loose Ends in Chondrule Formation by Shocks **[#2300]**
We discuss two unresolved issues in modeling nebular shocks: the appropriate input radiation boundary condition and the dust opacity. Resolving these issues and line cooling now allows a full calculation of shock-heated chondrule thermal histories.

Bouvier A. Wadhwa M. Simon S. B. Grossman L.
Magnesium Isotope Compositions of Chondrules from the Murchison and Murray Carbonaceous Chondrites **[#2193]**
We present new Mg isotope compositions of petrographically well-characterized chondrules from Murchison and Murray CM2 carbonaceous chondrites with the goal of understanding their formation processes and time scales.

Das J. P.
Fe/Mg-Fe/Mn Systematics of Chondrules and Their Host Chondrites: Clues for Their Evolution **[#1497]**
Fe-Mg-Mn diagram is used for chondrules and bulk of Semarkona (LL3.0), Chainpur (LL3.4), Allende (CV3), Renazzo (CR2) and Qingzhen (EH3) to understand effect of the major processes that have affected chondrites and chondrules during nebular and planetary stage evolution.

Fries M. Steele A.
Graphite Whiskers Discovered in CV3 Meteorites **[#2514]**
We report the serendipitous discovery of a small number of graphite whiskers (GWs), a rare polymorph of carbon, in a range of settings within several CV3 meteorites and present implications pertaining to meteoritics and astronomy for this finding.

Hewins R. H.
Minor Element Zoning of Olivine in Type IIA Chondrules in Semarkona **[#1669]**
P-rich zones, preserved because P diffuses slowly, mark periods of rapid growth and generally show continuous crystallization of olivine grains. They also mark onset of growth on resorbed relict grains. P X-ray maps can clarify the evolution of individual chondrules.

Varela M. E. Zinner E. Kurat G.
Chondrule Tieschitz IIIM: Clues to the Origin of Early Liquids? **[#1390]**
We report the results of an ASEM and SIMS study of Tieschitz IIIM, a porphyritic olivine chondrule that is very rich in microcrystalline mesostasis, from the Tieschitz (H3.6) unequilibrated ordinary chondrite.

Teitler S. A. Paque J. M. Cuzzi J. N. Hogan R. C.
Statistical Tests of Turbulent Concentration of Chondrules **[#2388]**
Statistical tests of several sets of chondrules support the hypothesis of sorting by an aerodynamic process, specifically the turbulent concentration mechanism. The tests rule out several other classes of sorting mechanisms.

Petaev M. I.
Revised Thermodynamic Properties of Ca Aluminates: Implications for the Condensation Sequences **[#2407]**
I provide a new dataset of thermodynamic properties of hibonite, grossite, and dmitryivanovite and discuss how it affects condensation sequences.

Jacobsen B. Matzel J. Hutcheon I. D. Ramon E. Krot A. N. Ishii H. A. Nagashima K. Yin Q.-Z.
The ^{36}Cl-^{36}S Systematics of Wadalite from the Allende Meteorite **[#2553]**
The AJEF wadalite shows very large ^{36}S excesses correlated with the respective $^{35}Cl/^{34}S$ ratios. The slope of the best-fit line through the data yields an inferred $^{36}Cl/^{35}Cl$ ratio at the time of wadalite formation of $(17.2 \pm 2.5) \times 10^{-6}$.

Bullock E. S. MacPherson G. J.
A Pristine Amoeboid Olivine Aggregate Protolith from the Vigarano CV3 Chondrite **[#2385]**
A recently discovered amoeboid olivine aggregate from Vigarano CV3 chondrite contains a refractory, melilite-rich spherule that will allow high-precision Al-Mg isotopic dating, and will help to constrain the ages of these types of inclusion.

Farkaš J. Yu G. Huang S. Petaev M. I. Jacobsen S.
Formation of CAIs: Constraints from the Calcium Isotope Composition of CAI (SJ101) from the Allende CV3 Chondrite **[#2036]**
We present results of mass-dependent and non-mass-dependent calcium (Ca) isotope variations in the Ca-Al Rich Inclusion (CAI) from the Allende meteorite.

VOLATILE AND ORGANIC COMPOUNDS IN CHONDRITES

Orthous-Daunay F. R. Quirico E. Lemelle L. Beck P. De Andrade V. Simionovici A. Derenne S.
Sulfur Speciation in Carbonaceous Chondrites HF/HCl Residues by S K-Edge XANES Microspectrometry **[#1777]**
Sulfur oxidation state of insoluble OM from 3 CI1, 5 CM2, Renazzo (CR2) and Tagish Lake was determined by S-XANES. Different redox ratios are reported among these chondrites, possibly evidencing chemical effects of hydrothermalism.

Court R. W. Sephton M. A.
Volatile Yields Upon Pyrolysis of Carbonaceous Chondrites as Determined by Quantitative Pyrolysis-Fourier Transform Infrared Spectroscopy **[#1556]**
We have used quantitative pyrolysis-fourier transform infrared spectroscopy to determine the production of water and carbon dioxide upon the stepped pyrolysis of a range of carbonaceous chondrites.

Hilts R. W. Herd C. D. K. Morgan D. Edwards L. Huang Y.
Carboxylic Acid Abundances in the Tagish Lake Meteorite: Lithological Differences and Implications for Formic Acid Abundances in Carbonaceous Chondrites **[#1925]**
Analysis of two different Tagish Lake rocks found: 1) a very low GCMS response for formic acid, 2) formic acid concns above 100 ppm and 3) that formic acid to higher homologue ratios indicate the average level of oxidation for the soluble organics.

Wilson K. B. Wilson T. L.
Radial Breathing Modes in Cosmochemistry and Meteoritics **[#1627]**
Radial breathing modes in Raman spectra are "smoking gun" signatures of some Q-phase candidates in cosmochemistry and meteoritics. These active vibrational modes are either ignored or are not being reported. The resolution of Q depends upon them.

CRASHING CHONDRITES: IMPACT, SHOCK, AND MELTING

Frank E. A. Wittmann A. Kring D. A.
Petrography and Metallographic Cooling Rate of H-Chondrite Impact Melt Breccia LAP 04751 **[#2034]**
An impact event melted a portion of the H-chondrite parent body, mixing with surviving clastic material. The melt-rich breccia was deposited as a thin unit at a depth <10 m, implying an ejecta blanket or the uppermost fraction of a breccia lens.

Schrader D. L. Lauretta D. S. Connolly H. C. Jr. McCoy T. J. Greenwood R. C. Franchi I. A.
NWA 4477: A Unique Impact Melt Breccia. **[#1854]**
We discuss a unique impact melt breccia, NWA 4477.

Ozawa S. Ohtani E. Terada K.
Pressure and Timing of the Shock Events Recorded in L6 Chondrites **[#1474]**
Shock pressures of two L6 chondrites (Sahara 98222 and Yamato 74445) were estimated based on the mineralogy of shock melt veins. We also estimated the impact age of Sahara 98222 based on U-Pb dating of phosphates in and around the shock melt veins.

Fürj J. Gyollai I. Bérczi Sz. Gucsik A. Nagy Sz. Veres M.
Raman Spectroscopy of Shocked Olivine in the Hungarian L-Chondrite, Mócs **[#1110]**
Mócs (L5) meteorite contains shock-metamorphic effects in olivines: (1) weak-moderate shock mosaicism, (2) PF's and PDF's, and (3) presence of highly deformed olivine grains indicated by wadsleyite peaks of their Raman spectra.

Hutson M. L. Hugo R. Ruzicka A. M. Rubin A. E.
Olivine Microstructures in the Miller Range 99301 (LL6) Ordinary Chondrite **[#1081]**
We used Transmission Electron Microscope (TEM) imaging to examine microstructures in MIL 99301 (LL6) olivine grains in order to understand more fully this meteorite's deformation and thermal history.

Gyollai I. Fürj J. Bérczi Sz. Gucsik A. Nagy Sz.
Petrographic Study of Thermal and Shock Metamorphism of the Hungarian L-Chondrites: Mezomadaras (L3,7), Knyahinya (L5), and Mócs (L6). **[#1066]**
We studied by optical microscopy and Raman spectroscopy three Hungarian L-chondrites and we observed mineralogical signals of the shock stages of Mezomadaras (S2-S3), Knyahinya (S4), and Mócs (S3-S5).

Izawa M. R. M. Flemming R. L. Banerjee N. R.
Shock Stage Assessment and Petrography of 11 Antarctic Enstatite Chondrites **[#1322]**
EH and EL chondrites from a range of metamorphic grades were assessed for petrographic indicators of shock. A micro X-ray diffraction technique was used to determine lattice mosaicity. Moscaicity and petrographic shock stage are well correlated.

Dixon L. Herd R. K. Samson C. Hunt P. A.
A Detailed Investigation of the Mineralogy and Textures of the L4 Ordinary Chondrite Saratov **[#1465]**
SEM documentation and textural interpretation of 370 chondrules >100 microns in diameter, in a single polished thin section of Saratov, is revealing their complex histories. A revised classification scheme for chondrules is envisaged, reflecting their origins and processing.

UREILITE STUDIES

Trappitsch R. Cosarinsky M. Hofmann B. Leya I.
Noble Gas Studies of the Ureilites Kenna and Ramlath As Samah 247 **[#1246]**
We present noble gas data on two ureilites, Kenna and RaS 247 (desert find). Our measurements indicate cosmogenic He and Ne release at low temperatures, Ar is mostly primordial. Total gas concentrations are highly variable within the samples.

Jakubowski T. Karczemska A. Kozanecki M. Gucsik A. Stanishevsky A. Mitura S.
Micro-Raman Spectroscopy of Diamonds from Hot Desert Ureilites **[#1382]**
The samples of all types of ureilites, from less shocked up to highly shocked, were examined using Raman spectroscopy and Scanning Electron Microscopy. The results show the presence of diamonds in all of our samples.

Garren M. K. Singletary S. J. Bell D. R. Busek P. R.
Ureilite Lithium Isotopic Composition **[#1668]**
Lithium abundances and isototpic compositions from three ureilites are reported. Spot analyses reveal spatial correlations between abundances and isotopic compositions with features such as cracks, grain boundaries and the ubiquitous reduced rims.

Gabriel A. D. Pack A.
Ureilite Vein Metal — Indigeneous or Impact Material? **[#2462]**
Ureilite vein metal is not in chemical and isotopic equilibrium with ureilite silicate. We discuss if the vein metal can be produced by solid/liquid-fractionation in the parent body or if an outside source is nessary.

Goodrich C. A. Van Orman J. A. Domanik K. Berkley J. L.
Metal in Ureilites: Petrologic Characterization **[#1132]**
Metal and siderophile elements in ureilites appear to be inconsistent with a smelting model. We address this problem with detailed petrographic and trace element characterization of the types of metal in ureilites.

Le Guillou C. Rouzaud J. N. Remusat L. Bourot-Denise M. Jambon A.
Coupled Raman/TEM Study of an Ureilite Carbon Phases Compared to Shocked Graphite Analogs: Implication for Shock History and Noble Gases Carriers Evolution **[#2108]**
Carbons in an ureilite compared with analogs of shocked graphite suggest the presence of two diamond generation. The disordered carbon identified as a diamond coating may contain the noble gases released at low temperature in the mass spectrometer.

PETROLOGY AND MINERALOGY OF THE SNC METEORITES

Bunch T. E. Irving A. J. Wittke J. H. Rumble D. III Korotev R. L. Gellissen M. Palme H.
Petrology and Composition of Northwest Africa 2990: A New Type of Fine-grained, Enriched, Olivine-Phyric Shergottite **[#2274]**
We characterize a fine-grained martian magmatic rock that is different from those previously described.

Satake W. Mikouchi T. Makishima J. Miyamoto M.
Comparison of Redox States Between Geochemically-Intermediate and Enriched "Lherzolitic" Shergottites **[#1717]**
We analyzed geochemically-intermediate (ALH77005 and LEW88516) and enriched (RBT04262 and NWA4468) lherzolitic shergottites to compare their redox states. Fe-XANES analysis of ulvospinel in enriched samples showed slightly higher Fe3+ abundance.

Shearer C. K. Burger P. V. Papike J. J. Karner J.
ComparisonsBetween RBT 04262 and lherzolitic Shergottites (ALHA 77005 and LEW 88516) **[#1300]**
In this poster, we compare lithology A in RBT 04262 to two other lherzolitic shergottites to gain a better understanding of the petrogenesis of RBT 04262 and the lherzolitic shergottites, and their relationship to the basalts that produced the complete suite of shergottites.

O'Sullivan K. M. Neal C. R.
The Crystal Stratigraphy of Shergotty **[#1709]**
Pyroxene crystal size distributions, residence times, and geochemical variations are presented.

Mikouchi T.
Petrological and Mineralogical Diversities Within the Lherzolitic Shergottites Require a New Group Name? **[#2272]**
"Pyroxene-oikocrystic" shergottite can be an appropriate group name of lherzolitic shergottite because recent discovery of new shergottites such as RBT 04262 and NWA 4468 has revealed petrological and mineralogical diversities of this group.

Pinet P. C. Clenet H. Heuripeau F. Chevrel S. D. Rosemberg C. Daydou Y. Toplis M. Baratoux D.
Mafic Mineralogy of Martian Meteorites Based on a Systematic Deconvolution Using an Improved Modified Gaussian Model (MGM) Approach **[#1612]**
An improved MGM deconvolution procedure tested on SNC reflectance spectra leads to reliable detection of complex mafic lithologies based on the band positions in the 1 and 2 μm domains, with implications for interpreting the martian spectra.

Hui H. Peslier A. Lapen T. J. Brandon A. Shafer J.
Northwest Africa 5298: A Basaltic Shergottite **[#2087]**
Martian meteorite NWA 5298 found in 2008 is a moderately-evolved "enriched" shergottite. It is mainly composed of pyroxene grains with complex composition zoning and lath-shaped maskelynite. Oxygen fugacity recorded by Fe-Ti oxides is about QFM.

Basu Sarbadhikari A. Liu Y. Day J. M. D. Taylor L. A.
Olivine-hosted Melt Inclusions in Olivine-Phyric Shergottite LAR 06319 **[#1173]**
A newly-found, Antarctic, olivine-phyric shergottite, LAR 06319 which contains an enriched REE signature are studied. The results on olivine-hosted MI and their implications on the evolution of the LAR 06319 parental melt are reported.

Galenas M. G.. Jones J. H. Danielson L. R.
Experimental Crystallization of Yamato 980459 **[#1920]**
Fractional and equilibrium crystallization experiments find a correlation between major element compositions and differences in minor element compositions between Y-980459 and QUE 94201 suggesting that Y-98 is not a parental melt for QUE.

Draper D. S.
Yamato 980459 Liquid Line of Descent at 0.5 GPa: Approaching QUE94201 **[#1696]**
Anhydrous equilibrium crystallization experiments on a synthetic Yamato 980459 composition at 0.5 GPa produce residual liquids approaching the composition of QUE 94201.

Karner J. M. Papike J. J. Shearer C. K. Burger P. V.
Chemical Signatures in Plagioclase from Martian Meteorites **[#1327]**
Plagioclase composition holds signatures of planetary origin and igneous history.

Channon M. B. Bonifacie M. Stolper E. M. Eiler J. M.
Oxygen Isotope Compositions of Mineral Separates from SNC Meteorites: Constraints on the Petrogenesis of Martian Magmas **[#2450]**
Oxygen isotope data of martian meteorites from whole rock measurements may not reflect the isotopic composition of martian magmas. This study uses mineral separates to reconstruct oxygen isotope melt values and constrain mantle characteristics.

Nagao K. Park J. Okazaki R. Imae N. Kojima H.
Noble Gas Distribution in the Yamato 000593 Nakhlite Deciphered by Laser Ablation Analysis and Mineral Separation **[#1682]**
Noble gases measured for olivine, plagioclase and pyroxene separates, and by laser ablation on thin plate prepared from Y-000593 nakhlite indicate that plagioclase and/or mesostasis are the main carrier of elementally fractionated martian atmosphere.

Cartwright J. A. Burgess R. Gilmour J. D.
Xenon Isotopes in Shergottites RBT 04262, DaG 489, Shergotty and EET 79001 **[#1907]**
Xenon isotope analysis has been performed on mineral separates of shergottites EET 79001, Shergotty, DaG 489 and RBT 04262. All meteorites show similar distribution of martian components, except for clear overprinting from terrestrial contamination.

MARTIAN METEORITES

Albarede F. Bouvier A. Blichert-Toft J.
More Old News from Martian Meteorites **[#1914]**
We report new Pb isotopic data on whole-rocks and minerals from RBT 04262 (shergottite), MIL 03346 (nakhlite), and ALH 84001. ALH 84001 carbonates and silicates give ages of ca. 4.1 Ga. All SNC formed in three episodes dated at 4.3, 4.1, and 1.3 Ga.

Jagoutz E. Bowring S. Jotter R. Dreibus G.
New U-Th-Pb Data on SNC Meteorite ALHA 84001 **[#1662]**
We report new Th-U-Pb data on ALHA 84001. A ^{206}Pb-^{207}Pb age of 4135 ± 12 Ga and U – Pb of 41173 ± 2,3 are found. However, ^{208}Pb systematic is not consistent with U –Pb evolution, Th-Pb system shows a much younger age of 2926 ± 410 Ma.

Righter M. Lapen T. J. Brandon A. D. Beard B. L. Shafer J. T. Peslier A. H.
Lu-Hf Age and Isotope Systematics of ALH 84001 **[#2256]**
Lu-Hf age and isotope data of ALH 84001 yields crystallization age of 4086 ± 30 Ma and an initial eHf of –4.76 ± 1.04, indicating this meteorite is derived from ancient enriched reservoir on Mars.

Shafer J. T. Brandon A. D. Lapen T. J. Righter M. Beard B. Peslier A. H.
Lu-Hf Age of Martian Meteorite Larkman Nunatek 06319 **[#1803]**
The Lu-Hf age of martian meteorite LAR 06319 is 197±29 Ma. An initial $\varepsilon^{176}Hf$ of -18.0 is similar to other enriched shergottites (Shergotty, Zagami, RBT 04262, and Los Angeles) and extend the existing data set for the enriched shergottite group.

Park J. Ming D. W. Garrison D. H. Jones J. H. Bogard D. D. Nagao K.
Noble Gas Analysis for Mars Robotic Missions: Evaluating K-Ar Age Dating for Mars Rock Analogs and Martian Shergottites **[#2186]**
Noble gas investigation was organized for the possibility of measuring noble gases in martian rocks and air by future robotic missions such as MSL. We suggest the possibility of K-Ar age dating by lab simulation experiments on MORB and martian meteorites.

Greshake A. Fritz J.
Discovery of Ringwoodite, Wadsleyite, and ?-$Ca_3(PO_4)_2$ in Chassigny: Constraints on Shock Conditions **[#1586]**
The olivine high-pressure polymorphs ringwoodite and wadsleyite as well as the high-pressure phosphate ?-$Ca_3(PO_4)_2$ were discovered in melt pockets of the martian dunite Chassigny attesting a minimum prevailing shock pressure of ~20 GPa.

Walton E. L. Irving A. J. Bunch T. E. Kuehner S. M. Herd C. D. K.
Extreme Shock Effects in Relatively Enriched Shergottite Northwest Africa 4797 **[#1464]**
NWA 4797 is distinguished by its strong degree of shock damage, representing a growing group of martian meteorites shocked to pressures >55 GPa, previously represented only by Dhofar 378.

Fritz J. Greshake A.
Petrographic Constraints on Shock Induced P/T Conditions in Shergottites **[#1581]**
Quantitative shock pressure barometry and post shock temperature calculations of rock forming minerals are presented. The two independent data sets are in good agreement with the petrographic observations in shergottites.

Kurihara T. Mikouchi T. Saruwatari K. Kameda J. Miyamoto M.
Fe-Ni Metal and Magnetite Nano-Particles in "Brown" Color Olivines from Martian Meteorites **[#1049]**
Our TEM study revealed that brown olivines in Dhofar 019, LAR 06319 and NWA 1950 contained magnetite nano-particles instead of Fe-Ni metal nano-particles. These results indicate that magnetite nano-particles are widely present in martian meteorites.

Hoffmann V. H. Mikouchi T. Kurihara T. Funaki M. Torii M.
Magnetic Signature of Experimentally Shocked San Carlos Olivines: Simulation of the Neoformation Processes of Nano-sized Fe-Ni and Magnetite Particles in Brown Colored Olivines of Some Martian Meteorites (SNC) **[#2194]**
The magnetic signature and phase composition of experimentally shocked San Carlos olivines is investigated. The basic idea is to simulate the likely neoformation processes of nano-sized Fe-Ni/Magnetite particles in brown colored olivines of some martian meteorites.

Niihara T. Kaiden H. Misawa K. Sekine T.
U-Pb Isotopic Systematics of Experimentally Shocked Baddeleyite **[#1562]**
We performed shock recovery experiments on baddeleyite at the shock pressures of 24, 34, and 47 GPa. The data on U-Pb isotope and corresponding ages for experimentally shocked baddeleyite are indistinguishable from those of unshocked baddeleyite.

PHOENIX LANDING SITE: PERCHLORATE AND OTHER TASTY TREATS

Sykulska H. M. Pike W. T. Vijendran S.
Microscopy Analysis of the Salt Content of Soil and Dust at the Phoenix Landing Site **[#2366]**
Colour and spatial information of the material in the soil is combined to give a measure of the salt concentration. Analysis of various samples allows lateral and vertical comparison of salt content of the soil.

Sutter B. Lauer H. V. Golden D. C. Boynton W. V. Morris R. V. Niles P. B. Ming D. W.
Thermal and Evolved Gas Behavior of Calcite Under Mars Phoenix TEGA Operating Conditions **[#1843]**
Calcite may have been detected by the Thermal Evolved Gas Analyzer (TEGA) at the Phoenix lander site. Laboratory thermal analyses of calcite under TEGA operating conditions will be presented to aid the interpretation of calcite detection by TEGA.

Niles P. B. Boynton W. V. Hoffman J. H. Ming D. W. Phoenix Science Team
A First Look at Carbon and Oxygen Stable Isotope Measurements of Martian Atmospheric CO_2 by the Phoenix Lander **[#1806]**
The TEGA instrument on the Mars Phoenix Lander has measured the stable isotope composition of martian atmospheric CO_2. The results indicate that martian atmospheric CO_2 is slightly depleted in both ^{13}C and ^{18}O compared to atmospheric CO_2 on Earth.

Catling D. C. Claire M. W. Quinn R. C. Zahnle K. J. Clark B. C. Kounaves S. Hecht M. H.
Possible Atmospheric Origins of Perchlorate on Mars **[#1567]**
The Phoenix Mars lander measured perchlorate as a key soluble anion in the soil at an abundance of ~1wt%. Here, we discuss how the perchlorate was likely formed from atmospheric oxidants acting on chlorine-bearing species in Mars' arid environment.

Fisher D. A. Hecht M. Kounaves S. Catling D.
Perchlorate Found by Phoenix Could Provide a Mobile Brine Sludge at the Bed of Mars Northern Ice Cap that Would Allow Flow with Very Low Basal Temperatures: Possible Mechanism for Water Table Re-Charge **[#2281]**
The north cap of Mars has basal temperature that precludes the flow of ice. Phoenix discovered polar soils contain perchlorate salts. These salts depress the melting point so it could form a sludge that provides a mobile bed that moves the ice outwards.

Ming D. W. Lauer H. V. Jr. Archer P. D. Jr. Sutter B. Golden D. C. Morris R. V.
Niles P. B. Boynton W. V.
Combustion of Organic Molecules by the Thermal Decomposition of Perchlorate Salts: Implications for Organics at the Mars Phoenix Scout Landing Site **[#2241]**
The presence of a strong oxidizer (i.e., perchlorate salt) in the soils at the Phoenix landing site will most likely combust organic materials during pyrolysis by the Thermal and Evolved Gas Ananlyzer.

Lauer H. V. Ming D. W. Sutter B. Golden D. C. Morris R. V. Boynton W. V.
Thermal and Evolved Gas Analysis of Magnesium Perchlorate: Implications for Perchlorates in Soils at the Mars Phoenix Landing Site Perchlorates in Soils at the Mars Phoenix Landing Site. **[#2196]**
Perchlorate salts were discovered in the soils around the Phoenix landing site on the northern plains of Mars.The purpose of this paper is to evaluate the thermal and evolved gas behavior of perchlorate salts using TEGA-like laboratory testbed instruments.

Marion G. M. Catling D. C. Claire M. Zahnle K. J.
Modeling Aqueous Perchlorate Chemistries with Applications to Mars **[#1959]**
The paper will examine thermodynamic modeling of perchlorate chemistries with applications to the Phoenix mission site.

Morris R. V. Golden D. C. Ming D. W. Graff T. G. Arvidson R. E. Wiseman S. M. Lichtenberg K. A. Cull S.
Visible and Near-IR Reflectance Spectra for Smectite, Sulfate, and Perchlorate Under Dry Conditions for Interpretation of Martian Surface Mineralogy **[#2317]**
Visible and near-IR reflectace spectra were acquired under dry conditions for smectite and for sulfate- and perclorate-bearing phases. The spectra are used for interpretaton of martian surface mineralogy.

Pike W. T. Sykulska H. Vijendran S. Phoenix Microscopy Team
Fractal Analysis of the Microstructure of the Martian Soil at the Phoenix Landing Site **[#1909]**
A fractal analysis of the Mars soil at the Phoenix site is presented. It indicates that the primary particles of the soil are up to 15 μm in size with larger particles formed by agglomeration resistant to fracture.

Shaw A. Arvidson R. E. Keller H. U. Lemmon M. Mellon M. T. Trebi-Ollennu A. Robinson M. Siebach K. Volpe R.
Phoenix Mission Trenching in Arctic Mars **[#2097]**
The Phoenix Mars Lander dug twelve trenches in polygonal terrain of the high northern latitudes. Forces measured while digging trenches help compare the properties of the soils in which the trenches were dug. The trenches sample polygons and troughs.

Markiewicz W. J. Kossacki K. J. Keller H. U. Hviid S. F. Goetz W. El Maarry M. R. Bos B. J. Woida R. Drube L. Leer K. Madsen M. B. Mellon M. T. Smith P.
Sublimation of Exposed Snow Queen Surface Water Ice as Observed by the Phoenix Mars Lander **[#1667]**
From the rate of sublimation of Snow Queen as imaged by the RAC we infer that the soil grain size is of the order of 1 micron which is consistent with atmospheric dust and Phoenix imaging at all scales.

Saraiva J. Antunes J. Bandeira L. Pina P.
Identification and Characterization of Small-Scale Polygons Around the Phoenix Landing Site **[#1323]**
This work presents a study of small-scale polygons in the area where the Phoenix probe landed. Large numbers of polygons are automatically identified and briefly characterized in geometric and topological terms, illustrating the potential of the methodology employed.

Cull S. C. Arvidson R. Mellon M. Wiseman S. McGuire P. Clark R. Titus T. Searls M.
Seasonal Ices at the Mars Phoenix Landing Site: Observations from HiRISE and CRISM **[#1814]**
CRISM spectra are used to determine when ices appear at the Phoenix landing site, how their grain sizes and relative abundances evolve through time, and what controls sublimation patterns during the spring defrosting period.

Searls M. L. Mellon M. T. Cull S. Hansen C. J.
Seasonal Frost at the Phoenix Landing Site **[#2402]**
This work provides a spatial and temporal characterization and analysis of the seasonal frost at the Phoenix landing site.

Levy J. S. Head J. W. III Marchant D. R.
Phoenix Landing Site Geomorphology: Surface Stability and Implications for the Martian Latitude-dependent Mantle **[#1625]**
Geomorphological observations of the Phoenix landing site suggest a history for local permafrost recently dominated by excess ice removal through sublimation, ongoing thermal contraction cracking, and limited cryoturbation by wet or dry processes.

Davis J. A. Lange C. F. Taylor P. A.
Numerical Study of the Effect of the Phoenix Mars Lander on the Temperature Sensors **[#2135]**
A numerical study of the effect of the Phoenix Mars lander on the temperature sensors show that under certain conditions, the heat produced by the lander can influence the temperature sensors.

Taylor P. A. Weng W. Cook C. Dickinson C. Akingunola A. Polkko J. Kahanpää H.
Pressure Data from the Phoenix Landing Site **[#1868]**
During the Phoenix mission surface pressures were measured at a frequency of 2 Hz for 150 sols. Seasonal and diurnal features of these data will be discussed. Short time scale features associated with convective vortices were also observed.

Nelli S. M. Renno N. O. Feldman W. C. Murphy J. R. Kahre M. A.
Reproducing Meteorological Observations at the Mars Phoenix Lander Site Using the NASA Ames GCM V.2.1 **[#1732]**
Using the NASA Ames General Circulation Model (GCM) v2.1, we reproduce atmospheric conditions at the Mars Phoenix Lander site in an effort to explain the measured atmospheric phenomena (water ice clouds, ground frosts, dust devils, etc.).

Bean K. M. Lemmon M. T. Phoenix Science Team
Surface Stereo Imager Observations of Dust Devils at the Phoenix Landing Site **[#1799]**
The Surface Stereo Imager observed 76 wind events during Phoenix's surface operations. There were 37 unique dust devils, and 11 strong gusts of wind. Dust devils were not observed until the last third of the mission.

Ellehøj M. D. Gunnlaugsson H. P. Taylor P. A. Gheynani B. T. Whiteway J. Lemmon M. T. Bean K. M. Tamppari L. K. Drube L. Von Holstein-Rathlou C. Madsen M. B. Fisher D. Smith P.
Dust Devils and Vortices at the Phoenix Landing Site on Mars **[#1558]**
Near continuous measurements of pressure and temperature by the MET instrumentation on the Phoenix Mars Lander are used to identify the passage of vertically oriented vortex structures at the Phoenix landing site (126W, 68N) on Mars.

Leer K. Drube L. Goetz W. Gunnlaugsson H. P. Lemmon M. Madsen M. B. Morris R. V. Smith P. Phoenix Science Team
Optical Study of Particles On Mars Phoenix Magnets **[#1923]**
Particles collected by magnets on the Phoenix Lander on Mars are compared to data from orbiter missions.

Drube L. Leer K. Madsen M. B. Goetz W. Morris R. V. Lemmon M.
Airborne Dust Experiment (iSweep) on the Phoenix Mars Lander **[#2266]**
The calibration targets for Phoenix also act as an experiment (called iSweep) looking at the airborne dust that is magnetically attracted to settle on its surface. Some results of which will be shown here.

Stein T. C. Arvidson R. E. Scholes D. M. Heil-Chapdelaine V. M.
Phoenix Analyst's Notebook: A Holistic Tool for Accessing Integrated Mission Data and Documents **[#1079]**
The Phoenix Analyst's Notebook (http://an.rsl.wustl.edu) provides access to the Mars Phoenix Lander mission data archives by integrating engineering and science data, observation planning and targeting, and documentation into web-accessible pages.

MARS POLAR ATMOSPHERES AND CLIMATE MODELING

Furfaro R. Panfili P. Luciani A. Kargel J. S. Ganapol B. Palmero-Rodriguez A. Mostacci D.
Deterministic Neutron Transport Modeling for Planetary Applications **[#1846]**
This paper shows how to model thermal and epithermal neutron fluxes leaking out from Mars using a deterministic approach. The model has been validated on Mars data and tuned for fast and accurate prediction of subsurface water-ice.

Helbert J. Head J. W. Marchant D.
The Berlin Mars Near Surface Thermal Model (BMST) — Modeling the Formation and Evolution of Sublimation Lags on Mars **[#1521]**
Phoenix for the first time directly studied ice on Mars and the SHARAD instrument detected clear evidence for glacial deposits in the equatorial regions of Mars. We study with the BMST model if these deposits are the remnants of an earlier climate cycle.

McMenamin D. S. McGill G. E.
Thermal Anomalies Suggest that Ongoing Clathrate Dissociation in Icy Sediment Contributes to Martian Atmospheric Methane **[#1848]**
Thermal anomalies in eroding icy sediments indicate sites of ongoing methane clathrate dissociation that release atmospheric methane on Mars.

Brown A. J. Wolff M. J.
Atmospheric Modeling of the Martian Polar Regions: One Mars Year of CRISM EPF Observations of the South Pole **[#1675]**
We have used CRISM Emission Phase Function gimballed observations to investigate atmospheric dust/ice opacity and surface albedo in the south polar region for the first Mars year of MRO operations. This covers the MY28 "dust event" and cap recession.

Hayne P. Paige D. A.
Clouds in the Polar Night of Mars: Modeling and Observations with the Mars Climate Sounder **[#1849]**
We present evidence from the Mars Climate Sounder and radiative transfer modeling, that polar cold spots are caused by carbon dioxide clouds.

Pankine A. Tamppari L. Smith M.
Water Vapor over Martian North Polar Cap from MGS TES **[#2145]**
We present retrievals of water vapor abundances from MGS TES data over martian north polar cap during spring and summer.

MARS POLAR INVESTIGATIONS

Litvak M. L. Boynton W. V. Kozyrev A. S. Mitrofanov I. G. Sanin A. B. Tretyakov V. I. Varenikov A. Golovin D.
Observation of Martian Seasonal Caps: Dimensions, Density, Mass, Inter Annual Variations **[#1254]**
Results of long term (eight years) observations of martian seasonal caps onboard Mars Odyssey are presented.

Pathare A. V. Chuang F. C.
The Mass Balance of Stratigraphic Anomalies in the Martian North Polar Layered Deposits **[#1400]**
The present-day mass balance of stratigraphic anomalies within north polar troughs is constrained by incorporating CRISM spectral observations of surface water ice into an NPLD sublimation model.

Fortezzo C. M. Tanaka K. L.
Unconformities Revealed by MRO Context Images in the Polar Layered Deposits of Planum Boreum, Mars **[#2270]**
Details of unconformities mapped using a CTX image mosaic in the martian north pole indicate that one regional, and multiple localized erosion or non-deposition episodes occurred during the formation of the polar plateau in the Gemini Scopuli region.

Rodriguez J. A. P. Tanaka K. L. Berman D. C.
Depression Systems in Western Planum Boreum, Mars: Distributions, Orientations, and Cross-Cutting Relationships **[#2371]**
Planum Boreum, in the north polar region of Mars, forms a domical plateau largely dissected by depression systems of various dimensions. In this investigation we discuss their distributions, orientations, and cross-cutting relationships.

Russell P. S. Byrne S. Fishbaugh K. Herkenhoff K. Thomas N. HiRISE Team
Heights and Slopes on Mars North Polar Scarps Using HIRISE Point-to-Point Stereo Measurements **[#2479]**
We present a technique for making vertical elevation-difference and slope measurements between two points that yields results more accurate than MOLA (at polar scarps) yet is not as complex and resource-intensive as producing a full scale DEM.

Guallini L. Rossi A. P. Marinangeli L. Biccari D. Pettinelli E. Seu R.
New Elements on Stratigraphy of South Polar Layered Deposits on Promethei Lingula Region and a Possible Structural Approach **[#1602]**
New stratigraphical/tectonical elements was found on Promethei Lingula south polar layer deposits. We assume two possible depositional cycles marked by an angular unconformity. Layers strain response could be useful to define sequence stratigraphy.

Betz E. O. Titus T. N. Cushing G. E.
Determining the Heights and Distributions of Swiss Cheese Features on Mars South Polar Residual Cap Using Photoclinometry **[#1363]**
Strange features known as "Swiss cheese" form in the thin CO_2 veneer of Mars south polar residual cap. Here we determine the heights and distributions of Swiss cheese features using photoclinometry in order to constrain the thickness of this veneer.

Langevin Y. Hansen C. Thomas N. Vincendon M. Titus T. Piqueux S. Bibring J.-P. Gondet B.
Investigations of Cryptic Regions of the South Seasonal Cap, 12/2008–02/2009 **[#2017]**
The origin of dust contamination in a major fraction of the cryptic region of the South seasonal cap of Mars has yet to be determined. An observation campaign in late 2008 / early 2009 with OMEGA, HIRISE, CRISM and THEMIS has been set up for adressing this issue.

Gardin E. Quantin C. Allemand P.
Defrosting Sequence on the Russell Megadune, Mars **[#2032]**
We have observed the complete defrosting sequence over the Russell megadune from small size dark spots to large dark streak spreading down the slope. Our results based on HiRiSE and CRISM data may question the current proposed model for defrosting features formation.

Westbrook O. W. Zuber M. T. Byrne S.
Southern Circumpolar Crater Ice Deposits on Mars **[#2147]**
Just beyond the martian south polar layered deposits (SPLD) are numerous impact craters containing mounded deposits that resemble outliers of the SPLD. We catalog and measure these crater-filling deposits and seek to understand their distribution, morphologies, and origins.

Moore M. Dasgupta A. Alva S. Casey S. Figueroa M. Hendershot C. Hwang D. Nagarajan S. Nguyen T. Szymanski J. Wilson R.
Defining Correlations Between Presence of Ice Deposits and Area Covered by Craters in Vastitas Borealis **[#1951]**
The Klein MSIP team gathered a number of THEMIS images to analyze. Areas of images covered by craters were correlated with areas covered by persistent ice deposits.

Kuzmin R. O. Zabalueva E. V. Christensen P. R.
Mapping of the Water Ice Amount in the Martian Surface Soil on the Periphery of the Retreating Seasonal Northern Polar Cap Based on the TES Data **[#1917]**
We present the results of the mapping of the water ice amount in the martian surface soil layer in the area around the Northern seasonal polar cap at the different stages of its recession.

Kuti A.
Thermal Behavior of Dokka Crater and its Surroundings in the North Polar Region of Mars **[#1006]**
The basic characterists of Dokka Crater and its surroundings in the north polar region of Mars are presented, focusing on the thermal properties and frost behavior. The results imply that the different thermal behavior is caused by H_2O ice.

Hovius N. Conway S. J. Barnie T. B. Besserer J.
Ice Filled Craters in Mars' North Polar Region — Implications for Sub-Surface Volatiles **[#2042]**
We present a study of impact craters above 65°N, to assess the sub-surface water budget, with emphasis on 17 craters containing lumps. We suggest these impacts formed a conduit to a periodically overpressurized aquifer, producing the lumps.

Swindle T. D. Thomas C. Mousis O. Lunine J. I. Picaud S.
The Trapping of Ar, Kr, and Xe in Martian Clathrates and the Possibility of Detecting Clathrates on Mars by Seasonal Changes in the Xe/Kr Ratio **[#1660]**
Calculations show that Xe would be much more readily trapped in multiple guest clathrates on Mars than would be Kr. Measurement of the Xe/Kr ratio over the course of a martian year would be a sensitive detector of seasonal formation of clathrate.

Blackburn D. G. Bryson K. Chevrier V. F. Roe L. A. White K. F.
Sublimation Kinetics of CO_2 Ice and Evolution of the Martian Polar Caps **[#1339]**
We report the experimentally measured sublimation rate of pure CO_2 ice under simulated martian conditions and compare them to data from MOLA, MOC, HiRISE, and CRISM. We predict the perennial CO_2 cap should disappear in approximately three martian years.

MARS NEAR-SURFACE ICE

Morgan G. A. Head J. W. III Marchant D. R.
The Use of Equilibrium Landforms to Identify Recent Climate Change on Mars: Insights from Field Studies in the McMurdo Dry Valleys of Antarctica **[#2217]**
Recent climatic change on Mars has been recorded in a series of equilibrium landform assemblages located in Noachis Terra. We explore these features through the detailed mapping of terrestrial analogs in the Antarctic Dry Valleys.

Boyce J. M. Mouginis-Mark P.
Martian Impact Crater Ejecta Run-Out Efficiency: Its Implications for Water in the Subsurface **[#1009]**
Martian impact crater ejecta efficiency provides information about the water content of the ejecta. Based on new estimates of martian ejecta run-out distances, they appears to require saturation with water during their emplacement.

Kress A. Head J. W.
Ring-Mold Craters on Lineated Valley Fill, Lobate Debris Aprons, and Concentric Crater Fill on Mars: Implications for Near-Surface Structure, Composition, and Age. **[#1379]**
Analysis of ring-mold crater populations on lineated valley fill, lobate debris aprons, and concentric crater fill on Mars and of ice-impact experiments suggest crater-count-derived ages may be erroneously old.

Drake J. S.
Thermokarst on Mars? Insights from a Survey of Rimless Depressions **[#1797]**
Rimless depressions on Mars have been mapped in THEMIS imagery from 50° north to 60° south latitude. Geomorphic evidence, along with MOLA observations of the features' depths, suggests that their interior stratigraphy is depositional in nature.

Head J. W. III Marchant D. R.
Inventory of Ice-related Deposits on Mars: Evidence for Burial and Long-Term Sequestration of Ice in Non-Polar Regions and Implications for the Water Budget and Climate Evolution **[#1356]**
We compile an inventory of non-polar ice deposits on Mars to estimate water abundance with time during different ancient climate conditions. We find that significant volumes are removed from the system and sequestered in non-polar ice reservoirs.

Putzig N. E. Phillips R. J. Head J. W. Campbell B. A. Egan A. F. Plaut J. J. Carter L. M. Seu R. SHARAD Team
Do Shallow Radar Soundings Reveal Possible Near-Surface Layering Throughout the Northern Lowlands of Mars? **[#2477]**
SHARAD soundings across the Northern Lowlands yield returns delayed by about 0.5 microsec from the surface return. These features may correspond to subsurface interfaces due to layering in the near surface, possibly including water ice.

Pearce G. D. Osinski G. R. Soare R. J.
Intra-Crater Glacial Deposits and Ice-Mantling in Utopia Planitia, Mars **[#2428]**
We describe glacial and periglacial features found within a crater in Utopia Planitia, northern plains of Mars and suggest that there is strong evidence for multiple emplacement events of ice-rich mantles.

Pedersen G. B. M. Head J. W. III
Overview of Possible Ice-related Morphologies in the Transition Zone Between Elysium and Utopia Basin, Mars **[#2081]**
Small scale ring mold-like craters, thermally distinct craters and craters with bipartite ejecta are observed. We evaluate their distribution and compile an overview in connection with other landforms, which have been ascribed to the presence of ice.

Orloff T. C. Kreslavsky M. A. Asphaug E.
Organization of Rocks on Patterned Ground in the Northern Latitudes of Mars **[#2205]**
The time and spatial scale of rock migration on the surface of patterned ground on Mars is studied by observing patterning effects around impact craters. Rock organization is linked to the degradation of craters and the patterned ground mechanism.

Kress A. Head J. W.
Lineated Valley Fill and Lobate Debris Aprons in the Deuteronilus Mensae Region, Mars: Implications for Regional Glaciation **[#1632]**
Studies of lineated valley fill and lobate debris aprons in the Deuteronilus Mensae region, Mars, reveal that they are endmembers of a continuum of morphologies with the same mode of origin, which is that of debris-covered glacier.

Balme M. R. Murray J. B. Gallagher C. Muller J-P. Kim J-R.
A Recent, Equatorial, Periglacial Environment on Mars **[#1837]**
We present geomorphological evidence for geologically recent freeze/thaw conditions in the equatorial Elysium Planitia region of Mars. This suggests a (perhaps transient) recent, warmer, martian climate than current models predict.

Zanetti M. Hiesinger H. Reiss D. Hauber E. Neukum G.
Scalloped Depression Development on Malea Planum and the Southern Wall of the Hellas Basin, Mars **[#2178]**
We offer support for a solar insolation model of scallop depression development from THEMIS-IR images, and suggest that scallops form from thermal contraction cracks in the surface of the latitude-dependent ice-rich dust mantle on Malea Planum.

Zanetti M. Hiesinger H. Reiss D.
Thickness Estimate of Ice-rich Mantle Deposits on Malea Planum, Southern Hellas Basin, Mars **[#2365]**
A quantitative estimate of the thickness of ice-rich dust mantles on Malea Planum has been determined using the crater diameter-rim height ratio for buried 'ghost' craters. Results show a marked thickening on the southern wall of Hellas Basin.

MARS: A VOLATILE-RICH PLANET

Withers A. C. Hirschmann M. M. Tenner T. J.
The Effect of Fe on OH- Content of Olivine: Implications for Extraction of H_2O from the Martian Mantle **[#1490]**
Experimental determinations of the effect of Mg# on H_2O storage capacity in olivine + opx suggests that extraction of H_2O from the martian mantle is similar to that of a LREE. By analogy to K we infer that ~50% of martian H_2O remains in its mantle.

Wood J. Filiberto J. Treiman A. H.
The Effect of Flourine on the Liquidus of an Adirondack-Class Martian Basalt **[#1105]**
As a preliminary study on the effect of F on phase equilibria, we have shown that F depresses the liquidus to a greater extent than water suggesting that fluorine is important during martian basalt genesis.

Brückner J. Dreibus G. Haubold R. Huisl W. Spettel B. Gellert R. Athena Science Team
Mobility of Phosphorus on the Martian Surface and in a Martian Meteorite **[#1613]**
The mobilization of P in an acidic environment was studied for meteorite Zagami by leaching experiments and for martian rocks by measurements of the APXS onboard the two Mars Exploration Rovers along their traverses.

Miura Y.
Formations of Martian Plagioclases and Flow Textures by Carbon Dioxides-rich Gas and Fluid Compared with Natural Rocks and Artificial Products on the Earth **[#1090]**
Carbon-bearing grains formed in basalts and syntheses are applied to carbon-fixing on martian plagioclases which are formed by impact pressures from carbon dioxides gas.

Nakamura N. Nyquist L. E. Reese Y. Shih C.-Y. Numata M. Fujitani T. Okano O.
Chlorine Isotopes as a Possible Tracer of Fluid/Bio-Activities on Mars and a Progress Report on Chlorine Isotope Analysis by TIMS **[#1946]**
We present a progress report on chlorine isotopic analysis using TIMS at NASA-JSC, and discuss the possible application of Cl isotopic analysis to martian meteorites in a search for fluid- and possibly biological activity on Mars.

Changela H. C. Bridges J. C.
TEM Study of Alteration Assemblages in the Nakhlites: Variation with Burial Depth on Mars **[#2302]**
TEM study of nakhlites shows a variation in secondary minerals between different meteorites. Lafayette from the greatest depth on Mars shows coarse crystalline Ca-Mn-Mg siderite and phyllosilicate whereas Y-000593 veins are amorphous silicate gel.

Greenwood J. P. Itoh S. Sakamoto N. Yurimoto H.
Hydrogen Isotope Measurements of Gypsum and Jarosite in Martian Meteorite Roberts Massif 04262: Antarctic and Houstonian Weathering. **[#2528]**
Ion microprobe measurements of hydrogen isotopes via spot mode and 2D ion imaging of gypsum and jarosite are best interpreted as last equilibrating with water in Houston and Antarctica, respectively.

MARS: GEOCHEMISTRY AND ALTERATION PROCESSES

Ling Z. C. Wang A. Li C.
Comparative Spectroscopic Study of Three Ferric Sulfates: Kornelite, Lausenite and Pentahydrate **[#1867]**
We have synthesized a new phase ferric sulfate with six structural waters, which is believed to be "lausenite". Its XRD, Raman and Vis-NIR spectral patterns are distinct from those of kornelite and pentahydrate.

Muirhead A. C. Bishop J. L. McKeown N. K.
The VNIR Spectral Properties of Iron Oxide/Oxyhydroxide Mixtures and Applications to Iron Oxides in the Mawrth Vallis Region of Mars **[#1652]**
The objective of this study is to measure the spectral properties of mixtures of FeOx minerals in order to better constrain the types and abundance of FeOx on Mars.

Beavon L. J. Lindsley D. H. McLennan S. M. Tosca N. J.
Experimental Constraints on Trace Element Mobility in Martian Basalt: Progress Report **[#1879]**
Low pH alteration experiments on a martian analog are being conducted to better understand the mobility of Ni, Zn, and Cr on the martian surface. Preliminary results will be presented.

Zhao Y. McLennan S. M. Tosca N. J.
Experimental Constraints on Trace Element Behavior during Martian Fe-Oxidation Processes at Meridiani Planum **[#1978]**
Trace elements Ni, Cr and Zn behavior during Fe-oxidation processes and reaction with precipitation products were experimentally investigated in this study. Preliminary results are reported here.

Hamilton V. E. Ruff S. W.
Mini-TES Spectra of Mazatzal and Other Adirondack-Class Basalts in Gusev Crater, Mars: Spectral/Mineralogical Evidence for Alteration **[#1418]**
We use Mini-TES data from the Spirit rover to demonstrate mineralogical evidence for sulfate in Adirondack-class rocks and the Mazatzal coating and to demonstrate for the first time that Adirondack-class basaltic exotics are present on the West Spur.

Gunnlaugsson H. P. Rasmussen H. Madsen M. B. Nørnberg P.
Inhomogenity of Basaltic Rocks at Gusev Crater on Mars **[#1656]**
Samples from Gusev crater on Mars show (Mössbauer-) inhomogeneities in the surface layer. Possible reasons for this are discussed and a simple explanation for the magnetic anomalies on Mars is offered.

Mølholt T. E. Gunnlaugsson H. P. Merrison J. P. Morris R. V. Nørnberg P. Madsen M. B.
Results from a Mössbauer and VNIR Study of Dust Generated from Olivine Basalt: Application to Mars **[#1622]**
It is shown that VNIR spectroscopy can greatly underestimate the ratio of olivine to pyroxene and olivine may be more abundant on Mars than hitherto believed. The possibilities of using electrodes to collect samples on Mars are discussed.

Fleischer I. Agresti D. Klingelhöfer G.
Mössbauer Hematite Temperature Study on Samples from the MER Landing Sites **[#1832]**
We use simultaneous fitting of Mössbauer spectra for a temperature-dependent study of hematite-bearing samples from both MER landing sites.

Le Mouélic S. Sarago V. Combe J.-Ph. Massé M. Bourgeois O. Mangold N. Bibring J-P. Gondet B. Langevin Y. Sotin C.
Global Mapping of Minerals on Mars with OMEGA Hyperspectral Data: Results of a Linear Unmixing Approach **[#1594]**
We use a linear unmixing algorithm to retrieve the main minerals contributing to the signal in OMEGA/Mars Express data. The result is a distribution map for each endmember selected in the input library, which covers the main mineral families.

Hughes C. G. Ramsey M. S. Bandfield J. L.
Detection of Small-Scale Mineral Deposits in Super-Resolved THEMIS TIR Data **[#2359]**
Super-resolved THEMIS TIR data allows more reliable detection of different subpixel-sized surfaces, and can be compared to Earth analogue sites or modeled further using more traditional approaches such as linear spectral deconvolution.

Roush T. L.
Estimated Optical Constants of Magnesite ($MgCO_3$) **[#1080]**
Carbonate minerals are of interest to the volatile and climate history on Mars. Spacecraft observations suggest the presence of magnesite at locations on the martian surface. The optical constants of magnesite are estimated and presented.

Lira C. Saraiva J. Pina P. Bandeira L. Antunes J.
A Mathematical Morphology Approach to the Analysis of Martian Soil Samples **[#2044]**
This work introduces a mathematical morphology tool to analyse the granulometry of soil samples *in situ* on Mars through image processing.

Needham A. W. Tomkinson T. Howard K. T. Grady M. M.
Clay Minerals in Nakhlites and on Mars **[#1969]**
Clay minerals, known to be present both in martian meteorites and on the surface of Mars, contain unique information about the planet's climate history. Analyses of terrestrial analogues and clay minerals in nakhlite meteorites are underway.

Viviano C. E. Moersch J. E. Piatek J. L.
Using THEMIS to Extend Mapping of Phyllosilicates on Mars **[#2107]**
We use a THEMIS spectral index to extend mapping of phyllosilicates in the Terra Sirenum region, suggesting possibilities for a THEMIS global phyllosilicate distribution map.

McKeown N. K. Bishop J. L. Wray J. J. Noe Dobrea E. Z. Silver E. A.
Textures and Morphologies of Phyllosilicate-bearing Units at Mawrth Vallis **[#2433]**
Coordinated analysis demonstrates that different phyllosilicate mineralogies identified in CRISM data have distinct textures in HiRISE images. This will help future rovers like MSL to identify different units and focus on unique outcrops.

Annex A. Marion-Spencer M. Jones M. Guthrie S. Grigsby B. Turney D.
CRISM Analysis of Graben in Terra Tyrrhena; A Search for Water in Equatorial Mars **[#1453]**
High school students lead CRISM and HiRISE study of Graben in Terra Tyrrhena, answering previous hypotheses about the formation of the graben and the presence of possible laccoliths.

Craig M. A. Osinski G. R. Flemming R. L. Cloutis E. A.
UV-Vis-NIR Reflectance Spectra of Shocked Carbonates from the Haughton Impact Structure, Devon Island, Canada: 0.35–2.5 μm; Implications for Carbonate Identification on Mars **[#1643]**
A preliminary look at the spectral effects of hypervelocity impact-induced shock metamorphism and melting in carbonates from the Haughton Impact Structure.

El Maarry M. R. Gasnault O.
A Preliminary Assessment of the Role of Impact Craters in Forming Hydrous Minerals on the Surface of Mars **[#1883]**
The role of impact craters in forming hydrous minerals on the surface Mars is discussed through correlations with the elemental hydrogen map from the gamma-ray spectrometer on board Mars Odyssey.

Fraeman A. A. Mustard J. F. Ehlmann B. L. Roach L. H. Milliken R. E. Murchie S. L.
Evaluating Models of Crustal Cooling Using CRISM Observations of Impact Craters in Terra Tyrrhena and Noachis Terra **[#2320]**
Occurrence of CRISM-detected hydrated silicates around Southern Highlands impact craters are used to assess models of crustal cooling. Preliminarily, lack of mineralogy-depth correlation favors cooling mediated by hydrothermal processes.

Schwenzer S. P. Abramov O. Kring D. A.
Impact-generated Hydrothermal Systems on Noachian Mars: The Path of Water **[#2328]**
We explore the path of water in impact-generated hydrothermal systems describing the mechanics of the fluid flux, the nature and distribution of alteration minerals and the amount of water stored in them.

Tornabene L. L. Osinski G. R. McEwen A. S.
Parautochthonous Megabreccias and Possible Evidence of Impact-induced Hydrothermal Alteration in Holden Crater, Mars **[#1766]**
Using CRISM with HiRISE, we report on the detection of phyllosilicates correlated with dikes within parautochthonous megabreccias originating from the well exposed basement of Holden Crater.

Barge L. M. Petruska J.
Experimental Tests of Micro-Concretion Nucleation in Porous Media **[#1910]**
We present an experimental study of nucleation and growth of spheroidal concretions in porous media.

Travis B. J. Feldman W. C.
Salt Deposits, Ice Lenses and Convective Brine Aquifers on Mars **[#1315]**
This abstract summarizes results of a numerical modeling study of possible brine aquifer dynamics in the shallow martian subsurface, subject to geothermal gradients, with implications for surface salt deposits and ice lenses.

Jänchen J. Morris R. V. Bish D. L. Hellwig U.
The H_2O Sorption Properties of a Martian Dust Analog **[#1395]**
Palagonitic dust is a geologically reasonable hydrated phase on the surface of Mars. Its presence as dust may account for the presence of the 3 μm absorption band as seen by OMEGA and CRISM at the martian surface for the entire planet.

Beck P. Pommerol A. Schmitt B. Brissaud O.
Experimental Study of Water Transport Across an Adsorbing Regolith **[#1291]**
We measured adsorption kinetics on analogs of the martian surface, we characterize the effect of adsorption on the transfer properties with implications on the coupling between the atmosphere and the sub-surface.

Robertson K. R. Bish D. L.
Thermal Behaviour of the Calcium-Sulfate-H_2O System **[#1829]**
Experimental results are presented here that provide a more thorough picture of dehydration rates in the calcium-sulfate-H_2O system. Our results suggest that gypsum desiccation will not occur over a diurnal or seasonal cycle under current martian conditions.

MARTIAN PHYLLOSILICATES: IDENTIFICATION, FORMATION, AND ALTERATION

Maturilli A. Helbert J. D'Amore M.
Identification of the Surficial Component from Martian Remote Sensing Infrared Spectra: Application to Mars Express PFS Measurements **[#1257]**
Target transformation and factor analysis techniques are applied to PFS LWC observations of the Nili Fossae region, where previous instruments detected phyllosilicates. PFS spectra are interpreted using the Berlin Emissivity Database (BED) spectral library.

Carter J. Poulet F. Bibring J.-P. Murchie S. Langevin Y. Mustard J. F. Gondet B.
Phyllosilicates and Other Hydrated Minerals on Mars: 1. Global Distribution as Seen by MEx/OMEGA **[#2028]**
This abstract presents the global spatial distribution of the phyllosilicate-bearing deposits on Mars as seen by MEx/OMEGA.

Makarewicz H. D. Parente M. Bishop J. L.
Determining the Composition of Phyllosilicates Using Automated Gaussian Modeling of Spectral Features **[#1358]**
Kaolinite-montmorillonite and nontronite-ferrihydrite mixture spectrawere analyzed using automated modified Gaussian modeling in order torelate relative band depths with endmember composition in lab spectra,and eventually in CRISM spectra on Mars.

Amador E. A. Bishop J. L. McKeown N. K. Parente M. Clark J. T.
Detection of Kaolinite at Mawrth Vallis, Mars: Analysis of Laboratory Mixtures and Development of Remote Sensing Parameters **[#2188]**
Laboratory mixtures and spectral parameters were created to better characterize and detect kaolinite in the Mawrth Vallis region of Mars where Al-phyllosilicates, including kaolinite and montmorillonite, have been detected.

Tosca N. J.
Clay Mineral Assemblages Derived from Experimental Acid-Sulfate Basaltic Weathering **[#1543]**
Basaltic weathering experiments lasting 295 days have yielded a variety of clay mineral assemblages. Linking clay mineral chemistry to aqueous chemistry provides insight into major controls on clay formation through basaltic weathering.

Hurowitz J. A.
Clay Mineral Formation and Evolution in an Experimental Basaltic Weathering Profile **[#2083]**
This work reports on a new experimental approach aimed at understanding basaltic weathering profile chemical evolution processes using a unique packed-bed flow through reactor design that enables *in situ* analysis of undisturbed alteration minerals.

Che C. Glotch T. D.
The Infrared Spectra Study of Dehydrated and Dehydroxylated Phyllosilicates **[#1482]**
We report the results of changes in the infrared spectra of thirteen phyllosilicates with exposure to increasingly higher temperatures. We hope this will increase the understanding of possible processes affecting phyllosilicate evolution on Mars.

Fairén A. G. Davila A. F. Marzo G. A. Roush T. L. McKay C. P.
Recent Liquid Water on Mars Inferred from Shock Decomposition Analysis of Phyllosilicates Within Impact Craters **[#1156]**
The analysis of the stability of phyllosilicates against shock pressure and temperature after an impact reveal recent water activity on Mars.

Altheide T. S. Chevrier V. F.
Acidic Weathering of Martian-Relevant Phyllosilicates **[#1012]**
Acidic weathering of phyllosilicates with varying pHs of sulfuric acid solutions demonstrates potential relationship between sulfates and phyllosilicates, and may also help explain recent observations of phyllosilicate layered deposits on Mars.

Gavin P. Chevrier V. Ninagawa K. Gucsik A. Hasegawa S.
Experimental Investigation of the Effect of Meteoritic Impacts on Clays on Mars **[#2069]**
Analysis of shock pressures and temperatures reached during impact experiments, as well as XRD and NIR spectral analysis, help determine whether clays found in association with impact craters on Mars were pre-existing or formed during the impact.

ASTROBIOLOGY

Kurosawa K. Sekine Y. Sugita S. Ohkouchi N. Ogawa N. O. Ishibashi K. Kadono T. Ohno S. Matsui T.
Cyanide Production by Chemical Reactions Between Impactor Material and an Ambient Atmosphere After Oblique Impacts **[#1636]**
We conducted laser ablation experiments in redox-neutral gas mixtures using graphite and Murchison meteorite. The results suggest that CN radicals generated by interactions between impactor material and an atmospheric N_2 are fixed into the condensates efficiently.

Hasenkopf C. A. Beaver M. R. Freedman M. A. Tolbert M. A. Toon O. B.
Optical Growth Measurements of Titan and Early Earth Organic Aerosol Analogs **[#1417]**
We report optical growth factors measured for Titan and early Earth aerosol analogs. Water uptake is observed for both analogs. This has important implications for the direct and indirect effects of aerosol that may have existed on Archean Earth.

Cooper G. Sant M. Asiyo C.
Anomalous Enantiomer Ratios in Meteoritic Sugar Derivatives **[#2537]**
The enantiomer (mirror-image) ratios of sugar acids in carbonaceous meteorites have been measured. D-enantiomer excesses are found in all acids measured thus far. This includes rare as well as common compounds.

Foucher F. Westall F. Bény J.-M. Brandstätter F. Demets R.
STONE-6 Experiment: Testing the Survival of Microfossils in Martian Analogues Rocks During Entry into the Earth's Atmosphere **[#1583]**
The aim of the STONE-6 experiment was to determine if martian sedimentary rocks, and the hypothetical microfossils they could contain, can survive the Earth's atmospheric entry.

LeVoci G. Burchell M. J. Tepfer D.
Survival of Seeds in Impacts at 1 km s^{-1} and Above **[#1239]**
Survival of viable seeds in impacts at 1 km/s is demonstrated in laboratory experiments using a light gas gun. Work is continuing to determine the upper limit on impact speeds for seed survival. The implications for Panspermia are discussed.

Edwards L. Huang Y. Schultz P. H.
Preservation of Organic Materials During Hypervelocity Impact Experiments **[#2524]**
Experiments at the AVGR explore the survivability of organic materials trapped within glasses produced by oblique and vertical hypervelocity impacts.

Howe K. L. Gavin P. Goodhart T. Kral T. A.
Methane Production by Methanogens in Perchlorate-supplemented Media **[#1287]**
Perchlorates, found on the martian surface, create a harsh environment. Methanogens are familiar with harsh environments and their growth was tested in perchlorate salt media. All four species of methanogens produced methane at all concentrations of each salt tested.

Conrad P. G. Fogel M. L. Glamoclija M. Kerr L. Mogensen C. Eigenbrode J. Mahaffy P. R. Steele A.
Metrics for Habitability Assessment **[#1384]**
We report an approach to evaluation of habitability potential on another planet, with special relevance to Mars Science Laboratory. We are developing a tool for optimizing the most critical measurements for extraterrestrial environmental assessment.

Vítek P. Jehlička J. Bezdek J. Francu E.
Degradation of β-Carotene Under UV-rich Irradiation Conditions: Implications for Martian Environment **[#1970]**
In this work, degradation of beta-carotene was studied, depending on exposure to the light obtained by metal halide lamp in order to simulate Mars irradiation mainly in the UV region. The protective role of the mineral matrix was also studied and is further discussed.

Allen C. C. Oehler D. Z. Baker D. M.
Mud Volcanoes — A New Class of Sites for Geological and Astrobiological Exploration of Mars **[#1749]**
Mud volcanoes are a unique low-T window into the Earth's subsurface and may prove to be significant sources of atmospheric methane. We report new work suggesting that features in Acidalia Planitia are most consistent with their being mud volcanoes.

Westall F. Foucher F. Cavalazzi B.
No Stromatolites on Mars? **[#1759]**
Easily identifiable microbial traces such as stromatolites are not to be expected on Mars because they could not have evolved before climate change. Martian life will be subtle and difficult to detect *in situ*.

Androes D. L. Dixon J. C. Zachry D. L.
The Evolution of Astronomically-forced Siliclastic Rhythmites of the Ancient Earth and their Correlation to Banded-Iron Formations **[#2323]**
Although the bulk of past research presumes that metamorphism, Milankovitch or climatic events have annihilated or overprinted any small-scale, orbitally-influenced, ubiquitous BIF laminations, recent research suggests preservation of small scale patterns is possible.

Socki R. A. Niles P. B. Blake W. Jr. Leveille R.
Covariant C and O Isotope Trends in Arctic Carbonate Crusts and ALH 84001: Potential Biomarker or Indicator of Cryogenic Formation Environment? **[#2218]**
Covariant C and O micro-scale isotope trends in arctic carbonate crusts mimic, to a lesser extent, those in ALH 84001 and are ideal terrestrial analogs for the isotopic composition of the ALH 84001 carbonates, implying a similar formation environment.

Lemelle L. Salome M. Westall F. Susini J. Simionovici S.
In Situ Search for Traces of Life in Extraterrestrial Samples Using X-Ray Spectromicroscopy at the Sulfur K-Edge **[#1842]**
Two selected case studies (Stardust keystones and Draken's Neoproterozoic cells) exemplify the relevance of micro-X-ray fluorescence at the S K-edge performed at the ID21 beamline of the ESRF to search for traces of life in extraterrestrial samples.

Jimenez-Lopez C. Romanek C. Rodriguez-Navarro A. Perez-Gonzalez T. Rodriguez-Navarro C.
Magnetites Formed from Thermal Decomposition of $(Ca,Mg,Fe)CO_3$: "Foreign" Cation Incorporation into the Estructure of Magnetite **[#1255]**
Pure magnetites are obtained from ankerite thermal decomposition. Chemical purity is typical of bacterial origin magnetites. Chemical purity of magnetites produced by thermal decomposition of ankerites containing different cations was analyzed.

Gánti T. Pócs T. Bérczi Sz. Horváth A. Kereszturi A. Sik A. Szathmáry E.
Ideal Microhabitats on Mars: The Astrobiological Potential of Polar Dunes **[#1618]**
Astrobiological potential of polar Dark Dunes: they may hold less oxidants, trap water-ice, mm layer of them shields UV radiation, allows light income for photosynthesis. Water uptake in nighttime, temperature in daytime is favorable for metabolism.

Banerjee N. R. Bridge N. J. Izawa M. R. M. Anderson L. D. Bebout G. E. Flemming R. L.
Glassy Subaqueous Lavas as a Habitat for Life on Earth, Mars, and Elsewhere? **[#1331]**
Biogeochemical and mineralogical traces of life preserved in modern and ancient terrestrial subaqueous lavas suggest basaltic rocks on Mars and other rocky bodies may represent an underappreciated habitat for life in the solar system.

Kong F. J. Zheng M. P. Wang A. L. Ma N. N.
Endolithic Halophiles Found in Evaporite Salts on Tibet Plateau as a Potential Analog for Martian Life in Saline Environment **[#1216]**
Mg-sulfates was found within salt deposits of the Da Langtan playa on Tibet plateau, similar as those found on Mars. Halophiles were isolated from the evaporative salts in the environment for analogs of the search for martian life in subsurface.

Cabrol N. A. Grin E. A. Wynne J. J.
Detection of Caves and Cave-bearing Geology on Mars **[#1040]**
Regions on Mars likely to contain caves and/or cave-bearing geology are identified using multispectral imagery from orbital missions and the exploration of terrestrial analogs for the characterization of associated thermal, and geo-signatures.

INSTRUMENT CONCEPTS, SYSTEMS, AND PROBES FOR INVESTIGATING ROCKS AND REGOLITH

El Shafie A. Ulrich R. Roe L.
Penetration Forces for Subsurface Regolith Probes **[#1205]**
Penetration and withdrawal forces have been measured for a variety of sizes and tip angles of penetrometers designed to carry instrumentation beneath the surface of a planetary body.

Pilgrim R. Ulrich R. Leftwich M.
Subsurface Spectroscopic Probe for Regolith Analysis **[#1219]**
A subsurface penetration probe is being developed for *in situ* FTIR analysis of the first 1/2 m of planetary bodies. The work describes the optical configuration.

Paulsen G. Zacny K. Maksymuk M. Wilson J. Mumm E. Craft J. Davis K. Kumar N.
Drilling in Ice Bound Lunar Regolith Simulant **[#1138]**
We describe drilling tests in frozen, water saturated lunar regolith simulant and present designs of the 3 m tall Mars chamber dedicated to 1 meter drilling tests.

Glass B. Thompson S. Hanagud S. Statham S. Cohen J. Lee P. Osinski G. Huffman S.
Planetary Drill Prototype Testing at an Impact Structure Palaeo-Hydrothermal Site **[#2197]**
A July 2008 field test effort updated and tested DAME drilling automation in a relevant planetary analog environment (a palaeo-hydrothermal chimney in permafrost inside Haughton Crater). Cores and cuttings were successfully retrieved and archived.

Johnson J. B. Mungas G. S. Zacny K. Albert D. G. Banerdt B. Buehler M. Elphic R. C. Lambert J. Sturm M. Johnson K.
A Lunar Regolith Characterization Kit (LRoCK) **[#1987]**
The Lunar Regolith Characterization Kit (LRoCK) project is a concept study to define a semi-autonomous instrument package for use by astronauts during future human lunar sortie missions.

Zacny K. Mungas G. Chu P. Craft J. Mumm E. Hedlund M. Paulsen G. Davis K.
MarsVac: A Two Step Regolith Sampling System **[#1068]**
A system for acquiring regolith consists of tubing embedded inside each leg of a lander. After landing, the tube will be pushed into regolith. With one puff of gas, the trapped regolith can be lifted/guided inside the tubing into a sample chamber.

Simionovici A. S. Lemelle L. Beck P. Ferroir T. Westphal A. Chazalnoel P. Debus A. Viso M. Vincze L. Solé A. V. Fihman F.
Methodology and Sample Holder for Analyses Under Quarantine of Martian Return Samples **[#2543]**
A method and a sample holder for analysis in quarantine conditions of Mars return samples is presented.

Scheeres D. J. Sánchez P. Dissly R. W. Asphaug E. I. Housen K. R. Swift M. R. Yano H. Roark S. E. Soto J. C.
Extra Low-Gear: A Micro-Gravity Laboratory to Simulate Asteroid Surfaces **[#2447]**
The conceptual design and application of a low-speed centrifuge for carrying out milli to micro-*G* gravity experiments to simulate the granular nature of the surface and interiors of asteroids and comets is described.

Bartlett P. W. Heys S. Drozdowski Z. Kennedy T. Wagner M.
Vertical Exploration Using Tethers **[#2146]**
Unobserved geologic features and epochs on multiple planetary bodies could be accessed using robotic tethers. Recent technology development shows the promise of tethers enabling steep slope mobility, downhole measurements and *in situ* sensing from aerial platforms.

Curtis S. A. Clark P. E. Minetto F. A. Calle C. I. Keller J. Moore M.
SPARCLE: Creating an Electrostatically Based Tool for Lunar Dust Control **[#1128]**
Here we present the results of our ongoing efforts to design and develop tools to remove dust on the lunar surface based on our characterization of the nature of dust particles and forces affecting them.

Anderson R. C. Peters G. H. Beegle L. Pounders E. Manatt K. Solitt L. Fleming G.
Particle Transport on the Mars Science Laboratory Mission: Effects of Triboelectric Charging **[#1648]**
One of the major challenges facing the 2009 Mars Science Laboratory (MSL) onboard analysis system is the ability to successfully transfer fine-grained powders from the sample acquisition unit to the analytical instruments that make the scientific measurements.

Brinckerhoff W. B. Zacny K. ten Kate I. L. Kusack A. Conrad P. G. Franz H. B. Eigenbrode J. Mahaffy P. R. Corrigan C. M. Onstott T. C.
Precision Subsampling System for In Situ Analysis at Mars (and Beyond) **[#2240]**
A new MIDP-supported effort seeks to develop a precision subsampling system (PSS) for Mars and other planetary bodies. The PSS will enable localized chemical and isotopic analyses of drill core layers and other small features in rock samples.

Dreyer C. Zacny K. Skok J. Steele J. Paulsen G. Szczesiak M. Nakagawa M. Schwendeman J.
Progress on the Development of a Thin Section Sample Preparation Device for Space Exploration **[#2463]**
We are researching the component step for thin section preparation with the aim of producing a device for space exploration. We show results of a prototype system that has produced a thin section adequate for petrographic analysis.

Furutani K. Ikeda E. Okada T. Saiki K. Ohue H.
Prototype of Cutting Machine by Wire-sawing in Vacuum for In-Situ Investigation of Rocks **[#1044]**
Cutting characteristics of rocks in air and vacuum were investigated for the preprocess of the scientific inspection. The machining amount of basalt with a wire saw in vacuum was saturated in a short time due to loading of pulverized debris.

Nuñez J. I. Farmer J. D. Sellar R. G. Gardner P. B.
The Multispectral Microscopic Imager (MMI) with Improved Spectral Range and Resolution **[#1830]**
The MMI advances the capabilities of current and planned microimagers, such as Phoenix' Robotic Arm Camera and Mars Science Laboratory's Mars Hand Lens Imager, by extending the spectral range into the infrared and increasing the number of spectral bands.

Michael G. Neukum G.
Image Enhancement of the Super Resolution Channel (SRC) of the Mars Express HRSC Experiment **[#1851]**
The poster describes and shows the application of the Richardson-Lucy algorithm to recover degraded images from the super resolution channel (SRC) of Mars Express HRSC.

Weinberg J. D. Dissly R. Nicks D. Miller K. L.
Applications and Field Testing of a Flash LIDAR System for Future Planetary Missions **[#2078]**
A flash LIDAR instrument is being developed by Ball Aerospace. This instrument enables multiple applications for planetary missions such as topographic mapping, ranging, surface mobility, autonomous rendezvous and docking, and descent and landing.

Istenes Z. Hargitai H. Tepliczky I.
The Information System of the HUNVEYOR-10 on the MDRS **[#2435]**
We created a portable and autonomous meteorological station, called HUME/HUNVEYOR-10, for the 71st. mission of the Mars Desert Research Station (MDRS), to measure continuously meteorological data, to take videos and to transmit them.

Bramall N. E. Stoker C. R. Price P. B. Allamandola L. J.
Detecting Organics In Situ Using Fluorescence **[#2470]**
Fluorescence spectroscopy is a powerful tool for the detection of a wide class of organics. We will discuss instruments we have developed and are developing.

Sharma S. K. Misra A. K. Acosta T. Bates D. Lucey P. G.
Compact Portable Remote Raman System for Planetary Exploration and Rapid Detection of Water and Hydrous Minerals **[#2398]**
We present a compact remote Raman system utilizing only a 85 mm Nikon camera lens for measuring good quality Raman spectra of various minerals, water, water-ice, CO_2-ice, organic and inorganic chemicals to a distance of 9-m with 1-s integration.

Vance S.
Mars Analog Tunable Laser Spectroscopy at a Site of Active Serpentinization **[#2005]**
We discuss measurements of isotope compositionsfrom spring samples collected at The Cedars, a site of active serpentinization and possibly an analog for the Nili Fossae, using tunable laser spectroscopy withinstrumentation similar to TLS on MSL.

Helbert J. Maturilli A. D'Amore M.
Mercury in a Box — In the Planetary Emissivity Laboratory (PEL) at DLR Berlin **[#1560]**
Analyzing the surface composition of Mercury is a challenging task. In support of MESSENGER and BepiColombo the upgraded Planetary Emissivity Laboratory can obtain emissivity measurement for fine grain sizes and at temperatures typical for Mercury's low-latitude dayside.

Bowles N. E. Calcutt S. Reininger F. Green S. F. Mortimer H.
The Asteroid Thermal Mapping Spectrometer: An Imaging Mid-IR Spectrometer for the Marco Polo NEO Sample Return Cosmic Vision Candidate Mission **[#1591]**
We describe the Asteroid Thermal Mapping Spectrometer (ATMS) instrument, a compact imaging mid-IR Fourier transform spectrometer currently being developed at the University of Oxford for NEO remote sensing applications.

Sobron P. Freeman J. J. Wang A.
Field Test of the Water-Wheel IR (WIR) Spectrometer on Evaporative Salt Deposits at Tibetan Plateau **[#2372]**
A new NIR reflectance spectrometer (WIR) was tested at the field sites on the Tibetan Plateau, a potential analog for the precipitation sequence and subsequent dehydration/degeneration of martian salts. Hydrated sulfates were identified.

Kozyrev A. S. Litvak M. L. Malakhov A. A. Mokrousov M. I. Mitrofanov I. G. Rogozhin A. A. Sanin A. B. Schulz R. Schvetsov V. N. Tretyakov V. I. Vostrukhin A. V.
Gamma-Rays and Neutron Spectrometers NS HEND — Tool for Study of Phobos Surface Composition **[#1865]**
NS HEND instrument, as the part of "Phobos-Grunt" mission, will be able to provide observational data for composition of Phobos regolith and content of natural radioactive elements K, U and Th, and also for content of hydrogen or water ice in the Phobos subsurface.

Elam W. T. Kelliher W. C. Shuler R. L. McLennan S. M. Carlberg I. A.
Improvements in X-ray Spectrometry for Planetary Surface Exploration **[#1820]**
There have been dramatic advances in X-ray spectrometry (XRS) hardware in recent years. Together they permit construction of XRS units with very low mass, power, and size yet have performance comparable to that of terrestrial laboratory units.

Grunthaner P. J. Bryson C. Gill D. Grunthaner F. Kelly M. DeFlores L. White V. Quinn R.
Ambient-Pressure X-Ray Photoemission Spectrometer for Surface Analysis of Planetary Surfaces **[#2294]**
Ambient-pressure X-ray photoemission offers the possibility of probing the surface chemistry of martian soils, rocks, and ices, including the atmospheric species interacting with these surfaces, to study geochemical surface processes.

Chemtob S. M. Yen A. Blake D. F.
The X-Ray Fluorescence Capabilities of CheMin IV: Data Reduction and Calibration **[#2171]**
CheMin, the primary instrument on the MSL rover for determining mineralogy, also features XRF capabilities. Here we present data reduction and calibration methods for determining composition of geologically relevant materials from CheMin XRF spectra.

Flemming R. L. McCausland P. J. A. Gellert R.
In Situ X-Ray Diffraction on the Moon, Mars and Asteroids **[#1888]**
In situ XRD can directly determine mineralogy of samples on planetary surfaces via crystal structural information, to compliment chemical data (e.g. APXS), with no need for sample extraction/pulverization. Lab-based e.g. are given using meteorites.

Sarrazin P. Dera P. Downs R. T. Blake D. F. Bish D. Gailhanou M.
Hybrid X-ray Diffraction for Planetary Mineralogical Analysis of Unprepared Samples **[#1496]**
A new type of X-ray diffraction (XRD) planetary instrument is being developed based on an innovative hybrid concept that allows performing both powder and single-crystal XRD measurements, making it possible to analyze minerals with limited or no sample preparation.

UP CLOSE AND PERSONAL: IN SITU ANALYSIS WITH LASER-INDUCED BREAKDOWN SPECTROSCOPY AND MASS SPECTROMETRY

Maurice S. Wiens R. Parès L. Bender S. le Roch N. Dalmau J. Berthé M. Langevin Y. Herkenhoff K. Bridges N. Saccoccio M. ChemCam Team
Characterization of the ChemCam (MSL) Imaging Capability **[#1864]**
The ChemCam instrument comprises a Remote Micro-Imager (RMI) to place the LIBS analyses in their geomorphologic context. We present RMI flight unit test results, including the characteristics and performances of this imaging capability on MSL.

Forni O. Clegg S. Wiens R. C. Maurice S. Gasnault O.
Multivariate Analysis of ChemCam First Calibration Samples **[#1523]**
We present a multivariate analysis of the first calibration of the ChemCam LIBS instrument on board MSL. We use two methods PCA and ICA on the same data set and compare them.

Mungas G. S. Dreyer C. B. Bauer A. J.
Elemental Abundance Measurement Using Micro-LIBS for Space Exploration **[#2264]**
LIBS elemental measurements suffer from inaccuracies we believe are fundamentally tied to uncertainty in the LIBS plasma thermal history. We propose a method to decode plasma temperature history with elemental abundance from observed emission lines.

Perkins J. J. Sharma S. K. Clegg S. M. Misra A. K. Wiens R. C. Barefied J. E.
Remote Laser-induced Breakdown Spectroscopy (LIBS) Analysis of Hydrated Sulfates **[#1397]**
We report here the use of remote LIBS for determining degree of hydration in sulfate minerals. With LIBS onboard MSL it will be possible to glean information about the degree of hydration along with major and minor elements on the surface of Mars.

Fabre C. Maurice S. Sautter V. Wiens R. Dubessy J. Boiron M. C. CHEMCAM Team
Onboard Calibration Silicate Targets for the Chemcam LIBS Instrument (MSL Rover) **[#1502]**
The MSL rover lander will carry rover-mounted calibration targets. The chemical compositions of the basaltic targets were checked using electron microprobe. The homogeneity is very good at the micrometric scale, even for the trace elements.

Rauschenbach I. Jessberger E. K. Hübers H. W. Pavlov S. G.
Miniaturized Laser-induced Breakdown Spectroscopy for Planetary Surface Analysis **[#1563]**
LIBS is currently under development for future lander missions to Mars and other planets and moons. Here we report on our study of different parameters that are of importance for a lightweight LIBS instrument specifically in the martian environment.

Cousin A. Maurice S. Parot Y. Michel Y. Le Roch N. Dalmau J. Parès L. Perez R. Cros A. Wiens R. ChemCam Team
ChemCam (MSL) Autofocus Capabilities **[#1684]**
ChemCam is a remote instrument to investigate martian geochemistry, using the LIBS technique, a board of the MSL rover. The aim of this work is to present the initial calibration of ChemCam, and to investigate the effect of the rocks' parameters on the autofocus function.

Laan E. C. van Westrenen W. Wielders A. Heiligers J. MoonShot Partners
MoonShot: A Combined Raman/LIBS Instrument for Lunar Exploration **[#1836]**
A consortium led by the Dutch Organisation for Applied Scientific Research with partners from Dutch industry and academia aims to provide a combined Raman/LIBS instrument as scientific payload for lunar and planetary exploration missions.

Vaniman D. T. Clegg S. Lanza N. Newsom H. Wiens R. C. ChemCam Team
Fabrication of Sulfate-bearing Ceramic Calibration Targets for the ChemCam Laser Spectroscopy Instrument, Mars Science Lander **[#2296]**
A need for sulfur-bearing calibration targets for LIBS analysis by ChemCam on the Mars Science Lander required development of low-fire ceramics. A range of sulfur contents can be obtained that mimic soil or rock at the potential landing sites.

Tucker J. M. Dyar M. D. Clegg S. M. Schaefer M. W. Wiens R. C. Barefield J. E. II
LIBS Analysis of Minor Elements in Geologic Samples **[#2024]**
The first investigation of minor element detection by LIBS for ChemCam calibration shows promise for identification and quantification of minor elements by statistical techniques.

Anderson F. S. Nowicki K.
In-Situ LDRIMS Geochronometry for the Moon and Mars **[#2290]**
Latest progress on the development of a Laser Desorption Resonance Ionization Mass Spectrometer (LDRIMS) instrument for *in situ* rubidium-strontium (Rb-Sr) geochronology.

Strashnov I. Blagburn D. J. Gilmour J. D.
Resonant Photoionization Mass Spectrometer for Determination of Isotopic Compositions of Krypton in Extraterrestrial Samples **[#1645]**
An ultra sensitive MS for determination of Kr has been developed. A four wave mixing in Xe is used for generation of vuv light necessary for the first resonant step of three color ionization scheme. Kr isotopic ratios of air samples and Stannern meteorite determined.

Mahaffy P. R. Hodges R. R. Benna M. Harpold D. N. Kasprzak W. K. Kellogg J. W. King T. T.
Neutral Mass Spectrometer Under Development for the Lunar Atmosphere and Dust Environment Explorer (LADEE) Mission **[#1217]**
Description of the Neutral Mass Spectrometer that is one of three instruments under development for the Lunar Atmosphere and Dust Environment Explorer (LADEE) Mission.

Nagashima K. Huss G. R. Kosaka K. Kunihiro T. Keil K. Krot A. N. Taylor G. J. Yurimoto H.
Development of Isotope Imaging System with Two-Dimensional Ion Detector SCAPS for ims-1280 Secondary Ion Mass Spectrometer **[#2066]**
We are developing a new imaging detector system using the SCAPS in combination with the University of Hawaii Cameca ims-1280 SIMS instrument. We present results of initial tests of the system as well as details of the system.

Davis A. M. Stephan T. Veryovkin I. V. Pellin M. J. Savina M. R.
The Ion Nanoprobe: A New Instrument for Studying the Isotopic and Elemental Composition of the Solar System and Beyond at the Few-Nanometer Scale **[#2472]**
The ion nanoprobe is a new instrument designed for isotopic, chemical, and possibly molecular analysis at lateral resolutions of a few nanometers. This instrument, now under construction, will be applied to a broad range of problems in cosmochemistry.

Hilchenbach M. Lang T. Hornung K. Thirkell L. Briois C.
UV-Laser Desorption Ion Source Applied to a Secondary Ion Mass Spectrometer **[#1162]**
We were focusing on using a new UV laser ion desorption source combined with a SIMS laboratory time-of-flight mass spectrometer, the latter being very similar to the COSIMA flight instrument onboard Rosetta.

Greer F. Fisher A. Corso T. MacAskill J. Willis P. A.
Nanospray Ionization for Coupling Capillary Electrophoresis with Mass Spectrometry for In Situ Titan Exploration **[#2200]**
This paper will present the status of our effort to develop a Lab-on-a-Chip instrument coupling microCE to MS via nanospray ionization enabling *in situ* detection and analysis of target compounds on Mars or the moons of the outer solar system.

JUPITER AND INSCRUTABLE IO

Visscher C. Sperier A. D. Moses J. I. Keane T. C.
Phosphine and Ammonia Photochemistry in Jupiter's Troposphere **[#1201]**
A photochemical model is developed for Jupiter's troposphere using updated constraints. The results suggest that diphosphine is an important aerosol component and that coupled ammonia-acetylene photochemistry is inhibited in Jupiter's atmosphere.

Williams D. A. Keszthelyi L. P. Crown D. A. Geissler P. E. Schenk P. M. Yff J. Jaeger W. L.
Volcanism on Io: Insights from Global Geologic Mapping **[#1403]**
We discuss latest insights into the volcano-tectonic evolution of Io based on global geologic mapping.

Bunte M. K. Williams D. A. Greeley R. Jaeger W. L.
Geologic Mapping of the Hi'iaka and Shamshu Regions of Io **[#1468]**
We present regional geomorphologic maps of the Hi'iaka and Shamshu regions of Io. The regions are characterized by varied volcanic and tectonic activity as well as progressional degradation. Volcano-tectonic interactions formed the Hi'iaka complex.

Barth B. Radebaugh J. Christiansen E. H.
Classification of Io's Paterae: Active vs Inactive **[#2397]**
On Io, the proportion of paterae with active volcanism, as judged from the presence of dark deposits within their margins, correlates with the total number of paterae in a longitudinal band and is highest in the sub-jovian and anti-jovian regions.

Allen D. Radebaugh J.
Ionian Volcanoes Reveal Their Temperatures **[#1475]**
Color temperature analyses were conducted on three hotspots using Cassini ISS data of the surface of Io in eclipse by Jupiter. The data for Pillan, Loki, and Wayland will be presented.

Keszthelyi L. P. Davies A. G. McEwen A. S.
Optimal Wavelengths for Studying Thermal Emission from Active Volcanoes on Io **[#1943]**
Eruption temperature of Io lavas can be constrained by new observations at ~0.8 and ~1 microns. Eruption style and heat flow are best studied at 2, 3, 4, 6, 8, 15, and 20 microns with 2, 5, and 8 microns being the most essential.

Rathbun J. A. Spencer J. R.
Ground-based Observations of Io in Support of the New Horizons Flyby **[#2177]**
We observed Io on 21 nights in 2006–2007 in support of the February, 2007 New Horizons flyby. We found that Tvashtar had been volcanically active for at least a month prior to the flyby and that at least four volcanoes were active on the Jupiter-facing hemisphere.

Borer N. Chen E. M. A. Choi D. S. Craft K. L. Fortenberry R. Harben J. Issacson P. Johnson A. Jones I. Mabry J. McDunn T. Millham R. A. Pankine A. Prater A. Cowardin H. M. Smith D. J. Snowden D.
Argus: A New Frontiers Mission to Observe Io **[#1062]**
A proposal to study Io, the most volcanically active solar system body. Study of volcanic activity, composition, tidal heating, atmospheric composition, mass wasting and magnetosphere interactions furthers understanding of dynamic planetary process.

McDoniel W. J. Goldstein D. Varghese P. Trafton L. Stewart B.
DSMC Modeling of 3D Vent Geometries for Ionian Plumes **[#2223]**
We study the effects of vent asymmetry on Io's volcanic plumes, with a focus on the difference between a disk source and a half annulus source, and show how the half annulus source can still lead to a fairly symmetric deposition ring.

TANTALIZING TITAN

Hayne P. McCord T. B. Barnes J. W.
Titan's Near Infrared Atmospheric Transmission and Surface Reflectance from the Cassini Visual and Infrared Mapping Spectrometer **[#1863]**
Using a ground calibration target method, we calculate Titan's atmospheric transmission and surface albedo in the 0.8 - 5.0 micron wavelength range. Two of Titan's most interesting features, Tui Regio and Hotei Regio, are depleted in water ice.

Rodriguez S. Crapeau M. Le Mouelic S. Paillou P. Barnes J. W. Brown R. H. Sotin C. Wall S.
Cassini VIMS and RADAR Altimeter Joint Study of Titan Surface **[#1596]**
Correlations between Cassini/Altimeter data and VIMS underlying images of Titan's surface suggest the presence of very local enrichments in water ice linked with smooth depressions, maybe hinting an ancient channel connected to a large basin.

Langhans M. Jaumann R. Stephan K. Brown R. H. Buratti B. J. Clark R. Baines K. H. Nicholson P. D. Lorenz R. D.
Fluvial Valleys on Titan — A Global Perspective **[#1681]**
Fluvial valleys on Saturn's largest moon, Titan, are investigated in this study. A global overview about the arrangement of fluvial channels is given. Spectral properties of fluvial regions were analysed based on Cassini-VIMS-data.

Burr D. M. Aliaga-Caro J. F. White B. R. Marshall J. R. Greeley R. Bridges N. T.
Numerical Modeling of Titan Aeolian Sediment Transport: Preliminary Threshold Wind Speed and Trajectory Results **[#2098]**
Preliminary numerical modeling of aeolian sediment transport parameters under Titan conditions is provided, for future testing in wind tunnel experiments.

Savage C. J. Radebaugh J.
Titan as a Laboratory for Linear Dune Formation **[#1005]**
We present results of a detailed morphological study of Titan's linear dunes showing sediment induration by liquids may be causing differences in dune width and interdune spacing between northern and southern hemispheres.

Neish C. D. Lorenz R. D. Kirk R. L.
Out of Africa: Radarclinometry of the Sand Seas of Namibia and Titan **[#1071]**
Far from the Namib; Dunes of organic solids; Mimic quartz cousins.

Stofan E. R. Farr T. Kirk R. L. Lopes R. M. Lorenz R. Lunine J. I. Mitchell K. L. Paillou P. Radebaugh J. Wall S. W. Wood C. A. Cassini Radar Team
Morphology of Four Flow Fields on Titan: Implications for Modes of Origin **[#1043]**
We describe four flow fields associated with channels that have been observed in Cassini Radar data of Titan.

Wood C. A. Stofan E. R. Paganelli F. Lorenz R. D.
Fluctus and Virgae of Titan **[#2277]**
Fluctus are bright flows on Titan with lobate margins and linear sources. If they are volcanic features they are evidence for tectonic control. Shiwanni Virgae is dune material that diverts around obstacles. They are not tectonic.

Janssen M. A. Le Gall A. Wye L. C. Zebker H. A. Lorenz R. D. Paillou P. Paganelli F. Cassini Radar Team
Anomolous Radar Backscatter from Titan's Xanadu **[#1916]**
We use simultaneously measured radar reflectivity and microwave emission from the Cassini Radar instrument to show that the radar backscattering seen across Titan's Xanadu region is too high to be explained by any known surface model.

Le Gall A. Janssen M. A. Lorenz R. D. Zebker H. Wye L. Paillou P.
Radar-Bright Channels on Titan **[#1533]**
The Cassini SAR observed channels in the Xanadu region of Titan which exhibit very large radar cross-sections. We propose the presence of (transparent) rounded, icy rocks with size larger than the radar wavelength (2.18 cm) to explain observations.

Lorenz R. D. Hayes A. Callahan P. Gim Y. Janssen M. Wall S. Le Gall A. Mitchell K. Zebker H. Wye L. Lunine J. Aharonson O. Kirk R. Wood C. Alberti G.
Ontario Lacus: Brilliant Observations of a Titan Lake by the Cassini Radar Altimeter **[#1990]**
Rad altimetry, Ontario, truly flat, Glints like a mirror..

Jaumann R. Neukum G.
The Surface Age of Titan **[#1641]**
Although the statistical precision of the Titan cratering results is not very high it is obvious that Titan's surface is partly as old as the other saturnian satellites and has been partly modified and heavily resurfaced .

Zahnle K. Korycansky D.
Some Possible Consequences of Menvra Impact on Titan **[#2390]**
The energy released by the Menvra impact was marginally large enough to melt and evaporate significant amounts of water, and thus cause rain. The energy of this and other impacts was large enough to evaporate significant amounts of methane.

Fukuzaki S. Sekine Y. Kurosawa K. Sugita S. Kadono T. Matsui T.
Impact Devolatilization of Ammonium Sulfate: Implications for the Origin of N_2 in Titan's Atmosphere **[#1575]**
We assess the role of devolatilization of $(NH_4)_2SO_4$ in Titan's crust by cometary impacts for the origin of N_2 by laboratory experiments. Our results suggest that the N_2 production for 4.5 Gyr reaches ~2.5–10 times that in the present atmosphere.

Berezhnoy A. A.
Nitrogen on Early Titan **[#1077]**
An early NH_3-rich Titan's atmosphere can be converted into the N_2-rich atmosphere without significant changes in the isotopic composition of N and H. The dissociative fractionation factor and the initial atmospheric mass of Titan are estimated.

ENIGMATIC ENCELADUS AND INTRIGUING IAPETUS

Hanna B. J. Yeoh S. K. Goldstein D. B. Varghese P. L. Trafton L. M.
Free-Molecular and Collisional Studies of Enceladus' Water Vapor Plumes **[#2389]**
The free-molecular and the direct simulation Monte Carlo (DSMC) codes are used to simulate the water vapor plumes observed on the south pole of Enceladus during the three orchestrated flybys in 2005 by Cassini.

Lisse C. M. Weaver H. A. Perry M. E. Turtle E. P. Hibbitts C. A. Dello Russo N.
Comparing Enceladus to Comets: Implications for Their Outgassing Activity **[#2299]**
Using results from Voyager and Cassini observations, we investigate the compositional similarities between Enceladus' plumes and cometary comae and compare the physical properties (densities, speeds, collimation) of the plumes and cometary jets.

Boice D. C. Goldstein R.
Is Enceladus a Comet? A Cometary Perspective **[#1506]**
The discovery of icy plumes emanating from Saturn's moon, Enceladus, by the Cassini spacecraft has raised questions about its cometary nature. Enceladus represents a transitional object, intermediate to the atmospheres of large satellites and the extended comae of comets.

Barr A. C.
Limits on Heat Transport and Resurfacing Rates Due to Mobile Lid Convection Beneath Enceladus' South Polar Terrain **[#2378]**
The high heat flux and intense surface deformation at Enceladus' south pole suggests that convective plumes reach close to the surface. I derive limits on the heat flux and resurfacing rate due to mobile lid convection.

Patthoff D. A. Kattenhorn S. A.
Establishing a Long-Term Fracture History of the South Polar Terrain on Enceladus **[#2513]**
Fracture mapping of the SPT on Enceladus will help to resolve the history of the tiger stripes and the surface of the moon through detailed analysis of the fracture types, orientations, and relative ages.

Hurford T. A. Bills B. G. Helfenstein P. Greenberg R. Hoppa G. V. Hamilton D. P.
Using Geological Implications of a Physical Libration to Constrain Enceladus' Libration State **[#1631]**
We describe how a physical libratrion might affect eruption variability, tidal shear heating and crack formation. These effects might be observable with Cassini data and allow the libration state to be constrained.

Morito H. Kimura J. Kawamura T. Morota T. Honda C. Kobayashi Y. Okada T.
Sublimation Impact for the Temporal Change of Albedo Dichotomy on Iapetus **[#1621]**
In this work, we evaluate the effect on icy sublimation and temporal change of surface albedo, and we try to reconstruct the original distribution the dark material on Iapetus.

Galuba G. G. Denk T. Neukum G.
Dark Crater Surfaces in Bright Areas on the Saturn Moon Iapetus **[#1792]**
The explanation why the Cassini Regio on Iapetus is dark is supplemented by an explanation why on the bright trailing side there are dark crater bottoms.

ICY SATELLITES: CRYPTIC CRATERS

Kirchoff M. R. Schenk P.
Impactor Populations in the Saturnian System: Constraints from the Cratering Records **[#2067]**
We use the cratering records of heavily cratered terrains of Mimas, Tethys, Dione, Rhea, and Iapetus to help constrain characteristics of impactor populations in the saturnian system.

Karpes B. A. Stoddard P. R.
The Cataloging of Craters on Enceladus **[#1306]**
We catalog craters of Enceladus, using publicly available images, and make some preliminary analysis.

Yozzo J. E. Kirchoff M. R. Schenk P.
Apex-Antapex Asymmetry of Impact Crater Density on Ganymede's Dark Terrain **[#2214]**
This abstract focuses on the asymmetry of impacts between Ganymede's apex and antapex of motion using the dark terrain of Ganymede and attempts to provide an explanation for the lack of a large predicted asymmetry.

Mukherjee P. Barlow N. G.
A Catalog of Impact Craters on Ganymede **[#2071]**
We are compiling a catalog of all impact craters on the jovian moon Ganymede which are larger than 3 km in diameter. We discuss preliminary results regarding interior morphologies associated with these craters.

Alzate N. Barlow N. G.
Analysis of Central Pit Craters on Ganymede and Implications for Pit Formation Models **[#1921]**
We have completed our survey of central pit craters on Ganymede. We discuss the characteristics and distributions of these central pit craters and the implications for central pit formation models.

ICY SATELLITES: GELID GEOLOGY/GEOPHYSICS

Schulson E. M.
Frictional Sliding of Cold Ice **[#1795]**
This paper reviews current knowledge of frictional sliding in water ice Ih, a fundamental process underlying tectonic activity within the icy crusts of Enceladus and Europa, and raises a number of questions.

Bland M. T. McKinnon W. B. Showman A. P.
Forming Ganymede's Grooves: Producing Large-Amplitude, Complex Deformation **[#1690]**
We present the first numerical simulations that realistically reproduce the complex deformation observed in Ganymede's grooved terrain. This deformation results from the inclusion of strain weakening effects in the ice rheology.

Damptz A. L. Dombard A. J.
Time-dependent Flexure on the Icy Satellites of Jupiter and Saturn **[#1316]**
In this work we explore the "static" assumption of models of lithospheric flexure that have been used on these icy satellites. We find that creep within the lithospheres is non-negligible, leading to progressive thinning of the lithosphere.

Goff-Pochat N. Collins G. C.
Strain Measurement Across Fault Scarps on Dione **[#2111]**
In this presentation we display the calculated surface strain over fault sets on Dione, and provide an analysis of the overall surface strain accommodated on Dione.

Wagner R. J. Neukum G. Stephan K. Roatsch T. Wolf U. Porco C. C.
Stratigraphy of Tectonic Features on Saturn's Satellite Dione Derived from Cassini ISS Camera Data **[#2142]**
Cassini ISS images were used to derive a stratigraphic sequence of tectonic landforms (troughs, ridges, scarps, lineaments) on Saturn's icy satellite Dione.

Kay J. P. Kattenhorn S. A.
Searching for Evidence of Active Tectonics on Europa **[#2454]**
Evidence of recent tectonic activity on Europa logically starts with the geologically young, ridgeless surface fractures. The temporal relationship between young fractures and their orientations could yield information about recent tectonic activity.

Coulter C. E. Kattenhorn S. A. Schenk P. M.
Topographic Profile Analysis and Morphologic Characterization of Europa's Double Ridges **[#1960]**
Ridges on Europa have very low slopes and limiting values of height/width that suggest viscoplastic gravitational collapse over time. Variability between ridges may point to disparate formation kinematics.

Singer K. N. McKinnon W. B.
Pits, Spots, Uplifts, and Small Chaos Regions on Europa: A Search for Regional Variations **[#2336]**
Mapping of a sample region illustrates how data obtained in ArcMap can be used to investigate the spatial and size frequency distribution of small features on Europa. We hope further mapping will shed light on the physics of feature formation.

Rodriguez N. J. Rathbun J. A. Spencer J. R.
Europa's Thermal Surface from Galileo PPR **[#2166]**
We present Galileo Photopolarimeter-Radiometer data of Europa and, from these, model the thermal inertia and bolometric albedo of the surface. We also derive an upper limit for detection of endogenic activity.

El Maarry M. R. Sierks H.
Geological, Geochemical and Engineering Considerations for Choosing a Landing Site on the Jovian Moon Europa **[#2014]**
Geological, geochemical, and engineering constraints on choosing a suitable landing site for lander on the jovian moon, Europa, are discussed briefly.

Stryk T. Stooke P. J.
Triton Crescent Imaging Revisited: Cartography and Geology **[#1710]**
Voyager 2 images of the outbound crescent of Triton are specially processed, added to a global map and interpreted geologically. Plains, hills, cantaloup-type areas and possible flows are mapped.

ICY SATELLITES: COOL CHEMISTRY AND SPECTACULAR SPECTROSCOPY

Hansen G. B. Apple S. K. Shin-White E.-J. Z.
Water Ice Abundance and Grain Sizes, and Non-Ice Materials on the Saturnian Satellite Phoebe from Cassini/VIMS Observations **[#2227]**
We are modeling Cassini-VIMS spectra from an observation of the Saturn satellite Phoebe with water ice and non-ice components, assuming linear mixing, to find abundances and grain sizes.

Stephan K. Jaumann R. Wagner R. Clark R. Cruikshank D. P. Hibbitts C. A. Roatsch T. Brown R. H. Buratti B. J. Filacchione G. Hansen G. B. McCord T. B. Baines K. H. Nicholson P. D.
VIMS Coverage of Saturn's Icy Satellite Rhea **[#1377]**
The present status of observing Saturn's satellite Rhea by the Cassini VIMS spectrometer will be presented showing that the derived spatial variations of Rhea's spectral properties appear to be similar to the neighboring satellite Dione.

Filacchione G. Cuzzi J. N. Clark R. N. Buratti B. J. Capaccioni F. Tosi F. Coradini A. Cerroni P. Adriani A. Cruikshank D. P. Jaumann R. Stephan K. Brown R. H. Nicholson P. D. Baines K. H. Nelson R. M. McCord T. B.
Revised Full-Disk Spectra by Cassini-VIMS of the Saturnian Minor Icy Moons **[#1780]**
This abstract concern with a detailed re-analysis of the disk-integrated spectra of the minor moons of Saturn (Atlas, Prometheus, Pandora, Janus, Epimetheus, Calypso and Telesto) obtained by Cassini-VIMS.

Hendrix A. R. Buratti B. J.
Multi-Wavelength Photometry of the Icy Saturnian Satellites: A First Look **[#2438]**
We present results from analyses of phase curves of Enceladus and Dione made using data from Cassini UVIS and VIMS. The investigation provides critical insight into the evolution of the moon regoliths and an understanding of their current environments.

Phillips C. B. Dalton J. B.
Combining Galileo SSI and NIMS Spectra for Europa **[#1367]**
We are combining spectral information from visible-wavelength color Galileo SSI images of Europa with multi-spectral near-infrared data from Galileo NIMS. These combination spectra will help us understand the composition of Europa's surface.

Collins G. C. Hibbitts C. A. Hansen G. B.
Investigation of Carbon Dioxide Distributions on Saturnian and Galilean Satellites Through Fusion of Spectrometer Data with Geological Maps **[#2327]**
We have converted spectrometer data from Cassini VIMS and Galileo NIMS into GIS layers that can be queried along with geological map data. This presentation shows examples from CO_2 band depth mapping on Dione and Ganymede.

Dupire C. Le Menn L. Grasset O. Le Mouélic S.
In Situ Infrared Studies of Water and CO_2 Frost Between 1 and 5 μm: From the Grain to the Icy Surfaces Signatures **[#1242]**
In situ infrared spectra and images of well controlled water and carbon dioxide ice grains have been experimentally acquired in the laboratory. The spectral influence of gaseous CO_2 in an icy matrix is discussed.

Palmer E. E. Brown R. H.
Carbon Dioxide on the Surface of Iapetus, Its Stability and Production [#2442]
CO_2 has been found on Iapetus, where it should be thermally unstable. We generate CO_2 using water ice and carbon grains using UV light as a source for Iapetus. We evaluate how CO_2 can be trapped on the surface.

Cook J. C. Olkin C. B. Desch S. J. Mastrapa R. M. Roush T. L. Verbiscer A. J.
Examination of the K-Band Spectrum of Charon: Possible Evidence for Multiple Ammonia Ices [#2222]
We present a new K-band (1.9–2.4 microns) spectrum of Charon and show there is evidence that the surface has different forms of ammonia ice.

Peeters Z. Hudson R. Moore M.
Carbonic Acid Stability in Solar System Ices **[#2561]**
We have investigated spectral properties and the stability of carbonic acid (H_2CO_3) at different temperatures upon irradiation with MeV protons. The results are extrapolated to life times in outer solar system bodies.

Choukroun M. Barmatz M. Castillo-Rogez J. C. Sotin C.
New Growth Setup of Planetary Clathrate Hydrate Analogs for Physical Properties Measurements [#2313]
We present a new high pressure – low temperature setup for the synthesis of large clathrate hydrate samples. We are ready to grow CO_2 clathrates, and to conduct initial measurements of their mechanical properties, with applications to Enceladus.

Dougherty A. J. Hogenboom D. L. Kargel J. S.
Volumetric and Optical Studies of High Pressure Phases of Na_2SO_4-$^{10}H_2O$ with Applications to Europa [#2033]
We use optical images of high-pressure phases of the Na_2SO_4-H_2O system,coupled with measurements of pressure, temperature, and volume changes, toreport eutectic transitions for pressures up to 325MPa, with implicationsfor modeling Europa's ocean.

Asteroids and Comets

De Sanctis M. C. Lasue J. Magni G. Capria M. T. Turrini D. Coradini A.
Models of ROSETTA Target Comet 67P/Churyumov-Gerasimenko **[#1510]**
We will present the results of a new quasi three-dimensional comet evolution model for non-spherically shaped cometary nuclei. We applied this model to comet 67P/Churyumov-Gerasimenko.

Emery J. P. Cruikshank D. P. Burr D. M.
Near-Infrared Spectroscopy of Trojan Asteroids: Evidence for Two Compositional Groups **[#1442]**
We present near-infrared spectra of ~70 Trojan asteroids. No clear absorption features are detected, but the data reveal two spectral groups. These results are in agreement with other observational evidence, and we suggest the groups indicate distinct compositions.

Hibbitts C. A. Jauhari S. Hagaman S. Lisse C.
Near-Far IR Spectra of Refractory Minerals Relevant to Comets **[#1932]**
We present our results for transmission spectra from ~ 2–200 μm and derived absorption constants for these and other materials relevant to comets, including pyrrhotite, other sulfides, carbonates, and several clay minerals.

Zolotov M. Yu.
Ceres: A Case for Porous, Undifferentiated, and Non-Icy Hydrated Body **[#2329]**
As opposed to previous deductions, this work argues for a porous internal structure of Ceres without a dense core and water mantle.

Li J.-Y. McFadden L. A. A'Hearn M. F. Feaga L. M. Russell C. T. Coradini A. De Sanctis C. Ammannito E.
UV Absorption Features of Asteroid 1 Ceres **[#2101]**
New images and spectra of asteroid Ceres at UV were obtained with HST/ACS/SBC. The absorption feature at about 280 nm in the spectrum of Ceres is confirmed.

Milliken R. E. Rivkin A. S.
Spectral Evidence for a Brucite-Carbonate Alteration Assemblage on Ceres **[#1481]**
We present a new interpretation for the 3 um hydration feature in Ceres' reflectance spectrum. The features in this wavelength region are consistent with brucite and Mg carbonate, suggesting alteration on Ceres is distinct from the chondrites.

Ostrowski D. R. Sears D. W. G. Gietzen K. M. Lacy C. H. S.
An Investigation of Phyllosilicates, C Chondrites, and C Asteroids Using Continuum Slopes of Near Infrared Spectra **[#1136]**
We have measured the near-IR spectra of five phyllosilicates heated in 100°C intervals to 1100°C. We conclude that the surfaces of C asteroids are essentially amorphous, being impact-dehydrated phyllosilicates.

Reynolds C. M. Reddy V. Gaffey M. J.
Compositional Study of 51 Nemausa: A Possible Carbonaceous Chondrite-like Asteroid **[#1285]**
This is a compositional study on the main-belt asteroid 51 Nemausa.

Cloutis E. A. Hardersen P. S. Reddy V. Gaffey M. J. Bailey D. T. Craig M. A.
Metal-Orthopyroxene and Metal-Olivine Mixtures: Spectral Reflectance Properties and Implications for Asteroid Spectroscopy **[#1332]**
The spectral reflectance properties of metal + mafic silicate mixtures indicate that mafic silicate band centers can be successfully recovered, and mafic silicate compositions derived, from analysis of the spectra.

Gietzen K. M. Lacy C. H. S. Ostrowski D. R. Sears D. W. G.
Low-Calcium and Calcium-Free Clinopyroxene Spectra and the Implications for UOC Material on Asteroids **[#1348]**
Many S asteroids have spectral bands for Ca-rich clinopyroxene, which distinguish them from most ordinary chondrites. Five low-Ca clinopyroxenes have the same spectral feature and this likens the asteroids to unequilibrated ordinary chondrites.

Burbine T. H. Buchanan P. C. Dolkar T. Binzel R. P.
Pyroxene Mineralogies of Near-Earth Vestoids **[#1922]**
We determine the mineralogies of seven near-Earth asteroids that have reflectance spectra similar to howardites, eucrites, and diogenites (HEDs). All of these observed near-Earth V-type asteroids have pyroxene mineralogies consistent with eucrites or howardites.

Chapman C. R. Enke B. Merline W. J. Nesvorný D. Tamblyn P. Young E. F.
Reflectance Spectra of Members of Very Young Asteroid Families **[#2258]**
We present SpeX infrared spectra for members of the dynamically young Datura, Iannini, Karin, and Veritas asteroid families (plus Koronis and Themis family controls). S-types are space-weathered on timescales of a few million years.

Fauerbach M. Marks S. A. Behrend R. Bernasconi L. Bosch J.-G. Conjat M. Rinner C. Roy R.
Shape Models of Minor Planets 242 Kriemhild and 287 Nephthys **[#1279]**
Lightcurve inversion of photometry has been shown to be a viable source to obtain information about physical attributes like rotation period, shape and spin axis orientation for asteroids. We will present results for 242 Kriemhild and 287 Nephthys.

Takeuchi H. Miyamoto H. Oku M.
Distributions and Morphological Characteristics of Bright Spots on Boulders Covering the Surface of Asteroid Itokawa **[#1566]**
We scrutinized the highest-resolution images of the asteroid Itokawa to identify 387 bright spots on the surfaces of 123 boulders. Our preliminary results indicate ~90% of these bright spots are formed as results of micrometeoroid impacts.

Dachev Ts. P. Semkova J. V. Maltchev S. Tomov B. Matviichuk Yu. N. Koleva R. Benghin V. Chernykh I. Shurshakov V. Petrov V. Angelis G. De.
Radiation Environment Study During Phobos Sample Return Mission by Charged Particle Telescope Liulin-Phobos **[#1297]**
This paper describes the Liulin-Phobos experiment, which will be flown onboard the future Phobos – Soil sample return mission to the satellite of Mars – Phobos. The main goal is the investigation of the radiation environment and doses on the path and on Phobos surface.

Hamelin M.
Surface and Near Surface Dynamics on Phobos: Possible Grooves Formation by Impact Ejecta **[#1764]**
The motion of a test mass on an ellipsoidal model of Phobos is computed and compared with the grooves patterns around Stickney. It is shown that trajectories are not generally down slope and that a gliding mass can take off over some distance.

Ipatov S. I. A'Hearn M. F.
Deep Impact Ejection from Comet Tempel 1 as a Triggered Outburst **[#1022]**
Results of our studies of velocities and rates of ejection testify that the Deep Impact collision with Comet 9P/Tempel 1 was a trigger of a large outburst that had a local peak of ejection at about 10 seconds and a sharp decrease at ~60 s.

Doressoundiram A. Roques F. Boissel Y.
Probing the Radial Distribution of the Kuiper Belt Using Stellar Occultations **[#1074]**
We conducted a survey for serendipitous occultations. We report on 19 hours of fast-photometry data. We run a complex procedure to analyse the lightcurve. The results bring strong constraints on the Kuiper Belt structure.

McEachern F. M. Cuk M. Stewart S. T.
Dynamical Evolution of the Hungaria Asteroids **[#2554]**
In this study we investigate some 30 of the largest Hungaria asteroids for which taxonomic classes have been assigned, specifically to shed light on their possible dynamical histories.

Bradley P. A. Plesko C. S. Weaver R. P. Clement R. R. C. Guzik J. A.
Pritchett-Sheats L. A. Huebner W. F.
Modeling the Dynamic Response of an Asteroid or Comet to a Nuclear Deflection Burst **[#2314]**
The most technically feasible method of deflecting a Potentially Hazardous Object is a nuclear stand-off burst. We show results from our initial models that use bursts ranging from 1 to 1000 kt on 100 meter diameter targets of various compositions.

COMET WILD 2: MINERALOGY AND MORE

Rost D. Henkel T. King A. Lyon I.
Study of Aerogel Surface Exposed to the Particle Flux of Comet Wild 2: An Update **[#2480]**
Surfaces of Stardust aerogel have been analyzed with latest technology ToF-SIMS, utilising a beam of 40kV C60 ions, most suitable to measure heavy organic compounds at high lateral resolution.

Stephan T.
TOF-SIMS Analysis of Cometary Fragments Extracted from a Stardust Aerogel Track **[#1698]**
TOF-SIMS of cometary fragments from Stardust aerogel show that terminal particles are less mixed with aerogel than material from bulbous cavities. For a comprehensive picture of Wild 2 matter, all material from along the tracks needs to be analyzed.

Stodolna J. Jacob D. Leroux H.
Mineralogy and Petrology of Stardust Particles Extracted from the Walls of Track 80 **[#1762]**
We report a TEM examination of a compressed wall piece extracted from track 80. The sample shows a large diversity of mineralogy suggesting that the incident particles was a complex fine grained aggregate.

Stodolna J. Jacob D. Leroux H.
ATEM Study of Four Thermally Modified Stardust Particles from Track 80 **[#1754]**
We compare the microstructure and composition of thermally modified particles extracted from track 80. Elements distribution attests for capture induced reduction process. No evolution of the thermal alteration is observed along the track.

Ogliore R. C. Butterworth A. L. Fakra S. C. Gainsforth Z. Marcus M. A. Westphal A. J.
Fe-bearing Mineral Groupings in Stardust Fragments **[#2215]**
The Fe-bearing minerals in 193 micron-sized fragments from 11 Stardust tracks are shown to cluster into five groups, giving clues to the heterogeneity scale of comet Wild2.

Schmitz S. Brenker F. E.
Microstructural Indications for Protoenstatite Precursor of Cometary $MgSiO_3$ Pyroxene: A Further High Temperature Component of Comet Wild 2 **[#1580]**
We investigated samples from comet Wild 2 using the TEM. Here we present evidence for the former existence of the high temperature $MgSiO_3$ polymorph protoenstatite as a precursor for the formation of clino- and minor orthoenstatite.

Leroux H.
Mineralogy of Track 77 (PUKI): Toward the Understanding of the Fine-Grained Components of Wild 2 **[#1809]**
Using TEM we show that samples from track 77 display a combination of non-equilibrated crystalline silicates and amorphous material, the latter originates from a fine-grained material thermally altered during the capture in the aerogel.

Joswiak D. J. Brownlee D. E. Matrajt G.
Mineralogical and Textural Changes of a Wild 2 Terminal Particle Pentlandite from Capture Heating in Aerogel **[#2150]**
A ~3 μm pentlandite grain observed in Stardust track 59 and derived from comet Wild 2 was disaggregated and thermally modified (partially) to monosulfide solid-solution (MSS) and heazlewoodite from heating during capture in silica aerogel.

Price M. C. Kearsley A. T. Burchell M. J. Hörz F. Cole M. J.
Comet 81P/Wild 2: The Updated Stardust Coma Dust Fluence Measurement for Smaller (Sub 10-Micrometre) Particles **[#1564]**
Presented is an updated coma dust fluence measurement for comet 81P/Wild 2 for sub-10 micron particles based upon new experimental data. We show this brings the cumulative particle size distribution closer to that measured by the DFMI.

Ishii H. A. Joswiak D. Bradley J. P. Teslich N. Matzel J. Hutcheon I. D. Brownlee D. Matrajt G. MacPherson G. McKeegan K. D.
Enabling Al-Mg Isotopic Measurements on Comet Wild 2's Micro-CAIs **[#2288]**
In order to enable Al-Mg isotopic measurements otherwise not possible on the micro-CAIs returned by Stardust from comet 81P/Wild 2, we combined TEM mineral mapping and precise and selective removal of interfering minerals by focused ion beam milling.

Leroux H. Jacob D. Cordier P.
Fine-grained Material Trapped in Stardust Track Walls **[#1785]**
Using TEM we describe micro-tracks in the Stardust aerogel medium. The size and composition of the cometary material present as discrete patches along these micro-tracks suggest that it originates from an ultrafine matrix, CI-like in composition.

Khodja H. Raepsaet C. Burchell M. J. Flynn G. J. Gainsforth Z. Herzog G. F. Keller L. P. Lanzirotti A. Rao W. Sutton S. R. Taylor S. Westphal A.
Characterization of 81P/Wild 2 Particles C2103,1,98,1,0, C2103,1,98,2,0, and C2065,1,97,1,0 **[#1746]**
Three aerogel-coated Stardust grains have organics and CI-like Cr/, Mn/, Ni,/ and Zn/Fe ratios. Some flight aerogel has 5 wt% C. C and N in 30×30 μm areas of Alais and Orgueil match CI values to within a factor of two. Coal shot into aerogel left a track but no terminal particle.

Wirick S. Flynn G. J. Frank D. Sandford S. A. Zolensky M. E. Tsou P. Peltzer C. Jacobsen C.
Carbon XANES Data from Six Aerogel Picokeystones Cut from the Top and Bottom Sides of the Stardust Comet Sample Tray **[#1340]**
Nine aerogel picokeystones were cut from the top (comet-side) and bottom of the comet sample tray tiles for C XANES spectra analyses. Six of these keystones have been analyzed and four types of C XANES spectra have been found in the non-track containing aerogel.

Hypervelocity Impacts: Stardust Models, LDEF, and ISPE

Dominguez G. Wilkins G.
Temperatures and Time Evolution of Hypervelocity Impact Generated Tracks in Aerogel **[#2535]**
I present a novel method for calculating the temperatures and dynamics of track in aerogel that are generated by the capture of hypervelocity projectiles.

Anderson W. W. Cherne F. J.
Material Models for Aerogel Dust Collectors **[#2549]**
A new material model is being developed for shocked aerogel that will significantly improve description of the effects of capture. The model takes into account chemistry and ionization of the silica and also provides estimates of transport properties.

Price M. C. Kearsley A. T. Burchell M. J.
Hydrocode Simulations of Aggregate Dust Particle Impacts Onto Stardust Al Foils **[#1617]**
3-D measurements of complex craters on Stardust foils allows models of their aggregate impactors to be constructed. Hydrocode modelling is used to validate these models. Its ability to recreate the morphology and formation of such craters is shown.

Stadermann F. J. Floss C. Brownlee D. E. Rodruck M.
Revisiting LDEF: High Resolution Elemental and Isotopic Characterization of Hypervelocity Impacts **[#2120]**
We have studied impact craters from the Long Duration Exposure Facility (LDEF) satellite which was flown in Low Earth Orbit for a duration of 69 months from 1984 through 1990.

Westphal A. J. Allen C. Bajt S. Basset R. Bastien R. Bechtel H. Bleuet P. Borg J. Brenker F. Bridges J. Brownlee D. E. Burchell M. Burghammer M. Butterworth A. L. Cloetens P. Cody G. Ferroir T. Floss C. Flynn G. J. Frank D. Gainsforth Z. Grün E. Hoppe P. Kearsley A. Lemelle L. Leroux H. Lettieri R. Marchant W. Mendez B. Nittler L. R. Ogliore R. Postberg F. Sandford S. A. Schmitz S. Silversmit G. Simionovici A. Srama R. Stadermann F. Stephan T. Stroud R. M. Susini J. Sutton S. Trieloff M. Tsou P. Tsuchiyama A. Tyliczszak T. Vekemans B. Vincze L. Warren J. Zolensky M. E.
Stardust Interstellar Preliminary Examination (ISPE) **[#1786]**
The Stardust Interstellar Preliminary Examination (ISPE) is a three-year effort to characterize the Stardust interstellar dust collection and collector using non-destructive techniques. We summarize the status of the ISPE.

Presolar Grains

Zinner E. Gyngard F.
FIB in the NanoSIMS **[#1046]**
The O and Mg isotopic analysis of small presolar spinel grains in the NanoSIMS is substantially improved if nearby grains of isotopically normal composition are sputtered away with the finely focused Cs primary ion beam.

Leitner J. Hoppe P. Zipfel J.
NanoSIMS Investigation of Presolar Silicates and Oxides in Primitive Solar System Materials **[#1512]**
Impact residues in 76 small Stardust craters were investigated, as well as 12500 μm^2 of matrix of the CR chondrite NWA 852, for their O isotopes. All residues are isotopically normal, and 27 presolar silicates and oxides were found in NWA 852.

Tachibana S. Nagahara H. Ozawa K. Tamada S. Ogawa R.
Condensation Experiments of Mg-rich Crystalline and Amorphous Silicates in Vacuum **[#2512]**
We compare results of two types of kinetic condensation experiments of Mg-silicates; "quench" and "cooling" experiments. Highly non-equilibrium condensates can be obtained in quench-type experiments at very low pressures.

Takigawa A. Tachibana S. Nagahara H. Ozawa K.
Condensation Anisotropy of Corundum Around AGB Stars and Its Effect on Infrared Spectra **[#1731]**
In order to understand the forming processes of refractory dust, we conducted condensation experiments of corundum at high and low supersaturation and investigated the e?ects of condensation conditions on the shape of dust and infrared spectra.

Verchovsky A. B. Fisenko A. V. Semjonova L. F. Wright I. P.
Preparations and Analysis of a New Set of Grain-size Fractions of Nanodiamonds from Kainsaz **[#1908]**
A new set of grain-size fractions of nanodiamonds from Kainsaz have been prepared and analysed. A three populations of nanodiamonds with different carbon isotopic compositions have been identified.

Kashiv Y. Kratz K.-L.
The α-Process in Supernova Presolar SiC Grains **[#2534]**
Preliminary results of the new High Entropy Winf model of nucleosynthesis in SN Type II are presented. It is shown that the Mo isotopic composition measured in SiC X grains could be explained by the primary a-process.

Fujiya W. Sugiura N. Hiyagon H. Takahata N. Sano Y.
Ion Probe Analysis of ^{54}Cr Isotopic Compositions of an Organic Residue from Murchison CM2 Chondrite **[#1486]**
We measured $^{54}Cr/^{52}Cr$ ratios of Cr bearing grains contained in an organic residue from Murchison CM2 chondrite using the NanoSIMS 50 to search for carriers of ^{54}Cr isotopic anomalies found in bulk carbonaceous chondrites.

Yokoyama T. Walker R. J. Alexander C. M. O'D. MacPherson G. J.
Osmium Isotope Anomalies in Chondrite Components: Refractory Inclusions, Chondrules, Metal and Presolar Grains **[#1489]**
We present precise Os isotope data for chondrite components (CAIs, chondrule, metal and IOMs). None of the CAIs, chondrule or metal show Os isotopic anomalies that are resolvable from the solar, while the IOMs possess large nucleosynthetic anomalies.

Jagoutz E. Jagoutz O. E. Ott U.
A Rb Osotopic Shift Due to Nucleosynthesis (S-Process)? **[#1815]**
We describe experimental procedures for high-precision measurements of Rb isotopes and briefly discuss evidence for a component in meteorites that may be due to enhanced abundance of Rb from the weak s-process.

King A. Henkel T. Chapman S. Rost D. Lyon I.
First Analysis of Gently Separated Presolar Graphite **[#2501]**
A gentle separation procedure has been used to isolate presolar graphite grains from the Murchison meteorite. This provides pristine samples with which to study stellar environments. We report the the first TOFSIMS analyses of a gently separated presolar graphite grain.

Davidson J. Busemann H. Alexander C. M. O'D. Nittler L. R. Schrader D. L. Orthous-Daunay F. R. Quirico E. Franchi I. A. Grady M. M.
Presolar SiC Abundances in Primitive Meteorites by NanoSIMS Raster Ion Imaging of Insoluble Organic Matter **[#1853]**
We present results obtained with NanoSIMS raster ion imaging to determine the abundance of presolar SiC in the insoluble organic matter (IOM) extracted from a number of different classes of chondrites (both carbonaceous and ordinary).

Gilmour J. D.
Late Loss of "Planetary" (Actually Presolar) P3 Gases from Nanodiamonds **[#1603]**
The relationship between Xe and Kr in the solar wind and P3 suggests P3 is presolar and includes a contribution from 129I that was alive in the early solar system, constraining the timing of trapping of P3.

Hynes K. M. Gyngard F.
The Presolar Grain Database: http://presolar.wustl.edu/~pgd **[#1198]**
We present a website containing a compilation of the available presolar grain isotopic data. The database is available for use by the entire cosmochemistry community and all data is available for download.

Hoppe P. Huth J. Ott U.
NanoSIMS Studies of Presolar Graphite Grains: Are C-Isotopic Ratios Grain-Size-Dependent? **[#1010]**
We performed C, N, O, and Si isotope measurements on presolar graphite grains with the NanoSIMS. While micrometer-sized graphite grains have predominantly isotopically light C, most of submicrometer-sized graphite grains have heavy C.

EARLY NEBULAR PROCESSES: MODELS AND ISOTOPES

Perret B. Timmes F. X.
Supernova Bullets Impinging Upon Molecular Clouds **[#1999]**
We present preliminary results of the contamination of molecular clouds by supernova ejecta in the form of bullets.

Muralidharan K. Stimpfl M. de Leeuw N. H. Deymier P. A. Runge K. Drake M. J.
Some - Perhaps Most - Water in the Earth Must Result from Adsorption on to Grains in the Accretion Disk **[#1882]**
We show that adsorption of water onto grains in the accretion disk must be a significant source of Earth's water. Using density functional theory we show that HDO may be preferentially retained relative to H_2O in adsorption/desorption kinetics.

Nielsen S. G. Prytulak J. Halliday A. N.
Vanadium Isotope Ratios in Meteorites: A New Tool to Investigate Planetary and Nebular Processes **[#1549]**
This abstract presents the first method that produces high precision vanadium isotope data for terrestrial rocks and meteorites. Vanadium isotope ratios may be used as a tool to test the X-wind model or as an indicator of planetary core formation.

Birck J. L. Petitat M. Luu T. H. Gounelle M.
^{54}Cr Anomalies in the Tagish Lake and Orgueil Carbonaceous Chondrites **[#1683]**
In this study we extend the survey of meteorites exhibiting Cr anomalies to Tagish Lake. We report the highest ^{54}Cr excess so far for the silicate fraction of this meteorite.

Chakrabarti R. Jacobsen S. B.
A Combined Silicon and Magnesium Isotopic Study of Bulk Meteorites and the Earth **[#2089]**
Si and Mg isotope ratios in bulk chondrites, Earth, Mars and achondrites are identical and suggests that the solar nebula was homogeneous with respect to Si and Mg isotopes.

Shi X. Yin Q.-Z. Ng C.-Y.
Testing "Self-Shielding" Model with Laboratory Experiment for the Oxygen Isotope Evolution in the Early Solar Nebula **[#2251]**
We point out weaknesses in recent experiments by Chakraborty et al (2008), and propose to use high-resolution VUV laser for photodissociation and photoionization of CO to directly test the self-shielding model under relevant temperature condition.

Barr A. C. Canup R. M.
Constraints on an Outer Solar System Late Heavy Bombardment from Callisto's Interior State **[#1309]**
A recent theory for the origin of late heavy bombardment impactors suggests an outer solar system source. Limits on the size of rocky core in Jupiter's moon Callisto are used to constrain the contribution of outer solar system impactors to the LHB.

Cuzzi J. N. Hogan R. C. Bottke W.
Primary Accretion: The Birth Population in the Asteroid and KBO Regions **[#2418]**
We explore the implications of a new theory of primary accretion, in which chondrule-sized objects are transformed directly into 10–100km size bodies in nebula turbulence, for the "birth function" of primitive bodies in the asteroid and Kuiper Belt regions.

Futó P. Gucsik A.
Compaction and Sticking of Planetesimals due to Porosity **[#1008]**
It was estimated using numerical methods that numbers, sizes and masses of planetesimals are ranging from 10^{16}–10^{20} kg in the boundary of the early inner solar system.

Ipatov S. I.
Formation of Binaries at a Stage of Rarefied Preplanetesimals **[#1021]**
The angular momentum of two identical collided rarefied preplanetesimals exceeded the angular momentum of the corresponding present binary that could be formed as a result of contraction of the rotating preplanetesimal originated at the collision.

Ciesla F. J. Collins G. S. Davison T. M.
The Thermal Evolution of Post-Impact Planetesimals **[#1086]**
We investigate the thermal evolution of energy that is deposited after the collision of two porous planetesimals. Regions of planetesimals can be shock heated to temperatures >1000 K, with the subsequent cooling lasting hundreds of thousands of years.

Korycansky D. G.
Modeling Rubble-Pile Impacts: Spheres vs. Polyhedra **[#1124]**
Rubble-pile collisions: spherical elements vs. polyhedra: does it make a difference?

Korycansky D. G. Asphaug E.
Some Further Results from Rubble-Pile Impact Calculations **[#1320]**
We present results on energy scaling and axis ratios of fragments from impact simulations of rubble-pile planetesimals.

Holland G. Ballentine C. J. Cassidy M.
Primordial Krypton in the Terrestrial Mantle is Not Solar **[#1824]**
Analysis of Kr isotopes in terrestrial well gas samples indicate the Earth's mantle contains a primitive component identical to the average value for carbonaceous chondrites, distinctly different from solar.

Tang H. Dauphas N. Craddock P. R.
High Precision Iron Isotopic Analyzes of Meteorites and Terrestrial Rocks: ^{60}Fe Distribution and Mass Fractionation Laws **[#1903]**
We present a new method for high precision Fe isotope analysis of bulk meteorites and terrestrial rocks to examine the ^{60}Fe distribution in the protoplanetary disk and assess Fe mass fractionation laws among geo- and cosmochemical processes.

Burkhardt C. Kleine T. Oberli F. Bourdon B.
Search for Mass-independent Molybdenum Isotope Anomalies in Iron Meteorites **[#2482]**
We present improved analytical techniques for the precise measurement of Mo isotope compositions of meteorites. Our first results for magmatic iron meteorites do not show any resolvable mass-independent Mo isotope anomalies. Further analyses are in progress.

Sanders I. S.
CAIs Made by Giant Impact **[#2275]**
Since CAIs in metal-rich chondrites may have formed in an impact plume, a case is made for CAIs in CV chondrites originating in a very early impact between planetary embryos.

Young E. D. Gounelle M. Smith R. L. Morris M. R. Pontoppidan K. M.
The Oxygen Isotopic Composition of the Solar System in a Galactic Context: New Results for CO in Young Stellar Objects and Implications for the Birth Environment of the Solar System **[#1967]**
We compare newly-acquired oxygen isotope ratio data for young stellar objects with new data for molecular clouds to show that the birth-place of the solar system was polluted by supernova ejecta.

SOLAR WIND AND GENESIS: MEASUREMENTS AND INTERPRETATION

Yamada A. Nanbu S. Hiraki Y. Seta T. Kasai Y. Ozima M.
Mass Independent Isotopic Fractionation of Oxygen in Earth Wind (EW) with Relevance to Exotic Oxygen in Lunar Metals **[#1478]**
To test suggestion by Ozima et al. (2008), we calculate photodissociation cross sections of O_2 for isotopomers using quantum chemistry method and estimate isotopic ratios at the altitude of 300–400 km.

McKeegan K. D. Kallio A. P. Heber V. Jarzebinski G. Mao P. H. Coath C. D. Kunihiro T. Wiens R. Allton J. Burnett D. S.
Oxygen Isotopes in a Genesis Concentrator Sample **[#2494]**
Oxygen isotopic compositions of solar wind collected by the Genesis concentrator sample are reported.

Heber V. S. Wiens R. C. Jurewicz A. J. G. Baur H. Vogel N. Wieler R. Burnett D. S.
Isotope Fractionation of Solar Wind Implanted into the Genesis Concentrator Target Determined by Neon in the Gold Cross and Implantation Experiments **[#1485]**
All four arms of the concentrator gold cross were analyzed for Ne, proving that the entire concentrator target was radially homogeneously irradiated. An implantation experiment showed, however, that backscatter loss of Ne from AuSS is not controllable.

Mabry J. C. Meshik A. P. Hohenberg C. M. Burnett D. S.
Real-Time Diffusive Losses of Light Noble Gases from Genesis Aluminum Collectors **[#1783]**
Genesis collector pieces were baked for an extended time in order to quantify the effect that diffusive losses of light noble gases from the Genesis collector materials have on the measured isotopic and elemental ratios.

Cetina C. Grabowski K. S. Knies D. L.
SIMS-AMS Method for Measuring Solar Wind Silicon in DLC Genesis Collectors **[#2550]**
We are illustrating the use of the NRL facility to determine the amount of solar wind silicon retained in DLC collectors. We are encouraging the Genesis science community to consider this method as an alternate solution in other cases.

Humayun M. Huang S.
Low-Level Magnesium Isotopic Analysis for the Genesis Mission **[#1272]**
A method for multicollector ICP-MS analysis of Mg isotopic composition on 1E12 atoms of Mg with 1‰ precision is presented, together with initial results.

Rodriguez M. C. Calaway M. C. Allton J. H. McNamara K. M. Hittle J. D.
Status of Reconstruction of Fragmented Diamond-on-Silicon Collector from Genesis Spacecraft Solar Wind Concentrator **[#1337]**
The Genesis concentrator was comprised of four quadrants: two of SiC, one of 13C diamond and one of DLC on silicon (this target did not survive the hard landing). This is a report on identifying the DLC pieces and finding their initial orientation.

Burkett P. J. Rodriguez M. C. Calaway M. C. Allton J. H.
Genesis Solar Wind Array Collector Cataloging Status **[#1373]**
A focused characterization task was initiated in May 2008 to document the largest array fragments in the Genesis solar wind collection. To date, the collection consists of 3460 samples. By area, total percentage of cataloged array material is 18%.

Calaway M. J. Rodriguez M. C. Allton J. H. Stansbery E. K.
Decontaminating Solar Wind Samples with the Genesis Ultra-Pure Water Megasonic Wafer Spin Cleaner **[#1183]**
The cleaning efficiency of the Genesis Ultra-pure Water Megasonic Wafer Spin Cleaner will be presented. Results show the effectiveness of the new cleaner removing particle contamination from Genesis silicon wafers implanted with solar wind.

EDUCATION AND PUBLIC OUTREACH

Hsu B. C. Weir H. M. Bleacher L. V.
Using Web 2.0 to Disseminate Information About NASA's Lunar Reconnaissance Orbiter **[#2280]**
The Lunar Reconnaissance Orbiter (LRO) is NASA's first step in establishing a permanent human presence on the Moon. In order to capitalize on the excitement of the mission, the LRO team makes use of social media networking and Web 2.0 platforms.

Davidson J. Bartlett S. Carter A. Cornwall M. A. Dryer B. J. Fernandes C. D. Harrison S. K. Janmohamed I. H. S. Mason J. P. Masteika V. Morris A. K. R. Otter S. Tomkinson T. Wilkinson P. T.
The European Student Moon Orbiter and its Biological Lunar Experiment: A Unique Outreach Mission to the Moon **[#2182]**
The ESMO mission provides an ideal opportunity to increase public awareness of lunar missions and to train the current generation of space/planetary science students whilst also conducting novel science via the BioLEx scientific payload.

Terazono J. Tanaka S. Sakamoto S. Watanabe J. Wakabayashi N.
Ten Years in Lunar and Planetary Exploration Outreach: "The Moon Station" Challenge **[#1231]**
This presentation summarizes the website for public outreach on Japanese lunar and planetary exploration. We will address the status, lessons and future prospects based on our ten years' web operation.

Runyon C. Shipp S. Tuthill G. Garver K.
What's New with the Moon Mineralogy Mapper/Chandrayaan-1 E/PO Program? **[#1725]**
The Moon Mineralogy Mapper (M3) team is actively engaged in E/PO activities that provide educators with exposure to lunar geology and experience with spectroscopy as a means of exploring and understanding the composition of the lunar surface.

Bérczi Sz. Gucsik A. Hargitai H. Józsa S. Kereszturi A. Nagy Sz. Szakmány J.
Concise Atlas of the Solar System (11): Petrographic Textures and Evolutionary Processes from the Chondritic Parent Bodies, Moon and Mars **[#1718]**
The 11th atlas of the Solar System helps students in a systematic approach to petrographic textures of planetary materials of processes on asteroids, Moon and Mars, arranged in their igneous units of their geological settings in the parent body.

Boros-Olah M. Hargitai H. Hirsch T. Kereszuti A. Muhi A. Tepliczky I.
HungaroMars2008: Analog Research in the Education of Planetary Sceince **[#1492]**
Between 13–26 of April 2008 a Hungarian crew worked at Mars Desert Research Station. The planetary science related educational aspects are summarized from the meteorolgical station, Husar-2D autonomous rover, geologic and geomorphologic analysis.

Gulick V. C. Deardorff G. Davatzes A. E. K. Kanefsky B.
Education and Public Outreach With the Mars Reconnaissance Orbiter's High-Resolution Imaging Science Experiment: A Virtual Science Team Experience **[#2354]**
Looking back over one Mars year, we report on the accomplishments of the HiRISE EPO program during the primary science phase of MRO.

Grigsby B. Capages C. Christensen P. R. Murchie S. Turney D. Beisser K. Seelos F. Seelos K. Harvel C. Barnouin-Jha O. Patterson W. McGovern A. Buczkowski D. Malaret E. Hash C. Ehlmann B. Roach L.
Involving Students in Authentic Research: First Year Results from the Mars Exploration Student Data Teams Project **[#2185]**
The Mars Exploration Student Data Teams (MESDT) program, created by Arizona State University's Mars Education Program, focuses on immersing teams of high school students in an authentic research Science, Technology, Engineering and Mathematics (STEM) based experience.

Bitter C. Buxner S. R.
Martian Multimedia: The Agony and Ecstasy of Communicating Real-Time, Authentic Science During the Phoenix Mars Mission **[#2172]**
The Phoenix Mars Mission faced robust communication challenges requiring real-time solutions. Managing the message from Mars and ensuring the highest quality of science data and news releases were our top priorities during mission surface operations.

Hines R. Stopar J. Taylor W. Minitti M. E. Wadhwa M.
Enhancing and Expanding Educational Outreach Programs at the Center for Meteorite Studies, Arizona State University **[#1875]**
New outreach and education programs are being developed at ASU's Center for Meteorite Studies, in conjunction with an improved and expanded web presence, to impact a broader local and international audience of students, educators, scientists and interested individuals.

Kolb K. J. Keller J. M. Novodvorsky I.
Investigating Alternative Conceptions about Water on Mars Held by Middle School Science Teachers **[#2143]**
We report on alternative conceptions about water on Mars that are held by middle school science teachers in AZ and CA.

Urquhart M. L.
Designing Standards-driven Space Science Educational Outreach for Formal Education **[#2408]**
Space science is an exciting topic for many students, but research is rarely on the specific topics typically found in K–12 standards. This paper discusses the importance of standards-based approaches to outreach intended for formal education.

Bleamaster L. F. III Crown D. A. Canizo T. L. Lebofsky L. A.
Planets are Places Too: Professional Development Workshops for K–8 Teachers **[#1695]**
The Planetary Science Institute, in partnership with the Tucson Regional Science Center, is offering a series of professional development workshops targeting elementary and middle school teachers within the Tucson, Arizona region.

Kadel S. D. Williams D. A.
Carrying the Fire: Classroom and Field-based Teacher Training Using a Newly Institutionalized E/PO Product **[#2448]**
The Worlds of Fire E/PO is institutionalized as a college course, GLG231AA Special Topics in Geology: Volcanoes of Northern Arizona, providing a classroom overview of volcanism on Earth and Io and a field excursion to volcanoes around Flagstaff, AZ.

Hegyi S. Göcze Z. Hegyi A. Kovács P. Baksa L. Bérczi Sz.
Field Trip Tasks and Simulations with Husar-2 Rover at the Mars Analog Desert Station, Utah, USA **[#1163]**
Husar-2d rover was used by Hungarian Crew No. 71 at MDRS, Utah, USA, 2008 April in surface activities in their high relief movements with high car-chassis, material collecting plate, geological, geographical, chemical mesurements.

Boice D. C. Asbell H. E. Reiff P. H.
Engaging Students in Research — Young Engineers and Scientists (YES) **[#1507]**
Young Engineers and Scientists (YES) is a community partnership between SwRI and local high schools in San Antonio, Texas. It provides high school students a bridge between classroom instruction and real world, research experiences in science and engineering.

McCoy T. J. Baldwin D. W. Olm W. Ironstrack G. M. Yingst R. A. Doudrick S. R.
Myaamionki: Ašiihkiwi Neehi Kiišikwi (The Place of the Miami: Earth and Sky) **[#1283]**
We report on a workshop and summer camp held within the Miami Tribe of Oklahoma to examine the overlap between science (planetary science, geology, and astronomy) and traditional ways of knowing derived from myaamia culture, including lessons learned.

Toyota T. Kasahara S. Narita N. Hirasawa T. Watanabe M. Kodera C. Homma N. Kaburagi Y. Yokoyama H.
Interdisciplinary Collaboration for Outreach by Young Scientists in a Japanese University **[#1606]**
In this paper, we introduce our activities for inter-disciplinary communication of young scientists in a Japanese university. We also report an educational activity of the astrobiology class at an elementary school in Japan.

ANCIENT MARTIAN CRUST: PRIMARY MINERALOGY AND AQUEOUS ALTERATION
Wednesday, 8:30 a.m. Waterway Ballroom 1

Chairs: **Joseph Michalski and Janice Bishop**

8:30 a.m. Mustard J. F. * Murchie S. L. Ehlmann B. L. Milliken R. E. Bibring J-P. Poulet F. Head J. W.
Stratigraphy of Noachian-aged Crust in the Nili Fossae-Syrtis-Isidis Region **[#2115]**
A section of well-exposed Noachian crust exists surrounding the Isidis Basin. Over thousands of km it is largely a breccia consisting of blocks of sedimentary and primary igneous rocks in a phyllosilicate-bearing matrix, and capped by impact melt.

8:45 a.m. Skok J. R. * Mustard J. F. Murchie S. L.
Identification of Primary Noachian Crustal Blocks on Mars with CRISM Observations **[#2180]**
The early Noachian crust of Mars has been obscured by impacts, alteration, and resurfacing, resulting in the earliest crust exposed as breccia blocks across the planet. We use spectral observations to constrain the mineralogy of these crustal blocks.

9:00 a.m. Tosca N. J. * Knoll A. H.
Juvenile Chemical Sediments and the Duration of Aqueous Activity on Ancient Mars **[#1538]**
A general lack of diagenetic maturation among martian chemical sediments suggests that liquid water could not have persisted at these localities much beyond initial precipitation.

9:15 a.m. Chevrier V. F. *
Early Martian Surface Conditions from Thermodynamics of Phyllosilicates **[#2515]**
Thermodynamic equilibria are used to determine the geochemical conditions during the Noachian era. Results show that CO_2 pressure and temperature can explain observations of various phyllosilicates and carbonates.

9:30 a.m. Velbel M. A. *
Mechanisms of Pyroxene Alteration to Smectite: Implications for Inferring Elemental Mobility in Martian Paleoenvironments **[#1415]**
Pyroxene and smectite compositions are an observational basis for inferring former chemical conditions that facilitated differential elemental mobility in systems in which the water that mediated the weathering reactions is no longer present.

9:45 a.m. Carter J. * Poulet F. Bibring J.-P. Murchie S. Langevin Y. Mustard J. F. Gondet B. Seelos F.
Phyllosilicates and Other Hydrated Minerals on Mars: 2. Detailed Analysis **[#2058]**
This abstract focus on the spectral diversity and the geological setting of phyllosilicate-bearing deposits detected on Mars.

10:00 a.m. Michalski J. R. * Poulet F. Bibring J.-P. Mangold N.
Combined Visible/Near Infrared and Thermal Infrared Analyses of the Nili Fossae Region, Mars **[#1365]**
We present evidence for two main classes of phyllosilicate minerals in the Nili Fossae region of Mars based on the combined use of TES and OMEGA data. Both dioctahedral Fe^{3+} and trioctahedral Fe/Mg^{2+} clay minerals exist together.

10:15 a.m. Bishop J. L. * McKeown N. K. DesMarais D. J. Noe Dobrea E. Z. Parente M. Seelos F. Murchie S. L. Mustard J. F.
The Ancient Phyllosilicates at Mawrth Vallis and What They Can Tell Us About Possible Habitable Environments on Early Mars **[#2239]**
Phyllosilicates observed at Mawrth Vallis indicate a wide range of past aqueous activity. The phyllosilicate stratigraphy, possible formation scenarios, and possible links to prebiotic chemistry and biosignatures are presented.

10:30 a.m. Ruff S. W. * Hamilton V. E.
New Insights into the Nature of Mineralogic Alteration on Mars from Orbiter, Rover, and Laboratory Data **[#2160]**
TES spectra now appear to support the identification in some places of phyllosilicates observed by OMEGA/CRISM. Enigmatically, spectra from Mini-TES in Gusev crater show no such phases on rocks that clearly are altered. Amorphous phases are implicated.

10:45 a.m. Gavin P. * Chevrier V.
Thermal Alteration of Nontronite and Montmorillonite: Implications for the Martian Surface **[#1027]**
We investigate the spectral properties of thermally altered nontronite and montmorillonite and compare them to those of clays detected in impact crater ejecta on Mars.

11:00 a.m. Dyar M. D. * Murad E. Sklute E. C. Bishop J. L. Muirhead A. C.
Mössbauer and Reflectance Spectroscopy of Iron Oxide Mixtures **[#2209]**
Mössbauer spectroscopy is used to identify and quantify abundances of iron oxide and hydroxide minerals in mixtures that are analogs for martian rocks and soils.

11:15 a.m. Ehlmann B. L. * Mustard J. F. Murchie S. L.
Detection of Serpentine on Mars by MRO-CRISM and Possible Relationship with Olivine and Magnesium Carbonate in Nili Fossae **[#1787]**
Reports the first orbital detection of serpentine on Mars' surface, made by CRISM in the Thaumasia and Nili Fossae regions. Evidence for serpentinization of an olivine-magnesium carbonate-serpentine bearing rock unit in Nili Fossae is discussed.

11:30 a.m. Glotch T. D. * Rogers A. D.
Reexamination of Global Carbonate Abundances Using TES Data **[#1605]**
In this study, we reexamine global carbonate abundances in the TES data set. Results of the study generally support previous work indicating that carbonates are not widely present on Mars at the outcrop scale.

SPECIAL SESSION: MESSENGER AT MERCURY: A GLOBAL PERSPECTIVE ON THE INNERMOST PLANET
Wednesday, 8:30 a.m. Waterway Ballroom 4

Chairs: **Sean C. Solomon and Brett Denevi**

8:30 a.m. Solomon S. C. * Freed A. M. Hauck S. A. II Head J. W. III Kerber L. Phillips R. J. Robinson M. S. Watters T. R. Zuber M. T.
MESSENGER's Newly Global Perspective on Mercury: Some Implications for Interior Evolution **[#1750]**
MESSENGER's first two flybys of Mercury have revealed a planet with a richer history of magmatism, deformation, and impact basin modification than heretofore appreciated, placing new constraints on the planet's formation and interior evolution.

8:45 a.m. Purucker M. E. * Johnson C. L. Anderson B. J. Korth H. Uno H. Blewett D. T. Sabaka T. J. Solomon S. C. Head J. W.
Mercury's Internal Magnetic Field from MESSENGER **[#1277]**
The internal magnetic field at Mercury is overwhelmingly of core origin, although small-scale fields of crustal origin may yet be shown to exist. None of the craters profiled during the MESSENGER flybys exhibit any magnetic signature.

9:00 a.m. Zurbuchen T. H. * Raines J. M. Gloeckler G. Slavin J. A. Krimigis S. M. Killen R. M. Sprague A. L. McNutt R. L. Jr. Solomon S. C.
First Ion Plasma Measurements in the Mercury Magnetosphere **[#2141]**
This paper discusses results from the two 2008 MESSENGER flybys. It addresses the relative importance of surface sputtering, chemical sputtering and micrometeoroid impact for the creation of Mercury's ionized exosphere.

9:15 a.m. Vervack R. J. Jr.* McClintock W. E. Bradley E. T. Killen R. M. Sprague A. L. Mouawad N. Izenberg N. R. Kochte M. C. Lankton M. R.
MESSENGER Observations of Mercury's Exosphere: Discoveries and Surprises from the First Two Flybys **[#2220]**
The MESSENGER flybys have provided excellent opportunities to probe the tenuous exosphere of Mercury, have led to the discovery of magnesium, and have revealed unexpected and puzzling structure in the spatial distributions of several species.

9:30 a.m. Lawrence D. J. * Feldman W. C. Goldsten J. O. Solomon S. C.
Identification of Neutron Absorbing Elements on Mercury's Surface Using MESSENGER Neutron Data **[#1761]**
Thermal neutrons provide a sensitive measure of elements such as Fe, Ti, Gd, and Sm. We present MESSENGER Neutron Spectrometer data along with an initial modeling analysis; implications for the abundance of neutron absorbing elements are described.

9:45 a.m. Izenberg N. R. * McClintock W. E. Holsclaw G. M. Blewett D. T. Helbert J. Solomon S. C. MESSENGER Team
Resolved Ultraviolet to Infrared Reflectance Spectroscopy of Mercury from the Second MESSENGER Flyby **[#1663]**
MESSENGER's MASCS instrument obtained resolved reflectance spectra from the ultraviolet to near-infrared (115–1450 nm) during the second Mercury flyby, sampling a variety of geologic terranes and units.

10:00 a.m. Denevi B. W. * Robinson M. S. Blewett D. T. Domingue D. L. Head J. W. III McCoy T. J. McNutt R. L. Jr. Murchie S. L. Solomon S. C.
MESSENGER Global Color Observations: Implications for the Composition and Evolution of Mercury's Crust **[#2247]**
A near-global view of Mercury from MESSENGER provides the first opportunity to perform a planet-wide assessment of Mercury's major geologic units and their significance.

10:15 a.m. Ernst C. M. * Murchie S. L. Barnouin-Jha O. S. Robinson M. S. Denevi B. W.
Exposure of Red Material by Impact Craters on Mercury: Implications for Buried Plains Material **[#1900]**
Occurrences of the red unit associated with impact craters on Mercury are examined using MESSENGER data to determine their extent, burial depth, and origin. The examination of one small area on Mercury reveals a complex local stratigraphy.

10:30 a.m. Blewett D. T. * Kerber L. Head J. W. Denevi B. W. Robinson M. S. Murchie S. L. Gillis-Davis J. J. Solomon S. C.
Mercury Pyroclastics: Color, Morphology, and Volatile Content **[#1793]**
We examine potential pyroclastic deposits with Mariner 10 and MESSENGER images. The best candidates have high reflectance and red spectral slope. Eruption physics calculations place constraints on magma volatile content, and suggest 1000s of ppm CO.

10:45 a.m. Zuber M. T. * Farmer G. T. Hauck S. A. II Ritzer J. A. Phillips R. J. Solomon S. C. Smith D. E. Head J. W. III Neumann G. A. Robinson M. S. Watters T. R. Johnson C. L. Oberst J. Barnouin-Jha O. McNutt R. L. Jr.
Observations of Ridges and Lobate Scarps on Mercury from Messenger Altimetry and Imaging and Implications for Lithospheric Strain Accommodation **[#1813]**
Ridges and scarps profiled by the Mercury Laser Altimeter on MESSENGER display offsets that significantly exceed those of martian wrinkle ridges. The structures can be used to constrain the early lithospheric structure and thermal state of Mercury.

11:00 a.m. Smith D. E. * Zuber M. T. Phillips R. J. Solomon S. C. Lemoine F. G. Neumann G. A. Head J. W. III Torrence M. H.
Does Mercury Have Lunar-like Mascons? **[#1802]**
In 2008 MESSENGER conducted two flybys of Mercury and experienced greater perturbation than expected. We investigated the possibility of gravity anomalies associated with surface features being the cause.

11:15 a.m. Prockter L. M. * Watters T. R. Chapman C. R. Denevi B. W. Head J. W. III Solomon S. C. Murchie S. L. Barnouin-Jha O. S. Robinson M. S. Blewett D. T. Gillis-Davis J.
The Curious Case of Raditladi Basin **[#1758]**
Raditladi Basin was imaged by MESSENGER during its flyby of Mercury. The basin appears to be very young – perhaps less than 1 Ga – and exhibits unusual extensional troughs. The presence of the troughs is at odds with Raditladi's apparent youth.

11:30 a.m. Head J. W. III* Solomon S. C. McNutt R. L. Jr. Blewett D. T. Chapman C. R. Domingue D. L. Gillis-Davis J. J. Hawkins S. E. III Helbert J. Holsclaw G. M. Izenberg N. R. McClintock W. E. Merline W. J. Murchie S. L. Phillips R. J. Prockter L. M. Robinson M. S. Denevi B. W. Sprague A. L. Strom R. G. Vilas F. Watters T. R. Zuber M. T.
The MESSENGER Mission to Mercury: New Insights into Geological Processes and Evolution from the First Two Encounters **[#2198]**
The first two Mercury MESSENGER mission encounters imaged much of the surface unseen by Mariner 10, establishing the widespread nature of volcanism, the presence of pyroclastic deposits, and the volcanic filling of impact craters and basins.

CAIs AND CHONDRULES: RECORDS OF EARLY SOLAR SYSTEM PROCESSES
Wednesday, 8:30 a.m. Waterway Ballroom 5

Chairs: **Kim B. Knight and Harold C. Connolly Jr.**

8:30 a.m. Simon S. B. * Sutton S. R. Grossman L.
First Ti-XANES Analyses of Refractory Inclusions from Murchison **[#1626]**
Ti valence in refractory phases is an important recorder of redox conditions in the early solar nebula. We report the valence of Ti in pyroxene, spinel and hibonite in spinel-hibonite and spinel-pyroxene inclusions and in a coarse hibonite grain.

8:45 a.m. Ma C. * Beckett J. R. Rossman G. R.
Allendeite and Hexamolybdenum: Two New Ultra-Refractory Minerals in Allende and Two Missing Links **[#1402]**
We report here two newly discovered ultra-refractory minerals from Allende: Allendeite, $Sc_4Zr_3O_{12}$, a new Sc- and Zr-rich oxide; and hexamolybdenum, (Mo,Ru,Fe), a Mo-dominant alloy.

9:00 a.m. Knight K. B. * Kita N. T. Davis A. M. Richter F. M. Mendybaev R. A.
Mg and Si Isotope Fractionation Within Three Type B Ca-Al-rich Inclusions **[#2360]**
Isotopic profiles of Mg and Si in melilite were measured within three Type B Ca-Al-rich inclusions from the CV3 chondrites Allende (USNM-3529.16 and AL-4884) and Leoville (USNM-3535.1) by secondary ion mass spectrometry.

9:15 a.m. Mendybaev R. A. * Richter F. M. Georg R. B. Davis A. M.
Evaporation Kinetics of Forsterite-rich Melts and Thermal Histories of FUN CAIs **[#2461]**
We present the results of our experiments on evaporation kinetics of forsterite-rich melts in vacuum. The results are used to place constraints on the thermal history of FUN CAIs.

9:30 a.m. Krot A. N. * Nagashima K.
Istopically Uniform, ^{16}O-Depleted CAIs in Metal-Rich Carbonaceous Chondrites. **[#1036]**
The metal-rich carbonaceous chondrites (CH, CB, and Isheyevo) contain a population of igneous CAIs, which are isotopically uniform and ^{16}O-depleted [$\Delta^{17}O \sim -7‰$] compared to CAIs from other chondrite groups ($\Delta^{17}O \sim -23.5‰$), suggesting a unique origin.

9:45 a.m. Petaev M. I. * Jacobsen S. B.
Nebular History of the Allende FoB CAI SJ101 **[#1388]**
We compare petrologic and chemical characteristics of a unique FoB CAI SJ101 with the results of thermodynamic modeling of condensation of its precursors in a system of solar composition and speculate about nebular formation history of this CAI.

10:00 a.m. Richter F. M. * Mendybaev R. A. Christensen J. Gaffney A. Ebel D.
Elemental and Isotope Fractionation of Chondrule-like Liquids by Evaporation into Vacuum **[#2321]**
The talk will present new experimental data on the evaporation kinetics of Na and K from a chondrule-like melt, and new isotopic data on the K isotopic fractionation of the evaporation residues.

10:15 a.m. Kropf A. Huss G. R. Krot A. N. Pack A. *
Closed System Behavior of Alkalis in Type-1 Chondrules — Understanding Chondrules as Igneous Systems **[#2464]**
New SIMS and high-current EPMA data on type-I chondrules from Semarkona show that they behaved as chemically closed systems during melting and olivine crystallization.

10:30 a.m. Weisberg M. K. * Ebel D. S. Connolly H. C. Jr. Kita N. T. Ushikubo T.
Petrologic-Geochemical Study of Chondrules in Enstatite Chondrites **[#1886]**
Chondrules in E3 chondrites differ markedly from chondrules in other chondrites. They are records of a highly reducing nebular environment and/or precursor assemblage. Oxygen isotope data is being collected to better constrain their history.

10:45 a.m. Ushikubo T. * Kimura M. Kita N. T. Valley J. W.
Oxygen Isotopic Compositions of Phenocrysts in Chondrules from the Primitive Carbonaceous Chondrite Acfer 094 **[#1383]**
We measured O isotopic compositions of 29 chondrules from Acfer 094. We found ^{16}O-poor relict olivine from three chondrules, suggesting that their precursors formed in a ^{16}O-poor environment and were processed in a relatively ^{16}O-rich environment.

11:00 a.m. Berlin J. * Jones R. H. Brearley A. J.
Identification of FeO-rich Relict Olivines in Type IIA Chondrules Using Fe-Mn Systematics **[#2399]**
We identified FeO-rich relict olivines in type IIA chondrules from Kainsaz (CO3.2) and Semarkona (LL3.0). Host chondrule olivines show linear trendlines in a Mn vs. Fe diagram, while relict grains plot in different regions of the diagram.

11:15 a.m. Nakashima D. * Matsuda S. Iio H. Bajo K. Nagao K.
Solar Wind Like Noble Gases in a Chondrule in the NWA 852 CR2 Chondrite **[#1674]**
We found through laser extraction noble gas analysis of the NWA 852 CR2 chondrite that a chondrule contains solar wind like noble gases in its interior, suggestive of solar gas acquisition before/during the chondrule formation.

11:30 a.m. Hezel D. C. * Armytage R. M. G. Georg R. B. Keren E. Russell S. S.
Combined Fe- and Si-Isotope Measurements of CV Chondrite Chondrules and CAIs **[#1772]**
Chondrules have variable Fe-isotopic, but similar Si-isotopic compositions. 3D tomography revealed 1–7 vol% sulfide/metal in Allende. We conclude that isotopic and chemical variabilites among chondrules were established during chondrule formation.

11:45 a.m. Schrader D. L. * Zega T. J. Lauretta D. S. Connolly H. C. Jr.
Microstructure of Sulfide-Assemblages in a Renazzo Type-II Chondrule as Revealed by Transmission Electron Microscopy **[#2181]**
We report on a combined focused ion beam scanning electron microscopy and transmission electron microscopy analysis of the microstructure of sulfide-assemblages in a type-II chondrule from Renazzo.

SMALL BODIES: SHAPES OF THINGS TO COME
Wednesday, 8:30 a.m. Waterway Ballroom 6

Chairs: **Al Conrad and Debra Buczkowski**

8:30 a.m. Conrad A. R. * Merline W. J. Drummond J. D. Carry B. Dumas C. Campbell R. D. Goodrich R. W. Chapman C. R. Tamblyn P. M.
Recent Results from Imaging Asteroids with Adaptive Optics **[#2414]**
We report results from recent high-angular-resolution observations of asteroids using adaptive optics (AO) on large telescopes.

8:45 a.m. Marchis F. * Descamps P. Durech J. Emery J. P. Harris A. W. Kaasalainen M. Berthier J.
The Cybele Binary Asteroid 121 Hermione Revisited **[#1336]**
The combination of adaptive optics, photometric and Spitzer mid-IR observations of the 121 Hermione binary asteroid system allowed us to confirm the bilobated nature of the primary derived a bulk density of 1.4 g/cc implying a rubble-pile interior.

9:00 a.m. Schmidt B. E. * Thomas P. C. Bauer J. M. Li J. -Y. Radcliffe S. C. McFadden L. A. Mutchler M. J. Parker J. Wm. Rivkin A. S. Russell C. T. Stern S. A.
The 3D Figure and Surface of Pallas from HST **[#2421]**
We present Pallas in three dimensions and surface maps.

9:15 a.m. Besse S. * Groussin O. Jorda L. Lamy P. Kaasalainen M. Gesquiere G. Remy E. OSIRIS Team
3-Dimensional Reconstruction of Asteroid 2867 Steins **[#1545]**
The OSIRIS imaging experiment has imaged asteroid Steins. We have combined three methods to retrieve the shape: limbs, Point of Interest and light curves. The mean radius of Steins is 2.7 ± 0.3 km, for a volume of 78 ± 30 km^3 and a surface of 98 ± 25 km^2.

9:30 a.m. Burchell M. J. * Leliwa-Kopystynski J.
The Large Crater on Asteroid Steins: Is it Abnormally Large? **[#1525]**
Comparison of the large crater on asteroid Steins (observed during the recent Rosetta fly by) to large craters on other small rocky bodies, shows that, whilst large, it is not abnormally so and follows an already established trend.

9:45 a.m. Heggy E. * Kataria T. Clifford S. M. Lasue J. Kofman W.
Dielectric Model of Comet 67P/Churyumov-Gerasimenko in Support of the CONSERT Radar Tomography Experiment On Board Rosetta **[#1944]**
We present parametric dielectric model of Comet 67P/Churyumov-Gerasimenko and corresponding radar wave propagation through the comet in Support of the CONSERT Radar Tomography Experiment on Board Rosetta.

10:00 a.m. Sánchez P. * Scheeres D. J.
Granular Mechanics in Asteroid Regolith: Simulating and Scaling the Brazil Nut Effects **[#2228]**
The simulation and scaling of granular mechanics flows in asteroid regolith is studied to interpret observations of asteroid surfaces and topography. We focus on the "Brazil Nut Effect" in gravitational fields of different magnitudes.

10:15 a.m. Asphaug E. *
Shattered Dirt: Surface Fracture of Granular Asteorids **[#1438]**
The fracture grooves prevalent on Eros, Phobos and other small bodies cannot be indicators of a competent rocky bedrock. They are expressions of soil cohesion exceeding the minuscule gravitational overburden in the upper meters.

10:30 a.m. Richardson J. E. *
The Seismic Effect of Impacts on Asteroid Surface Morphology: Three-Dimensional Modeling Results **[#2144]**
We investigate impact-induced seismic effects on cratered asteroid terrain, utilizing a two-stage modeling process: a numerical shake-table to compute regolith motion, which is then applied to a three-dimensional model of cratered terrain evolution.

10:45 a.m. Durda D. D. *
Constraining Source Crater Regions for Boulder Tracks and Elongated Secondary Craters on Eros **[#2173]**
Dynamical models of reaccretion of impact ejecta on asteroids are used to 'back track' the derived landing trajectories of selected boulders on Eros, placing constraints on the source regions for the primary impact craters.

11:00 a.m. Buczkowski D. L. * Barnouin-Jha O. S. Wyrick D. Prockter L. M.
Further Analyses of the 433Eros Global Lineament Map **[#1187]**
While some linear features identified on Eros are clearly formed by impact, others do not obviously follow any model predictions of lineation formation by impact and possibly represent a pre-existing internal structure. New analyses are presented.

11:15 a.m. Scheeres D. J. * Jacobson S. A.
Fission and Stability of Ellipsoidal Contact Binary Asteroids **[#2040]**
The initial relative equilibrium state for contact binary asteroids spun to fission are always unstable. Thus their initial evolutionary phase should be strongly unstable and the application of classical tidal results may not be correct.

11:30 a.m. Holsapple K. A. *
The Deformation of Asteroids from YORP Spin-Up **[#2053]**
YORP spin-up is a candidate for forming binary asteroids. Results of an analytical study of the deformation of a spinning ellipsoidal body with imposed increasing angular momentum are presented, and compared to a numerical N-body study.

SULFUR ON MARS: ROCKS, SOILS, AND CYCLING PROCESSES
Wednesday, 1:30 p.m. Waterway Ballroom 1

Chairs: Scott McLennan and Deanne Rogers

1:30 p.m. McLennan S. M. * Grotzinger J. P.
Sulfur and the Sulfur Cycle on Mars **[#2152]**
Elevated S in martian mantle/crust and absence of plate tectonics results in a S-enriched sedimentary mass. The S-cycle of Mars is analogous to the Earth's C-cycle, with long-term storage in the rock record and shorter-term S-recycling processes.

1:45 p.m. Milliken R. E. * Edgett K. S. Swayze G. Clark R. N. Thomson B. J. Anderson R. Bell J. F. III
Clay and Sulfate-bearing Rocks in a Stratigraphic Sequence in Gale Crater **[#1479]**
CRISM reflectance spectra of a >5 km thick sequence of strata in Gale Crater reveal the presence of diverse mineralogy, including clay-bearing rocks interbedded with sulfate-bearing rocks. Gale is one of four final MSL candidate landing sites.

2:00 p.m. Wiseman S. M. * Arvidson R. E. Morris R. V. Murchie S. L. Seelos F. P. |Andrews-Hanna J. C. CRISM Team
Hydrated Sulfate Deposits Detected Within Schiaparelli Crater, Mars **[#1798]**
Hydrated sulfate deposits are detected within Schiaparelli crater using CRISM spectral data. The hydrated sulfate deposits occur in association with likely sedimentary outcrop and may be related to hydrated sulfate deposits in Meridiani.

2:15 p.m. Niles P. B. * Michalski J.
The Origin of the Meridiani Sediments: The Key for Understanding the Formation of Sulfates and Layered Deposits on Mars **[#1972]**
The provenance of the Meridiani deposits is best explained by reworking of acid-weathered sublimation residue from a large scale ice/dust deposit. The acid weathering is hypothesized to have occurred inside of the ice powered by solar radiant energy.

2:30 p.m. Lichtenberg K. A. * Arvidson R. E. Morris R. V. Murchie S. L. Bishop J. L. Glotch T. D. Noe Dobrea E. Mustard J. F. Andrews-Hanna J. Roach L. H. CRISM Team
Stratigraphy and Relationship of Hydrated Minerals in the Layered Deposits of Aram Chaos, Mars **[#2326]**
Hydrated minerals such as hematite and monohydrated, polyhydrated, and Fe-OH sulfates in Aram Chaos, Mars show stratigraphic relationships indicative of their formation history as a depositional unit in an aqueous environment.

2:45 p.m. Roach L. H. * Mustard J. F. Murchie S. L. Bishop J. L. Ehlmann B. L. Milliken R. E. Lichtenberg K. Parente M.
Hydrated Mineral Stratigraphy in Ius Chasma, Valles Marineris **[#1834]**
Kieserite, a polyhydrated sulfate, hydrated silica, Fe/Mg phyllosilicate, and a hydrated silicate (possibly consistent with an acid-leached phyllosilicate) are found in light-toned units within Ius Chasma, Valles Marineris.

3:00 p.m. Flahaut J. * Quantin C. Allemand P.
Geology and Mineralogy of the Interior Layered Deposits in Capri/Eos Chasma (Mars), Based on CRISM and HiRiSE Data **[#1639]**
We studied HiRiSE and CRISM data over Capri Chasma, a small canyon of Valles Marineris. Layered Deposits in this area show various hydrated minerals signatures, as abundant sulfates, implying a strong past water activity there.

3:15 p.m. Rogers A. D. * Reeder R. J. Glotch T. D.
Infrared Spectroscopy of Amorphous Sulfate Phases **[#1202]**
Stability experiments have indicated that amorphous sulfate phases may be important constituents of martian surface materials. IR spectral properties of X-ray amorphous Mg- and Fe-sulfate phases are described and compared with their crystalline counterparts.

3:30 p.m. Freeman J. J. * Wang A. Ling Z. C.
Ferric Sulfates on Mars: Mission Observations and Laboratory Investigations **[#2284]**
A change was observed in the Pancam spectra of Tyrone salty soils after 190 sols exposure at Gusev. Based on the results of laboratory experiments, we suggest dehydration, amorphization, and phase transition of copiapites to be the potential causes.

3:45 p.m. Hausrath E. M. * Golden D. C. Galindo C. Sutter B. Morris R. V. Ming D. W.
Column Experiments to Interpret Weathering in the Columbia Hills, Mars **[#2423]**
Column dissolution experiments were performed to interpret weathering in the Columbia Hills, Mars. Results suggest that the formation of an amorphous aluminum phosphate and gypsum are likely, and that Si and Ti are relatively immobile.

4:00 p.m. Golden D. C. * Ming D. W. Sutter B. Clark B. C. Morris R. V. Boynton W. V. |Hecht M. H. Kounaves S. P.
Sulfur Mineralogy at the Mars Phoenix Landing Site **[#2319]**
The sulfur mineralogy of the soils at Phoenix lander site was derived using Thermally Evolved Gas Analyzer (TEGA) data in combination with known geochemistry of the martian polar regions. The most likely S mineral phase at the Phoenix site is anhydrite.

4:15 p.m. Vaniman D. T. * Bish D. L. Chipera S. J.
Bassanite on Mars **[#1654]**
There are several ways to desiccate gypsum on Mars and form bassanite but rehydration in presence of ice at cold, dry conditions tends to form only bassanite or gypsum plus bassanite. This product may provide a paleoclimate or paleogeothermal marker.

4:30 p.m. Halevy I. * Schrag D. P.
Experimental Inhibition of Carbonate Precipitation by Sulfite Minerals **[#1030]**
Experiments show that sulfite minerals inhibit carbonate precipitation at pH ~7, consistent with the presence of clays and absence of carbonates on early Mars. Subsequent oxidation of these sulfites yields acid and mixtures of sulfates and Fe-oxides.

MERCURY: EVOLUTION AND TECTONICS
Wednesday, 1:30 p.m. Waterway Ballroom 4

Chairs: **Thomas Watters and Mark Wieczorek**

1:30 p.m. Robuchon G. * Tobie G. Choblet G. Cadek O. Mocquet A.
Thermal Evolution of Mercury: Implication for Despinning and Contraction **[#1866]**
Mercury's surface exhibits specific features, lobate scarps, that suggest that Mercury has experienced a change of shape during its history. We perform 3D simulations to evaluate: evolution of the temperature, despinning, shape and stress field.

1:45 p.m. Watters T. R. * Murchie S. L. Robinson M. S. Head J. W. Chapman C. R. Solomon S. C. Denevi B. W. André S. L. Fassett C. I. MESSENGER Team
A Newly Discovered Impact Basin on Mercury Revealed by MESSENGER **[#1817]**
Images obtained from the second MESSENGER flyby of Mercury in October 2008 have revealed a large, previously unrecognized impact basin in the southern hemisphere.

2:00 p.m. Freed A. M. * Solomon S. C. Watters T. R. Phillips R. J. Zuber M. T.
Could Pantheon Fossae be the Result of the Apollodorus Crater-forming Impact within the Caloris Basin, Mercury? **[#1362]**
We use finite element models to explore the idea that the Apollodorus crater-forming impact induced the formation of the radially oriented graben of the Pantheon Fossae complex near the center of the Caloris basin, Mercury.

2:15 p.m. Klimczak C. * Nahm A. L. Schultz R. A.
Evaluation of the Origin Hypotheses of Pantheon Fossae, Mercury **[#1251]**
By means of a detailed study of the graben pattern on MESSENGER image PIA10397, a strain analysis along five concentric traverses, and an analysis of the loading of the mercurian lithosphere, different origin hypotheses of the Pantheon Fossae structure are evaluated.

2:30 p.m. Rothery D. A. * Massironi M.
Beagle Rupes — Evidence for a Basal Decollement of Regional Extent in Mercury's Lithosphere **[#1702]**
Beagle Rupes is a thrust bounded by transpressive lateral ramps. To remain in the elastic lithosphere, the dip of the fault must become shallower at depth. This is evidence for thin-skinned tectonics, with out-of-sequence thrusts, on Mercury.

VENUS GEOLOGY, VOLCANISM, TECTONICS, AND RESURFACING
Wednesday, 3:00 p.m. Waterway Ballroom 4

Chairs: **David Senske and Martha Gilmore**

3:00 p.m. Kreslavsky M. A. * Ivanov M. A. Head J. W.
The Geological History of Venus: Constraints from Buffered Crater Densities **[#1096]**
We apply buffered crater density technique to a new global geological map of Venus (Ivanov, 2008) and obtain robust constraints on relative timing of resurfacing history. We show that the atmospheric mass in the past was not significantly different.

3:15 p.m. Hansen V. L. * López I.
Venus Preserves a Rare Record of Early Terrestrial Planet Processes **[#2064]**
Geologic relations and thermal modeling indicate that ribbon tessera terrain (rtt) records a unique and ancient era of Venus evolution. A new global geologic map of rtt preserves a rare record of early terrestrial planet evolution processes.

3:30 p.m. Basilevsky A. T. * Raitala J. Head J. W.
Venus: Estimates of Absolute Time Duration of Corona Activity **[#1827]**
In the representative sample of coronae of Venus (55 coronae) we have found six coronae whose activity lasted for several hundred million years. Four of them which, represent the evolution of individual mantle plumes have astrum-like components.

3:45 p.m. Senske D. A. * Plaut J. J.
Geologic Evidence for a Thick Volcanic Crust in Part of Tellus Tessera, Venus **[#1707]**
Geologic mapping is performed to provide insight into the make-up of part of Tellus Tessera and suggests that some of this terrain may be a thick sequence of volcanic deposits.

4:00 p.m. Gilmore M. S. *
Tellus Regio, Venus: Evidence of Tectonic Assembly of Tessera Terrain and Implications for Exploration **[#2015]**
SW Tellus Regio is formed from the collision of distinct tessera units and plains materials.

4:15 p.m. White O. L. * Stofan E. R. Guest J. E.
A New Survey of Intermediate Volcanoes on Venus **[#1148]**
A new catalogue of intermediate volcanoes on Venus broadly incorporates four volcano types: cones, domes, shields and calderas. Frequency, size, altitude, latitudinal distribution and total areal cover statistics are presented for each type.

4:30 p.m. Aubele J. C. *
Shield Fields and Shield Plains on Venus: Contrasting Volcanic Units Exemplified in Shimti Tessera (V-11) and Vellamo Planitia (V-12) Quadrangles **[#2396]**
Shield fields and shield plains appear to represent different volcanic styles and may represent different temporal associations in Venus geologic history.

ASTEROID–METEORITE CONNECTIONS
Wednesday, 1:30 p.m. Waterway Ballroom 5

Chairs: **Andrew Rivkin and Phil Bland**

1:30 p.m. Hildebrand A. R. * Milley E. P. Brown P. G. McCausland P. J. A. Edwards W. Beech M. Ling A. Sarty G. Paulson M. D. Maillet L. A. Jones S. F.
Characteristics of a Bright Fireball and Meteorite Fall at Buzzard Coulee, Saskatchewan, Canada, November 20, 2008 **[#2505]**
A bright fireball was widely observed across Alberta, Saskatchewan and Manitoba from 17:26:40 to 17:26:45 MST during late twilight on November 20, 2008.

1:45 p.m. Bland P. A. * Spurný P. Towner M. C. Bevan A. W. R. Singleton A. T. Chesley S. R. Bottke W. F. Jr. Shrbený L. Borovicka J. McClafferty T. Vaughan D. Benedix G. K. Deacon G. Hough R. M.
A Eucrite Delivered from an Aten-type Orbit: The Last Link in the Chain from 4 Vesta to Earth **[#1664]**
A likely scenario is that our meteorite is a fragment of a Vestoid, derived from the innermost region of the main belt, delivered from the ν_6 resonance, evolving onto an Aten-type orbit, before entering the atmosphere over south-western Australia.

2:00 p.m. Gaffey M. J. *
Identifying Asteroidal Ordinary Chondrite Assemblages and Petrographic Types from VNIR Spectra **[#1412]**
Existing spectral calibrations are sufficient to identify asteroidal ordinary chondrite assemblages from VNIR (~0.7–2.5 μm) spectra, but have limitations due to systematic mineralogical variations between and within the H-, L-, and LL-types.

2:15 p.m. Beck A. W. * McSween H. Y. Jr.
Interpretation of the Origin of Olivine in Diogenite Breccias **[#1127]**
This study proposes that the presence of olivine in diogenites is caused by the brecciation and incorporation of harzburgite fragments. This is based on textural observation and chemical analyses of olivine and two distinct orthopyroxene phases in ten diogenite breccias.

2:30 p.m. Lim L. F. * Emery J. P. Moskovitz N. A.
Diogenite-like Features in the Spitzer IRS (5–35 μm) Spectrum of 956 Elisa **[#2204]**
We report preliminary results from the Spitzer IRS (Infrared Spectrograph) observations of the V-type asteroid 956 Elisa. Several features of this spectrum suggest the presence of diogenitic material at a relatively coarse particle size.

2:45 p.m. Delaney J. S. *
The Surface of 4 Vesta: A Petrologist's View **[#1600]**
Vesta has provinces with distinct spectral characteristics. The regolith is best represented by howardites. The howardite meteorites provide the optimum sample suite for constraining the Dawn spectral data.

3:00 p.m. McFadden L. A. * Ammonito E. Cloutis E. A. Coradini A. deSanctis M. C. Fulchignoni M. Hadamcik E. Hiroi T. Kolokolova L. Levasseur-Regourd A. C. Psarev V. Renard J. -B.
Coordinated Laboratory Studies of Meteorites Supporting Rosetta Mission's Asteroid Flyby Target: 2867 Steins **[#2287]**
Aubrite ALH7 8113,82 is studied to support Rosetta flyby of Steins, an E-type asteroid. Two questions are, what is the spectrally active material in Steins at 500 nm? Is Steins a fragment from an aubrite?

3:15 p.m. Bottke W. F. * Nesvorný D. Vokrouhlický D. Morbidelli A.
The Gefion Family as the Probable Source of the L Chondrite Meteorites **[#1445]**
Fragments from the Gefion asteroid family-forming event 470 My ago are the probable source of the tiny fossil L-chondrite meteorites found in an marine limestone quarry in Sweden as well as the larger L-chondrites reaching Earth today.

3:30 p.m. Rivkin A. S. * Thomas C. A. Trilling D. E. Enga M. T. Grier J. A.
Small Koronis-Family Objects as a Probe of Space Weathering: Broadband Spectrophotometry from Magellan and Kitt Peak **[#1774]**
Broadband spectrophotometry of 1–5 km Koronis family objects shows them spanning the range from S-class to Q-class colors. This is consistent with space weathering rather than composition as the cause for similar findings in the NEO population.

3:45 p.m. Roth A. S. G. * Baur H. Heber V. S. Reusser E. Wieler R.
Cosmic-Ray-produced Helium and Neon in Chondrules in Allende and Murchison **[#1838]**
Most chondrules in Allende and Murchison show nearly identical cosmic ray exposure ages. Six chondrules in Murchison show large cosmogenic gas excesses, most likely acquired during tens of Ma of exposure in a parent body regolith.

4:00 p.m. Fieber-Beyer S. K. * Gaffey M. J. Hardersen P. S.
Near-Infrared Spectroscopy of 3:1 Kirkwood Gap Asteroids 1379 Lomonosawa and 974 Lioba: Plausible Parent Bodies of L- and LL-Chondrites **[#1115]**
We present a mineralogical assessment of 3:1 Kirkwood Gap asteroids, 1379 Lomonosawa and 974 Lioba, using data obtained May 19 and 20, 2008 UT using the NASA Infrared Telescope Facility.

4:15 p.m. Sunshine J. M. * Day J. M. D. Ash R. D. McCoy T. J. Bus S. J. Klima R. L. Hiroi T.
Searching for the Evolved Crust of Oxidized Asteroids **[#1965]**
The spectral properties of the unique GRA 06128/9 meteorites are examined so similar asteroids can be recognized. Giving the geochemical links to brachinites, they may occur near previously identified brachinites-like asteroids.

4:30 p.m. Sasso M. R. * Macke R. J. Britt D. T. Rivers M. L. Ebel D. S. Friedrich J. M.
Physical Properties of Incompletely Compacted Equilibrated Ordinary Chondrites: Implications for Asteroidal Structure and Impact Processing **[#1670]**
We detail our synchrotron x-ray microtomographic investigations into the 3D nature of pore spaces in several unusual chondrites. Implications for asteroidal structures and the historical mechanical processing of these materials will be discussed.

IMPACTS I: MODELS AND EXPERIMENTS
Wednesday, 1:30 p.m. Waterway Ballroom 6

Chairs: **Kai Wünnemann and Keith Holsapple**

1:30 p.m. Hammond N. P. * Nimmo F. Korykansky D.
Hydrocode Modeling of the South Pole Aitken Basin-forming Impact **[#1455]**
We model vertical lunar impacts to investigate whether the formation of the South Pole Aitken Basin excavated lunar mantle.

1:45 p.m. Plesko C. S. * Asphaug E. Weaver R. P. Wohletz K. H. Korycansky D. G.
Initial Conditions of an Impact-generated Greenhouse Event from Hydrocode Models of Large Impacts on Noachian Mars **[#2167]**
We model impacts into Mars-like stratigraphies to constrain initial conditions and energy partitioning of hypothesized impact-generated greenhouse events. Early results show impactors as small $d = 50$ km may trigger a greenhouse event.

2:00 p.m. Senft L. E. * Stewart S. T.
The Role of Phase Changes During Impact Cratering on Icy Satellites **[#2130]**
We conducted simulations of impacts onto the Jovian satellite Ganymede using a new EOS for H_2O. We find that including the high-pressure solid phases produces more complex crater formation phenomenology.

2:15 p.m. Collins G. S. * Davison T. Elbeshausen D. Wünnemann K.
Numerical Simulations of Oblique Impacts: The Effect of Impact Angle and Target Strength on Crater Shape **[#1620]**
Impact craters are asymmetric if the impactor's trajectory is below a threshold angle of incidence. Lab experiments and 3D numerical simulations show that the threshold angle is higher if target strength is high and cratering efficiency is low.

2:30 p.m. Stöffler D. * Meyer C. Reimold W. U. Artemieva N. A. Wünnemann K.
Ries Crater and Suevite Revisited: Part I Observations **[#1504]**
A reevalution of the geologic setting and properties of suevite at the Ries Crater reveals a new hypothesis based on "phreato-magmatic"-like explosions of a clast-laden impact melt sheet induced by surficial water.

2:45 p.m. Artemieva N. A. * Wünnemann K. Meyer C. Reimold W. U. Stöffler D.
Ries Crater and Suevite Revisited: Part II Modelling **[#1526]**
Presented numerical models cannot reproduce the previous hypotheses on suevite origin as plume-related non-ballistic ejecta. We suggest an alternative explanation.

3:00 p.m. Kimberley J. * Ramesh K. T. Barnouin-Jha O. S. Swaminathan P. K. Ernst C. M.
Visualization of High- and Low-Rate Compressive Failure of Quartz **[#2337]**
Quasistatic and dynamic compression experiments were performed on single crystal quartz specimens. In cases where the specimens were loaded below catastrophic failure crack propagation was observed only during the unloading of the specimen.

3:15 p.m. Mikouchi T. * Ohsumi K. Ichiyanagi K. Adachi S. Nozawa S. Koshihara S. Zolensky M.
Nano-Second Time-Resolved Synchrotron X-Ray Diffraction Study of Olivine Under Laser-induced Shock Compression **[#2250]**
We performed *in situ* nano-second time-resolved synchrotron X-ray diffraction analysis of olivine by synchronization of X-ray and laser pulses. We could successfully obtain 0–30 ns Laue diffraction images at the shock pressure of 1.2–6.5 GPa.

3:30 p.m. Bell M. S. *
Relative Shock Effects in Mixed Powders of Calcite, Gypsum, and Quartz: A Calibration Scheme from Shock Experiments **[#1321]**
A systematic experimental shock study of calcite, gypsum, and quartz powders mixed 1:1:1 was carried out in order to calibrate shock pressures in naturally shocked carbonates and sulfates to shock effects in quartz.

3:45 p.m. Ishibashi K. * Yagi T. Matsui T.
Determination of the Decomposition Boundary of $CaCO_3$ at High Temperature: Implications for Impact-induced Degassing of $CaCO_3$ **[#1569]**
We experimentally determined the decomposition boundary of $CaCO_3$ up to ~5000 K and ~10 GPa with a technique of laser-heated diamond-anvil cell. Then, impact-induced degassing of $CaCO_3$ is discussed using the newly determined decomposition boundary.

4:00 p.m. Hermalyn B. * Schultz P. H. Heineck J. T.
Early-Stage Ejecta Velocity Distribution **[#2492]**
This study investigates high speed early-time departures from the accepted power-law relationship of ejecta velocity over a range of projectile diameters by utilizing a new high speed 3D-Particle Imaging Velocimetry technique.

4:15 p.m. Kraus R. G. * Stewart S. T.
Thermodynamics of Impacts onto Icy Mixtures: Peak and Post-Shock Temperature Measurements in an Ice-Sand Mixture **[#2508]**
We present the first experimental shock and release temperature data on ice-sand mixtures.

4:30 p.m. Schultz P. H. * Anderson J. L. B. Hermalyn B.
Origin and Significance of Uprange Ray Patterns **[#2496]**
Arcuate uprange crater rays occur on the Moon, Mercury, and Mars. This pattern reflects depends on the evolution of initial coupling that depends on both impactor (density, speed and angle) and target (porosity).

SOLAR WIND AND GENESIS: MEASUREMENTS AND INTERPRETATION
Wednesday, 1:30 p.m. Montgomery Ballroom

Chairs: **Kathy Kitts and Nadia Vogel**

1:30 p.m. Meier M. M. M. * Schmitz B. Baur H. Wieler R.
A Regolith Pre-Exposure Signature in Fossil Micrometeorites from an Asteroid Collision 470 Million Years Ago **[#1153]**
Some 25% of fossil micrometeorites (MM) from an asteroid collision 470 Myrs ago have Ne-21 CRE ages of 10–50 Myrs due to regolith preexposure, requiring to revisit the cometary origin interpretation of a similar pattern observed in recent MM and IDP.

1:45 p.m. Vogel N. * Heber V. S. Baur H. Burnett D. S. Wieler R.
Preliminary Genesis Bulk Solar Wind Ar, Kr, and Xe Abundances in Comparison to Young Lunar Regolith and Solar Photosphere Data **[#1964]**
We present preliminary Genesis bulk solar wind Ar, Kr, and Xe isotope and element compositions. These are compared to SW abundances inferred from young lunar regoliths and to photospheric data to rule on fractionation between the Sun and the SW.

2:00 p.m. Grimberg A. * Bühler F. Wieler R. Bochsler P.
Comparison of Solar Wind Noble Gas Data from Genesis with Apollo/SWC — New Results from Implantation Experiments **[#1537]**
We will show new results from extensive implantation experiments to adress differences of isotopic and elemental solar wind noble gas data between Genesis and Apollo/SWC.

2:15 p.m. Heber V. S. * Wiens R. C. Bochsler P. Wieler R. Burnett D. S.
Fractionation Processes in the Solar Wind Revealed by Noble Gases Collected by Genesis Regime Targets **[#2503]**
Significant differences in isotopic and elemental compositions of noble gases among the different SW regimes were found. Here we discuss fractionation processes in the solar wind.

2:30 p.m. Meshik A. P. * Hohenberg C. M. Pravdivtseva O. V. Mabry J. C. Allton J. H. Burnett D. S.
Relative Abundances of Heavy Noble Gases from the Polished Aluminum Solar Wind Collector on Genesis **[#2037]**
Here we report the results of our Ar-Kr-Xe analysis of solar wind captured by the Genesis Polished Aluminum Collector.

2:45 p.m. Kitts K. * Choi Y. Eng P. Sutton S. R.
X-Ray Standing Wave Based Internal Reference Method for Quantification of Implanted Fe in Genesis Samples **[#1439]**
We present a new internal reference method for XSW and XRF that does not require a separate standard and compare that directly to the implant standard method and present the absolute Fe solar wind abundance in Genesis sapphire 50722.

3:00 p.m. Veryovkin I. V. * Tripa C. E. Zinovev A. V. Pellin M. J. Burnett D. S.
Solar Wind Calcium and Chromium in GENESIS Bulk Silicon Collector: Simultaneous Measurements by RIMS **[#2422]**
First results for simultaneous RIMS measurements of solar wind Ca and Cr in Genesis collectors are reported.

3:15 p.m. Pepin R. O. * Becker R. H. Schlutter D. J.
Solar Wind Nitrogen in Genesis Gold-on-Sapphire (AuOS) Collectors **[#2103]**
We report direct measurements of the isotopic composition of solar wind nitrogen in nitrogen extracted from Genesis gold-on-sapphire (AuOS) collectors by a low-temperature amalgamation technique. The measured $\delta^{15}N$ value is ~ +325‰.

3:30 p.m. Marty B. * Zimmermann L. Burnard P. G. Burnett D. L. Heber V. S. Wieler R. Bochsler P. Wiens R. C. Sestak S. Franchi I. A.
In Search of Solar Wind Nitrogen in Genesis Material: Further Analysis of a Gold Cross Arm of the Concentrator **[#1857]**
We have analysed nitrogen and noble gases in another gold cross arm of the Genesis concentrator by laser ablation - static MS. Results define a correlation that points to a light N isotope composition within the range of Jupiter atmospheric value.

MARS: AQUEOUS PROCESSES
Thursday, 8:30 a.m. Waterway Ballroom 1

Chairs: Rebecca Williams and Mary Chapman

8:30 a.m. Williams R. M. E. * Weitz C. M.
Stratigraphic Context for Inverted Channels on the Plains North of Juventae Chasma: Implications for Post-Noachian Martian Climate Change **[#1935]**
Fluvial features in negative and inverted relief are preserved in a layered section on plains north of Juventae Chasma. The record of geologic events preserved here suggests that clement climate conditions were episodic in the post-Noachian period.

8:45 a.m. McGowan E. M. * McGill G. E.
Putative Water Related Features: Cydonia Mensae and Utopia Planitia, Mars **[#1295]**
Analogous spatial relationships between putative shorelines, pitted cones and giant polygons in are found in both Cydonia Mensae and Utopia Planitia.

9:00 a.m. Erkeling G. * Reiss D. Hiesinger H. Jaumann R.
Morphologic, Stratigraphic and Morphometric Investigations in Eastern Libya Montes, Mars: Implications for Long-Term Fluvial Activity **[#1604]**
The Noachian highlands of Libya Montes represent one of the oldest regions on Mars that have been degraded by intensive, long-term and repeated fluvial processes which led to the formation of widespread and mature "dendritic valley networks."

9:15 a.m. Baker D. M. * Head J. W. Marchant D. R.
Flow Patterns of Lobate Debris Aprons and Lineated Valley Fill North of Ismeniae Fossae, Mars **[#1822]**
Flow patterns are mapped within lobate debris aprons and lineated valley fill north of Ismeniae Fossae, Mars. Flowlines are sourced in plateau alcoves and form large, well-integrated systems, consistent with a debris-covered glacier interpretation.

9:30 a.m. Howard D. A. *
Modeled Catastrophic Outflow at Aram Chaos Channel, Mars **[#2179]**
The first hydraulic modeling of Aram Chaos channel is presented indicating that fluvial flow may have created enough stream power to sculpt the channel in a single catastrophic outflow event.

9:45 a.m. Kargel J. S. * Furfaro R. Rodriguez J. A. P. Candelaria P. Prieto-Ballesteros O. Marion G. M. Crowley J. Hook S.
No-Rainfall Origin of Melas Chasma Valley Networks by Salt Dehydration: Numerical Thermal Model **[#2063]**
Salts in Melas Chasma should produce large positive thermal anomalies and warm hypersaline conditions at shallow depths. Dewatering may yield brine eruptions, and we argue that in Melas Chasma valley networks were produced this way, not by rainfall.

10:00 a.m. Chapman M. G. * Neukum G. Dumke A. Michaels G. van Gasselt S. Kneissl T. Zuschneid W. Hauber E. Mangold N.
Evidence of Late-Stage Fluvial Outflow in Echus Chasma, Mars **[#1374]**
This abstract discusses a highlight of a mapping-based study of the Echus Chasma and Kasei Valles system: a fracture in Echus Chasma, identified to have sourced at least one late-stage flood, and possibly other lava and water floods.

10:15 a.m. Hauber E. * Preusker F. Trauthan F. Reiss D. Carlsson A. E. Hiesinger H. Jaumann R. Johansson H. A. B. Johansson L. Johnsson A. McDaniel S. Olvmo M. Zanetti M.
Morphometry of Alluvial Fans in a Polar Desert (Svalbard, Norway): Implications for Interpreting Martian Fans **[#1658]**
We analyze field measurements and high-quality image (20 cm/px) and topographic (50 cm/px) data of alluvial fans in Svalbard, an arcic polar desert, as analogues for martian fans. Remotely-sensed morphometric data alone are insufficient for unambiguous interpretations.

10:30 a.m. Ori G. G. * Di Achille G. Pondrelli M.
Deltas on Mars **[#1579]**
Deltaic depositional systems are an important component in the geological history of Mars. Deltaic deposits provide evidence of a complex and vast hydrological system and are the most prominent features suggesting the existence of long-lasting standing bodies of water.

10:45 a.m. Weitz C. M. * Noe Dobrea E. Williams R. M. E. Metz J. Quantin C. Parente M. Grotzinger J.
MRO Observations of Fluvial Features, Sulfates, and Other Landforms in the Melas Chasma Basin **[#1874]**
We have used new data acquired from the Mars Reconnaissance Orbiter (MRO), including HiRISE, CTX, and CRISM, to analyze fluvial features, sulfates, and other landforms in the Melas Chasma Basin.

11:00 a.m. Parker T. J. *
East Acidalia Shoreline Morphology at MRO CTX Image Scales **[#2551]**
Current work to revisit sites along the lowland/upland boundary where landforms interpreted to be shorelines were identified, using CTX images georeferenced to MOLA topography.

11:15 a.m. Wray J. J. * Milliken R. E. Swayze G. A. Dundas C. M. Bishop J. L. Murchie S. L. Seelos F. P. Squyres S. W.
Columbus Crater and Other Possible Paleolakes in Terra Sirenum, Mars **[#1896]**
Diverse, interbedded sulfate and clay minerals are observed in light-toned, layered deposits inside several large degraded craters in the Terra Sirenum region of Mars. These may be lacustrine sediments precipitated under a range of pH conditions.

11:30 a.m. Di Achille G. * Hynek B. M. Searls M. L.
New Evidence for the Shalbatana Vallis Paleolake, Mars, from the High Resolution Imaging Science Experiment (HiRISE) **[#1939]**
Sub-meter scale High Resolution Imaging Science Experiment (HiRISE) images of Shalbatana Vallis, Mars, reveal the first direct evidence of martian strandlines along a delta formed within an intravalley lake during the Hesperian (~3.4 Ga).

MAGMATIC VOLATILES AND ERUPTIVE CONDITIONS OF LUNAR BASALTS
Thursday, 8:30 a.m. Waterway Ballroom 4

Chairs: **Justin Hagerty and Brad Jolliff**

8:30 a.m. Friedman B. Saal A. E. * Hauri E. H. Van Orman J. Rutherford M. J.
The Volatile Content of the Apollo 15 Picritic Glasses **[#2444]**
We report over 200 new volatile data on volcanic glasses from the Apollo 15 mission. These new data extend the range of previously reported H_2O, C, F, S and Cl contents, and confirm the presence of significant dissolved magmatic volatiles in lunar volcanic glasses.

8:45 a.m. McCubbin F. M. * Nekvasil H. Jolliff B. L. Carpenter P. K. Zeigler R. A.
Inhomogeneous Distribution of Magmatic Volatiles in the Lunar Interior: Clues from the Mineral Apatite **[#2246]**
The variations in apatite volatile contents (F, Cl, OH) between Mare basalts and the magnesian and alkali-suite rocks indicate that the lunar interior may be stratified with respect to magmatic volatiles.

9:00 a.m. Agee C. B. * Duncan M. S.
The Effect of CO_2 on Density of Molten Apollo 14 Black Glass at High Pressure **[#1266]**
We present new experimental data on the effect of pressure on CO_2 in lunar magmas.

9:15 a.m. Grimm R. E. * McSween H. Y. Jr.
Water and the Electrical Conductivity of the Lunar Mantle **[#1958]**
Tens of ppm H_2O in ultramafic minerals can fit the lunar conductivity profile, without recourse to high alumina content.

9:30 a.m. Barr J. A. * Grove T. L.
Toward Developing a Garnet Lherzolite Saturation Model for Lunar Low-Ti, Ultramafic Green Glass Compositions **[#2161]**
To evaluate the possible role of primordial lunar mantle in the derivation of the low-Ti ultramafic green glasses, a model of garnet lherzolite melting must be developed for relevant lunar compositions.

9:45 a.m. Liang Y. * Hess P. C.
Simple Models for Trace Element Fractionation During Melting and Melt Migration in an Upwelling Heterogeneous Lunar Mantle **[#2117]**
The lunar mantle is chemically and lithologically heterogeneous. In this paper, we present simple models for trace element fractionation during melting and melt migration in a heterogeneous lunar mantle and discuss their implications for lunar magma genesis.

10:00 a.m. Wilson L. * Head J. W.
Lunar Volcanism: Factors Controlling Intrusion Geometries and Eruption Conditions **[#1160]**
We review theoretical factors controlling geometries of dikes that either do or do not reach the surface to feed eruptions. We then compare the surface expressions of the consequences of both kinds of event with observed lunar volcanic features.

10:15 a.m. Thomson B. J. * Grosfils E. B. Bussey D. B. J. Spudis P. D.
The Thickness of Mare Basalts in Imbrium Basin Estimated from Penetrating Craters **[#1727]**
Here we report basalt thicknesses values in Imbrium Basin derived from analyses of Clementine UV-VIS multispectral images of large craters that penetrate (or failed to penetrate) the mare. The mare volume is ~2× greater than some previous estimates.

10:30 a.m. Oshrin J. Neal C. R. *
Crystal Size Distributions and Basalt Evolution: More from Fra Mauro **[#1706]**
Crystal size distributions have been used to calculated residence times for plagioclase crystals. Trace element data from different crystal populations are also presented.

10:45 a.m. Kramer G. Y. * Hawke B. R. Giguere T. A. Heitman G. McCord T. B.
The Mare Basalts of Eastern Frigoris **[#2369]**
The ejecta composition of small, immature impacts into Eastern Mare Frigoris reveal low-Fe, very low-Ti mare basalts, which may even be high alumina basalts.

11:00 a.m. Hawke B. R. Giguere T. A. * Blewett D. T. Boyce J. M. Cahill J. Gillis-Davis J. J. Hagerty J. J. Lucey P. G. Peterson C. A. Smith G. A. Spudis P. D. Taylor G. J.
Remote Sensing and Geologic Studies of the Northeastern Portion of the Lunar Nearside: Final Results **[#1483]**
Almost all of the light plains units immediately east and southeast of eastern Mare Frigoris are shown to be cryptomare deposits. The buried or obscured mare flows are dominated by VLT and low-TiO_2 mare basalts.

11:15 a.m. Kiefer W. S. *
Gravity Observations of the Aristarchus Plateau on the Moon: Implications for the Volcanic and Impact Histories of the Plateau **[#1106]**
Gravity anomalies in this region wrap around the fault-bounded eastern margin of the Aristarchus Plateau and place constraints on the impact-induced uplift history of the plateau.

11:30 a.m. Hagerty J. J. * Lawrence D. J. Hawke B. R. Gaddis L. R.
New Estimates of Thorium Abundances for the Rima Bode Pyroclastic Glass Deposit **[#1852]**
We use forward modeling of Lunar Prospector Gamma Ray Spectrometer thorium data to show that the Rima Bode pyroclastic glass deposit contains elevated thorium abundances.

COMPARATIVE PLANETOLOGY
Thursday, 8:30 a.m. Waterway Ballroom 5

Chairs: **Patrick McGovern and Kathleen Nicoll**

8:30 a.m. Montési L. G. J. *
Fabric Development, Shear Zone Formation, and the Possibility of Plate Tectonics on Earth and Venus **[#2350]**
The presence of plate tectonics on Earth and not Venus can be explained by the formation of ductile shear, which is possible as a consequence of layer development in a polyphase material on Earth, but not if all phases are dry.

8:45 a.m. McGovern P. J. * Watters T. R.
Interaction of Membrane Stresses and Magma Ascent at Large Impact Basins on Mars and Mercury **[#1765]**
We use a simple mathematical model of the broad-scale loading effects induced by impact basins to investigate how such loading may control magmatism within and around basins on Mars (Borealis, Utopia, and Hellas) and Mercury (Caloris).

9:00 a.m. Lee C.-T. A. * Luffi P. Dalton H. A.
Application of New Thermobarometers to Constraining the Origin of Magmas on Mars, Venus, Earth, the Moon, and the Eucrite Parent Body **[#1467]**
New thermobarometers are presented that can estimate T-P of magma generation on Earth, Mars and other planetary bodies, providing constraints on lithosphere thickness and planetary thermal state (emphasis will be on Mars).

9:15 a.m. Horodyskyj U. N. * Wyatt M. B.
Compositional Variations with Depth in Icelandic Cores: Applications to Integrated Mars Remote Sensing Data Sets **[#2527]**
To better constrain the regional effects and depth of alteration at high-latitudes on Mars, we are examining compositional variations with depth in Icelandic basaltic cores.

9:30 a.m. Nicoll K. * Chan M. A. Parker T. J. Jewell P. W. Komatsu G. Okubo C. H.
Bonneville Basin Analogues for Large Lake Processes and Chronologies of Geomorphic Development on Mars **[#1962]**
We present an inventory of geomorphic analogues for Lake Bonneville and Mars, with focus on potential standing-water features. The goal is to understand water as a geomorphic agent at a variety of temporal and spatial scales.

9:45 a.m. Halevy I. * Schrag D. P. Pierrehumbert R. T.
Radiative Transfer in the Early Atmospheres of Mars and Earth **[#1029]**
Small differences in the formulation of CO_2 absorption in a line-by-line model result in large differences in the radiative forcing provided by 0.1—5 bars of CO_2. This uncertainty pervades any modeling study of the early planetary climate.

INTERSTELLAR MATTER: ORIGINS AND RELATIONSHIPS
Thursday, 10:00 a.m. Waterway Ballroom 5

Chair: **Frank Stadermann**

10:00 a.m. Duprat J. * Dobrica E. Engrand C. Aléon J. Gounelle M. Leroux H. Marrocchi Y. Meibom A. Mostefaoui S. Rouzaud J.-N. Robert F.
Extreme Deuterium Enrichment in Organic Matter from Cometary Antarctic Micrometeorites **[#1724]**
Deuterium rich organic matter, with D/H up to 30 times the terrestrial value, has been identified in ultra-carbonaceous micrometeorites from central Antarctic snow, strongly suggesting a cometary origin for these objects.

10:15 a.m. Floss C. * Stadermann F. J. Yada T. Noguchi T. Nakamura T.
Anomalous Nitrogen Isotopic Compositions in the Stardust-rich Antarctic Micrometeorite T98G8: Affinities to Primitive CR Chondrites and Anhydrous IDPs **[#1082]**
We report the presence of abundant N isotopic anomalies in T98G8, an Antarctic micrometeorite that contains high abundances of presolar grains. Its mineralogical and isotopic characteristics suggest a link to IDPs or certain CR chondrites.

10:30 a.m. Bonal L. * Huss G. R. Krot A. N. Nagashima K.
Highly ^{15}N-enriched Chondritic Clasts in the CB/CH-like Isheyevo Meteorite **[#2046]**
We report the discovery of chondritic clasts in the CB/CH-like meteorite Isheyevo, characterized by bulk ^{15}N-enrichment such as $\delta^{15}N = 1000–1300‰$ and where hotspots (up to $\delta^{15}N = 4000‰$) are present. Their origin will be discussed.

10:45 a.m. Ishii H. A. * Bradley J. P. Bonal L. Krot A. N. Huss G. R. Nagashima K. Hutcheon I. D. Teslich N.
Transmission Electron Microscopy on Highly ^{15}N-Enriched Chondritic Clasts in the Isheyevo Meteorite **[#2467]**
To explore the possible origin and carrier(s) of extreme ^{15}N enrichments in unique chondritic clasts in the Isheyevo CH/CB-like meteorite, TEM analyses are being undertaken. Initial results from bulk-enriched and hotspot areas are presented.

11:00 a.m. Briani G. * Gounelle M. Marrocchi Y. Mostefaoui S. Robert F. Leroux H. Meibom A.
Ultra-Pristine Extra-Terrestrial Material with Unprecedented Nitrogen Isotopic Variation **[#1642]**
A xenolith in the chondrite Isheyevo shows pristine mineralogy and the most extreme N isotopic variation measured in any solar system material – but no H and C isotopic anomalies. This poses new challenges for models for light element fractionation.

11:15 a.m. De Gregorio B. T. * Stroud R. M. Nittler L. R. Cody G. D. Kilcoyne A. L. D.
Isotopically Anomalous Organic Globules from Comet 81P/Wild 2 **[#1130]**
Two Stardust cometary organic globules contain anomalous δD or $\delta^{15}N$ (but not both), indicating a presolar origin.

IMPACTS II: CRATERS AND EJECTA
Thursday, 8:30 a.m. Waterway Ballroom 6

Chairs: **Peter Schulte and Tamara Goldin**

8:30 a.m. van Soest M. C. * Wartho J.-A. Monteleone B. D. Hodges K. V. Koeberl C. Schmieder M. Buchner E. Spray J. G. Bezys R. K. Reimold W. U.
(U-Th)/He Dating of Single Zircon and Apatite Crystals — A New Tool for Dating Terrestrial Impact Structures **[#2041]**
The low temperature (U-Th)/He technique has been utilized to date individual crystals from the Manicouagan, Lake Saint Martin, and Bosumtwi impact structures. New (U-Th)/He zircon ages are in agreement with ages obtained via other dating methods.

8:45 a.m. Sapers H. M. * Osinski G. R. Banerjee N.
Re-Evaluating the Rochechouart Impactites: Petrographic Classification, Hydrothermal Alteration and Evidence for Carbonate Bearing Target Rocks **[#1284]**
A systematic classification of the Rochechouart impacts is proposed. Evidence for post-impact hydrothermal alteration was observed. A carbonate clast within the lithic impact breccia suggests the existence of carbonate in the pre-impact target rocks.

9:00 a.m. Mohr-Westheide T. * Reimold W. U.
Chemical Analysis of Small-Scale Pseudotachylitic Breccia in Archean Gneiss of the Vredefort Dome, South Africa **[#1528]**
Results of a new microchemical investigation of small-scale pseudotachylitic breccias from the Archean gneiss of the Vredefort dome are reported. Limited mixing and for small veinlets local melt formation are observed.

9:15 a.m. McDonald I. Koeberl C. * Gurov E.
A Meteoritic Component in Melt Rocks from the Boltysh Impact Structure, Ukraine: First Assessment **[#1252]**
A chondritic component has been detected in impact melt rocks from the Boltysh impact structure, Ukraine.

9:30 a.m. Schmieder M. * Jourdan F. Hietala S. Moilanen J. Öhman T. Buchner E.
A High-Precision Late Mesoproterozoic $^{40}Ar/^{39}Ar$ Age for the Keurusselkä Impact Structure (Finland) **[#1028]**
The Kirkkoranta pseudotachylitic breccia dike is the first finding of impact-related melt lithologies known from the deeply eroded Keurusselkä impact structure, Finland. $^{40}Ar/^{39}Ar$ dating yielded a late Mesoproterozoic (Stenian) age of the rock.

9:45 a.m. Kofman R. S. * Herd C. D. K. Walton E. L. Froese D. G.
The Late Holocene Whitecourt Meteorite Impact Crater: A Low-Energy Hypervelocity Event **[#1942]**
The Whitecourt Meteorite Impact Crater resulted from the low-energy hypervelocity impact of an iron meteoroid. The crater is 36 m in diameter with meteorites scattered up to 70 m from the rim. The crater and ejecta blanket are all well-preserved.

10:00 a.m. Kenkmann T. * Reimold W. U. Khirfan M. Salameh E. Konsul K. Lehmann T. Khoury H.
The Impact Crater Jebel Waqf as Suwwan in Jordan: Effects of Target Heterogeneity and Impact Obliquity on Central Uplift Formation **[#1592]**
We present results of a field campaign to the first large impact crater of the Middle East, which has recently been discovered. A superb exposure of the central uplift allows block sizes to be measured and the impact direction to be derived.

10:15 a.m. Herrick R. R. * Schenk P. M.
Surveys of Elliptical Crater Populations on the Saturnian Satellites and Mercury **[#2352]**
Planetary impacts at the lowest impact angles form elliptical craters. The angle at which this occurs can be inferred from a planet's cratering record. Here we compare five saturnian moons and Mercury to previous work for moon, Mars, and Venus.

10:30 a.m. Schmitz B. * Heck P. R. Alwmark C. Kita N. T. Peucker-Ehrenbrink B. Ushikubo T. Valley J. W.
Determining the Impactor of the Ordovician Lockne Crater: Oxygen Isotopes in Chromite Versus Sedimentary PGE Signatures **[#1161]**
Oxygen isotopic results for chromite from the Lockne cCater and new PGE results show that the claims by Tagle and Schmitt (2008, LPSC abstr. #1418) that the Lockne Crater was caused by a nonmagmatic iron meteorite lacks substance entirely.

10:45 a.m. Schulte P. * Deutsch A. Salge T.
A Dual-Layer Chicxulub Ejecta Sequence with Shocked Carbonates from the Cretaceous-Tertiary (K/T) Boundary, ODP Leg 207, Western Atlantic **[#1859]**
An up to 2-cm thick Chicxulub ejecta deposit marks the Cretaceous-Tertiary boundary in ODP Leg 207 (Western Atlantic). High-resolution analysis reveals the presence of spherules as well as shocked tectosilicates and carbonate clasts.

11:00 a.m. Goldin T. J. * Melosh H. J.
Planet Earth Set to Broil: Thermal Radiation from Chicxulub Ejecta Reentry **[#2342]**
We model the thermal radiation transfer due to the atmospheric reentry of hypervelocity Chicxulub impact ejecta. Self-shielding of downward radiation by the spherules limits the magnitude and duration of the thermal pulse at the Earth's surface.

11:15 a.m. Ferrière L. * Robin E.
Composition and Origin of Ni-rich Spinel from the Cretaceous-Tertiary Boundary **[#1812]**
The main objective of our study is to characterize, at the nanometric scale, the internal microstructure of Ni-rich spinel from the K/T boundary, to better understand and constrain their formation conditions.

11:30 a.m. Harris R. S. * Schultz P. H.
Microscopic Fragments of an Angrite-like Asteroid in 5.28 Ma Impact Melt Breccias from Bahia Blanca, Argentina **[#2453]**
Meteoritic fragments preserved in a 5.28 Ma impact melt are mineralogically similar to angrites. We report the details and implications of their petrology and geochemistry.

MARS: TECTONICS AND DYNAMICS
Thursday, 1:30 p.m. Waterway Ballroom 1

Chairs: **Leslie Bleamaster and Jeffrey Andrews-Hanna**

1:30 p.m. Schultz R. A. * Nahm A. L.
Transient and Long-Term Displacement-Length Scaling of Planetary Faults **[#1075]**
We examine the relationship between fault displacement profiles and displacement-length scaling relations to identify transient and long-term fault growth.

1:45 p.m. Wyrick D. Y. * Smart K. J.
Discrete Element Modeling of Dike-induced Deformation **[#1647]**
Discrete element models of dike-induced deformation suggest the most distinctive topographic signature of an underlying dike are parallel ridges formed by contractional folding bounding a trough rather than an extensional fault-bounded graben.

2:00 p.m. Evans A. J. * Andrews-Hanna J. C. Zuber M. T.
Quantitative Constraints on Surface Erosion via Admittance Localization for Arabia Terra, Mars **[#2368]**
This research focuses on constraining erosion in Arabia Terra based on flexural modeling coupled with the observations.

2:15 p.m. Nahm A. L. * Schultz R. A.
Evaluation of the Orogenic Belt Hypothesis for the Formation of the Thaumasia Highlands, Mars **[#1069]**
The orogenic belt hypothesis for the formation of the Thaumasia Highlands is tested using critical taper wedge mechanics. We find that conditions required for their formation as an orogenic belt are improbable for Mars.

2:30 p.m. Bleamaster L. F. III*
A Dynamic Mechanism for Valles Marineris Formation **[#2552]**
I propose that although Tharsis uplift plays an important role in Valles Marineris formation, a Tharsis-driven tectonic history is incomplete and secondary to the long-lived dynamic influence of northern Borealis basin subsidence and adjustment of the northern lowlands.

2:45 p.m. Andrews-Hanna J. C. *
The Opening of the Valles Marineris Canyons on Mars: Stress Focusing Along the Buried Dichotomy Boundary Beneath Tharsis **[#1094]**
The Valles Marineris canyons formed as a result of Tharsis loading over the preexisting crustal dichotomy boundary, which generated a narrow belt of strongly extensional stresses just south of the boundary at the present-day location of the canyons.

3:00 p.m. Zhong S. * Sramek O.
The Causes and Consequences of the Crustal Dichotomy and Their Implications for the Early Evolution of Mars **[#2432]**
Endogenic and exogenic formation mechanisms for the crustal dichotomy and their consequences on mantle dynamics, melting and volcanism are critically compared and examined.

3:15 p.m. Šrámek O. * Zhong S.
Dynamic Stress at Martian Surface in the Model of Rotation of the Lithosphere **[#2491]**
We compute dynamic stresses at martian surface in the model of rotation of the lithosphere and we will discuss the implications for the martian tectonics.

3:30 p.m. Wen L. *
Dynamics of Mars and Origin of Tharsis **[#1436]**
A large fraction of the longest-wavelength observed Mars' geoid and topography (l = 2,3) has to come from a thermo-chemical anomaly in the deep lower mantle beneath Tharsis, which also explains its presence and, formation and evolution of Tharsis.

3:45 p.m. Schumacher S. *
Influence of Regional Crustal Variations on the Global Temperature Field of Mars **[#1520]**
The effects of regional crustal variations on the present-day temperature distribution of Mars are shown using 2D-models. The results indicate that the thermal anomalies generated can be larger than those caused by a potential mantle plume.

4:00 p.m. Kiefer W. S. * Li Q.
Mars Is Not Dead: Mantle Convection Controls the Observed Lateral Variations in Lithospheric Thickness on Present-Day Mars **[#1416]**
Mantle convection is a natural explanation for the observed lateral variations in lithospheric thickness on present-day Mars. Lithospheric flexure at the north polar cap of Mars is consistent with an interior with moderately vigorous convection.

4:15 p.m. Li Q. * Kiefer W. S.
Layered Mantle Convection and Magma Production on Mars: Effects of Dense Layer Properties **[#1399]**
We explore the effects of a chemically dense deep layer and its properties on martian mantle dynamics. Our focus is on the viscosity and radioactivity contrast between the dense layer and upper portion of the mantle.

4:30 p.m. King S. D. *
Mars Mantle Structure: Results from Calculations with an Imposed Hemispheric Lithospheric Step **[#1680]**
I examine spherical convection with a step viscosity increase in the lithosphere. With a low-viscosity channel below the lithosphere small-scale convection develops at the step within the first 100 MY. I discuss application to Tharsis.

MARS ANALOGS I: GEOLOGICAL
Thursday, 1:30 p.m. Waterway Ballroom 4

Chair: **R. Aileen Yingst**

1:30 p.m. Clarke J. D. A. * Bourke M. C.
Recognition Criteria of Spring Deposits on Mars at all Scales: Evidence from the Dalhousie Springs Analog (Australia) **[#1102]**
Spring deposits at Dalhousie have a suite of distinctive characteristics at all scales that allows their recognition. These characteristics are found in many terrestrial spring deposits. These may assist in the recognition of such deposits on Mars.

1:45 p.m. Yingst R. A. * Kuhlman K. R.
Microscale Characteristics of Particles Deposited by the 1996 Skeiðarársandur Jökulhlaup: A Potential Terrestrial Analog to Mars **[#1326]**
As part of our effort to characterize and create a database of important martian analogs at the microscale, we here report on the characteristics of particles deposited by the 1996 Skeiðarársandur jökulhlaup.

2:00 p.m. Zimbelman J. R. * Garry W. B. Irwin R. P. III
Precision Topography of Pluvial Features in Western Nevada as Analogs for Possible Pluvial Landforms on Mars **[#1370]**
Ten DGPS topographic surveys from Surprise Valley, on the Nevada-California border, provide insights into the precision required to identify and correlate pluvial features.

2:15 p.m. Wang A. * Zheng M. P.
Evaporative Salts from Saline Lakes on Tibetan Plateau: An Analog for Salts on Mars **[#1858]**
We report the initial results from a field campaign to a sulfate-dominated lacustrine system on the Tibetan Plateau. Results from *in situ* and laboratory measurements of the collected salt samples will be presented.

2:30 p.m. Ulrich M. * Morgenstern A. Guenther F. Roessler S.
Investigation of Thermokarst Features in NE Siberia as Possible Terrestrial Analogues of Martian Scalloped Depressions **[#1076]**
We investigate permafrost degradation in ice-rich, fine-grained deposits in NE Siberia as terrestrial analogues for martian degraded volatile-rich mantle deposits focusing on the influence of solar insolation on thermokarst morphology.

2:45 p.m. Xiang S. M. * Huang D. H.
Analogue Research in China's Lunar Exploration **[#1458]**
We conduct analogue research on the northwestern China stony desert pavements which appears to have similar surface material as the Moon and Mars, tremendous temperature cycling and almost lifeless.

EXPLORING THE DIVERSITY OF LUNAR LITHOLOGIES WITH SAMPLE ANALYSES AND REMOTE SENSING
Thursday, 3:00 p.m. Waterway Ballroom 4

Chairs: **Paul Lucey and Allan Treiman**

3:00 p.m. Lucey P. G. * Cahill J. T. S.
The Composition of the Lunar Surface Relative to Lunar Samples **[#2424]**
Remote sensing measurements of plagioclase abundance and Mg' (Mg/Mg+Fe) show a compositionally heterogeneous lunar surface with three major compositional types: ferroan anorthosites, Mg-suite and mare basalt.

3:15 p.m. Klima R. L. * Pieters C. M. Dyar M. D.
Pyroxene Spectroscopy: Probing Composition and Thermal History of the Lunar Surface **[#2155]**
We present a quantitative analysis of spectra of 8 lunar pyroxenes in the context of an extensive study of compositionally controlled synthetic pyroxenes to determine which spectral properties can be related to elevated amounts of Ti^{3+} and/or Al^{3+}.

3:30 p.m. Zeigler R. A. * Korotev R. L. Jolliff B. L.
A Study of Apollo 16 Feldspathic Glasses: Locally Produced or Ballistically Deposited? **[#2533]**
This study presents the results of a coordinated major-, minor-, and trace-element study of Apollo 16 glasses, concentrating on the feldspathic glasses, in order to ascertain their likely provenances.

3:45 p.m. Cook D. L. * Berger E. Faestermann T. Herzog G. F. Knie K. Korschinek G. Poutivtsev M. Rugel G. Serefiddin F.
^{60}Fe, ^{10}Be, and ^{26}Al in Lunar Cores 12025/8 and 60006/7: Search for a Nearby Supernova **[#1129]**
We measured the short-lived nuclides ^{60}Fe, ^{10}Be, and ^{26}Al in two lunar cores (12025/28 and 60006/7). Live ^{60}Fe was detected in the topmost sample of 12025/8. Possible sources of the ^{60}Fe are discussed, including debris from a nearby supernova.

4:00 p.m. Shearer C. K. * Burger P. V. Guan Y.
Vapor Element Transport in the Lunar Crust and Implications for Lunar Ore Deposits **[#1299]**
Troilite veins and replacement textures occur in numerous lunar samples. Here we differentiate between the several proposed transport models and thereby gain a clearer understanding of volatile element transport in the relatively dry lunar crust.

4:15 p.m. Fuller M. * Weiss B. P.
The Paleomagnetic Record of the Apollo Samples **[#1192]**
Analyses of demagnetization characteristics of the Apollo samples give promise of distinguishing primary NRM carried by Mare basalts from impact related shock magnetization and other contamination.

CHONDRITE ACCRETION AND EARLY HISTORY
Thursday, 1:30 p.m. Waterway Ballroom 5

Chairs: **Denton Ebel and Rhiannon Mayne**

1:30 p.m. Howard K. T. * Benedix G. K. Bland P. A. Cressey G.
Modal Mineralogy of CV3 Chondrites by PSD-XRD: Mineralogic Insights into a Complex Evolutionary History **[#1235]**
CV3 chondrites Vigarano, Efremovka, Allende, Mokoia, Grosnaja and Kaba are amongst the most studied rocks in existence. By XRD we define the first quantitative modal mineralogy of these samples and explore implications of our data to petrogenesis.

1:45 p.m. Ebel D. S. * Leftwich K. Brunner C. E. Weisberg M. K.
Abundance and Size Distribution of Inclusions in CV3 Chondrites by X-Ray Image Analysis **[#2065]**
Chondrule, matrix, CAI and AOA abundances and log-normal clast size distributions for Allende, Mokoia, Nova 002, Leoville and Vigarano are determined with a new technique. Oxidized CVs have ~2× matrix and ~50% chondrule area compared to reduced CVs.

2:00 p.m. Zanda B. * Bland P. A. Le Guillou C. Hewins R. H.
Volatile Element Distribution in Matrix and Chondrules of Carbonaceous and Ordinary Chondrites **[#1810]**
Presolar diamond, H_2O, C, N and volatiles in OCs and CCs correlate with matrix abundance. Matrix accreted with a uniform composition throughout chondrite groups for the first four species, but chondrule-matrix complementarity is possible for volatiles.

2:15 p.m. Kunihiro T. * Maruyama S. Watanabe M. Nakamura E.
Elemental and Isotopic Abundances of Lithium in Chondrule Constituents in the Allende Meteorite **[#1500]**
We report data on the distribution of Li elemental and isotopic abundances in chondrule constituents and in the neighboring matrix of the Allende meteorite.

2:30 p.m. Weiss B. P. * Carporzen L. Elkins-Tanton L. T. Ebel D. S.
Evidence for Internally Generated Magnetic Fields on the CV Chondrite Parent Planetesimal **[#2237]**
Paleomagnetic analyses of Allende suggest that the CV parent body generated a dynamo field in a convecting metallic core. This would imply that the parent planetesimal is partially differentiated and has a relic, chondritic surface.

2:45 p.m. Nimmo F. *
Energetics of Asteroid Dynamos and the Role of Compositional Convection **[#1142]**
Asteroid dynamos require core cooling rates of < 0.1 K/Myr if compositional convection driven by a light element (e.g. sulphur) occurs, but 1-100 K/Myr otherwise. Parent bodies of several existing meteorites cooled fast enough to generate dynamos.

3:00 p.m. Elkins-Tanton L. T. * Weiss B. P.
Chondrites as Samples of Differentiated Planetesimals **[#1293]**
The physical and compositional effects of an internal magma ocean on the solid, undifferentiated outer shell of a planetesimal provides a starting model from which to explain a variety of observations of chondrite meteorites.

3:15 p.m. Hewins R. H. * Ganguly J. Mariani E.
Diffusion Modeling of Cooling Rates of Relict Olivine in Semarkona Chondrules **[#1513]**
Diffusive exchange profiles between relict olivine and melt-grown olivine in Semarkona Type IIA chondrules were oriented by EBSD to correct D. Results for Fe-Mg (D from Dohmen) and Cr (Ito and Ganguly) are concordant at 300°–400°C/hr.

3:30 p.m. Wittmann A. * Weirich J. R. Swindle T. D. Rumble D. III Kring D. A.
Petrography of MIL05029, the First Accretional Impact Melt from the L-Chondrite Parent Body **[#1426]**
Petrographic characteristics, radioisotopic age, and the thermal history of MIL05029, an igneous rock with L-chondritic affinity, suggest formation as an impact melt in a 15–60 km diameter crater during accretion of the L-chondrite parent body.

3:45 p.m. Mayne R. G. * McCoy T. J.
Metamorphism and Melting in an "Unmetamorphosed" Mesosiderite **[#1728]**
We present SEM and EMP analyses from two silicate clasts within Crab Orchard specifically to compare the degree of metamorphism of these clasts to similar clasts in eucrites and to understand the igneous processes that occurred upon mixing with the metal.

4:00 p.m. Rubin A. E. *
Shock Effects in EH6 Chondrites and Aubrites: Implications for Collisional Heating of Asteroids **[#1353]**
Many EH4-EH7 chondrites have been impact melted, implying that collisional heating is responsible for EH-chondrite metamorphism. Two aubrites show evidence of post-shock annealing, a process that appears to be common among asteroids.

4:15 p.m. Humayun M. * Keil K. Bischoff A.
Siderophile Elements in Metal from Northwest Africa 2526, an Enstatite Chondrite Partial Melt Residue **[#1744]**
Siderophile elements confirm that metal in NWA 2526, an enstatite chondrite partial melt residue, equilibrated with C- and S-bearing metallic liquids, and provide a chemical link to Si-bearing iron meteorites.

4:30 p.m. van Niekirk D. * Humayun M. Keil K.
In Situ Determination of Siderophile Trace Elements in EL3 Meteorites **[#2049]**
Siderophile elements in kamacite from Metal-Silicate-Sulfide assemblages from EL3 chondrites confirm that these assemblages formed as partial melts, not nebular condensates, supporting an origin as impact melts.

SCIENCE INSTRUMENTS FOR THE MARS SCIENCE LANDER
Thursday, 1:30 p.m. Waterway Ballroom 6

Chairs: Leslie Tamppari and Noah Petro

1:30 p.m. Gellert R. * Campbell J. L. King P. L. Leshin L. A. Lugmair G. W. Spray J. G. Squyres S. W. Yen A. S.
The Alpha-Particle-X-Ray-Spectrometer(APXS) for the Mars Science Laboratory (MSL) Rover Mission **[#2364]**
The new APXS for the MSL Rover mission was successfully tested, calibrated and delivered to NASA/JPL. The data acquisition time compared to MER was decreased by about a factor of 3, allowing a full *in situ* chemical analysis within ~3 hours at temperatures below ~–5C.

1:45 p.m. Wiens R. C. * Clegg S. Bender S. Lanza N. Barraclough B. Perez R. Maurice S. Dyar M. D. Newsom H. Chemcam Team
Initial Calibration of the ChemCam LIBS Instrument for the Mars Science Laboratory (MSL) Rover **[#1461]**
The ChemCam laser-induced breakdown spectroscopy (LIBS) flight instrument was calibrated at distances up to 7 m with 65 standards. We report in terms of quantitative elemental abundances, sample classification, and remote dust removal from samples.

2:00 p.m. SAM Team Mahaffy P. R. * Cabane M. Conrad P. G. Webster C. R.
Sample Analysis at Mars (SAM) Instrument Suite for the 2011 Mars Science Laboratory **[#1088]**
The measurement capabilities of the Sample Analysis at Mars (SAM) Instrument Suite for the 2011 Mars Science Laboratory (MSL) are described. MSL explores present and past habitability of Mars and the SAM focus is volatiles, isotopes, and organics.

2:15 p.m. Litvak M. L. * Mitrofanov I. G. Shvecov V. N. Timoshenko G. N. Kozyrev A. S. Malakhov A. V. Mokrousov M. I. Sanin A. B. Tretyakov V. Vostrukhin A. Golovin D. V. Varenikov A.
DAN/MSL Instrument: Road from Field Tests to the Estimation of Hydrated Minerals in the Martian Subsurface **[#1250]**
Results of DAN/MSL field tests and predictions for operations onboard MSL rover are presented.

2:30 p.m. Gómez-Elvira J. * Castañer L. Lepinette A. Moreno J. Polko J. Sebastian E. Torres J. Zorzano MP. REMS Team
REMS, an Instrument for Mars Science Laboratory Rover **[#1540]**
REMS (Rover Environmental Monitoring Station) is part of the MSL instrument suite. All qualification and protoflight tests have been accomplished, as well most of the calibration ones. A description of the flight model status and calibration tests is presented.

2:45 p.m. Hassler D. M. * Andrews J. Bullock M. Grinspoon D. Neal K. Posner A. Rafkin S. Tyler Y. Vincent M. Weigle E. Zeitlin C. Beaujean R. Boehm E. Boettcher S. Burmeister S. Kortmann O. Martin C. Muller-Mellin R. Wimmer-Schweingruber R. F. Reitz G. Brinza D. Cucinotta F. Cleghorn T.
The Radiation Assessment Detector (RAD) on the Mars Science Laboratory (MSL) **[#2297]**
The Radiation Assessment Detector (RAD) will detect and analyze the most hazardous energetic particle radiation on the surface of Mars as a key element of the Mars Science Laboratory (MSL) mission.

3:00 p.m. Blake D. F. * Vaniman D. Anderson R. Bish D. Chipera S. Chemtob S. Crisp J. DesMarais D. J. Downs R. Farmer J. Gailhanou M. Ming D. Morris D. Stolper E. Sarrazin P. Treiman A. Yen A.
The CheMin Mineralogical Instrument on the Mars Science Laboratory Mission **[#1484]**
The CheMin mineralogical instrument aboard MSL will for the first time return definitive and quantitative mineralogical data from the Mars surface. During MSL's 2-year mission, CheMin will provide XRD data from as many as 72 separate rock or soil samples.

MARTIAN GULLIES: MORPHOLOGY AND ORIGINS
Thursday, 3:15 p.m. Waterway Ballroom 6

Chairs: **Timothy Titus and Nina Lanza**

3:15 p.m. Schon S. C. * Head J. W. Fassett C. I.
Unique Chronostratigraphic Marker in Depositional Fan Stratigraphy on Mars: Evidence for ~1.25 Ma Old Gully Activity and Surficial Meltwater Origin **[#1677]**
Gully fan morphology indicates multiple periods of depositional activity with date-able secondary craters from a nearby rayed-crater emplaced during an intermediate period in deposition, which provides a maximum age for recent activity of this gully.

3:30 p.m. Parsons R. A. * Nimmo F.
Fluvial Discharge Rates of Martian Gullies: Slope Measurements from Stereo HiRISE Images and Numerical Modeling of Sediment Transport **[#1947]**
Based on fluvial discharge and sediment transport theory from Kleinhans [2005], groundwater is a plausible mechanism for forming gullies on Mars if the supplying aquifer is permeable and ~10s of m thick. Our model suggests gullies form rapidly (~h).

3:45 p.m. Coleman K. A. * Dixon J. C.
Martian Gully Morphologies **[#1230]**
Numerous morphologically distinct forms on Mars are referred to using the term "gullies". We analyzed HiRISE and MOC images and began to build a database of morphologies seen in gullies on Mars. To date seven distinct morphologies have been identified.

4:00 p.m. Xu D. * Zeng Z. Yue Z. Wang J. Zhang Z. Birnbaum S. J. Xie H. Yan D.
A Case Study of an Application of Fractal Theory to Gully's Alcove on Mars **[#2481]**
Poleward facing gullies have higher fractal values than those of equator-ward facing ones in crater of Mars and provides evidence for the hypothesis, formation of gullies is related to snow and ice accumulation and melting due to climatic processes.

4:15 p.m. Morgan G. A. * Head J. W. III Marchant D. R. Dickson J. Levy J.
The Effect of Varying Annual Snow Accumulation on Gully Formation in Anarctica: Comparisons Between 'Wet' and 'Dry' Seasons and Implications for Gully Formation on Mars **[#2331]**
The sensitivity of gully activity to snow volume in Antarctica demonstrates the importance of snow accumulation, in addition to temperatures permitting melt generation, in determining the location of gully activity.

4:30 p.m. Lanza N. L. * Meyer G. A. Okubo C. Newsom H. E. Wiens R. C.
Preliminary Evidence for a Debris Flow Gully Slope-Area Relationship on Mars and Implications for a Source Liquid **[#2225]**
We compare morphometric characteristics of terrestrial gullies associated with debris flows with a subset of martian gullies to test the hypothesis that these martian gullies are formed by saturation and failure of the regolith.

POSTER SESSION II
Thursday, 6:30 p.m. Town Center Exhibit Area

MERCURY

Gómez-Perez N. Wicht J.
Magnetic Field at Mercury: Effects of External Sources on Planetary Dynamos **[#1634]**
In Mercury, magnetospheric currents induce a magnetic field at the top of the core. We study dynamo simulations with the presence of an external field and find that fully convective cores result in weakened dipole fields.

Johnson C. L. Uno H. Purucker M. E. Anderson B. J. Korth H. Slavin J. A. Solomon S. C.
Mercury's Magnetic Field: Assessing the Effects of External Fields on Internal Field Models **[#1385]**
MESSENGER data confirm the presence of an intrinsic magnetic field at Mercury. Here we discuss several approaches to modeling magnetospheric fields, and the implications for assessing internal field structure and its origin.

Blewett D. T. Denevi B. W. Robinson M. S. Purucker M. E.
Do Lunar-like Swirls Occur on Mercury? **[#1352]**
Lunar swirls are unusual high-albedo markings. Mercury swirls were tentatively identified by Mariner 10. We examine potential swirls with MESSENGER, and consider the implications for the origin of swirls and the agent of space weathering.

Frigeri A. Federico C. Pauselli C. Coradini A.
Fostering Digital Geologic Maps: The Digital Geologic Map of Mercury from the USGS Atlas of Mercury, Geologic Series **[#2417]**
We present the digital geologic map of Mercury generated from the merge of the USGS Atlas of Mars, Geologic Series originally published by the USGS, and based on Mariner data. This single map offers several advantages over a series of distinct maps.

André S. L. Watters T. R.
Tectonic Features Revealed in MESSENGER Images Detailed Within Mariner 10 Stereo Topography **[#2341]**
Tectonic landforms were revealed in MESSENGER images within areas imaged by Mariner 10. Some of these landforms are recognizable in Mariner 10 derived stereo topography. We present topographic data for some newly identified tectonic features.

Barnouin-Jha O. S. Zuber M. T. Oberst J. Preusker F. Smith D. E. Neumann G. A. Solomon S. C. Hauck S. A. II Phillips R. J. Head J. W. III Prockter L. M. Robinson M. S.
Assessing the Relationship Between Crater Depth and Diameter on Mercury with Topographic Measurements by MESSENGER **[#1638]**
Altimetry and imaging data acquired by the MErcury Surface, Space ENvironment, GEochemistry, and Ranging (MESSENGER) spacecraft allow reassessing the relationship between crater depth and diameter on Mercury.

Gillis-Davis J. J. Blewett D. T. Denevi B. W. Robinson M. S. Solomon S. C. Strom R. G. MESSENGER Team
Pit-Floor Craters on Mercury: Characteristics and Modes of Formation **[#2234]**
We classify pit craters on Mercury into two categories on the basis of morphology and size: small irregular-sized pit craters and larger-sized, steep-sided pit craters. We conclude that differences in pit morphology relates to the mode of formation.

Fassett C. I. Head J. W. Blewett D. T. Chapman C. R. Dickson J. L. Murchie S. L. Strom R. G. Watters T. R.
Caloris Impact Basin: Exterior Geomorphology, Stratigraphy, Morphometry, Radial Sculpture, and Smooth Plains Deposits **[#1899]**
MESSENGER data allow new consideration of the stratigraphy and geology of materials surrounding the Caloris basin. We discuss radial impact sculpture and secondaries associated with the basin, as well as the origin of the plains outside of its rim.
Izenberg N. R. Blewett D. T. McNutt R. L. Chabot N. L. Chapman C. R. Denevi B. W. Robinson M. S. Prockter L. M. Murchie S. L.
MESSENGER Views of Crater Rays on Mercury **[#1676]**
High-reflectance crater materials and extensive ray systems are notable in imaging from MESSENGER's two Mercury flybys in 2008. These images provide the opportunity to make comparisons with lunar rays and Earth-based radar images of Mercury.

Domingue D. L. Denevi B. W. Ernst C. M. Holsclaw G. M. Izenberg N. R. McClintock W. E. Murchie S. L. Robinson M. S.
Regional Color Photometry of Mercury's Surface **[#1301]**
Using images from both flybys of Mercury, the photometric properties of the planet in general, and of spectral units is examined.

Helbert J. D'Amore M. Maturilli A. Izenberg N. R. Sprague A. L. Holsclaw G. M. Head J. W. McClintock W. E. Blewett D. T. Solomon S. C.
Compositional Units on Mercury Along MESSENGER Ground Tracks from Principal Component Analysis of Spectral Observations **[#1529]**
We have started analysis of the MESSENGER MASCS surface spectra using a principal component approach. The main goal of this analysis is to identify surface units along the ground tracks and characterize them.

Riner M. A. Lucey P. G. Desch S. J. McCubbin F. M.
Opaques in Mercury's Crust: Additional Evidence for a Low-FeO Magma Ocean **[#2062]**
Laboratory spectra of opaque oxides together with MESSENGER observations of Mercury's surface suggest Mercury's crust is not the lunar highlands, modified, but is a unique array of lithologies produced by crystallization of a low-FeO magma ocean.

Warell J. Sprague A. L. Kozlowski R. W. Helbert J.
Surface Composition and Chemistry of Mercury: Hapke Modeling of MESSENGER/MASCS Reflectance Spectra **[#1902]**
We present results of modeling of published MASCS/VIRS reflectance spectra from the first MESSENGER Mercury flyby using multicomponent mixtures with microphase iron in Hapke's radiative transfer model.

Warell J. Kozlowski R. W. Sprague A. L. Helbert J. Önehag A. Trout G. Rothery D.
Ground-based Infrared Spectroscopy of Mercury's Near-Global Surface with IRTF/SPEX: Complementing MESSENGER Compositional Observations **[#1931]**
Using SpeX at the NASA IRTF telescope we have obtained disk-resolved spectra of Mercury and lunar sites in the wavelength range 0.8-5.5 mum. These will be compared to MESSENGER data, searched for IR spectral features, and modeled to determine surface properties.

Kozyrev A. S. Gurvits L. I. Litvak M. L. Malakhov A. A. Mokrousov M. I. Mitrofanov I. G. Rogozhin A. A. Sanin A. B. Owens A. Schvetsov V. N. Tretyakov V. I. Vostrukhin A. V.
Studying Mercury Surface Composition by Mercury Gamma-Rays and Neutron Spectrometers (MGNS) from BepiColombo Spacecraft **[#1372]**
MGNS instrument, selected for the payload of the BepiColombo mission, is shown to have necessary capabilities to characterize the elementary composition of subsurface layer of Mercury and to test the presence of water ice deposits at both polar regions of the planet.

PURSUING LUNAR EXPLORATION

Wilson T. L. Lee K. T.
Photon Luminescence of the Moon **[#1918]**
The space-radiation-induced photon luminescence existing on the Moon is derived from SEP and GCR sources. Its spectrum is present in the upper X-ray and lower ?–ray portion of the electromagnetic spectrum. Dose mitigation measures are addressed.

Petro N. E. Bleacher J. E. Clark P. E. Mest S. C. Lewis R.
Optimizing Lunar Surface Science: Comparison of Shackleton Base Scenario and Sortie Surface Scenarios at the Nectaris Basin, Marius Hills, and Olivine Hill **[#2206]**
The work reported here responds to the need to provide the Constellation program with science requirements for a surface system architecture and metrics for surface operations. We compare surface scenarios for an outpost at Shackleton to three sorties.

Fong T. Broxton M. Deans M. C. Helper M. Hodges K. V. Schaber G. G. Schmitt H. H. Smith T.
Traverse Planning for Robotic Recon and Human Exploration of Hadley Rille **[#1233]**
We recently conducted a lunar traverse planning exercise at NASA Ames. The objective was to plan an EVA traverse for a hypothetical, manned mission to the Apollo 15 region and then identify where ground-level data (acquired by robotic scouting) would help refine the plan.

Ruberg R. Wood C. A. Reese D. D. Lightfritz C. Harrison A.
MoonWorld: Virtual Fieldwork in Second Life **[#2229]**
MoonWorld is a Second Life simulation that models the Moon as a tool for learning lunar science through virtual fieldwork. Avatars climb into craters to collect samples and observe structure to understand crater formation.

Boldoghy B. Kummert J. Varga T. P. Szilágyi I. Darányi I. Bérczi Sz. Varga T. N. Hudoba G. Jr.
Buildings of Great Inner Space Created with Low Asset Requirement and High Efficiency for the Moon **[#2458]**
For constructing lunar base buildings of great inner space we propose a plan, architectural concept, and building technology of using local materials by various technologies, baking, bagging and moving of the regolith to cover the building.

SOURCES AND ERUPTION OF LUNAR BASALTS

Arai T. Misawa K. Tomiyama T. Yoshitake M. Irving A. J.
Constraints on Lunar KREEP Magmatism: A Variety of KREEP Basalt Derivatives in Lunar Meteorite NWA 4485 **[#2292]**
Lunar meteorite NWA 4485 include a variety of lithic clasts derived fromKREEP magmatism. Pyroxene composition and zoning trends indicate that the KREEP basalt clasts in this meteorites are moderately equilibrated relative to Apollo KREEP basalts.

Burger P. V. Shearer C. K. Papike J. J.
The Multi-Stage Cooling History of Lunar Meteorite NWA 032 as Recorded by Phenocrystic Olivine and Pyroxene **[#2043]**
This study examines previously undocumented oscillatory zoning in phenocrystic pyroxene grains from lunar meteorite NWA 032, and its implication for the crystallization history of this sample.

Hauri E. H. Saal A. E. Van Orman J. Rutherford M. J. Friedman B.
New Estimates of the Water Content of the Moon from Apollo 15 Picritic Glasses **[#2344]**
In this abstract, we report the results of new SIMS measurements of water on over 200 new samples of picritic glasses recovered from the Apollo 15 mission. Our new measurements suggest an upward revsion of current estimates for the water content of lunar magmas.

van Kan Parker M. Agee C. B. van Westrenen W.
Density of Molten "Apollo 17 Orange Glass" **[#1722]**
The density of molten intermediate-high titanium bearing Apollo 17 orange glass was determined at lunar mantle pressures and temperatures using the sink/float technique.

van Kan Parker M. van Westrenen W. van Sijl J.
Computational Study of Trace Element Partitioning Between Orthopyroxene and Melt: Implications for Substitution Mechanisms in Earth and Moon **[#1714]**
A computational study of element partitioning between orthopyroxene and silicate melt highlighting the possible effects of iron content and charge balancing mechanisms on partition coefficients.

Krawczynski M. J. Sutton S. R. Grove T. L. Newville M.
Titanium Oxidation State and Coordination in the Lunar High-Titanium Glass Source Mantle **[#2164]**
XANES and EXAFS spectra from synthetic HiTi lunar glasses determine coordination of Ti in the HiTi source region. The amount of Ti^{3+} present affects the olivine-opx equilibrium, and the total amount of Ti^{3+} present requires a pyx bearing source.

Fernandes V. A. Korotev R. L. Renne P. R.
^{40}Ar-^{39}Ar Ages and Chemical Composition for Lunar Mare Basalts: NWA 4734 and NWA 4898 **[#1045]**
^{40}Ar-^{39}Ar ages are reported for lunar mare basalts NWA 4734 and NWA 4898. The age obtained for NWA 4734 is 2.766 ± 0.022 Ga (same as NWA 032/479) and for NWA 4898 is 3.520 ± 0.060 Ga, the same as Rb-Sr age reported by Gaffney et al. (2008).

Donohue P. Neal C. R.
Apollo 17 High-Titanium Basalt Petrogenesis Revealed by Crystal Size Distributions and Mineral Geochemistry **[#1805]**
Crystal Size Distributions (CSDs) and mineral geochemistry are presented for ilmenite crystals in a Type B2 (70275,35) lunar sample, and two Type C (74255,55 and 74275,312) lunar samples.

Liu Y. Spicuzza M. J. Valley J. W. Taylor L. A.
Oxygen Isotopes of Lunar Rocks: Different Sources for Different Hi-Ti Basalts? **[#2291]**
New oxygen isotopes of lunar mare basalts show difference among high-Ti basalts.

Haloda J. Tycova P. Thöni M. Jelenc M.
The Petrogenesis and Chronology of Lunar Meteorite Northeast Africa 003-A: Sm-Nd and Rb-Sr Isotopic Studies **[#1247]**
The Sm-Nd age of lunar mare basalt NEA 3.089 ± 0.064 Ga represents the crystallization age of the meteorite, suggesting that NEA 003-A can be a product of younger low-Ti mare basalt volcanism within the Apollo 15 olivine-normative basalt suite.

Wilson L. Head J. W.
Lunar Volcanic Eruptions: Range of Eruption Styles and Implications for Magma Ascent and Emplacement **[#1159]**
We characterize the range of volcanic feature morphologies observed on the Moon in a manner suitable to allow them to be related to the conditions under which eruptions and intrusions took place.

CHEMICAL AND PHYSICAL PROPERTIES OF THE LUNAR REGOLITH

Spudis P. D. Taylor G. J.
A Major KREEP-Basalt — Mare Basalt Unconformity on the Moon **[#1039]**
The Station 2 boulder at Apollo 15 preserves a major 500 Ma unconformity between early Imbrian-age non-mare KREEP basalts and late Imbrian-age mare basalt. These samples may represent a paleoregolith, an ancient regolith preserved between two lava flows on the Moon.

McKay D. S. Cooper B. L. Riofrio L. M.
New Measurements of the Particle Size Distribution of Apollo 11 Lunar Soil **[#2051]**
We have initiated a major new program to determine the grain size distribution of nearly all lunar soils collected in the Apollo program. The use of a laser diffraction instrument improves upon previous work using sieving.

Johnson J. R. Shepard M. K. Paige D. A. Foote E. J. Grundy W.
Spectrogoniometric Measurements and Modeling of Apollo 11 Soil 10084 **[#1427]**
Laboratory visible/near-infrared multispectral goniometer observations of Apollo 11 soil 10084 were acquired using the Bloomsburg University Goniometer to provide constraints on Hapke radiative transfer models for comparison to lunar analog soils.

Seddio S. M. Jolliff B. L. Korotev R. L. Zeigler R. A.
A Newly Characterized Granite from the Apollo 12 Regolith **[#2285]**
The newly characterized lunar sample 12032,366-19 is a pristine lunar granite with a unique texture and mineral assemblage and no impact-generated glass or brecciated material.

Johnson D. Jolliff B. Zeigler R. Carpenter P.
Distribution of Ti in Glass and Mineral Components of Lunar Soils 10084 and 71501; Grain Size Fraction 100 to 210 μm **[#2346]**
The grain size and shape of ilmenite and the distribution of Ti in components of Apollo 11 and Apollo 17 soils are discussed.

Seddio S. M. Korotev R. L. Jolliff B. L. Zeigler R. A.
Petrographic Diversity in Apollo 12 Regolith Rock Particles **[#2415]**
A set of 52 lithic fragments of the Apollo 12 regolith are analyzed to understand the petrographic diversity that the site contains focusing on regolith breccias, KREEP impact-melt breccias and other high-Th samples, and basalts.

Ling Z. C. Wang A. Jolliff B. L. Li C. Liu J. Bian W. Ren X. Mu L. Su Y.
Raman Spectroscopic Study of Quartz in Lunar Soils from Apollo 14 and 15 Missions **[#1823]**
Quartz, a rare but important mineral indicator for Moon, is detected from soil 14163 and 15273 by Raman point-count procedures. The two major Raman peaks of quartz show considerable red shift, indicating different shock effect on these grains.

Isaacson P. J. Pieters C. M. Klima R. L. Hiroi T. Sarbadhikari A. B. Liu Y. Taylor L. A.
The Lunar Rock and Mineral Characterization Consortium (LRMCC): Integrated Analyses and Mineral Endmembers from Mare Basalts **[#1821]**
The LRMCC has conducted coordinated mineralogy/petrology and spectroscopy analyses of four lunar basalt samples and associated mineral separates. The dataset provides key ground truth and constraints on spectral mixing and space weathering models.

Nemchin A. A. Pidgeon R. T. Grange M. L.
REE Patterns in Lunar Zircons **[#1509]**
Zircon grains from breccia sample 14321 show significant REE variation, indicating that these zircons formed in the rocks with a wide compositional range.

Yakovlev O. I. Gerasimov M. V. Dikov Yu. P.
Temperatures of Formation of HASP and GASP Particles **[#1261]**
Comparison of chemical composition of HASP glasses and GASP particles with compositions of residual melt and corresponding equilibrium vapor for lunar mare basalt show correlation to experimental data at ~1870–1650°? and mass loss in the range 20–50%.

Edmunson J. Cohen B. A. Spilde M. N.
Characterizing the Effect of Shock on Isotopic Ages I: Ferroan Anorthosite Major Elements **[#2094]**
Ferroan anorthosites 62236 and 67075 do not show major element mobility due to shock in microprobe analysis. The shock pressure of 67075 is estimated at <50 kilobars.

Sharp Z. D. Shearer C. K. Jr. Barnes J. D.
The Chlorine Isotope Composition of the Moon **[#2351]**
The chlorine isotope composition of leached pyroclastic glass (Apollo 17) were measured using gas source mass spectrometry and found to be -0.74‰ (vs SMOC), different from bulk Earth (0‰). The Cl bulk concentration is 80 ± 20 ppm.

ten Kate I. L. Glavin D. P. VAPoR Team
Evolved Gas Analysis of Two Lunar Simulants, Apollo 16 Regolith and a Carbonaceous Meteorite (Murchison) Using VAPoR **[#2232]**
Volatile Analysis by Pyrolysis of Regolith (VAPoR) on the Moon using mass spectrometry is one technique that should be considered for *in situ* analysis of lunar regolith. Here we present evolved gas analysis data obtained with the VAPoR breadboard.

LUNAR DUST AND TRANSIENT SURFACE PHENOMENA

Wohl C. J. Belcher M. A. Hopkins J. W. Connell J. W.
Topographical Modification of Materials for Lunar Dust Adhesion Mitigation **[#1121]**
The surface energy of polymer films was reduced by topographical modification, towards lunar dust adhesion mitigation. Contact angle goniometry and microscopy characterized the modified surfaces. Laser ablation afforded high fidelity topographies.

Tranfield E. Rask J. C. Wallace W. T. Kerschmann R. Loftus D. J.
Enhanced Chemical Reactivity of Crystalline Quartz by Mechanical Grinding **[#2529]**
We have developed a technique for mechanically grinding crystalline silica which increases the chemical reactivity of the material as judged by the terephthalate assay. This technique uses a modern, commercially available ball mill.

Wallace W. T. Jeevarajan A. S.
Understanding the Activation and Solution Properties of Lunar Dust for Future Lunar Habitation **[#2483]**
Grinding of lunar dust results in increased hydroxyl radical production in solution. Lower pH and grinding causes lunar simulant to release increased amounts of ions into solution.

Horanyi M. Sternovsky Z. Gruen E. Srama R. Lankton M. Gathright D.
The Lunar Dust EXperiment (LDEX) on the Lunar Atmosphere and Dust Environment Explorer (LADEE) Mission **[#1741]**
LDEX is designed to map the variability of the spatial and size distributions of dust grains in the lunar environment.

Wilson T. L.
Lunar Dust and Dusty Plasma Physics **[#1314]**
Lunar dust is addressed using the physics of dusty plasmas. Equations for small dust grains on the Moon are given and related to MHD effects of plasma precipitation as it orbits through the Earth's plasma sphere, magnetosphere, and the solar wind.

Taylor L. A. Liu Y. Zhang A.
Shape and Size Relationship of Several Lunar Dusts: Preliminary Results **[#2106]**
The abstract reports preliminary results of shape and size relationship of several lunar dusts.

Irwin S. A. Durrance S. T. Buhler C. R. Calle C. I.
Method to Investigate the Charging of Lunar Dust Particles **[#2521]**
Charging characteristics of lunar dust particles are studied experimentally with borosilicate glass beads in a constant electric field, within an environmental chamber at various humidities.

Cook A. C. Grande M.
Preliminary Analysis of Transient Lunar Phenomena Catalog Data **[#2429]**
We have completed a new catalog of Transient Lunar Phenomena and have performed an initial statistical analysis on this.

Crotts A. P. S. Berger A. Cecil G. Cseresnjes P. Ebel D. Hickson P. Joner M. Pfrommer T. Marka S. Morehead R. Radebaugh J. Schultz P.
Status of a Program Monitoring Optical Lunar Surface Transients **[#2373]**
We are observing the lunar near side intensively with a network of robotic imaging telescopes tuned to detect small transient changes in photometry (on timescales of ~1 to 100 min). We also describe a parallel program to detect quasi-permanent photometric surface changes.

Daly R. T. Radebaugh J. Austin D. E.
Computational Study of the Lunar Time-of-Flight Mass Spectrometer (LTMS): Meteorite Impacts and Outgassing Events **[#2411]**
A miniature mass spectrometer uses imaging pattern analysis to determine the location, magnitude, and composition of meteorite impacts and regolith outgassing on the lunar surface. Simulations examine range, detection limit, and spatial resolution.

LUNAR DATABASES AND DATA RESTORATION

Archinal B. Lunar Geodesy and Cartography Working Group
Activities of the NASA LPRP Lunar Geodesy and Cartography Working Group **[#2095]**
We describe the purpose, operation, activities, and future plans of the NASA Lunar Precursor Robotic Program Lunar Geodesy and Cartography Working Group. New standards/recommendations and the need to geodetically control lunar datasets are discussed.

Gaddis L. Becker T. Weller L. Hare T. Isbell C.
Lunar Orbiter Digital Frame Mosaics: Ready for Prime Time **[#2437]**
This abstract announces the availability of Lunar Orbiter (LO) projected and cosmetically processed frame mosaics. Frames from medium- and high-resolution cameras from LO missions III, IV, and V are available via the Lunar Orbiter Frame Viewer web tool at USGS.

Williams D. R. Schultz A. B. Hills H. K. Guinness E. A. Lowman P. D. Taylor P. T.
Restoration of Apollo Data by the PDS Lunar Data Node **[#1991]**
The Lunar Data Node (LDN) has been formed to put relevant, scientifically important Apollo data into accessible digital form for use by researchers and mission planners. We will report on progress made since last year and plans for future data restorations.

Broxton M. J. Moratto Z. M. Nefian A. Bunte M. Robinson M. S.
Preliminary Stereo Reconstruction from Apollo 15 Metric Camera Imagery **[#2282]**
We present preliminary results from automated stereo processing of 70 image pairs from the Apollo 15 Metric Camera. Geo-registration of these data is discussed, as well as a new algorithm for improved sub-pixel stereo matching.

McClanahan T. P. Evans L. G. Starr R. D. Mitrofanov I.
Fast Ray Tracing of Lunar Digital Elevation Models **[#2092]**
Methods for optimizing ray-tracing processes for radiation analysis of digital elevation models (DEM)'s. Point-vector methods are demonstrated using Clementine DEM to determine degree of illumination as a function for large scale DEM analysis, complex orbital ephemeris.

Lee E. M. Gaddis L. R. Weller L. Richie J. O. Becker T. Shinaman J. Rosiek M. R. Archinal B. A.
A New Clementine Basemap of the Moon **[#2445]**
The new basemap of the Moon based on ULCN2005 will be distributed through USGS Map-A-Planet web site (http://www.mapaplanet.org). The image geometry was verified for accuracy, and radiometric and photometric corrections applied and mosaicked.

Losiak A. Wilhelms D. E. Byrne C. J. Thaisen K. Weider S. Z. Kohout T. O'Sullivan K. Kring D. A.
A New Lunar Impact Crater Database **[#1532]**
The aim of this abstract is to describe a new database of lunar impact craters which integrates information concerning the locations and ages of craters, as well as various measured and calculated physical characteristics.

Korotev R. L. Zeigler R. A. Irving A. J. Bunch T. E.
Keeping up with the Lunar Meteorites – 2009 **[#1137]**
We report results of compositional analyses of 16 new lunar meteorite stones for which names have been approved since our report of last year and speculate about pairing relationships on the basis of composition and preliminary petrographic data.

Isaacson P. J. Liu Y. Patchen A. Pieters C. M. Taylor L. A.
Integrated Analyses of Lunar Meteorites: Expanded Data for Lunar Ground Truth **[#2119]**
Lunar meteorites are a valuable opportunity to expand our lunar sample library. We have conducted preliminary mineralogy/petrography/spectroscopy analyses needed to apply them as ground truth and to determine their geologic context with remote data.

Welten K. C. Owens T. L. DePaolo D. J.
Thermal Ionization Mass Spectrometry Studies of Sm and Gd Isotopic Shifts in Lunar Meteorites Due to Neutron Capture: A Progress Report **[#2449]**
We will present preliminary TIMS measurements of Sm and Gd isotopic shifts in lunar meteorites due to neutron-capture effects. These studies will provide more insight in the evolutionary history of meteorites on the lunar surface.

Carpenter P. K. Zeigler R. A. Jolliff B. L. Vicenzi E. P. Davis J. M. Donovan J. J.
Advances in Electron-Probe Microanalysis and Compositional Mapping: Applications to Lunar Samples **[#2531]**
Advances in instrumentation and analytical techniques using EPMA and XRF have been applied to the study of lunar samples. The analysis of multiphase sample volumes using defocused beam analysis presents a central problem to both microanalysis and the study of lunar samples.

Snape J. F. Joy K. H. Crawford I. A.
A Trace-Element Investigation of Lunar Meteorite Northeast Africa 001 **[#1539]**
A trace-element investigation of NEA 001 (a feldspathic polymict breccia). Our results have revealed that several VLT basalt clasts in the sample have unusual REE profiles and positive Eu anomalies.

Foreman A. B. Korotev R. L. Zeigler R. A. Wittmann A. Kring D. A. Irving A. J. Kuehner S. M.
Petrographic and Geochemical Analysis of Feldspathic Lunar Meteorite Shisr 161 **[#2304]**
We present petrographic and geochemical analyses of the lunar meteorite Shisr 161 – a feldspathic regolith breccia compositionally similar to the NWA 3163/4483/4881 granulites.

Takeda H. Karouji Y. Ogawa Y. Otsuki M. Yamaguchi A. Ohtake M. Arai T.
Matsunaga T. Haruyama J.
Iron Contents of Plagioclases in Dhofar 307 Lunar Meteorite and Surface Materials of the Farside Large Basins **[#1565]**
FeO contents of clear plagioclase crystals in Dhofar 307 lunar meteorite, have been determined in connection with spectral data of the Kaguya mission and propose a model of formation of such breccia in a large basin of the farside.

Liu Y. Zhang A. Thaisen K. G. Anand M. Taylor L. A.
Mineralogy and Petrography of a Lunar Highland Breccia Meteorite, MIL 07006 **[#2105]**
Mineralogy and petrography of a new lunar feldsphathic breccia, MIL 07006.

Rahilly K. E. Treiman A. H.
Granulite Clasts of Intermediate Mg in Lunar Meteorite ALHA 81005: Chemical Compositions and Origins* **[#1168]**
Many granulite clasts in lunar highland meteorites have Mg* (molar Mg/(Mg + Fe)) between those of ferroan anorthosite (FAN) and magnesian anorthositic granulite (MAG). Compositions of these clasts are inconsistent with simple mixing of MAG and FAN, but require multiple origins.

Fernandes V. A. Irving A. J. Kuehner S. M. Gellissen M. Korotev R. L. Bandfield J. L.
Petrology, Bulk Composition, Ar-Ar Age and IR Emission Spectrum of Lunar Granulite Northwest Africa 4881 **[#2009]**
Petrology, bulk composition, ^{40}Ar-^{39}Ar age and IR emission spectrum data of lunar granulite Northwest Africa 4881 will presented and showing the combination of laboratory and remotely sensed data is idea to search for meteorite provenance.

Joy K. H. Burgess R. Hinton R. Fernandes V. A. Crawford I. A. Kearsley A. T. Irving A. J. EIMF Team
U-Pb and Ar-Ar Chronology of Lunar Meteorite Northwest Africa 4472 **[#1708]**
We report Ar-Ar and U-Pb chronology studies of KREEP-rich lunar meteorite NWA 4472.

Liu D. Wan Y. Zhang Y. Dong C. Jolliff B. L. Zeigler R. A. Korotev R. L.
Age of Zircons in the Impact-Melt Breccia in SaU 169 Lunar Meteorite: Beijing SHRIMP II Study **[#2499]**
Age dating of zircon grains using SHRIMP methods yields an age of 3918 Ma for the mafic impact-melt breccia lithology in SaU 169, which is chemically and petrographically identical to a group of impact melt breccias from Apollo 12.

Nishiizumi K. Caffee M. W. Vogel N. Wieler R. Leclerc M. D. Jull A. J. T.
Exposure History of Lunar Meteorite Northwest Africa 5000 **[#1476]**
Cosmogenic radionuclides and noble gases were measured in NWA 5000. After ~600 Myr residence in the lunar regolith, it was ejected from a depth of ~335 g/cm^2 on the Moon. The minimum transit time was 1.3 kyr with a short terrestrial age.

CHONDRITES, THEIR CLASTS, AND ALTERATION

Le Guillou C. Rouzaud J. N. Findling N. Düber S.
Experimental Graphitization and Oxidation Kinetic of Nanodiamond: Implication for Nebular Thermal Processing **[#2070]**
Graphitization/oxidation kinetic of nanodiamonds is investigated to determine which reaction governs diamonds destruction in chondrites. Graphitization prevails and kinetic parameters indicate a high temperature (~1300°C) short time (hours) event.

Dyl K. A. Bischoff A. Ziegler K. Wimmer K. Young E. D.
Metamorphic Conditions within the Villalbeto de la Peña L-Chondrite Parent Body Based on Petrologic and UV Laser Fluorination Oxygen Isotopic Studies on an Unique Fragment **[#2506]**
Oxygen isotope data from a foreign feldspar fragment in Villalbeto de la Peña (L6) record an isotopic profile across the object. This and NaSi-CaAl exchange suggest the presence of a volatile phase responsible for the fragment's alteration.

Lehner S. W. Buseck P. R.
The Highly Unequilibrated EH Chondrite, Sahara 97072, May Be a Primitive Breccia **[#2154]**
We have investigated a breccia lump in the unequilibrated enstatite chondrite Sahara 97072, which we interpret to be a primitive breccia.

Macke R. J. Britt D. T. Consolmagno G. J.
Enstatite Chondrite Physical Properties: Density, Porosity and Magnetic Susceptibility **[#1598]**
We measured density, porosity and magnetic susceptibility for 26 stones from 16 enstatite chondrites. We find no difference between EH and EL in these properties. Despite some outliers, enstatite chondrites grouped tightly in these properties.

Zhang A. Guan Y. Hsu W. Liu Y. Patchen A. D. Taylor L. A.
An Unusual Lithic Clast in the Grove Mountains 021536 CM2 Chondrite: Petrography, Mineralogy, and Oxygen Isotopes **[#1270]**
This abstract reports petrography, mineralogy, and oxygen isotopic compositions of an unusual lithic clast in a new CM2 chondrite GRV 021536.

Lyon I. Spring N. King A. Henkel T. Rost D.
The Li and Trace Element Budget of Acfer 094 Matrix **[#2335]**
Acfer 094 matrix has been studied by TOFSIMS elemental and isotopic analysis. Unusual minerals including a Li and Cr silicate has been found. These unusual minerals may account for a significant fraction of the budget of lithium and chromium in Acfer 094.

Matsuda S. Nakashima D. Iio H. Bajo K. Nagao K.
Laser Microprobe Noble Gas Analysis of Chondrules in the NWA 801 CR2 Chondrite **[#1628]**
Chondrules in NWA 801 show variations in cosmogenic ^{3}He and ^{21}Ne concentrations, suggesting cosmic-ray exposure on the parent body. In addition, we found solar-like noble gases in a chondrule in NWA 801.

Chizmadia L. J. Cabret-Lebrón E.
La Paz 031117: A New Primitive CO3 Carbonaceous Chondrite **[#2031]**
Lap031117 has AOIs with an avg olivine composition of 0.56mol% Fa with a standard deviation of 0.21. Type II chdls have an avg Cr_2O_3 content of 0.39wt% and the std dev is 0.12. These two properties are consistent with Lap031117 being subtype 3.0.

Ivanova M. A. Moroz L. V. Kononkova N. N.
Altered Material in CH/CB Chondrite Isheyevo **[#1259]**
Isheyevo is a metal-rich meteorite with similarities to both CH and CBb chondrites. Here we report results on mineralogical and IR-microspectroscopic studies of several lithic clasts and layered chondrules with rim of altered materials from Isheyevo.

Petitat M. Gounelle M. McKeegan K. Mostefaoui S. Marrocchi Y. Meibom A. Zolensky M. E.
Kaidun Carbonates: Re-Examining the ^{53}Mn-^{53}Cr Systematics **[#1666]**
In this work, we used a NanoSims to characterize ^{53}Mn-^{53}Cr internal isochrons on individual dolomite grains found in two different CI-lithologies of Kaidun.

Blinova A. I. Herd C. D. K. Zega T. De Gregorio B. Stroud R.
Preliminary SEM and TEM Study of Pristine Samples of Tagish Lake Meteorite **[#2039]**
We present preliminary SEM and TEM study of the prestine dark-dusty and compact-coherent lithologies from Tagish Lake meteorite.

Nakashima D. Matsuda S. Iio H. Bajo K. Ebisawa N. Nagao K.
Noble Gases in the NWA 852/801 CR2 Chondrites **[#1661]**
NWA 852/801 are solar noble gas rich meteorites and petrologically similar, suggesting they are paired. The constituents had been exposed to solar winds and cosmic-rays for > 57 Ma on the parent body surface followed by meteoroid flight of ~ 9 Ma.

Kuehner S. M. Irving A. J. Rumble D. III Nicklin I. Gregory D. A.
Exotic, Primitive Micrometeorite Clasts Related to CM Chondrites in Polymict Eucrite Breccia Northwest Africa 5232 **[#2315]**
Dark CM chondritic clasts in a eucrite breccia contain characteristic phosphosulfides.

Gordon S. H. Hammond S. J. Howard L. E. Bland P. A.
Dark Inclusions: Clasts of CM-type Material Within Allende **[#1713]**
Dark inclusions of Allende (CV3) are found to be CM in origin. Trace and minor element determinations carried out by solutions ICP-MS show very similar volatile element depletion patterns for the two materials.

Izawa M. R. M. Barker I. Moser D. E. Flemming R. L. McCausland P. J. A.
Colour SEM-Cathodoluminescence Investigation of the Tagish Lake C2 Chondrite **[#1757]**
Colour + UV SEM-CL imaging reveals variations in at least three constituents of Tagish Lake. Intra- and inter-grain differences appear to be uncorrelated with major element chemistry, but may identify trace element records of thermochemical evolution.

Morlok A. Neff D. Libourel G.
Alteration of Metal in CR2 Chondrites as Analogue for Long Term Corrosion Processes: Raman Studies of Corrosion Rims **[#1296]**
We use alteration features of metal and glass in CR2 chondrites as analogues for corrosion features of steel and Si-glass in the long term repository of nuclear waste. This presentation focuses on Raman analyses of corrosion rims around metal grains in Al Rais and GRO 95577.

Hiyagon H. Yamakawa Y. Sasaki M. Uchiyama K. Ushikubo T. Lin Y. Kimura M.
Rare Earth Element Fractionation in Fine-grained Inclusions from the Ningqiang and Other Carbonaceous Chondrites: Origin of Positive Ce-Eu-Yb Anomalies **[#1493]**
Fine-grained inclusions sometimes show positive anomalies in Ce, (Eu) and Yb often associated with HREE-depletions (Modified Group II). We suggest that they are produced by addition of a Ce-Eu-Yb-rich component onto Group II-like precursors.

Zolensky M. E. Briani G. Gounelle M. Mikouchi T. Ohsumi K. Weisberg M. K. Le L. Satake W. Kurihara T.
Searching for Chips of Kuiper Belt Objects in Meteorites **[#2162]**
We report progress towards locating pieces of Kuiper Belt Objects in meteorites.

ACHONDRITES: PRIMITIVE AND NOT SO PRIMITIVE

Nyquist L. E. Shih C.-Y. Reese Y. D.
Early Petrogenesis and Late Impact(?) Metamorphism on the GRA 06128/9 Parent Body **[#1290]**
Sm-Nd analyses of GRA06128 and GRA06129 determine its crystallization age to be 4.550 ± 0.034 Ga. Plagioclase, whole rock, and leachate (phosphate) samples give a secondary isochron age of 3.4 ± 0.4 Ga probably dating an impact event on the parent body.

Day J. M. D. Sunshine J. M. Ash R. D. Walker R. J. Liu Y. Rumble D. III McDonough W. F. Taylor L. A.
Making Crust in the Asteroid Belt: Evidence from GRA 06128/9 and Brachinites **[#2012]**
The GRA 06128/9 achondrite meteorites are thought to be fragments of evolved asteroidal crust. We examine their petrogenesis, possible link to brachinites and search for their parent body in the solar system.

Sanborn M. E. Wadhwa M.
Rare Earth Element Geochemistry of Angrites Northwest Africa 4590 and Northwest Africa 4801 **[#1345]**
We report ion microprobe analyses of rare earth element abundances in minerals of the plutonic angrites NWA 4590 and NWA 4801. Based on these results, implications are presented for the petrogenetic history of these two angrites and their relationships to other angrites.

Irving A. J. Rumble D. III Kuehner S. M. Gellissen M. Hupé G. M.
Ultramafic Achondrite Northwest Africa 5400: A Unique Brachinite-like Meteorite with Terrestrial Oxygen Isotopic Composition **[#2332]**
We characterize a remarkable brachinite-like specimen, which is perhaps a sample of proto-Earth or Theia.

Crowther S. A. Whitby J. A. Busfield A. Holland G. Busemann H. Gilmour J. D.
The I-Xe System in Lodranites Suggests Impact-related Rapid Cooling **[#1595]**
The I-Xe system of three lodranites has been investigated. Two metal and one silicate separate from GRA 95209 gave ages consistent with each other (and the I-Xe age of Acapulco feldspar), suggesting the parent material underwent a period of rapid cooling.

IRON METEORITES

Yang J. Goldstein J. I. Michael J. R. Kotula P. G.
Composition and Thermal History of the IVB Iron Meteorites **[#1186]**
Cooling rates across IVB iron group vary more than a factor of six, which is against the constant cooling rate as shown in previous studies. Implications to the early evolution of asteroids will be discussed.

Qin L. Dauphas N.
Cosmogenic Stable Isotope Effects in Carbo **[#2278]**
Samples from the same iron meteorite, Carbo, show resolvable variations in $\varepsilon^{182}W$. The variations are correlated with ^{3}He and depth from pre-atmospheric center. These are best explained by cosmogenic effects. No variation in $\varepsilon^{184}W$ can be resolved.

Garvie L. A. J. Németh P.
The Structure of Canyon Diablo "Diamonds" **[#1346]**
"Diamond" from the Canyon Diablo meteorite is composed of a nanoscale intergrowth of diamond and lonsdaleite, with [0–11] zone axis of diamond parallel to [010] of diamond.

METEORITE METHODOLOGY

Pourmand A. Dauphas N.
The Lu and Hf Isotopic Compositions of Meteorites: A Comparative Study of Alkali Flux Fusion and HF Parr Bomb Dissolution **[#2452]**
We compare Lu and Hf isotopic compositions and concentrations of Allende standard material dissolved in HF Parr bombs and alkali flux fusion in high-purity graphite, glassy carbon and platinum crucibles. Results from 12 meteorites are also presented.

Patzer A. Pack A. Gerdes A.
Determination of High-Precision Zr/Hf Ratios in Bulk Meteorites Using LA-ICP-MS **[#2522]**
We will present high-precision Zr/Hf data of different meteorite classes.

Minnick M. A. Strait M. M. Flynn G. J. Durda D. D.
Investigation of the Hydration of Anhydrous Chondrite Meteorites **[#2224]**
The purpose of our investigation was to examine the possibility and effectiveness of hydrating bulk meteorites from anhydrous samples to be used for fragmentation studies currently examining the origin of interplanetary dust particles.

Beck A. W. McSween H. Y. Jr. Mittlefehldt D. W. Lee C.-T. A.
Fused Bead Analysis in Diogenite Meteorites **[#1177]**
This study examines the accuracy of fused bead analysis in diogenites. We find elemental heterogeneity in the beads along with the presence of quench crystals. These findings suggest that fused bead cannot be used to accurately determine bulk chemistry of diogenites.

Shirai N. Humayun M. Irving A. J.
The Bulk Composition of Coarse-grained Meteorites from Laser Ablation Analysis of their Fusion Crusts **[#2170]**
We determined elemental abundances for an angrite, NWA 4590, and a shergottite, NWA 4468, from laser ablation analysis of broad areas of their fusion crusts.

ANTARCTIC MICROMETEORITES

Dobrica E. Engrand C. Leroux H. Rouzaud J. N. Duprat J.
Transmission Electron Microscopy of Ultracarbonaceous Antarctic Micrometeorites of Possible Cometary Origin **[#1534]**
TEM observations of ultracarbonaceous Antarctic micrometeorites show intimate mixing of disordered carbon and fine-scale assemblages of minerals like Mg-rich olivine, pyroxenes and Fe-Ni sulphides and alloys.

Imae N. Iwata N.
Compositions of Relict Olivines and Pyroxenes in Micrometeorites: In Comparison with Unequilibrated Chondrites **[#1501]**
Relict olivines and pyroxenes survived the atmospheric entry heating among Antarctic micrometeorites tend to be similar to the CR2 and CO3.0 chondrites rather than the CM2 and Tagish Lake chondrites.

Taylor S. Herzog G. F. Jones K. W.
Tomography of Metal Beads in Micrometeorites **[#1692]**
To better understand metal bead formation in micrometeorites (MMs) we measured the shapes and size distribution of beads relative to their host MMs in section and mapped the internal structure of MMs using synchrotron computed microtomography.

Badjukov D. D. Brandstaetter F. Raitala J. Kurat G.
Unmelted FeNi Metal Micrometeorites from the Novaya Zemlya Glacier **[#1499]**
We report on the texture and mineralogy of two FeNi metal and one metal-chromite particles, which possibly are the first unmelted metal micrometeorites found so far.

Suavet C. Alexandre A. Franchi I. A. Gattacceca J. Sonzogni C. Folco L.
Greenwood R. C. Rochette P.
Oxygen Isotope Ratios of Large Cosmic Spherules: Carbonaceous and Ordinary Chondrite Parent Bodies **[#1776]**
Oxygen isotopes measurements of 33 cosmic spherules, using IR-laser fluorination/mass spectrometry, indicate that 30% of them are above the terrestrial fractionation line, i.e., are unrelated to carbonaceous chondrites but rather to ordinary and R chondrites.

Onoue T. Yasuda C. Haranosono T. Morita K. Nakamura T.
Cosmic Spherules from Triassic Deep-Sea Sediments in Japan **[#1228]**
We report the textures and major element compositions of cosmic spherules from the Triassic deep-sea sediments that accumulated in a mid-oceanic basin of the ancient Pacific Ocean.

HEDs and Vesta

Warren P. H. Rubin A. E. Ziegler K.
Northwest Africa 5415: A Howarditic Impact-Melt Breccia with Zoned Relict Orthopyroxenes and Augites, and Corroded, Complexly Mantled Fo-59 Olivines **[#2545]**
NWA5415 is unusual among HEDs for its clear manifestation of origin by large-scale impact melting. Our section's five relict olivines display reaction textures (pyroxene coronas) formed by immersion in melt on the Si-rich side of the ol-px liquidus.

Roszjar J. Srinivasan G. Bischoff A. Mezger K. Whitehouse M.
Hf-W Ages of Zircons — New Constraints on the Evolution of the Eucrite Parent Body **[#1655]**
We determined Hf-W ages from zircons found in four basaltic eucrites using the Cameca 1270 ion microprobe. The consistent crystallization ages suggest, that the eucrite zircons formed in between a short time period after core-mantle segregation.

Greenwood R. C. Haack H. Buchanan P. C. Franchi I. A. Smith C. L. Johnson D. Burbine T. H.
Searching for the Missing Mantles of Disrupted Asteroids: Evidence from an Olivine-rich Clast in the Vaca Muerta Mesosiderite **[#2456]**
As part of an investigation into the olivine-rich material in mesosiderites we have looked in detail at a clast from Vaca Muerta which may represent preserved mantle material.

Ghosh A. Day R.
Thermal Simulation of a Magma Ocean on Asteroid 4 Vesta **[#1850]**
We present a thermal model of a magma ocean scenario on 4 Vesta.

Scott E. R. D. Greenwood R. C. Franchi I. A. Sanders I. S.
Oxygen Isotopic Constraints on the Origin and Parent Bodies of Eucrites, Howardites, and Diogenites **[#2263]**
Our oxygen isotopic analyses of 18 eucrites and four diogenites suggest that Vesta was isotopically homogeneous and that five of these eucrites with abnormal O isotopic compositions plus NWA 011 come from five Vesta-like bodies.

Righter K. Sutton S. Danielson L. Pando K. Le L. Newville M.
Using Vanadium in Spinel as a Sensor of Oxygen Fugacity in Meteorites: Applications to Mars, Vesta, and Other Asteroids **[#2213]**
Some meteorites do not contain mineral assemblages required to apply traditional oxy-barometers. Here we introduce a technique using vanadium X-ray absorption features in spinels to characterize the oxygen fugacity of meteoritic dunites, pyroxenites, and chondrites.

Irving A. J. Bunch T. E. Kuehner S. M. Wittke J. H. Rumble D. III
Peridotites Related to 4 Vesta: Deep Crustal Igneous Cumulates and Mantle Samples **[#2466]**
NWA 5480 may be a sample of Vesta-Related Mantle, but 4Vesta may be just one part of a former, larger body (Opis).

Bogard D. Garrison D.
Ar-Ar Impact Heating Ages of Eucrites and Timing of the LHB **[#1131]**
Ar-Ar ages indicate impact resetting ~4.48 Ga ago for unbrecciated eucrites and ~3.4–4.1 Ga for brecciated eucrites. These impacts likely are related to the late heavy bombardment (LHB) of the Moon.

DUST FORMATION AND TRANSFORMATION

Flynn G. J. Durda D. D. Minnick M. A. Strait M.
Production of Cosmic Dust by Hydrous and Anhydrous Asteroids: Implications for the Production of Interplanetary Dust Particles and Micrometeorites **[#1164]**
Comparison of the debris from hypervelocity disruption of four hydrous CM2 meteorites to that from the anhydrous meteorite Saratov indicates the hydrous meteorites significantly overproduce dust in the 10^{-4} to 10^{-7} gram mass range.

Rietmeijer F. J. M. Hadamcik E. Pun A. Renard J.-B. Nuth J. A. III Levasseur-Regourd A. C.
Light Scattering by Fluffy Low-Silica Al-Fe-SiO and Ca-SiO Smokes Obtained by Non-Equilibrium Vapor Phase Condensation **[#1742]**
The effects of grain size, grain size distributions and bulk composition on maximum polarization and the phase angle function were studied for vapor phase condensed Ca-SiO and low-silica Al-Fe-SiO smokes, serving as analogs for comet dust.

Roskosz M. Leroux H.
Subsolidus Transformation of Amorphous Interstellar Dusts After Injection in a Protoplanetary Disk **[#1745]**
Subsolidus reheating of amorphous interstellar silicate dust analogs produces an unexpected diversity of minerals and a large redistribution of elements. Some of these phases look very similar to condensation and high-temperature products.

INTERSTELLAR ORGANIC MATTER

Dobrica E. Engrand C. Quirico E. Montagnac G. Duprat J.
Immature Carbonaceous Matter in CONCORDIA Antarctic Micrometeorites **[#1688]**
Raman spectroscopy of Antarctic micrometeorites reveals abundant and highly disorganized carbonaceous matter in all types of unmelted to partially melted particles. The cyanide functional group was found in an ultracarbonaceous micrometeorite.

Floss C. Stadermann F. J.
Interstellar Components in the Primitive CR3 Chondrites QUE 99177 and MET 00426 **[#1083]**
QUE 99177 and MET 00426 contain abundant N- and C-anomalous phases of interstellar origin. High abundances carbonaceous matter with C isotopic anomalies in these meteorites suggests that their scarcity in other samples is due to secondary processes.

Croat T. K. Bernatowicz T. J. Stadermann F. J.
Auger and NanoSIMS Investigations of Pristine Presolar SiC Surfaces **[#1887]**
From Auger Electron Spectroscopy of 15 pristine SiC surfaces (prepared without harsh acids) and subsequent NanoSIMS measurement of three SiCs, we find evidence for C-rich, Si-poor coatings and C and N isotopic distinctions between surface and bulk.

De Gregorio B. T. Stroud R. M. Nittler L. R. Cody G. D.
Variety of Organic Matter in Stardust Return Samples from Comet 81P/Wild 2 **[#2260]**
Cometary organics show a wide variety of morphology and chemistry, including a growing population of N-rich organic matter.

Nuth J. A. III
Fischer-Tropsch-Type Catalytic Activity in the Primitive Solar Nebula: Results of New Experimental Studies Using Graphite and Noble Gases **[#2401]**
A carbonaceous coating forms via Fischer-Tropsch type reactions that is a better catalyst than amorphous iron silicates. Such a coating on grain surfaces could explain rich deposits of macromolecular carbon found in primitive meteorites and could have other consequences.

EARLY SOLAR SYSTEM CHRONOLOGY

Moynier F. Dauphas N. Podosek F.
A Search for ^{70}Zn Anomalies in Meteorites **[#1646]**
^{70}Zn is homogeneously distributed in the early solar system at a precision of 0.70 ε which confirms the homogeneity in planetary bodies of neutron rich isotopes around the iron peak.

Parai R. Jacobsen S. B.
Precise Determination of Initial Solar System $^{87}Sr/^{86}Sr$ and Implications for Early Solar System Chronology **[#1995]**
We measure Sr isotopes in CAIs, angrites, lunar anorthosites and eucrites to determine initial solar system $^{87}Sr/^{86}Sr$ with better precision than previous studies, thus providing better resolution of early solar system chronology.

Bowers M. R. Collon P. Kashiv Y. Lamm L. Lu W. Paul M. Robertson D. Schmitt C.
Proposed Measurements of ^{36}Cl Cross Sections for In-Situ Production in the Early Solar System **[#2113]**
An overabundance of ^{36}S in CAIs was interpreted as evidence for the extinct ^{36}Cl. We are planning to measure the ^{36}Cl production cross sections in the relevant E < 20 MeV/A range for irradiation from a young Sun with accelerator mass spectrometry.

Hans U. Kleine T. Bourdon B.
The Chronology of Accretion and Volatile Depletion of Differentiated Protoplanets Inferred from Rb-Sr Systematics of Angrites **[#2440]**
We present new high-precision Sr isotope data for plagioclase separates from angrites and use these data to constrain the chronology of volatile depletion and accretion of the angrite parent body.

Chaussidon M. Barrat J.-A.
^{60}Fe in Eucrite NWA 4523: Evidences for Secondary Redistribution of Ni and for Secondary Apparent High $^{60}Fe/^{56}Fe$ Ratios in Troilite **[#1752]**
High apparent $^{60}Fe/^{56}Fe$ ratios have been found in troilite from the eucrite NWA 4523. These ratios are likely explained by a redistribution of Ni isotopes after the decay of ^{60}Fe.

Brennecka G. A. Weyer S. Wadhwa M. Janney P. E. Anbar A. D.
$^{238}U/^{235}U$ Variations in CAIs: Implications for Pb-Pb Dating **[#1061]**
Data obtained from CAIs of the Allende meteorite challenges the assumed uniformity of $^{238}U/^{235}U$ used in the Pb-Pb age equation for meteoritic material. Such data may require revision of the absolute age of the first solids in the solar system.

Chen J. H. Papanastassiou D. A.
Nickel Isotopic Compositions in Pallasites and Iron Meteorites **[#1844]**
Fe-Ni measurements in pallasites do not show preserved evidence of *in situ* ^{60}Fe decay (1.5 Ma half life) but still place pallasite formation within 15 Ma of unequilibrated chondrites.

Quitté G. Cosmidis J. Poitrasson F.
Nickel Nucleosynthetic Anomalies in Leachates of Carbonaceous Chondrites **[#2324]**
Ni isotopes were measured in sequentially digested carbonaceous chondrites. Orgueil leachates show deficits in ^{60}Ni and ^{62}Ni, while anomalies in Allende and Murchison can generally not be resolved from the standard isotope composition.

Yin Q.-Z. Amelin Y. Jacobsen B.
Project Milestones: Testing Consistent Chronologies Between Extinct ^{53}Mn-^{53}Cr and Extant U-Pb Systematics in the Early Solar System **[#2060]**
New ^{53}Mn-^{53}Cr data are presented for four "milestones" with well-known Pb-Pb ages. We demonstrate consistent chronologies between extinct ^{53}Mn-^{53}Cr and U-Pb systematics in the Early Solar System. ^{53}Mn/^{55}Mn heterogeneity could be tested with future work.

Liu M.-C. Nittler L. R. Alexander C. M. O'D. Lee T.
A Search for Internal ^{26}Al Isochrons in CM Hibonite **[#1739]**
We conducted a high spatial-resolution investigation of the internal Mg isotopic distribution in a spinel-hibonite spherule from Murchison to seek an internal ^{26}Al isochron.

Ito M. Ganguly J.
Mg Diffusion in Minerals in CAIs: New Experimental Data for Melilites and Implications for the Al-Mg Chronometer and Thermal History of CAIs **[#1753]**
We evaluate the relative robustness of CAI minerals for Al-Mg chronometer, and the possible resetting of Mg isotopic composition during the period of residence of the CAIs in the protoplanetary disk and by thermal processes in the parent body.

Spivak-Birndorf L. J. Wadhwa M.
^{26}Al-^{26}Mg Systematics in Brachina and the Unique Achondrite GRA 06129 **[#2131]**
We report an investigation of the ^{26}Al-^{26}Mg chronology of the possibly related achondrites, Brachina and GRA 06129. Both meteorites show evidence of very early crystallization (~2–3 Myr after Solar System) followed by later thermal metamorphism.

COMPARATIVE PLANETOLOGY

Sharkov E. Bogatikov O.
Irreversible Evolution of the Terrestrial Planets: Geological and Petrological Data **[#1065]**
All terrestrial planetary bodies have been self-developed systems, evolved on the close scenario, which provides cardinal change of tectonomagmatic processes at the middle stages of their evolution; except the Earth, they are "dead" bodies now.

Stoddard P. R. Jurdy D. M.
Topographic Comparisons of Uplift Features on Venus and Earth: Implications for Venus Tectonics **[#2236]**
Topographic profiles of regiones and rifts on Venus are compared to hotspots and mid-ocean spreading centers on Earth. Principal component analysis shows that the continental Yellowstone hotpot corresponds well with Venus regions.

Litherland M. M. McGovern P. J.
Effects of Planetary Radius on Lithospheric Stresses and Magma Ascent on the Terrestrial Planets **[#2201]**
We model how varying planetary curvature affects the lithospheric stress beneath a load. We then examine how this can assist or inhibit magma ascent beneath volcanoes and basins on differently sized planets.

Baptista A. R. Craddock R. A. Mangold N.
Small Martian Shield Volcanoes and Terrestrial Analogues **[#2102]**
We are conducting field studies in Hawaii and in Iceland to understand the formation of parasitic shield volcanoes and their related lava flows. The rheological properties of Mars Syria Planum small shields volcanoes make them a good analog.

Gadányi P. Gucsik A. Bérczi Sz.
Pseudokarstic Subsidences Induced by Subsurface Melting of Tephra-covered Firn — Analogues for Martian Subsidences in the Dyngjufjöll Massif, Iceland **[#2353]**
The subsidences from the selected area of Iceland can aid to understand more about the newly discovered ice shields on Mars and their morphological features and climatic environments.

Tretyakov V. I. Kozyrev A. S. Litvak M. L. Malakhov A. V. Mitrofanov I. G. Mokrousov M. I. Sanin A. B. Vostrukhin A. A.
Comparison of Neutron Environment and Neutron Component of Radiation Doze for Space around Earth and Mars from Data of Instruments HEND/MarsOdyssey and BTN/ISS **[#1292]**
Data from two similar instruments — HEND onboard NASA's Mars Odyssey and BTN onboard International Space Station — allows us to compare the neutron environment in the space near Mars and Earth and estimate the neutron dose for interplanetary flights.

Schmedemann N. Neukum G. Denk T. Wagner R.
Impact Crater Size-Frequency Distribution (SFD) on Saturnian Satellites and Comparison with Other Solar-System Bodies **[#1941]**
Our research shows high similarities of impact crater-SFDs between the inner Solar-System bodies, the saturnian satellites and the asteroid body-SFD.

Garry W. B. Zimbelman J. R. Bleacher J. E. Crumpler L. S.
Topography and Inflation Features of the 1859 Mauna Loa Lava Flow, Hawai'i: Applications to Inflated Flows on Mars **[#1200]**
Topography and inflation features from the distal end of the 1859 lava flow on Mauna Loa volcano Hawai'i will be compared to possible inflated flows on Mars.

Bleacher J. E. Garry W. B. Zimbelman J. R. Richardson P. W.
Field Observations of Rootless Vents over the Pohue Bay Lava Tube, Hawai'i: Comparisons with Olympus Mons Lava Fans, Mars **[#1980]**
Field studies of rootless vents over lava tubes on Hawai'i suggest that most Olympus Mons lava fans are also rootless eruption points. Rift zones, if present, are likely responsible for a smaller population of flank fans.

Shockey K. M. Gregg T. K. P.
The Spatial Relationship Within Fields of Shield Volcanoes **[#2056]**
We statistically examine the spatial distribution of volcanic edifices within fields on the terrestrial planets.

IMPACTS I: MODELS AND EXPERIMENTS

Ivanov B. A.
Multiphase Equations of State for Planetary Impact Study II **[#2283]**
First results of the construction of the ANEOS-base multiphase EOS of forsterite are presented. The new EOS promises more accurate impact melt calculations in high-velocity planetary impact modeling.

Carter R. T. Jandir P. S. Kress M. E.
Estimating the Drag Coefficients of Meteorites for All Mach Number Regimes **[#2059]**
Most models that describe the descent of meteorites use a constant drag coefficient. We present a numerical method to calculate drag coefficients as a function of Mach number.

Wünnemann K. Elbeshausen D. Collins G. S.
Structural Evidence for the Direction of Impact at Complex Craters: Insight from 3D Numerical Modeling **[#1593]**
We use 3D hydrocode modeling of impact crater formation to investigate the effect of the angle of incidence on structural asymmetries in the resulting crater morphology.

Kurta A. T. Wünnemann K. Kenkmann T.
Morphometry and Structure of Eroded Complex Impact Craters: A Parameter Study Using Hydrocode Modeling **[#1948]**
The crater diameter and the size of the central uplift and the ring syncline change with the amount of erosion a complex impact crater has undergone. We systematically analyse these quantities as a function of depth utilizing numerical simulations.

Elbeshausen D. Wünnemann K. Collins G. S.
Oblique Impacts in Frictional Targets — Implications for Crater Size and Scaling **[#1559]**
We conducted more than 200 3D-hydrocode simulations to reveal the effect of the impact angle on crater size and the role of friction in oblique impacts. We prove whether existing scaling laws can be extended to describe both the effect of obliquity and friction.

Ernst C. M. Barnouin-Jha O. S. Ramesh K. T. Swaminathan P. K. Kimberley J.
Strain Rate and Dynamic Fracturing in Planetary-Scale Impacts **[#2523]**
Using numerical simulations and new dynamic fragmentation models, we investigate what strain rates might be generated during large scale impacts and assess implications for fragmentation considering new dynamic fragmentation models.

Potter R. W. K. Collins G. S. Elbeshausen D. Wünnemann K.
The Effect of Asteroid Shape, Velocity and Target Material on Asteroid Survivability **[#1610]**
Numerical simulations of asteroid impacts show that a substantial fraction of the asteroid remains solid (does not melt or vaporize) if the impact is near escape velocity, into a deep water layer or if the impactor is significantly prolate.

Ormö J. Lepinette A. Lindström M. Sturkell E. Shuvalov V. Housen K. Holsapple K.
Dynamics of the Water Resurge at Marine-Target Impact Craters Analyzed with a Combination of Low-Velocity Impact Experiments and Numerical Simulation **[#1571]**
Projectile impact experiments complement numerical simulations when illustrating the processes involved in the formation and modification of marine-target craters.

Holsapple K. A. Housen K. R.
Deep Impact: An Outburst Triggered by an Impact? **[#1936]**
The Deep Impact ejecta apparently had more kinetic energy than the impactor. We suggest some possible reasons, and present the results of experiments that may give clues to the interpretation of the event.

Housen K. R.
Dynamic Strength Measurements on Granite and Basalt **[#1701]**
Dynamic strength measurements on granite and basalt are reported and compared with measurements of flaw size distributions.

Sugita S. Kurosawa K. Kadono T. Hironaka Y. Otani K. Shiroshita A. Ozaki N. Miyanishi K. Sekine Y. Nakamura K. Fukuzaki S. Sano T. Sakaiya T. Fujiwara T. Mochiyama T. Takarada S. Fujioka S. Shigemori K. Ohno S. Tachibana S. Matsui T.
In-Situ Spectroscopic Observation of Silicate Vaporization Due to >10 km/s Impacts Using a Laser-driven Launcher **[#2493]**
A high-power laser was used to accelerate heavy metal (Ta) flyers to 9 km/s, to shock heat and compress silicate samples to near critical conditions. High-speed spectroscopic observation reveals that diopside vaporizes around 4 GPa and 8000 K.

Stickle A. Schultz P. H. Crawford D. A.
The Role of Shear in Oblique Impacts **[#2357]**
Shear failure plays a significant role in hypervelocity impacts. Experimental results are compared to CTH models to determine regions of shear and extensional failure in a variety of targets.

Schultz P. H.
Uprange Plumes and Nature of the Comet 9P/Tempel 1 **[#2386]**
Hypervelocity impact experiments were performed for a variety of targets in order to assess conditions leading to reverse vapor plumes during early stages of crater formation with implications for deep impact.

IMPACTS II: CRATERS AND EJECTA

Koeberl C. Bartosova K. Brandstätter F.
Melt Particles in the Chesapeake Bay Impact Structure Eyreville Drill Core — A Progress Report **[#1715]**
Geochemical studies of melt fragments in a Chesapeake Bay crater drillcore indicate that no widespread homogenization of the melt took place.

Watson J. S. Gilmour I. Kelley S. P. Jolley D. W.
Scientific Drilling of the Boltysh Impact Crater, Ukraine **[#1719]**
We have re-drilled the Boltysh impact crater and have recovered a near continuous record of ~400 m of organic-rich sediments together with 15 m of suevite.

Albin E. F. Harris R. S. King D. T. Jr. Jaret S. J. Jarrett R. E.
Alternate Twin Deformation in Plagioclase: Possible Evidence of Shock Deformation in Charnockitic Rocks Associated with the Woodbury Structure **[#2544]**
Charnockitic rocks associated with the Woodbury structure contain evidence of possible shock metamorphism in plagioclase grains.

Milam K. A.
Deformation Fabrics and Their Cross-Cutting Relationships in the Central Uplifts of Large Impact Structures **[#2455]**
Deformation fabrics and the petrogenetic sequence observed in smaller complex craters (<20 km in diameter) are now being observed in the larger complex impact structures.

Ferrière L. Koeberl C. Reimold W. U. Hecht L. Bartosova K.
The Origin of "Toasted" Quartz in Impactites Revisited **[#1751]**
The toasted appearance of quartz is caused by an increase in light scattering due to the presence of numerous vesicles. Toasted quartz is formed by vesiculation after pressure release, at high post-shock temperatures.

Morrow J. R. Weber J. C.
Comparison of Low-Pressure Shock-Metamorphic Effects in Quartz from Barringer Crater, Arizona, and Kentland Dome, Indiana **[#1913]**
Low-pressure (=10 GPa) shock effects in quartz from Coconino Ss., Barringer Crater, and St. Peter Ss., Kentland Dome, are compared. Although showing overall similar post-shock microfabrics, very different PFs and incipient PDFs are developed.

Schmieder M. Buchner E. Kröchert J.
'Ballen Silica' in Impactites and Magmatic Rocks **[#1020]**
Recent studies pointed out that 'ballen silica' is an impact-diagnostic feature. However, ballen-textured α-cristobalite was also reported in rocks not related to impact.

Poelchau M. H. Kurta A. T. Kenkmann T.
Signatures of an Oblique Impact in the Central Uplift of Martin Crater, Mars **[#1796]**
The internal, layered structure of Martin Crater's central peak reveals a preferential orientation of strike that is perpendicular to the impact direction. Preliminary results are presented and implications for the cratering process are discussed.

Crasselt C. Reimold W. U.
Impact Related Pseudotachylitic Breccias in the Schurwedraai and Baviaan-Krantz Alkali Granite Complexes in the Collar of the Vredefort Dome, South Africa **[#2085]**
Structural and petrographic observations and chemical data of pseudotachylitic breccia occurrences in alkali granite of the collar of the Vredefort Dome are discussed with regard to the possible formation of these enigmatic melt breccias.

Wartho J-A. Schmieder M. van Soest M. C. Buchner E. Hodges K. V. Bezys R. K. Reimold W. U.
New (U-Th)/He Zircon and Apatite Ages for the Lake Saint Martin Impact Structure (Manitoba, Canada) and Implications for the Late Triassic Multiple Impact Theory **[#2004]**
New (U-Th)/He single crystal zircon and apatite ages for the 40 km Lake Saint Martin impact structure suggests that this crater is too now old to be included in the postulated ca. 214 Ma Late Triassic multiple impact event.

Buchner E. Moilanen J. Öhman T. Schmieder M.
Shock-Molten Sandstone Clasts in Impact Melt Rocks: Age Constraints for the Paasselkä Impact Structure (SE Finland) **[#2169]**
Partially molten sandstone clasts in impact melt rocks suggest a new <1.4 Ga age for the Paasselkä impact structure, SE Finland.

Ormö J. Hill A. Self-Trail J. M. Frisk Å. M.
A Method to Determine the End of Impact-related Sedimentation at Marine-Target Craters: Geochemistry and Micropaleontology of the Transition from Resurge to Secular Deposits at the Lockne, Tvären, and Chesapeake Bay Impact Structures **[#1318]**
Stable isotope and major element analysis is proving to be a necessary complement to inadequate visual inspection for distinguishing the end of impact-related sedimentation at marine-target craters.

Bliss K. M. Morrow J. R. Weber J. C. Vice M.
Evaluation of XRD and Raman Peak Broadening in Shock-Metamorphosed Carbonates from Carbonate-Target Bolide Impact Structures **[#2211]**
Carbonate samples were analyzed from eight confirmed carbonate-target impact structures and other high temperature-pressure settings to determine whether XRD and micro-Raman peak broadening in the resulting spectra is unique to impact settings.

Cernok A. Kring D. A.
Were Carbonate Impact Melts Produced from the Carbonate-rich Target Lithologies at Meteor Crater, Arizona? **[#1825]**
During the Meteor Crater impact event mafic silicate melts intensively degassed of CO_2 were produced. Recently, existence of carbonate melt has been reported. To test this concept, we analyzed interior fall-back breccia and ejected melt particles.

Orr Key W. R. Schultz R. A.
Fault Formation at Impact Craters in Porous Sedimentary Rock Targets **[#1073]**
We present results of a study in which the mechanics of faulting at high strain rates in porous sedimentary rocks were evaluated at the Upheaval Dome impact crater in southeast Utah.

Byrne C. J. Lordi N. G.
Radial Profiles of Lunar Basins and Large Craters **[#1351]**
The centers and diameter of large lunar impact features are derived from radial elevation profiles. Some published basins are not confirmed, some parameters are significantly different, and new basins are identified.

Bray V. J. Schenk P. M. Melosh H. J. Collins G. S. Morgan J. V.
Dimensions of Central Pits in Ganymede Craters **[#1350]**
Central pit craters are an unusual class of impact crater seen most commonly on the icy Galilean satellites and Mars. We will present topographic profiles of central pit craters on Ganymede, using these data to construct scaling trends.

Goeritz M. Kenkmann T. Wünnemann K. van Gasselt S.
Asymmetric Structure of Lunar Impact Craters Due to Oblique Impacts? **[#2096]**
Based upon observations of asymmetric lunar mare craters we investigated deviations of the central peak positions from the geometric center of the craters. We found slight correlations between the peak offset and the impact direction.

Vijayan S. Vani K. Sanjeevi S.
Crater Mapping and Analysis Using Cartosat 1 DEM **[#2427]**
Impact craters study using DEM: Analog to lunar mare crater.

Plescia J. B.
Wetumpka Impact Structure, Alabama: Gravity Survey **[#1218]**
A gravity survey of the Wetumpka impact shows a simple anomaly — a central low (–5.75 mGal) surrounded by a high (+2.5 mGal). There is no suggestion of a buried central uplift.

King D. T. Jr. Petruny L. W.
Upper Cretaceous Chalk at Wetumpka Impact Structure, Alabama: Post-Impact Sediment? **[#2381]**
Wetumpka impact structure, a 7.6 km diameter, Late Cretaceous marine impact feature, contains coeval chalk deposits that represent both displaced target megablocks and post-impact sediments with the interior and exterior terrains.

Glidewell J.
Seismic Data Through the Hico Structure: A Possible Impact Feature in North-Central Texas **[#2563]**
The Hico Structure in north-central Texas has been proposed to be an impact feature. Recent seismic data through the feature support this theory.

Kirkland L. E. Herr K. C. Adams P. M.
Remote Sensing of Geologic Materials at Man-Made Craters **[#2153]**
We use ground and airborne infrared remote sensing to explore geologic materials exposed by large manmade craters at the Nevada Test Site. The site and methods are analogs to rover and satellite exploration of the Moon and Mars.

Mihályi K. Gucsik A. Szabó J. Bérczi Sz.
Facts, Theories and Further Questions Around the Ries-Steinheim Simultaneous Impact Event: A Review **[#1542]**
This proposed paleoeographic reconstruction study can aid to understand more about the environmental effects of a terrestrial impact event such a double-type one: Ries-Steinheimer impact events and their influences on the paleoecological envrionment.

Danilin A. N.
A New Astrobleme in the Polar Urals (Russia) **[#1001]**
A reasonable assumption is made that one of the largest ancient astroblemes in the Earth is in the Polar Urals (Russia).

Rajmon D.
Circular Geomorphologic Feature Near Urengoy, West Siberia **[#1881]**
Circular polygonal feature 4.5 km in diameter near Urengoy in West Siberia is unique in the wider area. Geologic review indicates that a meteorite impact or transpression tectonics are the most likely formation mechanisms.

Bron K. T.
The Tookoonooka Tsunami Sequence: Evidence for Marine Impact in Australia's Lower Cretaceous **[#2560]**
The Tookoonooka subsurface impact structure (Australia) is located in the lower Cretaceous Eromanga Basin sedimentary succession. An ejecta-bearing tsunami sequence with basin-wide extent was discovered, and provides clear evidence that Tookoonooka was a shallow marine impact.

Aden D. J. Milam K. A. Kah L. C. Gilleaudeau G. J.
An Anomalous Breccia in the Mesoproterozoic (~1.1 Ga) Atar Group, Mauritania: Potential Evidence for an Impact-generated Tsunami **[#2003]**
Inital observations reveal that an anomalous high-energy breccia in the Mesoproterozoic Atar Group, Mauitania, is a possible candidate for an ancient tsunamite, which may have been triggered by a marine impact event.

Deutsch A. Berndt J. Mezger K. Schulte P.
The Pristine Chicxulub Ejecta Sequence at ODP Leg 207: A Micro-Chemical Study **[#1245]**
A La-ICP-MS study across the uppermost 6 mm of the exceptionally well preserved K/T boundary in Site 1259C (ODP Leg 207)allows assessing which components have contributed to the Chicxulub ejecta layer.

Jaret S. J. Kah L. C. French B. M.
Petrographic Investigation of Ejecta from the Tenoumer Impact Crater, Mauritania **[#1281]**
To improve our understanding of the excavation, shock metamorphism, and impact melting in simple craters, we undertook a mineralogical and petrological study of ejecta and impact melt from the Tenoumer impact crater, Mauritania.

Bölitz M. C. Langenhorst F.
Liquid Immiscibility and Gas Content in Dark Schlieren of Libyan Desert Glass **[#2018]**
We report microprobe and gas analyses of dark schlieren in Libyan Desert Glass (LDG). Schlieren contain two immiscible metastable silicate liquids that have formed by rapid cooling. High volatile contents in schlieren point to hydrous phases as precursor materials.

Harris R. S. Duncan M. S. Roden M. F. Schroeder P. A.
Discovery of In Situ Impact Glass in Upper Eocene Coastal Plain Strata, Jefferson County, Georgia **[#2502]**
We report the discovery of *in situ* impact glass fragments in an upper Eocene ejecta. Their compositions are consistent with microtektites in the North American strewn field.

Adolph L. Deutsch A.
Glass Spherules Related to the El'gygtgyn Impact Crater (Siberia) **[#1116]**
We report the results of a geochemical investigation on glass spherules from a terrace deposit outside the rim of the El'gygytgyn impact crater (NE Siberia, Russia). These spherules are very homogeneous yet differ in their composition from dacitic to basaltic-andesitic.

Das P. K. Misra S. Basavaiah N. Newsom H. Dube A.
Rock Magnetic Evidence of Asteroid Impact Origin of Ramgarh Structure, India **[#1466]**
The magnetic properties of spherules and other materials from the Ramgarh structure in India have high NRM, possibly associated with formation of the impact structure.

Miura Y.
Impact-related Indicators of Grains with Akaganeite Composition Found at Takamatsu, Nio, Kuga (Japan) and Carancas (Peru) **[#2565]**
Chlorine (Cl)-bearing Fe and Ni phases (as akaganeite composition) originated from impacts of meteoroids are found at Takamatsu, Nio, Kuga and Carancas compared with awaruite and artificial grains.

Hargitai H.
Water Ejecta of Marine Impacts and Ice Meteorites **[#2439]**
There is a debate on ice meteorites of extraterrestrial origin — but what if ice meteorites are made locally? A possibility of ice meteorites mady be marine impacts.

Cagen K. T. Abbott D. Nitsche F. West A. Bunch T. Breger D. Slagle A. Carbotte S.
Impact Ejecta in a Possible Tsunami Layer in the Hudson River: Regional or Local Event? **[#2276]**
Recent discoveries point to a tsunami event in the New York metropolitan area approximately 2300 BP. Our discovery of impact ejecta deposited by the tsunami in the Hudson River suggests that the tsunami was caused by an impact in the Atlantic Ocean.

Buchner E. Schmieder M. Strasser M. Strasser A. Kröchert J.
Impacts on Spherules **[#1017]**
Characteristic marks of low- and high-speed particle contacts (microcratering), respectively, may reveal a possible tool to discriminate between iron spherules of anthropogenic/industrial (low-speed) and cosmic/impact (high-speed) origin.

Abbott D. H. Gerard-Little P. Costa S. Breger D.
Odd $CaCO_3$ from the Southwest Indian Ocean Near Burckle Crater Candidate: Impact Ejecta or Hydrothermal Precipitate? **[#2243]**
Unusual carbonate crystals from the vicinity of Burckle Crater candidate may be impact ejecta or hydrothermal precipitates from ridge crest vents. However, they occur with translucent C impact spherules, native metals, and well preserved mineral fragments and glass.

Huang J. Xiao L. Wang K.
Xifeng Circular Basin: Another Failed Potential Crater in China **[#1035]**
There has been no substantiated impact crater in China. In 2006, a possible one was discovered in Xifeng County, Guizhou Province. By analysis of morphology, stratigraphy and impact metamorphism, we propose that it is not an impact crater but a reformed syncline.

Watters W. A. Zuber M. T.
Relating Target Properties to the Planimetric Shape of Simple Impact Craters **[#2556]**
We investigate the dependence of planimetric crater shape on the properties of geological targets, by comparing the distribution of morphometric quantitiesderived from the rim trace of fresh impact craters captured in HiRISEand MOC images.

Hamilton C. W. Fagents S. A.
The Tartarus-Colles Cone Group and Its Implications for Explosive Lava-Water Interactions in the Grjota Valles Region of Mars **[#1924]**
Terrestrial volcanic rootless cones (VRCs) are the products of explosive-lava water interactions. We describe the Tartarus-Colles cone group on Mars and provide morphological and geospatial evidence to support the interpretation that these landforms are VRCs.

Lanz J. K. Saric M. B.
Possible Traces of Hydrothermal Venting in Aeolis Planum, Mars **[#1014]**
We have studied pitted cones and ridges north of Aeolis Planum that show striking differences to other cone complexes on Mars. We propose that they were formed by hydrothermal venting processes similar to hydrothermal vent complexes on Earth.

Kerber L. Head J. W. Madeleine J. B. Forget F. Wilson L.
The Dispersal of Pyroclasts from Apollinaris Patera, Mars **[#2176]**
Using a Mars global circulation model, we model the dispersal of ash from Apollinaris Patera, varying parameters such as plume height, grain size, and season. We test the hypothesis that Apollinaris could be a source for the Medusae Fossae formation.

Lang N. P.
Another Look at the Summit Caldera of Apollinaris Patera **[#2370]**
This project focuses on documenting the structural and volcanic evolution of the summit caldera on Apollinaris Patera.

Fagan A. L. Sakimoto S. E. H.
Formation Constraints on Martian North Polar Volcanic Edifices **[#1976]**
Comparisons of topographic characteristics between Icelandic volcanoes and martian north polar edifices imply that many of the latter may be of subglacial origin and thus suggest a potential former ice sheet with a minimum thickness of 80–550m.

Tyson S. Wilson L. Gilbert J. S. Lane S. J.
A New Mechanism for Caldera Formation Resulting from Interactions Between Magmatic Heat and Cryospheric Ice **[#1716]**
We propose a new mechanism of caldera formation that does not require local removal of magma.

Tyson S. Wilson L. Lane S. J. Gilbert J. S.
Hecates Tholus: Defrosting a Volcano **[#1158]**
We explore how magmatic heat influences the survival of the cryosphere and any possible snowpack at the summit of Hecates Tholus.

Byrne P. K. van Wyk de Vries B. Murray J. B. Troll V. R.
An Overview of Volcano Flank Terraces on Mars **[#2192]**
Using MOLA, HRSC, and CTX images, and laboratory analogue modelling, we report on the nature, origin, and context of volcano flank terraces on Mars.

Spagnuolo M. G. Pio Rossi A.
Analog Modelling for Pit Craters and Its Relation to Extensional Features on Mars **[#1307]**
We performed analog modelling to study pit crater formation on Mars. Preliminary results show that pit craters in fact form in the presence of unconsolidated material over hard layers but no faults are developed.

Cushing G. E. Titus T. N.
Kilauea Pit Craters as Mars Analogs: A New Direction for Cave-Detection Techniques **[#1203]**
Some Kilauea pit craters provide access to extensive cave networks, and from the outside, appear morphologically similar to anomalous pit craters found on Mars. Thermal comparisons may enable future studies to indirectly identify caves on Mars.

Lopez T. Baratoux D. Rabinowicz M. Antoine R. Ayoub F. D'Uston L.
What Does Control the Thermal Behaviour of the Pits Near Arsia Mons? **[#1912]**
The THEMIS instrument onboard Mars Odyssey imaged deep pits, localised North of Arsia Mons, in the visible and infrared channels.We present a detailed thermal study of these pits to evaluate several hypotheses that could explain their thermal behavior.

Leverington D. W.
Reconciling Channel Formation Processes with the Nature of Elevated Hesperian Outflow Systems at Valles Marineris **[#1469]**
A volcanic origin for relatively small outflow systems at uplands adjacent to Valles Marineris is in accord with channel characteristics, regional geological context, and solar system analogs.

Basilevsky A. T. Neukum G. Kneissl T. Dumke A.
Geologic Analysis of HRSC Images of the Area East of the Mangala Valles Head Graben, Mars **[#1833]**
This study shows that the lava flows associated with a graben being the continuation to the east of the head graben of the Mangala Valles formed around ~0.5 Ga ago and thus correlate with one of the episodes of the Mangala Valles flood activity.

Crown D. A. Berman D. C. Rivas R. Ramsey M. S.
Arsia Mons Lava Flows: Insights into Flow Field Emplacement and Stratigraphy from CTX and HiRISE Images **[#2252]**
This research focuses on lava flows south of Arsia Mons and utilizes high-resolution images as well as topographic and thermal infrared data to examine development of channel and levee systems, local sequences of flow emplacement, and degradation of flow field surfaces.

Hiesinger H. Pasckert J. H. Reiss D.
Rheology of Lava Flows on Elysium Mons, Mars **[#1983]**
We have mapped 25 individual lava flows in the Elysium Mons region and measured their dimensions. On the basis of these measurements, we have calculated the yield strengths, effusion rates and viscosities of the lava flows.

Hiesinger H. Rohkamp D. Sturm S. Thiessen F. Reiss D.
Geology, Ages, Morphology, and Morphometry of Thumbprint Terrain in Isidis Planitia, Mars **[#1953]**
We constructed a map of thumbprint terrain and measured the heights, lengths, basal diameters, and the diameters of the central depressions. We dated the geologic units on which the thumbprint terrain occurs and superposed rampart craters.

Milazzo M. P. Keszthelyi L. P. Jaeger W. L. Rosiek M. Mattson S. Verba C. Beyer R. A. Geissler P. E. McEwen A. S. HiRISE Team
The Distribution of Columnar Lavas on Mars as Seen by HiRISE **[#2159]**
On Mars, water floods mix with hot lavas; joints form. HiRISE sees from space.

Korteniemi J.
Interpreting Remote Sensing Data: Martian Dikes vs. Other Features **[#2084]**
Examples of structures which may be (mis)interpreted as magmatic dikes or their surface manifestations.

Pedersen G. B. M. Head J. W. III Wilson L.
Early Amazonian Dike Swarms in Utopia Basin, Mars: Nature of Substrate and Estimates of Effusion Rates **[#1541]**
Hundreds of narrow, linear ridge segments are found in the transition zone between Elysium Rise and Utopia Basin. The linear ridges are interpreted to be dikes and the multiple ridge systems are interpreted to be dike swarms.

Woerner W. R. Coraor E. K. McCubbin F. M. Nekvasil H. Lindsley D. H.
The Effect of Pressure on Residual Liquid Compositions from Crystallization of a Humphrey-like Magma: Implications for Crustal Stratigraphy in Martian Volcanic Provinces **[#2203]**
Experiments indicate that Humphrey-like liquids ponding at the base of a thickened crust in major volcanic provinces on Mars would produce a pigeonite-rich cumulus layer at depth and highly silica-undersaturated sodic residual liquids.

Usui T. McSween H. Y. Jr. Clark B. C. III
CO_2-related Noachian Alkaline Magmatism on Mars: Evidence from High-Phosphorous Wishstone-Class Rocks in Gusev Crater **[#1055]**
We demonstrate that high-phosphorous tephrites (Wishstone class) in Gusev crater formed in association with carbonatitic melt/fluid. This could yield insights into the effects of CO_2 (an effective greenhouse gas) on Noachian magmatism.

Hutchins K. I. Agee C. B. Draper D. S.
Experimental Constraints on the Source Regions of the Shergottites and Gusev Basalts **[#1845]**
Rover data from rocks sampled at Gusev Crater on Mars combined with data from the martian basaltic meteorites (shergottites) suggest there are at least two distinct basalt source regions in the martian mantle.

Boisson J. Heggy E. Clifford S. M. Frigeri A. Plaut J. J. Farrell W. M. Putzig N. Picardi G. Orosei R. Lognonné P. Gurnett D. A.
The Geoelectrical Properties of Athabasca Broken-Rafted Plate Terrain as Derived from the MARSIS Radar Sounding Data **[#2001]**
To test the volcanic or fluvial formation hypothesis of Athabasca rafted plate terrain, we investigate the geoelectrical properties of the subsurface in this zone derived as derived from MARSIS radar data.

MARS: TECTONICS AND DYNAMICS

Wang Y. Wen L. Weidner D. J.
Constraining Composition of Mars Using Geophysical Constraints and Mineral Physics Data **[#1880]**
We construct 1-D density models of Mars for different mantle and core compositions, and calculate the hydrostatic gravity, moment of inertia and flattening factor, and then compare the predictions with the observations to constrain Mars composition.

Nunes D. C. Smrekar S. E. Konopliv A. S.
Survey of Gravity Admittance for Mars from the High-Resolution Mars Reconnaissance Orbiter Data **[#2011]**
We examine martian admittance spectra obtained with high-resolution gravity data from MRO, contrasting signatures from northern lowlands, southern highlands, and major volcanoes.

Spagnoulo M. G. Grings F. Perna P. Karszenbaum H. Ramos V. A.
Interpreting SHARAD Radargrams Using Interaction Models and Geological Constraints to Study Faults Zones in Mars **[#2163]**
The objective of this work is to present evidence of the SHARAD capabilities to retrieve information about the structure of a fault zone located at North-East of Ismeniae Fossae.

Roberts J. H. Lillis R. Manga M.
Giant Impacts on Early Mars and the Cessation of the Martian Dynamo **[#1265]**
The global magnetic field on Mars disappeared during the mid-Noachian, at the end of a sequence of giant impacts. We find that impact heating can reduce the CMB heat flow by up to 40%, and may have led to the cessation of dynamo activity.

Bills B. G. Ghent R. R. Nimmo F.
Tidal Dissipation in Mars: Where and How? **[#1712]**
Tidal dissipation in Mars is surprisingly vigorous. Tides raised by Phobos dissipate 3.3 MW. We consider several possible mechanisms for this dissipation, including tidally driven water flow in crustal aquifer systems.

Ruedas T. Tackley P. J. Solomon S. C.
Water, Melting, and Convection in the Martian Mantle **[#1463]**
In numerical thermochemical convection models of the partially molten martian mantle, radionuclides and water are being redistributed. This leads to a stiff upper mantle and a longer-wavelength thermal structure in water-bearing models.

Miskovic A. Grove T. L.
Stability of Hydrous Silicates and Deep Melting of the Early Martian Mantle **[#2539]**
Experimental phase relations predict that hydrous silicates can be buried deep in a growing planet. Relations between hydrous minerals and vapor-saturated solidus in martian mantle are investigated during the early planetary differentiation.

Kite E. S. Manga M. Perron J. T.
Evidence for Past Kilometer-Scale Overturn(s) in Deformed, Layered Terrain Near the Deepest Point on Mars **[#1248]**
In NW Hellas, wind has exhumed layered terrain showing ductile deformation. A km-scale cellular pattern is identified, consistent with thermal and/or compositional convection. 'Frozen-in' convection within an impact melt sheet is consistent with observations.

Zeng Z. Zhang Z. Birnbaum S. J. Xie H. Yang W.
Global Dynamical Significance of Zigzag Fractures in South Polar Ice Cap of Mars **[#1225]**
Regional zigzag fractures and an echelon fractures developed in the south polar ice cap of Mars implies an accelerating spinning of Mars about its axis after the formation of the cap and proves the formation mechanism of the spiral trough in the cap.

Lucas A. Mangeney A. Mège D. Bouchut F.
Landslide Scar Geometry Effect on Flow Spreading: Application to Martian Landslides **[#1770]**
The geometry of the landslide scar may play a role mass spreading but it is usually unknown. Numerical tests have been performed so as to figure out this effect. Application to martian cases and implications in terms of mass balance will be discussed.

MARTIAN STRATIGRAPHY: UNDERSTANDING THE GEOLOGIC HISTORY OF MARS THROUGH THE SEDIMENTARY ROCK RECORD

Garchar L. A. Calvin W. M.
Characterization of Outcrop Rock Targets in Meridiani Planum Using Pancam and Mini-TES Spectra **[#1019]**
We hope to gain insight into the compositional variability of outcrop rocks through analysis of concurrent Pancam and Mini-TES spectra. We have analyzed color and spectral data from Pancam and unmixed the Mini-TES using surface component end-members.

Fan C. Xie H. Schulze-Makuch D. Ackley S.
A Likely Formation Mechanism of the Hematite-rich Spherules in the Equatorial Region of Western Mars **[#1470]**
We argue that the hematite-rich spherules were originally formed in Valles Marineris and transported to Meridiani Planum accompanied with accretion of finer volcanic materials, abrasion of basaltic fragments and break down of the spherules during the wash-out flows.

D'Arcangelo S. Pondrelli M. Rossi A. P. Michael G.
Geological Characterization of the Layered Deposits of the Crommelin Crater (Mars) **[#1601]**
The layered deposits cropping out in the Crommelin crater have been analyzed and mapped and their origin has been hypothesised as related to possible spring processes.

Chuang F. C. Weitz C. M.
Characteristics and Regional Distribution of Intracrater Layered Deposits in Arabia Terra, Mars **[#2057]**
Using several datasets from the Mars Reconnaissance Orbiter mission, we are assessing the morphology and other characteristics of intracrater layered deposits with regard to their regional distribution in Arabia Terra.

Rossi A. P. Pondrelli M. Hauber E. Baliva A. Michael G. Ori G. G. Pompilio L. Parente M. Ivanov A. Neukum G.
Stratigraphic Architecture and Structural Control on Sediment Emplacement in Becquerel Crater (Mars) **[#1588]**
We investigate the link between structure and sedimentation on becquerel light-toned deposits and their relation with regional tectonic features in Arabia Terra.

Anderson R. B. Bell J. F. III Milliken R. E.
Geologic and Thermophysical Unit Mapping of the Proposed Mars Science Laboratory Landing Site and Traverse Path in Gale Crater **[#2030]**
We present a unit map of the proposed MSL landing site and traverse path in Gale crater, with descriptions and preliminary interpretations of key units on the crater floor and in the layered mound.

Sowe M. Roach L. H. Hauber E. Jaumann R. Mustard J. F. Neukum G.
Comparison of Interior Layered Deposits in Chaotic Terrains **[#1938]**
The characterization of ILDs using high-resolution image, elevation and spectral data demonstrated differences in terms of erosional shape, thickness, elevation, material competence and possibly mineralogy, but similarities in morphology.

Raitala J. Kostama V.-P.
Deformation of the Light Blocks on the Floor of Ius Chasma **[#1574]**
Layered blocks on the floor of Ius Chasma provide tectonics, cross-cuts and insights into the development, materials, layering, strata forming events and early geology on the tableland surrounding Ius.

Fueten F. Abdulla Y. Stesky R. MacKinnon P. Hauber E. Zegers T. Gwinner K.
Detailed Observation of an ILD Within Southern Coprates Chasma, Valles Marineris, Mars **[#1324]**
Attitudes of the lowest layers of an ILD on the southern edge of Coprates Canyon within Valles Marineris suggest deposition on local basement topography. This ILD postdates the formation of this part of Valles Marineris.

Wendt L. Gross C. McGuire P. C. Combe J.-P. Neukum G.
Analysis of Juventae Chasma Sulfate Mound B using the Multiple-Endmember Linear Spectral Unmixing Model (MELSUM) on CRISM Data **[#1531]**
MELSUM, is a novel, efficient method to analyze hyperspectral NIR data using a linear mixing model. It identifies monohydrated and polyhydrated iron and magnesium bearing sulfates as the spectral components of this outcrop.

Racher H. Slingerland M. Fueten F. Stesky R. MacKinnon P. Hauber E. Gwinner K. Zegers T.
Structural Analysis of an Interior Layered Deposit in Southern Coprates Chasma, Mars **[#1472]**
A triangular shaped ILD in Southern Coprates Chasma within Valles Marineris is interpreted as a rotated fault block. The rotation can be interpreted as a back rotation consistent with the opening of a rift valley.

Roach L. H. Mustard J. F. Murchie S. L. Bishop J. L. Ehlmann B. L. Lichtenberg K.
Parente M. CRISM Science Team
Sulfate and Hematite Stratigraphy in Capri Chasma, Valles Marineris **[#1826]**
We present sulfate and red hematite stratigraphy within the central Interior Layered Deposit of Capri Chasma, Valles Marineris, from spectral analysis of CRISM data.

Le Deit L. Bourgeois O. Mège D. Le Mouélic S. Massé M. Hauber E. Jaumann R. Bibring J.-P.
Geological History of a Light-toned Formation Draping the Plateaus in the Region of Valles Marineris, Mars **[#1856]**
We perform a geological analysis of layered deposits cropping out on the plateaus around Valles Marineris in order to determine their possible formation scenario and the role of water in their geological history.

Farrand W. H. Rice J. W. Jr. Glotch T. D.
Evidence of the Presence of Jarosite and Diagenetic Activity in the Mawrth Vallis Region **[#2080]**
CRISM and HiRISE data over the Mawrth Vallis region are examined and we find evidence for diagenetic activity and find a localized occurrence with a distinctive spectral signature which we identify as jarosite. Implications for the history of the region are discussed.

Crumpler L. Arvidson R. Blaney D. Cabrol N. deSouza P. Farrand W. Farmer J. Greeley R.
Hurowitz J. Lewis K. McCoy T. McEwen A. McSween H. Ming D. Morris R. V. Rice J. W. Jr.
Rice M. Ruff S. Schmidt M. Schröder C. Squyres S. Yen A. Yingst A.
Field Reconnaissance Geologic Mapping of the Columbia Hills, Gusev Crater from MER Spirit Rover and HiRISE Observations **[#2045]**
This study presents the results of the first field reconnaissance geologic mapping on another planetary surface. We show that geologic units on Mars are complex like their terrestrial counterparts, but can mapped at human and rover scales of observation.

Gurgurewicz J.
Mineralogy of Noctis Labyrinthus on the Basis of OMEGA/MEX and PFS/MEX Data **[#1576]**
The OMEGA/MEx and PFS/MEx data have been used to study the diversification of the mineral composition of the Noctis Labyrinthus region, which is situated in the western end of the Valles Marineris canyon on Mars.

Quantin C. Flahaut J. Allemand P.
Buried Layers Beneath South Rim of Valles Marineris Revealed by Central Uplift of Impact Craters **[#1651]**
Our study of exhumed layers in central peak of impact craters revealed extended buried layers below the southern plateau of Valles Marineris. According to their origin elevation, these layers could be exposed in the deepest parts of Valles Marineris.

MARS: VALLEYS AND VALLEY NETWORKS

Hoke M. R. T. Hynek B. M.
Valley Network Formation on the Ancient Highlands of Mars Occurred in the Late Noachian and Early Hesperian Epochs **[#1885]**
We compare valley network N(2) crater numbers with isochrons to place the end of their formation in the L. Noachian and E. Hesperian Epochs. Analysis of their crater populations indicates five of these networks experienced multiple periods of formation.

Luo W. Stepinski T. F.
Global, Computer-generated Map of Valley Networks on Mars **[#1311]**
The new, global map of valley networks on Mars has been created entirely by a computer algorithm parsing topographic data. Dependencies between dissection density and its potential controlling factors are derived and discussed.

Yamaguchi Y. Miyamoto H. Tanaka K. L. Palmero Rodriguez J. A.
Mapping Valley Networks in the Noachian Terrain around Naktong Vallis, Mars: Topographic Control on Drainage Density **[#1630]**
We find that a positive correlation exists between the mean slope and the drainage density of valley networks in Naktong Vallis on Mars, indicating that precipitation-fed surface runoff played a significant role in the valley formations.

Bodager E. C. Sweitzer-Lamme J. W. Tobias M. J.
An Analysis of Potential Fluvial Patterns on Mars' Surface Utilizing THEMIS **[#1955]**
Application of THEMIS rendered visual evidence for analysis of evidence and indicators of fluvial systems on Mars' surface. Results formulated by examining the thermal inertia of the area of interest.

Fassett C. I. Dickson J. L. Head J. W.
Small, Young Fluvial Features in Icy Terrains on Mars **[#1185]**
We describe small valleys found in association with ice-rich terrains on Mars (lobate debris aprons and viscous flow features). The most probable mechanism for their formation is the melting of ice, likely during the Amazonian.

Dickson J. L. Fassett C. I. Head J. W.
Young Valley Networks on Mars: Persistent Flow of Water in Lyot Crater, an Amazonian Impact Basin Microenvironment **[#1184]**
We document a suite of sinuous valley networks on the floor of Lyot Crater that incise a mantling unit dated as mid-Amazonian. We interpret the valley networks to be fluvial in origin and to have been sourced by mid- or late-Amazonian glacial units.

Newsom H. E. Lanza N. L. Ollila A. M. Wiseman S. M. Roush T. L. Marzo G. A. Tornabene L. L. Crumpler L. S. Okubo C. H. Osterloo M. M. Hamilton V. E.
Inverted Channels on the Floor of Miyamoto Crater, Mars, Viewed by the HiRISE Camera **[#1396]**
Curvilinear ridges on the western floor of Miyamoto crater have similar characteristics to positive relief channel deposits seen on Earth near Green River, UT that are interpreted as exhumed, inverted, fluvial paleochannel deposits.

Marzo G. A. Roush T. L. Lanza N. L. McGuire P. C. Newsom H. E. Olilla A. M. Wiseman S. M.
Mineralogy of the Inverted Channel on the Floor of Miyamoto Crater, Mars **[#1236]**
Miyamoto Crater contains an inverted paleochannel deposit. Based on CRISM and HRSC observations, the paleochannel appears located in an area rich in Fe/Mg-smectite uniquely associated with the lowest terrain in the area.

Burr D. M. Williams R. M. E.
The Stanislaus Table Mountain: Observations of a Lava-capped Inverted Paleochannel for Interpretation of Inverted Paleochannels on Mars **[#1633]**
Inverted fluvial features on Mars may form through a variety of processes. Investigations into a lava-capped paleochannel on Earth provide observations that aid in distinguishing among formation mechanisms and assessing paleochannel preservation.

Bouley S. Craddock R. A. Mangold N. Ansan V.
Comparison of Different Crater Counting Methods Applicated to Parana Valles **[#1097]**
The exact timing of valleys networks is still not well understood. We set out to test the reliability of different counting methods applied to Parana Valles using a large dataset of HR images that allow to reduce uncertainties in age determination.

Dohm J. M. Hare T. M.
Coupling Viking Information with Themis and Mola Data Results in Significant Improvement in Paleoerosional Detail of Warrego Valles **[#1949]**
Here we report preliminary findings on the re-evaluation of the Viking-based, published geologic map information of the Thaumasia region through detailed investigation of the Warrego rise region, which includes Warrego Valles.

Musiol S. Cailleau B. Neukum G.
A Model of Pore-Fluid Flow Applied to the Formation of Outflow Channels in the North-Eastern Hellas Region on Mars **[#1023]**
The numerical calculations are done with the finite-elements software ABAQUS. We analyse stresses and pore-fluid flow in the lithosphere under the assumption of a poroelastic martian crust, and compare our results to surface structures.

Mars: Aqueous Processes in Valles Marineris and the Southern Highlands

Lucchitta B. K.
Lakes in Valles Marineris, Mars (I): Walls, Mounds, Moats, and Volcanoes **[#2068]**
Synthesis of research concerning lakes in the Valles Marineris suggests that the interior layered deposits were emplaced in a wet environment. Addressed are exhumation from the walls; eolian, fluvial, or volcanic origin; moats and inclined layers.

Lucchitta B. K.
Lakes in Valles Marineris, Mars (II): Valleys, Channnels, Shallow Lakes, and Age **[#2345]**
Synthesis of research concerning lakes in the Valles Marineris suggests that interior layered deposits were emplaced in a wet environment. Addressed are the provenance of water; shallow, deep, and late lakes; ancestral basins; and age relations.

Popa C. Esposito F. Colangeli L.
Tithonium Chasma on Mars: Evidences for Water Related Processes Time Span on Mars **[#1611]**
Tithonium Chasma system west of VM present sulfate outcrops in ambiguous relationship with material that cuts through. We discuss the implications of their presence to the limits of water-dry transitions on Mars.

Gross C. Wendt L. Dumke A. Neukum G.
Further Evidence for Multiple Flooding Events at Juventae Chasma and Maja Valles, Mars **[#1890]**
We investigate the age relationship of Juventae Chasma to the adjacent Maja Valles to gain an explanation for the evolution of rhythmic LLD. We use impact crater size-frequency distributions for dating of the surface in the region.

Kostama V.-P. Raitala J. Ivanov M. A. Aittola M. Korteniemi J. Lahtela H. Törmänen T.
Hydrologic History of the Eastern Hellas Basin Region, Mars **[#1582]**
The eastern Hellas Basin rim region displays evidence for continued fluvial and glacial activity from Noachian-early Hesperian to Amazonian. The observations and analysis of the region suggest a complex and multitemporal fluvial activity.

Irwin R. P. III Maxwell T. A. Howard A. D. Higbie M. A.
Floor Materials of Open Paleolake Basins on Mars **[#2358]**
In Terra Cimmeria, Mars, Noachian craters with etched floor deposits are clustered in relatively dust-free areas, suggesting locally efficient aeolian erosion of crater floor sediments or more volcanic resurfacing closer to the dichotomy boundary.

Annex A. Grigsby B. Turney D. Zimbelman J. R. Rice J. W. Jr.
Preliminary Analysis of Tinto Vallis and Palos Crater; A Proposal for CRISM Targeting **[#1459]**
Preliminary CRISM study results of the Tinto Vallis and Palos crater paleo lake system. CTX, THEMIS, and TES data indicate water related minerals could be present in and around Palos, justifying the need for high resolution CRISM targets.

Baker D. M. Head J. W.
The Origin of Eridania Lake and Ma'adim Vallis: An Investigation of Closed Chaos Basins, Hesperian Ridged Plains, and Tectonic Constructs on the Floor of a Large Hypothesized Paleolake on Mars **[#1835]**
The stratigraphy of structures and units is analyzed on the floor of a potential paleolake south of Ma'adim Vallis, Mars. Closed chaos basins are potential sources of groundwater inputs, and may have been modified by later lava flow loading.

MARS: AQUEOUS GEOMORPHOLOGY

de Villiers G. Kleinhans M. Postma G. Hauber E. de Jong S. de Boer P. L.
Types of Martian Fan-shaped Sedimentary Deposits **[#1901]**
Our objectives are to qualify and quantify the morphological elements of martian fan-shaped sedimentary deposits with the use of Mars Express-HRSC data. Based on size, shape, and gradient, we describe different types of fan-shaped deposits.

Pondrelli M. Rossi A. P. Marinangeli L. Baliva A.
The Holden and Eberswalde Deltaic Systems: Lithofacies and Depositional Environments **[#1619]**
The Holden and Eberswalde fan deltas have been analyzed in order to map the lithofacies assemblage, to recognize sedimentary processes and to infer depositional environments.

Kleinhans M. G. van de Kasteele H. E. Hauber E. de Villiers G. Postma G. de Jong S. de Boer P. L.
Palaeoflow and Sediment Delivery Reconstructions from Martian Delta Morphology by Combined Modelling and HRSC DTM Analysis **[#1495]**
Morphology of crater lake deltas indicates formative time scale, sediment flux and water flux. Our new morphological model predicts quantitative morphology which we compare to DTM data. Five studied deltas formed in less than ten years.

Di Achille G. Hynek B. M.
Possible Primordial Oceans on Mars: Evidence from the Global Distribution of Ancient Deltas? **[#1977]**
Terrestrial marine deltas share the characteristic of being formed at the mean global sea level. By using the global distribution of martian deltas, we report preliminary results of a test for the possible ancient ocean on Mars.

Berman D. C. Feldman W. C. Rodriguez J. A. P.
Volatile-driven Morphologies Relating to Zones of High WEH in Xanthe Terra **[#1333]**
The MO Neutron Spectrometer has detected moderate concentrations of WEH in western Xanthe Terra. We utilize new high-resolution images to analyze the morphologies of craters and small channels to look for evidence of water-rich degradation.

Howard A. D. Moore J. M.
Subaqueous Mega-Slides on the Floor of Hellas **[#1376]**
Extensive subaqueous mass movements have been involved in the emplacement and deformation of the Hellas Basin floor deposits, followed by intensive eolian erosion.

Craft K. Lowell R. Kraal E.
Models of Martian Hydrothermal Systems and Impliations for Geomorphology **[#1535]**
Systems driven by magmatic intrusions are first investigated by applying boundary layer theory to obtain results for heat and fluid fluxes and then by using numerical modeling to explore other parameters including ice-melting and brine formation.

Harrison K. P.
An Alternative View of Martian Chaotic Terrain Formation **[#1743]**
Martian chaotic terrains have traditionally been regarded as groundwater source regions for outflow channels. However, the near ubiquitous presence of upstream fluvial inlets suggests that their status as source regions should be revisited.

Oehler D. Z. Allen C. C.
Mud Volcanoes in the Martian Lowlands: Potential Windows to Fluid-Rich Samples from Depth **[#1034]**
Mud volcanoes in the martian lowlands may provide access to relatively unaltered samples of fluid-rich strata from depths that would otherwise be unreachable. The Chryse-Acidalia region is particularly prospective for such structures.

Neather A. C. Wilson L. Lane S.
Muddy CO_2-driven Brine Fountains at Mangala Valles, Mars **[#1154]**
We compare the mass flux provided by a theorised CO_2-driven water fountain with the flux required to emplace the apparently muddy deposits seen around the eastern arm of Mangala Valles, Mars, concluding that the fountain is a reasonable explanation.

Kereszturi A. Horváth A. Sik A. Kuti A. Bérczi Sz. Gánti T. Pócs T. Szathmáry E.
Possible Liquid-like Water Produced Seepage Features on Mars **[#1111]**
Seepage-like features emanate from Dark Dune Spots, and their seasonal changes were observed on northern dunes of Mars. Based on observations and theoretical computations, they may form by the movement of interfacial water-lubricated dune grains.

MARTIAN GULLIES: MORPHOLOGY AND ORIGINS

Schon S. C. Head J. W.
Terraced Cutbanks and Longitudinal Bars in Gully Channels on Mars: Evidence for Multiple Episodes of Fluvial Transport **[#1691]**
Longitudinal bars and multiple terraced cutbanks suggest distinct episodes of fluvial transport in gully channels. The low preservation potential of these high-slope, steep-sided, non-lithified features implies that they are latest Amazonian in age.

Kneissl T. Reiss D. van Gasselt S. Neukum G.
Northern-Hemisphere Gullies on Mars – Distribution and Orientation from the Evaluation of HRSC and MOC-NA Data **[#1590]**
We evaluated HRSC and MOC-NA data covering the northern hemisphere in order to analyse geographical and latitudinal distribution, geological context and orientation of gullied slopes.

Bryson K. L. Sears D. W. G.
Evaporation Effects on the Formation of Martian Gullies **[#1368]**
We analyze HiRISE images of martian gullies and adjacent dunes to evaluate the hypothesis that evaporation is a limiting factor in gully formation.

Johnsson A. Olvmo M. Reiss D. Hiesinger H.
Latitudinal Survey of Periglacial Landforms and Gullies of Eastern Argyre and Poleward on Mars **[#2405]**
We perform an investigation of periglacial landforms and gullies of eastern Argyre and poleward. Aim of study is to characterize the environment with a focus on landform zonation and its linkage to topography, geology, surface conditions and climate.

Dove A. R. Toon O. B. Heldmann J. L.
Observations and Modeling of the Mass and Energy Balance of Terrestrial Snowpacks to Constrain Martian Snowpack Models **[#1730]**
In order to improve martian snowpack models, we utilize numerical modeling and observations of terrestrial snowpacks to gain a better understanding of the physical processes that drive snowpack metamorphosis.

Rivera-Valentin E. G. Gavin P. Coleman K. A. Dixon J.
Liquid Water and Water-Ice Slush Flume Simulations of Gully Synthesis Varying Exit Aperture Diameter **[#1355]**
In an attempt to better understand the proposed wet gully synthesis hypothesis, this project undertakes the task of simulating liquid water and water-ice slush flows within a flume. We specifically study the effects of varying exit aperture diameter.

Dickson J. L. Head J. W.
The Formation and Evolution of Youthful Gullies on Mars: Gullies as a Late-Stage Product of Mars' Most Recent Ice Age **[#1768]**
We place new data of gullies from MRO in the context of data from MGS to explain the formation and evolution of gullies within the last several million years from the repeated melting of cold-trapped wind-blown snow.

Roehm C. L. Soare R. J. Osinski G. R. Costard C.
Crater-Rim Gully Formation in Utopia Planitia: Hydrological Support of the Periglacial Origin Hypothesis **[#2245]**
In this study, we present preliminary data derived from MOC imagery comparing the volumetric capacity of ejecta-based depressions with the volumetric dimensions of nearby crater-rim gullies.

Reiss D. Hiesinger H. Hauber E. Zanetti M. Preusker F. Trauthan F. Reimann G. M. Raack J. Carlsson A. E. Johnsson A. Olvmo M. Jaumann R. Johansson H. A. B. Johansson L. McDaniel S.
Morphologic and Morphometric Comparision of Gullies on Svalbard and Mars **[#2362]**
We compare terrestrial analogs on Svalbard morphologically and morphometrically with martian gullies in order to constrain the formation process (fluvial and/or debris flow).

Araki S. Williams R. M. E. Dombard A. J.
Examining Formation Mechanisms of Martian Gullies Using Mars Reconnaissance Orbiter Context Imagery **[#2497]**
We surveyed Context imagery to construct a database of gully features and used image-based observations to test gully formation mechanisms. Thus far we find that no one formation mechanism can explain the gully features observed.

Gulick V. C. Davatzes A. E. K.
MRO's HiRISE Coverage of Fluvial Landforms on Mars During its Primary Science Phase **[#2562]**
MRO HiRISE imaging of fluvial features is summarized, with a focus on gully forms.

Hart S. D. Gulick V. C. Parsons R. A. Barnhart C. J.
Gully Slopes and Discharges on Lyot Crater's Central Peak **[#2349]**
This study focuses on two large gullies present on the local topographic high of the central peak of Lyot crater. We use HiRISE stereo images to create high resolution gully profiles and cross sections, and calculate discharge estimates based on these measurements.

Kolb K. J. McEwen A. S. Pelletier J. D. HiRISE Science Team
Measuring Slopes of Gully Fan Apices Using Digital Elevation Models **[#2268]**
We measure channel gradients above the highest observable extent of deposition in gullies to assess the involvement of liquid water in gully-carving flows.

Conway S. J. Balme M. R. Murray J. B. Towner M. C.
Debris Flow as a Mechanism for Forming Martian Gullies **[#1950]**
Recently active gullies presents an apparent paradox, as the conditions on Mars prevent the survival of surface water. We compare the morphology of these gullies to those on Earth and tentatively suggest debris flow as forming the martian gullies.

Lucas A. Mangeney A. Mangold N. Mège D. Bouchut F.
New Insights into the Dynamics of Martian Gullies **[#1784]**
Numerical simulations have been performed so as to figure out the dynamics of dry granular media. Comparisons with bright deposits gully show that a pure dry granular media could not explain their bright deposits.

Costard F. Védie E. Font M. Lagarde J. L.
Laboratory Simulations of Martian Gullies over Sand Dunes: Impact of the Permafrost Table **[#1289]**
Some unusual linear gullies over sand dunes (Russell crater, Mars) are characterized by their long and narrow channels. This study focuses on the formation of these gullies by means of laboratory simulations within a cold room.

Chevrier V. F. Ulrich R. Altheide T. S.
Viscosity of Liquid Ferric Sulfate Solutions and Application to the Formation of Gullies on Mars **[#1424]**
Viscosity of ferric sulfate solutions has been experimentally measured and used in a numerical model of gully flow. Results show that boulders up to four meters can be moved in the channel, explaining size segregation observed by MRO-HiRISE.

Mars: Dunes, Dust, and Wind

Ellehøj M. D. Johnsen S. J. Madsen M. B.
D/H Fractionation in the Atmosphere-Ground Ice System on Mars **[#1561]**
The solid-vapor fractionation processes of Deuterium/Hydrogen (D/H) in the ground ice-atmosphere system on Mars are investigated through experiments and modeling. Preliminary results mainly from the experimental work are presented.

Segura T. L. Colaprete A.
Global Modeling of Impact-induced Greenhouse Warming on Early Mars **[#1056]**
We have modeled the climate effects of impacts on early Mars. The model includes evaporation/precipitation of water, water and CO_2 cloud microphysics, the radiative and latent heating effects of water and CO_2 clouds, and water cloud coalescence.

Metzger S. Balme M. Pathare A.
Meteorologic Conditions and the Formation of Terrestrial Dust Devils **[#1229]**
We examine the relationship between ground surface solar heating, ambient meteorologic conditions and the formation of terrestrial dust devils.

Wurm G. Teiser J. Reiss D. Kelling T.
Lifting Dust on Mars by Greenhouse Effects and Thermophoresis **[#1516]**
The GT-effect, a combination of a (solid state) greenhouse effect and thermophoresis can efficiently lift dust from a surface at low pressure. We discuss how this effect might lift dust from the martian surface.

Hayward R. K. Titus T. N. Michaels T. I. Colaprete A. Verba C. A. Christensen P. R.
Aeolian Dunes as Ground Truth for GCM and Mesoscale Modeling on Mars **[#1212]**
Aeolian dunes preserve a record of atmosphere/surface interaction, serving as ground truth for atmospheric models. We compare dune centroid azimuth and slipface orientation to a General Circulation Model and a mesoscale model.

Gardin E. Allemand P. Quantin C.
A Global Morphological Study at High Resolution on the Dune Fields on Mars **[#2510]**
Dune fields are possible recorders of paeloclimat. The high availible resolution images permit to complete the GIS of the MD3.

Bandeira L. Marques J. S. Pina P.
Automatic Delimitation of Regions with Aeolian Features on Mars **[#1288]**
This text describes an adaptive approach based on HOG features and SVM classifier to detect automatically regions with dune fields on Mars.

Toyota T. Kurita K.
Dark Halo: Enigmatic Features of Dark Streaks at Martian Volcanoes **[#1597]**
Interactions between the atmosphere and the ground surface cause observable changes in the surface patterns. Here we report a new kind of time-variable surface pattern called "Dark Halo" near the top of high altitude volcanoes in Tharsis region.

Chuang F. C. Beyer R. A.
Modification of Martian Slope Streaks **[#2104]**
This study focuses on features that were not identified or were uncommon in previous studies of slope streaks including ridge-like structures, terminal deposits, and mantle deposits.

Grant J. A. Wilson S. A. Noe Dobrea E. Fergason R. L. Griffes J. L. Moore J. M. Howard A. D.
HiRISE Views an Enigmatic Deposit in the Electris Region of Mars **[#1871]**
The Electris region of Mars defines a broadly distributed, unconformable deposit whose characteristics appear most consistent with emplacement as loess.

Tirsch D. Jaumann R. Pacifici A. Poulet F. Roach L. H. Mustard J. L. Bibring J.-P. Neukum G.
Dark Layers as Local Sources for the Dark Intra-Crater Dunes on Mars **[#1004]**
We present morphological indications and mineralogical evidence for dark layers acting as local sources for the dark dune material on Mars.

Szynkiewicz A. Ewing R. C. Fishbaugh K. E. Bourke M. C. Bustos D. Pratt L. M.
Geomorphological Evidence of Plausible Water Activity and Evaporatic Deposition in Interdune Areas of the Gypsum-rich Olympia Undae Dune Field **[#2038]**
New morphological features (e.g., cross-bedding strata, bright patches), revealed by HiRISE for the gypsum-rich Olympia Undae Dune Field, appear to indicate the change(s) in paleoenvironmental conditions likely controlled by climate fluctuations in the North Pole of Mars.

Horgan B. H. N. Bell J. F. III
Insights from Ferrous Mineralogy into the Transport of Martian North Polar Materials **[#2457]**
NIR spectra of the north polar region of Mars indicate the presence of various pyroxenes and olivine. The distribution of these minerals suggests a complex relationship between the regional sedimentary units, and that saltation affects composition.

Lahtela H. Titus T. N. Geissler P. E. Roach L. H. Verba C. A. Mustard J. F. Murchie S. L. Brown A. J. Seelos F. Seelos K. Calvin W. M. Parente M. Cornwall C.
Coordinated HiRISE/CRISM Observation on Gypsum Signature in Martian Polar Dunes **[#2254]**
Our independent HiRISE/CRISM study conformed that the source for sypsum signature in Mars north polar dunes is in the dark dunes themselves, not in the bright bedrock.

Diniega S. Byrne S. Glasner K.
Controls on the Spacing and Size of Martian Polar Dunes from a Buried Ice Table **[#1434]**
Dune fields often exhibit a stable characteristic dune size and spacing. We consider the possible effect of topography on dune scaling during dune formation and evolution, and consider the effect of an evolving ice table under martian polar dunes.

Necsoiu M. Leprince S. Dinwiddie C. Hooper D. Walter G.
Recent Migration Rates of the Great Kobuk Sand Dunes, Alaska: Technologic and Scientific Implications for Planetary Dune Systems **[#2074]**
A novel method based on correlation of optical satellite imagery was applied to dune migration rates in Kobuk Valley, AK. This method could be applied to monitor other morphological processes on planetary surfaces and remote terrestrial locales.

Howald T. V. Schieber J.
Preparing for MSL — Experimental Eolian Erosion of Soft Sedimentary Rocks **[#1872]**
An eolian erosion device was constructed to explore long-term eolian abrasion of soft sediments with wind velocities and sediment types that are more likely to be encountered on the martian surface.

Durham W. B. Pathare A. V. Stern L. A. Lenferink H.
Does the Brittle-to-Ductile (Mobility) Transition of Icy Sand Packs Coincide with the Maximum Packing Density? **[#1703]**
We present preliminary experimental data indicating a correspondence between the brittle-to-ductile transition of icy sand packs and the maximum packing density of sand in such packs.

MARS: REMOTE SENSING

Bandfield J. L. Mayorga L. C. Edwards C. S. Glotch T. D.
An Integrated Analysis of Martian Surface Compositions Using Near Infrared Through Thermal Infrared Spectroscopic Data **[#1072]**
TES, THEMIS, and CRISM spectroscopic data are used to analyze sites of mineralogical interest on Mars. The combined wavelength coverage provides a more complete perspective of surface compositions and their formation processes.

Lane M. D. Glotch T. D. Dyar M. D. Bishop J. L. Pieters C. M. Klima R. Hiroi T. Sunshine J. M.
Thermal Infrared Spectroscopy of a Synthetic Olivine Series (Forsterite-Fayalite) and Interpretation of the Nili Fossae, Syrtis Major, and Isidis Regions of Mars **[#2469]**
Synthetic olivines in the forsterite to fayalite solid solution series were made (14 different Fo values) and their midinfrared spectra were applied to Mars. Olivine was mapped in the Nili Fossae, Syrtis Major, and Isidis basin regions.

Osterloo M. M. Hamilton V. E. Anderson F. S. Koeppen W. C.
THEMIS Detections of Forsterite-Fayalite Compositions Within Terra Tyrrhena **[#1405]**
The objective of this study is to determine if the Thermal Emission Imaging System (THEMIS) can detect variations in the Mg-Fe content of olivines on the martian surface. We have selected four sites within Terra Tyrrhena to conduct our analysis.

Tsang S. W. R. Eckert-Erdheim A. M. Williams L. H.
Thermal Emissions Spectroscopy of Olivine **[#1206]**
Many scientists have noticed the absorptions in olivine move closer to 0 wavenumbers as the Fe content increases, but no one has quantified this phenomenon. The model that we have created will enable scientists to determine Fo values remotely.

Nuding D. L. Cohen B. A.
Characterization of Rock Types at Meridiani Planum, Mars Using MER 13-Filter Pancam Spectra **[#2023]**
A database of Pancam spectra shows the diversity of rocks on Meridiani Planum. It is difficult to distinguish cobble groups with simple methods. We identified a group of possible meteorites near Eagle Crater that may be related to Heat Shield Rock.

Ashley J. W. Ruff S. W. Knudson A. T. Christensen P. R.
Mini-TES Measurements of Santa Catarina-Type, Stony-Iron Meteorite Candidates by the Opportunity Rover **[#2468]**
Most meteorites found on Mars can be regarded as witness samples for surface-volatile interactions. We report on the Mini-TES evaluation of 12 cobbles located near Victoria Crater, and conclude that at least three of these are similar to meteorite candidate Santa Catarina.

Schröder C. Ashley J. W. Chapman M. G. Cohen B. A. Farrand W. H. Fleischer I. Gellert R. Herkenhoff K. E. Johnson J. R. Jolliff B. L. Joseph J. Klingelhöfer G. Morris R. V. Squyres S. W. Wright S. P. Athena Science Team
Santorini, Another Meteorite on Mars and Third of a Kind **[#1665]**
The rock fragment Santorini is similar in chemical and mineralogical composition to two other fragments investigated earlier during Oportunity's mission. These rocks are of meteoritic origin and probably fragments of the same originally larger body.

Karunatillake S. Squyres S. W. Wray J. J. Taylor G. J. Gasnault O. McLennan S. M. Boynton W. El Maarry M. R. Dohm J. M.
Chemically Striking Martian Regions and Stealth Revisited **[#1302]**
The Mars Odyssey GRS chemical maps establish chemically striking regions. They represent the surface to tens of cm depths, complementing tens-of-micron sampling depths of infrared spectra. We discuss the one region that overlaps with classic Stealth.

Plaut J. J. Safaeinili A. Campbell B. A. Phillips R. J. Putzig N. E. Nunes D. C. Seu R.
A Widespread Radar-Transparent Layer Detected by SHARAD in Arcadia Planitia, Mars **[#2312]**
The subsurface sounder SHARAD on MRO has detected a widespread radar-transparent layer up to 50–90 m thick in the Arcadia region of Mars.

Stillman D. E. Grimm R. E. Harrison K. P.
The Anomalous Radar Transparency of Central Elysium Planitia and Amazonis Planitia **[#2412]**
The only ice-free rocky units that SHARAD has been successful at penetrating into are in Elysium and Amazonis Planitia. These are the youngest units on Mars and probably have low radar loss because they have been insufficiently exposed to water.

Mouginot J. Kofman W. Grima C. Safaeinili A. Plaut J. J.
Martian Surface Radar Reflectivity by MARSIS **[#1546]**
Martian radar surface reflectivity by MARSIS - Calibration - Simulation - Analysis.

De Angelis G. Dachev Ts. P. Semkova J. V. Maltchev S. Tomov B. Matviichuk Yu. Koleva R. Benghin V. Chernykh I. Shurshakov V. Petrov V.
Models for the Radiation Environment of Planet Mars and of Its Moon Phobos **[#1308]**
Models of radiation environment induced by Galactic Cosmic Rays (GCR) and Solar Particle Events (SPE) on Mars and Phobos have been developed, as well as for the mission cruise phase, and used for the Liulin-Phobos experiment onboard the Phobos-Soil mission.

Sefton-Nash E. Catling D. C. Wood S. E.
Developments in Deriving Best-Fit Thermal Inertia of the Surface of Mars Using THEMIS Images **[#1773]**
We improve the resolution and accuracy of derived thermal inertia of the martian surface by 1) Implementing a validity test for THEMIS images based on a thermal model and 2) Using HRSC topography to produce high resolution slope and azimuth data.

Fergason R. L. Christensen P. R.
New View of the Martian Surface: THEMIS Global Thermal Inertia Mosaic **[#1997]**
We are generating a new global thermal inertia mosaic using THEMIS IR data at 256 m per pixel. This mosaic has facilitated an improved understanding of geologic processes acting on local scales, including the nature of moderate TI surfaces.

Edwards C. S. Bandfield J. L. Christensen P. R. Fergason R. L.
Global Distribution of Bedrock and the Nature of the Upper Martian Crust **[#2022]**
THEMIS thermal inertia data were used to map the distribution of interpreted bedrock on Mars. Most of the instances are concentrated in the southern highlands and globally few instances were identified, indicating large scale crustal processing.

Piatek J. L.
Thermophysical Properties of Terrestrial Rock and Debris-covered Glaciers as Analogs for Martian Lobate Debris Aprons **[#2127]**
A survey of the thermophysical properties of terrestrial rock and debris-covered glaciers suggests these properties may be used to distinguish between massive debris-covered ice and intimate rock/ice mixtures in martian lobate debris aprons.

Tanaka K. L. Dohm J. M. Irwin R. Kolb E. J. Skinner J. A. Jr. Hare T. M.
Progress in Global Geologic Mapping of Mars **[#1975]**
We describe new and updated aspects of our Mars global geologic mapping effort, including use of data sets, mapping approaches and progress, current issues, and future work.

Mest S. C. Crown D. A.
Geologic Mapping of MTM-30247, -35247 and -40247 Quadrangles, Reull Vallis Region of Mars **[#1930]**
Geologic mapping of MTMs -30247, -35247, and -40247 characterizes the upper reaches of Reull Vallis, located in the eastern Hellas region of Mars. Crater size-frequency distributions will be generated for mapped units using high-resolution images.

Crown D. A. Bleamaster L. F. III Mest S. C. Mustard J. F.
Geologic Mapping of the NW Rim of Hellas Basin, Mars **[#1705]**
Geologic mapping of the NW rim of Hellas basin is providing new constraints on the magnitudes, extents, and history of volatile-driven processes as well as a geologic context for mineralogic identifications.

Philippoff A. J. Tornabene L. L. McEwen A. S. Baker V. R. Melosh H. J.
Berman D. C. HiRISE Science Team
Geomorphic Mapping of Hale Crater, Mars **[#1737]**
Presented here is a geomorphic map of Hale Crater that highlights the channels found within and emanating from Hale's ejecta blanket and the implications they may have for the early climate and landscape evolution of Mars.

Griffin L. J. Zimbelman J. R.
Geologic Mapping of Western Medusae Fossae Formation, Mars (MC 23-NW): Redefining Unit Boundaries and Features to Reveal a History of Tectonism, Wind Erosion, and Episodic Water Flow **[#1196]**
Mapping has revealed substantial patches of layered materials that are interpreted to be outliers of Medusae Fossae Formation (MFF) materials. Eroded MFF materials show evidence suggesting localized folding, plus exhumed fluvial features.

Skinner J. A. Jr. Fergason R. L. Tanaka K. L.
Occurrence and Origin of Lobate Materials in the Highland-Lowland Boundary of Southern Utopia Planitia, Mars **[#2459]**
The southern Utopia HLB has been interpreted as colluvial sequences associated with HLB scarp erosion. We re-examine these interpretations and present evidence for the existence of extensive flow-related geologic processes.

Pina P. Antunes J. Bandeira L. Saraiva J.
Analyzing the Large Extension of Polygonal Terrain in the Northern Plains of Mars **[#2035]**
This work describes a plan for the automated analysis of the large extension of terrain covered by polygonal networks on the northern plains of Mars.

Dumke A. Spiegel M. van Gasselt S. Neukum G.
Valles Marineris, Mars: High-Resolution Digital Terrain Model on the Basis of Mars-Express HRSC Data **[#1985]**
High resolution digital terrain models (DTM) are necessary for geoscientific studies of Mars. To get a more comprehensive view of regional processes on Mars, images as well as topographic data have to be mosaicked photogrammetrically.

Chen Y. Hwangbo J. W. Li R.
Photogrammetric Processing of High-Resolution Planetary Orbital Imagery for Large-Area Topographic Mapping **[#2129]**
A photogrammetric method to process HiRISE stereo images is described. This bundle adjustment based method removes inconsistencies between differnt HiRISE images covering the same area to generate topographic products of the best quality.

Li R. Chen Y. He S. Yang L. Tang M. MER Science Team
Rover Localization: Comparison between Bundle Adjustment-based and HiRISE Orbital Image-based Methods **[#2208]**
A bundle adjustment-based rover localization method has been developed. Rover positions are also estimated by matching a ground image orthophoto to a HiRISE orthophoto. We estimated the differences in traverse positions between the two methods.

Daubar I. J. McEwen A. S.
Depth to Diameter Ratios of Recent Primary Impact Craters on Mars **[#2419]**
Very recent small martian primary craters confirmed by HiRISE have a depth/diameter ratio of ~ 0.26, close to expected for primaries and significantly higher than that measured for secondaries or many small fresh craters of unknown origin.

Barlow N. G.
Martian Central Pit Craters: Summary of Northern Hemisphere Results **[#1915]**
We have completed our survey of central pit craters in the northern hemisphere of Mars. We present results on the characteristics and distributions of these central pit craters.

DeVries R. J. Barlow N. G.
Central Pit Craters in the Southern Hemisphere of Mars **[#1929]**
We are conducting a survey of the characteristics and distributions of central pit craters in the southern hemisphere of Mars. We present the early results of this study.

Bray V. J. Tornabene L. L. McEwen A. S. Mattson S. S.
Measurement of Small-Scale Pits in the Corinto Crater, Mars **[#1389]**
HiRISE imagery has revealed small-scale pits in fresh martian impact craters. We are collecting measurement of pit dimensions in the Corinto crater, so that the possible relation of pit-concentration and terrain subsidence can be quantified.

Komatsu G. de Pablo M. A. Ormö J. Tornabene L. L.
Small Craters from Oblique Impacts and the Origin of an Unusual Streak in Elysium Planitia, Mars **[#1779]**
We present a HiRISE image revealing details of small craters (<100 m) that are probably secondaries formed by oblique impacts. We also discuss working hypotheses for the formation mechanisms of the light-toned streak associated with one of them.

Wyant M. A. Frey H. V. Davatzes A. K.
Relative Age Dating of Martian Geologic Units Through a Study of Buried Impact Structures Using an Improved Crustal Thickness Model **[#1767]**
The improved crustal thickness model for Mars allows for the identification of buried impact structures at greater resolution. Using this model we can look at individual regions of the planet and discern relationships between the units relative ages.

MARTIAN MINERALOGY: CONSTRAINTS FROM MISSIONS AND LABORATORY INVESTIGATIONS

Bishop J. L. Dyar M. D. Majzlan J. Lane M. D.
Spectral Properties of Copiapites with Variable Cation Compositions and Implications for Characterization of Copiapite on Mars **[#2073]**
The spectral properties of synthetic copiapite samples were analyzed for comparison with martian data. Changes with Fe vs Mg abundances are most notable in IR spectra near 2, 9,11, 18 and 45 μm and in the relative areas of Mössbauer doublets 1 and 2.

Cloutis E. A.
Reflectance Spectra of Low Atomic Weight ("APXS-Blind") Na-bearing Minerals: Nitrates, Nitrites, Borates, Hydroxides, and Peroxides **[#1176]**
The reflectance spectra of a number of low atomic-weight element-bearing phases, including nitrates, nitrites, borates, hydroxides, and peroxides show a diversity of features, largely related to O + H and cation-OH absorptions.

Fairén A. G. Davila A. F. Duport L. G. Amils R. McKay C. P.
Mars: Cold and Wet **[#1155]**
The role of solutes depressing the melting point of water in a frozen martian environment supports the idea that the majority of the water on Mars was forming super-cooled liquid solutions with large masses of ice covering parts of them.

Hahn B. C. McLennan S. M. Tosca N. J. Reeder R. J.
Trace Element Behavior in Martian Evaporite Minerals: Experimental Constraints **[#1194]**
We detail a series of laboratory investigations determining the partitioning coefficients of the trace elements Ni, Zn, and Cr into a suite of precipitating sulfate evaporite minerals observed on the martian surface.

Altheide T. S. Chevrier V. F. Denson J. Nicholson C.
Evaporation of Sulfate and Chloride Brines on the Surface of Mars **[#1011]**
When evaporated under simulated martian conditions, brines composed of sulfates and chlorides demonstrate lower evaporation rates than pure water, due to ion interactions and, depending on concentration and temperature, salt crystallization.

Xu W. Parise J. B.
$(H_3O)Fe(SO_4)_2$, A New Phase Formed by Dehydrating Rhomboclase **[#1816]**
The stability of rhomboclase with respect to temperature and humidity was examined by *in situ* XRD method, and a new phase $(H_3O)Fe(SO_4)_2$ was found, which needs to be considered when analyzing sulfate mineralogy on Mars.

Rice M. S. Bell J. F. III Cloutis E. A. Wang A. Ruff S. W. Craig M. A. Bailey D. T. Johnson J. R. de Souza P. A. Farrand W. H.
Silica-rich Deposits and Hydrated Minerals at Gusev Crater, Mars **[#2134]**
The Si-rich materials discovered by Spirit have distinct Vis-NIR features in their Pancam spectra that may result from adsorbed water or hydrated minerals. We find that spectrally similar materials are widespread throughout the Columbia Hills.

McGlynn I. O. McSween H. Y. Jr. Fedo C. M.
Mineralogical Characterization of Soils in Gusev Crater and Meridiani Planum, Mars **[#2249]**
The mineralogy of soil sediments at Gusev Crater and Meridiani Planum sites are evaluated combining APXS and MB data from the Mars Exploration Rovers. Soils are basaltic with minimal chemical weathering, are globally similar with local variability.

Ehlmann B. L. Mustard J. F. Poulet F.
Modeling Modal Mineralogy of Laboratory Mixtures of Nontronite and Mafic Minerals from Visible Near-Infrared Spectral Data **[#1771]**
Initial results assessing the efficacy of Shkuratov and Hapke radiative transfer models in estimating modal mineralogy from visible near infrared (VNIR) spectral data for various laboratory mixtures of phyllosilicate and light and dark mafic minerals.

MARS ANALOGS: CHEMICAL AND PHYSICAL

Blackburn D. G. Ulrich R. Elwood Madden M. E. Leeman J. R. Chevrier V. F.
Experimental Study of the Kinetics of CO_2 Hydrate Dissociation Under Simulated Martian Conditions **[#1341]**
We performed an experimental study of the kinetics of CO_2 hydrate dissociation under simulated martian conditions, which indicated the hydrates are heat-transfer limited and do not exhibit anomalous self-preservation behavior at 6 mbar.

Gillot J. Roskosz M. Depecker C. Roussel P. Leroux H.
Calcite Formation from Nanoporous Amorphous Silicates in Interaction with Carbon Dioxyde **[#1755]**
In situ infrared spectroscopy and X-ray diffraction reveal that amorphous porous silicate dusts react readily with CO_2 to form calcite at ambiant temperature. Dry carbonation can then account for the formation of carbonates observed around stars.

Gillot J. Roskosz M. Depecker C. Roussel P. Leroux H.
Sol-Gel Synthesis and Crystallization of Magnesium and Calcium Rich Silicate Dust Analogs **[#1763]**
A new sol-gel method optimized to synthesize amorphous and porous silicate dust analogs is proposed. The crystallization of such analogs is metastable and polyphasic. Their high reactivity is probably due to high surface/volume ratio.

ten Kate I. L. Zuray M. S. Mahaffy P. R.
Dust Storm Electrification in a Mars Chamber — First Results **[#2273]**
Analogue studies and numerical simulations suggest that in martian dust devils and dusty convective storms large-scale electric fields are generated. A laboratory setup has been built to investigate their effects on the composition of the atmosphere.

Needham A. W. Smith C. L. Howard K. T. Sephton M. A. Martins Z. Foster N. J.
Franchi I. A. Russell S. S.
Gamma Irradiation Effects in Mars Analogues **[#1971]**
The effects of gamma irradiation on geological samples continue to be investigated in preparation for potential sterilisation of samples returned from the surface of Mars in the coming decades.

Cereti A. Mellon M. T. Sizemore H. G. Phillips R. J.
Measurements of Dielectric Properties of Mars Analog Soils with Variable Temperature and Moisture Content **[#2189]**
We performed impedance spectroscopy of various martian analog soils, with varying temperature and moisture content, to investigate how the complex dielectric permittivity depends on these factors, as this parameter can strongly affect radar signals propagation.

Ukstins Peate I. Cabrol N. A. Grin E. A. French R. Dressing C. Franklin T. Parsons K.
Piatek J. Chong G.
Mechanisms for Planetary Spherules Formation and Alteration: Salar Grande, Chile — An Example of Volcanic/Aqueous Processes Interactions **[#1435]**
Silica nodules and hematite spherules are observed at Salar Grande and Monturaqui, Atacama Desert, Chile. The Planetary Spherules Project investigates formation, deposition and alteration processes as analogs to Gusev Crater and Meridiani, Mars.

Chan M. A. Potter S. L. Bowen B. B.
Overview of Iron Oxide Concretions and Implications for Mars: Current Knowledge and Gaps **[#2187]**
Terrestrial concretion analogs indicate that small Mars "blueberries" likely formed quickly by diffusive mass transfer, under conditions of abundant iron supply in chemically reactive host rock.

Pompilio L. Tampella G. Lisotti A. Rossi A. P. Sgavetti M.
Multi-Resolution Approach to the Spectral Analysis of Martian Outcrops **[#1801]**
Here we present demonstrative results of the multi-resolution approach to the interpretation of the spectral variability of a multispectral survey for a terrestrial area, through multispectral Landsat TM5 data.

Kraft M. D. Alvarado C. M. Sharp T. G. Rampe E. B.
Spectral Indexing of Chemical Weathering in the Mid-Infrared: New Means to Evaluate Weathering on Mars **[#2289]**
Features of mid-infrared spectra from a large suite of weathered basalt can be indexed to distinguish weathered and unweathered surfaces, suggesting that weathering can be studied on Mars without using spectral modeling methods.

Mayer D. P. Arvidson R. E. Wang A. Sobron P. Zheng M. P.
Mapping Minerals at a Potential Mars Analog Site on the Tibetan Plateau **[#1877]**
A new mineral facies map of lacustrine deposits from the cold, arid Qaidam Basin, China shows hydrated sulfates, carbonates, chlorides and phyllosilicates. This area may offer insight into the history of evaporite deposits identified on Mars.

McKeown N. K. Noe Dobrea E. Z. Bishop J. L. Silver E. A.
Coordinated Lab, Field, and Aerial Studies of the Painted Desert, AZ, as a Potential Analog Site for Phyllosilicates at Mawrth Vallis, Mars **[#2509]**
One hypothesis for clay formation at Mawrth Vallis is an altered ash-fall, like bentonites in the Painted Desert, AZ. We compare lab, field, and aerial data to determine if silicate spectral features are accurately captured in aerial datasets.

Sanders N. H. Sailer D. S. Kelley E. M. Clarke R. S. Davis S. J. Eckert-Erdheim A. M. Tsang S. W. R. Benson S. M. Fuerst A. J. Heyer K. M. Lee N. F. Oliver B. L. Sclotterer G. J. Suitt C. B.
Effects of Fine Sediment Mantle on the Thermal Inertia Signature of Underlying Materials **[#1195]**
Results of modeling the effect that overlying fine sediment has on materials underneath suggest that even as little as .5 cm of overlying fine sediment essentially masks the thermal signature of any underlying material.

Zheng M. P. Wang A. Kong F. J. Ma N. N.
Saline Lakes on Qinghai-Tibet Plateau and Salts on Mars **[#1454]**
The Qinghai-Tibet Plateau stands in the east of Asia, with an area of ~2.5 million km^2 and an average elevation of ~4500 m, and its general terrain slopes. It is a unique physicogeographical unit and also the youngest plateau on the Earth.

Irwin R. P. III Fortezzo C. M. Tooth S. E. Howard A. D. Zimbelman J. R. Barnhart C. J. Benthem A. J. Brown C. C. Parsons R. A.
Origin of Theater-headed Tributaries to Escalante and Glen Canyons, Utah **[#1644]**
Theater-headed tributaries to Glen Canyon, Utah, are important analogs to martian valley networks. Our field study suggests a hybrid model involving seepage weathering of Navajo sandstone, sheet fracturing, and transport of debris by flash floods.

Wynne J. J. Titus T. N. Jhabvala M. D. Cushing G. E. Cabrol N. A. Grin E. A.
Distinguishing Caves from Non-Cave Anomalies Using Thermal Infrared: Lessons for the Moon and Mars **[#2451]**
Research has shown one example differentiating caves from non-cave anomalies in the Mojave Desert, CA. This work has important implications for detecting caves on the Moon and Mars.

Grudzinski B. P. Luo W. Pederson D.
Estimating Hydraulic Conductivity from Drainage Patterns Derived from DEM – A Case Study in the Oregon Cascades **[#2112]**
This study introduces a new method of estimating hydraulic conductivity from drainage dissection pattern derived from digital elevation model (DEM). Tests in Cascades region, Oregon show promising results. It has the potential to be applied to Mars.

Williams R. M. E. Irwin R. P. III
Morphology of Lava-Capped Inverted Valleys Near St. George, Utah: Analogs for Martian Sinuous Ridges **[#2413]**
We report on the morphological attributes of multiple lava-capped mesas near St. George, Utah that preserve portions of the ancestral Virgin River drainage in inverted relief.

Pain C . F. Clarke J. D. A.
Relief Inversion: Australian Analogs of a Common Feature of Martian Landscape Evolution **[#1100]**
The Australian continent is particularly favourable for the formation and preservation of inverted relief and therefore provides a wide range of potential analogs for similar features on Mars.

Kraal E. R.
Hyperarid Fans in the Atacama Desert are an Interesting Analog to Martian Fans **[#1104]**
Alluvial fans in the Atacama Desert, Chile are valuable analogs for understanding fan formation in hyperarid conditions that may be similar to those experienced on Mars.

Byram S. K. Ukstins Peate I. Reagan M. K. Cabrol N. A. Grin E. A.
U-Th Geochronological Constraints on Paleolake Levels and Climate Change Recorded in Carbonate Sedimentation at Laguna Lejía, Northern Chile **[#2137]**
The unique climate of the Atacama Desert makes it a useful analogue to the environment on early Mars. Paleoterrace deposits at Laguna Lejía record rapid climate change and give insight into the organisms that survive in such extreme environments.

Weidinger T. Istenes Z. Hargitai H. Tepliczky I. Bérczi Sz.
Micrometeorological Station at the Mars Analog Field Work, Utah, April, 2008 **[#1282]**
The 71st crew of MDRS, Utah, meteorological station dataset of near surface layers of temperate belt and desert environments, were compared as terrestrial to martian conditions showing differences between the two planetary environments.

Merrison J. P. Holstein-Rathlou C. Gunnlaugsson H. P. Nornberg P.
A Forthcoming European Mars Simulation Wind Tunnel Facility **[#1544]**
A unique European Mars Simulator Facility is close to completion at Aarhus University in Denmark. It is intended for scientific study and instrument testing and will be accessible to international collaborators and space agencies.

MARS ANALOGS: SULFATES AND SULFIDES

Wang A. Freeman J. J.
Pathways and Rates of Mg-Sulfate Dehydration and Rehydration on Mars **[#2029]**
New understandings are developed based on a study of the stability field and phase transition pathways of Mg-sulfates in 50°C =T = –10°C and 7% <RH< 100%. Especially, the rates of reactions were extracted.

Liu Y. Wang A. Freemen J. J.
Raman, MIR, and NIR Spectroscopic Study of Calcium Sulfates: Gypsum, Bassanite, and Anhydrite **[#2128]**
The spectral peak assignments for fundamental vibration modes in Raman and MIR, for overtone and combination modes in NIR of Ca-sulfates, will help the interpretation of the mission data from current and future exploration to Mars and Venus.

Freeman J. J. Wang A.
Hydrated Magnesium Sulfates Below 0°C — Stable Phases and Polymorphs **[#2301]**
We found a low-T polymorph of epsomite at –10°C and mid-RH during an experimental study of stability fields and phase boundaries of hydrated Mg-sulfates. Meridianiite was found stable at –10°C and RH > 90%.

Grindrod P. M. Heap M. J. Meredith P. G. Sammonds P. M.
Strength and Elastic Moduli of Magnesium Sulfate Hydrates Under Martian Conditions **[#1515]**
We present experimentally-derived values of unconfined compressive strength and elastic moduli of mono- and poly-hydrated magnesium sulfates, which control the mechanical behaviour of similar equatorial deposits on Mars.

Kong W. G. Wang A. Freemen J. J. Sobron P. S.
A Comprehensive Spectroscopic Study (Raman, MIR, Vis-NIR, LIBS, XRD) of Synthetic Fe^{2+}, Fe^{3+}, Mg^{2+}, Al^{3+} Copiapites **[#1659]**
Fe^{2+}, Fe^{3+}, Mg^{2+}, and Al^{3+} copiapites were synthesized and investigated by Vis-NIR, Raman, and MIR. These studies will help *in situ* mineral ID, and to link the remote sensing data with the observed ferric sulfates during ground exploration on Mars.

Hyde B. C. King P. L.
Quantification of Structural H_2O and Total H_2O Contents in Iron Sulfate Minerals Using Diffuse Reflectance Infrared Fourier Transform Spectroscopy **[#1895]**
H-bearing Fe-sulfates are found on Mars. Better characterization includes H_2O/OH- quantification. Kubelka-Munk theory and the NOPL method were applied to biconical diffuse reflectance data. NOPL produces better fits. Both methods are mineral dependent.

Chipera S. J. Sarrazin P. Alcantar-Lopez L. Vaniman D. T. Bish D. L. Blake D. Chiari G.
Real-Time XRD/XRF at a Mars-Analog Sulfate Site in Leadville, Colorado, Using a CheMin-Heritage Instrument **[#1328]**
Real-time XRD/XRF of an acid-sulfate deposit demonstrates the value of *in situ* analysis in the study of ephemeral minerals and hydrates susceptible to rapid alteration and significantly aids in the identification of similar chemical species.

Sansano A. Sobron P. Lafuente B. Medina J. Rull F.
Raman Analysis of Sulfate Sequence of Precipitation from Iron-rich Waters of Rio Tinto River **[#2076]**
Rio Tinto area is considered a referent as an extremophilic scenery of iron rich. Raman spectroscopy is a powerful technique that allows studying these. This work shows the aplication of this technique on natural and simulated evaporitic samples.

Sobron P. Wang A.
Raman and LIBS: A Definitive Combination for the Characterization of Natural Samples from the Rio Tinto Mars Analog **[#2400]**
A combined Raman and LIBS study on natural sulfates from Rio Tinto demonstrated a fully characterization of Gypsum, Al/Mg-copiapite and Na/NH4-jarosite. It was proven to be a powerful tool for min/geochemical investigations at planetary surfaces.

Gómez-Ortiz D. Fernández-Remolar D. C. Prieto-Ballesteros O. Gómez F. Amils R.
Hydrogeological Study of the Rio Tinto Mars Analog: Implications for Mars Underground Water Fluxes **[#1550]**
A hydrogeological survey, including different tests of tracer injection, has been carried out in order to unravel the groundwater flow scheme of the Rio Tinto martian analog.

Calvin W. M. Shoffner J. D.
Remote Sensing Image Analysis at Leviathan Mine, Ca: A Sedimentary Sulfate Mars Analog Site **[#1210]**
An open pit mine site provides exposures of a wide variety of sulfate minerals. We have mapped the site using multi-spectral satellite data and high spatial resolution hyperspectral data. The results have implications for remote mapping of sulfates on Mars.

Cavalazzi B. Barbieri R. Ori G. G. Westall F. Cady S. L. Gennaro S. Lui A. Canteri R. Bersani M. Lazzeri P. Pepponi G.
Unusual Fe-rich Framboids from Devonian Carbonate Mounds (Sahara Desert, Morocco) Investigated by HR-SEM and ToF-SIMS: Fossil Analogues of OAM-SRB Consortia? **[#1113]**
Microaggregates from fossil mounds are likely related to hydrothermal and methane venting. The aggregates are considered a fossil analogue of living MOA and SRB. The detection of carbonate rocks on Mars make this finding remarkable for astrobiology.

Dyar M. D. Holden J. F. Bishop J. L. Lane M. D.
Spectroscopic Characterization of Hydrothermal Sulfide Chimneys at the Juan de Fuca Ridge **[#2221]**
We present here results of the study of a small sample suite from the Juan de Fuca Ridge using Mössbauer, mid-IR thermal emission, and visible, near-IR, and mid-IR diffuse reflectance spectroscopy.

MISSIONS: APPROACHES, ARCHITECTURES, ANALOGS, AND ACTUALITIES

Clark K. Stankov A. Pappalardo R. T. Greeley R. Blanc M. Lebreton J.-P. Van Houten T.
The Europa Jupiter System Mission **[#2338]**
The two sister spacecraft of the EJSM—the Jupiter Europa and Jupiter Ganymede Orbiters—perform a choreographed dance exploring the Jupiter system and studying the processes that led to the diversity and interactions of its associated components.

Coustenis A. Lunine J. Matson D. Hansen C. Reh K. Beauchamp P. Lebreton J.-P. Erd C.
The Joint NASA-ESA Titan Saturn System Mission (TSSM) Study **[#1060]**
The NASA-ESA Titan Saturn System Mission designed for an in-depth exploration of Titan and Enceladus. The mission comprises both remote (orbiter dedicated to Titan) and *in situ* (montgolfiere, lander) elements. Launch would be around 2020.

Green J. R. Dudzinski L. A. Sutliff T. J. Spilker T. R. Arakelian T.
Small Radioisotope Power Systems for Planetary Science Mission Applications **[#2484]**
NASA's RPS Program anticipates development of a small RPS for mission applications. We will present the current state of the art and invite the science community to actively participate in defining the requirements for this new capability.

Chicarro A. F.
Mars Express — Science Summary After Five Years in Orbit **[#1392]**
ESA's Mars Express has been orbiting Mars for over five years, providing unprecedented results on the interior, subsurface, surface, atmosphere and space environment of the Red Planet, allowing Europe to chart a future Mars exploration program.

McEwen A. Keszthelyi L. Spencer J. Thomas N. Johnson T. Christensen P. Wurz P. Glassmeier K.-H. Shinohara C. Girard T. Heinsohn G. Furfaro R. Gardner T. Cheeseman D. Beatty R. Ludwinski J. Kowalkowski T. Yen C. Elliot T. Turtle E. Strohbehn K. Janesick J. Falco C. Evans R.
Io Volcano Observer (IVO) **[#1876]**
IVO is a concept mission for Discovery, and would make multiple fast polar flybys of Io and acquire remote sensing an *in situ* measurements to address key questions about volcanic processes, tidal heating, and affects on the Jupiter environment.

Sollitt L. S. Kroening K. Malmstrom R. Segura T. Spittler C.
Mission Concepts to 4015 Wilson-Harrington **[#2391]**
We present a number of different architectures for mission concepts to 4015 Wilson-Harrington, a body which exhibits features of both comets and asteroids. We examine orbiter/lander missions as well as sample return missions, in different size classes.

Bellerose J. Yano H.
Requirements and Constraints for Exploration of Binary Asteroid Systems: From Didymos to Hektor **[#2443]**
Many questions remain regarding close orbit operations at a binary. We present important requirements and constraints including recent work on out-of-plane orbits, influence of the SRP, and contact binaries.

Blome H.-J. Wilson T. L.
Hyperbolic Orbits and the Planetary Flyby Anomaly **[#1704]**
The virial theorem in astrophysics is used to show that energy is not being conserved during the gravity assist procedure used in planetary flybys. These involve hyperbolic trajectories. So the so-called flyby anomaly exists at a very fundamental level.

Jenniskens P. Dissly R. Boyd I. D. ReVelle D. O. Nuth J. A. Worden S. P.
ASIMA — Asteroid Impact Analyzer: A Proposed Close-to-Home Planetary Mission to Probe the Diversity of Comets and Asteroids **[#2305]**
The proposed Asteroid Impact Analyzer (ASIMA) is a Partner Mission of Opportunity that will measure how the bulk carbon-to-metal ratio varies among comets and asteroids.

Foing B. H. Batenburg P. Drijkoningen G. Slob E. Poulakis P. Visentin G. Page J. Noroozi A. Gill E. Guglielmi M. Freire M. Walker R. Sabbatini M. Pletser V. Monaghan E. Boche-Sauvan L. Ernst R. Oosthoek J. Peters S. Borst A. Mahapatra P. Wills D. Thiel C. Wendt L. Gross C. Petrova D. Lebreton J. P. Zegers T. Stoker C. Zhavaleta J. Sarrazin P. Blake C. McKay C. Ehrenfreund P. Chicarro A. Koschny D. Vago J. Svedhem H. Davies G. ExoGeoLab Team EuroGeoMars Team
ExoGeoLab Lander/Rover Instruments and EuroGeoMars MDRS Campaign **[#2567]**
We describe ExoGeoLab a planetary surface instruments research incubator, and the EuroGeoMars campaign at the Mars Desert Research station aimed at validating a procedure for martian surface *in situ* and return science.

Lee P. Gernhardt M. Abercromby A. Braham S. Chase T. Comtois J.-M. Deans M. Effenhauser R. Fong T. Frankel C. Glass B. Hodgson E. Hoffman S. J. Jones J. A. Nelson J. Schutt J. W. Vasquez M.
Moon/Mars Science and Exploration in Pressurized Rovers: Early Lessons from Analog Studies at the Haughton-Mars Project Site, Devon Island, High Arctic **[#2498]**
Pressurized rovers will be key science "instruments" in the future humanexploration of the Moon and Mars. Lessons from long-range vehicular field traverses conducted at the Haughton-Mars Project site, Devon Island, HighArctic, are presented.

Ori G. G. Flamini E. Dell'Arciprete I. Taj-Eddine K.
A Facility of the Agenzia Spaziale Italiana to Test Operations, Instruments and Landing Systems for Mars Exploration: The PLANLAB Project of the Ibn Battuta Centre at Marrakech (Morocco) **[#1587]**
The Agenzia Spaziale Italiana in collaboration with the IRSPS has started a program (PLANLAB) to prepare and execute tests of rovers, landing systems, instruments and operations related to the exploration of Mars.

Garry W. B. Hörz F. Lofgren G. E. Kring D. A. Chapman M. G. Eppler D. B. Rice J. W. Jr. Lee P. Nelson J. Gernhardt M. L. Walheim R. J.
Science Operations for the 2008 NASA Lunar Analog Field Test at Black Point Lava Flow, Arizona **[#1649]**
Surface science operations on the Moon will require merging lessons from Apollo with new operation concepts that take advantage of the Constellation Lunar Architecture. We will present science operations for two prototype lunar rovers.

Cottingham C. M. Roark S. E. Deininger W. D. Dissly R. W. Epstein K. W. Waller D. M. Scheeres D. J.
Small Surface Probes for Enhanced Asteroid and Comet Rendezvous Missions **[#2310]**
This poster will discusses system concepts, architectures, and technology development work to mature critical components for low-cost surface probes for small solar system bodies.

Lawrence D. J. Elphic R. C. Weinberg J. D. Delory G. T. Dissly R. Evanyo J. Crider D. H. Lucey P. G. Fong T. Vondrak R. Zacny K. Yachbes I.
Exomoon — A Discovery and Scout Mission Capabilities Expansion Concept **[#1451]**
This submission describes a Discovery class landed mission concept for the *in situ* investigation of volatiles in the lunar polar cold traps. This mission is enabled by the use of the Advanced Stirling Radioisotope Generators (ASRG), currently in development by NASA.

Gilyén A. Szvoboda P.
Development of the Hungarosphere: The Husar-11 Rover Within a Transparent Spherical Space Probe Model with Special Planetary Surface Activities **[#1170]**
We built a spherical Hungaroszféra (Husar-11) rover: with transparent plexy body, camera can see bottom, it moves by inner driving, no spur outsteming from the sphere, can move on fluids, all instruments are defended from dust pollution.

Pasztor A. Simon T. Nagy Sz. Bérczi Sz.
Husar-8 Rover Swarm Collective Activity Around Humveyor-8: Planetary Robotics at the Kecskemét College, GAMF Faculty, Hungary **[#1491]**
By constructing the HUSAR-8 model the GAMF Faculty at Kecskemét College began student robotics program with swarm strategy for navigation on the field trip in order to develop teaching programming and trigger student personal activity.

Perl S. M. DeLaurentis D. A. Caldwell B. S. Crossley W. A.
Adapting System-of-Systems Engineering for the Advancement of the Mars Exploration Program **[#1911]**
To introduce the System-of-Systems (SoS) methodology for modeling the data network of the Mars Science Laboratory (MSL) mission. The goal of this protocol is to obtain the best science data return with a finite and varying amount of resources.

Clark P. E. Millar P. S. Beaman B. Choi M. Cooper L. Feng S. King R. Leshin L. Lewis R. Yeh P. S. Young E. Lorenz J.
Science Packages and Tools Designed for the Lunar Surface **[#1126]**
Lunar surface science packages may need to operate without radioisotope-based power systems available for Apollo. We demonstrate here that alternative state-of-the-art design and components can meet the power and mass constraints of earlier packages.

Griffes J. L. Grotzinger J. Grant J. Vasavada A. R. Golombek M. McEwen A.
Analysis of Four Potential Mars Science Laboratory Landing Sites Using HiRISE **[#1800]**
An overview of the four landing sites remaining under consideration for the 2011 Mars Science Laboratory Mission: Holden Crater, Gale Crater, Eberswalde Crater, and Mawrth Vallis.

Golombek M. Grant J. Vasavada A. R. Grotzinger J. Watkins M. Kipp D. Noe Dobrea E. Griffes J. Parker T.
Selection of Four Landing Sites for the Mars Science Laboratory **[#1404]**
This abstract describes the four landing sites under consideration and the selection process for the Mars Science Laboratory (MSL) after discussion of seven downselected sites at the third Landing Site Workshop and a subsequent project meeting.

Golombek M. P. Haldemann A. F. C. Simpson R. A. Fergason R. L. Putzig N. E. Huertas A. Arvidson R. E. Heet T. Bell J. F. III Mellon M. T. McEwen A. S.
Relationships Between Remote Sensing Data and Surface Properties of Mars Landing Sites **[#1409]**
The surface characteristics and material properties found at the landing sites are used as "ground truth" for interpreting orbital and Earth-based remote sensing data of Mars.

NOT JUST SKIN DEEP: ELECTRON MICROSCOPY, HEAT FLOW, RADAR, AND SEISMOLOGY INSTRUMENTS

Thaisen K. G. Taylor L. A. Gaskin J. A. Jerman G. Ramsey B. D.
An ESEM/SEM Study of Lunar Soil and the Potential for a Miniaturized Version on the Moon **[#1697]**
A PIDDP funded program involving the miniaturization of an Environmental Scanning Electron Microscope with Energy Dispersive Spectroscopy capability for potential use on rovers.

Gaskin J. G. Jerman G. A. Ramsey B. D. Ferguson C. K. Abbott T. O. O'Brien S. Joy D. C. Thaisen K. G. Taylor L. A. Sampson A. R. Rhodes E. A. Darlington E. H. Bussey B. J. Harvey R. P. Spudis P. D.
Miniature Scanning Electron Microscope for In-Situ Planetary Studies: Electron Gun Development **[#2318]**
We are developing a miniaturized scanning electron microscope that will permit *in situ* morphological and chemical characterization of lunar soil. Work presented here concerns the development and testing of the electron gun component of this system.

Stojic A. Brenker F. E.
Argon Ion Slicing (ArIS) of Mineral and Rock Samples: A Novel Tool to Prepare Large Electron Transparent Thin Films for TEM Use **[#1807]**
A new approach to TEM sample preparation is presented using Argon Ion Slicing a novel technique which provides larger electron transparent thin films than had been possible so far.

Smrekar S. E. Mungas G. Peters G. Hudson T. L. Morgan P.
Lunar Heat Flow Simulation and Testing Chamber **[#2055]**
Heat flow is a key indicator of planetary thermal and chemical evolution. We have constructed a vacuum chamber to provide a testbed for evaluating heat flow instrumentation and measurement issues and calibration techniques prior to flight.

Grott M. Spohn T. Richter L. Wieczorek M. A. Knollenberg J. Smrekar S. E. Kargl G. Ambrosi R. M. HP^3 Instrument Team
HP^3 — A Heat Flow Probe Proposed for the International Lunar Network **[#1107]**
HP^3, the heat flow and physical properties package, is proposed to be flown on the International Lunar Network mission. It will measure the thermal conductivity and thermal gradient to a depth of at least 3 m, allowing for a direct determination of the planetary heat flow.

Wawrzaszek R. Seweryn K. Grygorczuk J. Banaszkiewicz M. Gurgurewicz J. Neal C. R. Huang S. Kömle N.
The Heat-Flow Probe Hardware Component (HPHC) of the LGIP Package **[#1511]**
This work is focused on the integration of the Heat Flow Probe Hardware Component – instrument in the L-GIP Package, designed for direct measurements of the thermal energy flux from the interior of the Moon using mole device developed in SRC PAS.

Nagihara S. Zacny K. Taylor P. T. Milam M. B. Mumm E. Maksymuk M. Fink P. Hernandez W.
Heat Flow Probe Deployment Options for the International Lunar Network Missions **[#1165]**
The present work describes instrument design options for a lunar heat flow probe that can meet the logistical constraints and the science objectives of the International Lunar Network lander missions planned in the next decade.

Ciarletti V. Corbel C. Cais F. Plettemeier D. Hamran S. E. Øyan M. WISDOM Team
Performances of the WISDOM GPR Designed for the Shallow Sounding of Mars **[#2367]**
WISDOM is the UHF GPR selected to be onboard the rover of the ExoMars mission. It is designed to characterize the shallow subsurface structure of Mars prior to drilling operation. The first measurements performed on Earth show very promising results.

Zacny K. Mumm E. Fink P. Hernandez W. Paulsen G. Maksymuk M.
Telescopic/Pneumatic Heat Flow Deployment for the International Lunar Network Missions **[#1070]**
We describe a method of deploying heat flow probe for the International Lunar Network that consists of a telescopic probe with deployable isolated thermal anchors. The pneumatic hammer and gas flushing uses left over helium from a propulsion system.

Asphaug E. Safaeinili A. Belton M. J. S. Scheeres D. J. Chesley S. Yeomans D.
Deep Interior: High-Resolution Volumetric Radar Imaging of a Comet Nucleus **[#2109]**
Deep Interior uses a SHARAD-type radar to acquire 10 Tb of global echoes from a comet nucleus, a data set that will resolve the whole-body geology to better than 10 m in 3D.

Neal C. R. Weinberg J. D. Lognonné P. Hood L. Mimoun D. Wawrzaszek R.
Banaszkiewicz M. LGIP Team
Lunar Geophysical Instrument Package as a Payload for the International Lunar Network **[#1447]**
This submission describes the characteristics of the Lunar Geophysical Instrument Package (LGIP), its suitability as a payload for the ILN and the distinct advantages of using a common integrated suite of instruments.

Heggy E. Fong T. Kring D. Deans M. Anglade A. Mahiouz K. Bualat M. Lee P.
Horz F. Bluethmann W.
Potential of Probing the Lunar Regolith Using Rover-mounted Ground Penetrating Radar: Moses Lake Dune Field Analog Study **[#2183]**
We present Ground Penetrating Radar results of the Moses-Lake survey performed in June 2008 using two rover mounted probing instruments. Our results explore the utility of GPR to explore subsurface volatiles and structural elements in Lunar analog terrains.

Grimm R. E. Delory G. T.
Magnetotelluric Sounding of Terrestrial Planet and Satellite Interiors **[#2382]**
Simultaneous measurement of ambient electric and magnetic fields enables subsurface soundings from a single platform.

Schibler P. Lognonne P. Mimoun D. Zweifel P. Roll R. Kreuse I. Pike W. T. Calcutt S. Debus A.
Planetary Protection Policy Applied to HPL-ExoMars Seismometer **[#1312]**
The scope of this presentation is to describe how the instrument project will be conducted so as to meet the planetary protection requirements specified for ExoMars mission.

Batenburg P. A. W. Foing B. H. Drijkonigen G. G. Gill E. K. A. Poulakis P. Visentin G. Page J.
Pletser V. Peters S. Borst A. Mahapatra P. ExoGeoLab Team EuroGeoMars Team
Reflection Seismology Systems for Planetary Geology: First Tests at ESTEC ExoGeoLab and MDRS, Utah **[#2536]**
The authors investigated the use of reflective seismology for Planetary geology within ESA's ExoGeoLab pilot project. During the EuroGeoMars expedition tests were performed to test the influence of surface coupling and composition on data quality.

Oosthoek J. H. P. Kleuskens M. H. P.
3D Interpretation of SHARAD Radargram Data **[#2473]**
SHARAD radar data is interpreted in 3D using reservoiring engineering software. Here, the radar data is treated as seismic data. This enables us to distinguish between layers, which could help to better understand the formation process of the icecap.

Salamuniccar G. Loncaric S.
Morphometry, Votes-Analysis and Calibration Improvements of Crater Detection Algorithms Based on Edge Detectors and Radon/Hough Transform **[#1084]**
Six previously implemented Crater Detection Algorithms (CDAs) were improved using morphometry measurements (some new and some improved), votes-analysis and calibration. The results were analyzed using the Framework for Evaluation of CDAs (FECDA).

Robbins S. J. Hynek B. M.
Towards a New Catalog of Lobed Martian Craters Compared with a New Global Crater Database, Complete to 1.5 km **[#2460]**
Presenting preliminary results of a new crater database, focusing on lobed crater characteristics. Database is complete to at least 1.5 km-diameter craters and contains more characteristics of each crater than previous catalogs.

Nava R. A. Skinner J. A. Jr. Hare T. M.
Using Distributional Characteristics of Superposed Large-Scale Crater Clusters as Temporal Indicators of Geologic Processes **[#2530]**
We present a GIS-based tool that utilizes standard geoprocessing scripts to use the occurrence and orientation of large crater clusters as stratigraphic makers.

Stepinski T. F. Urbach E. R.
The First Automatic Survey of Impact Craters on Mars: Global Maps of Depth/Diameter Ratio **[#1117]**
The catalog of 75,919 craters on Mars is compiled by a computer algorithm. Using crater depths listed by this catalog, global maps of depth/diameter ratio are created. Such maps indicate existence of cryosphere at depths that varies with latitude.

Stepinski T. F. Bagaria C.
Automatic Mapping of Martian Physiography: Application to Tharsis Region **[#1118]**
Physiographic map of Tharsis region on Mars is created automatically by a computer algorithm. The map summarizes all relevant topographic features and presents them in a handy visual format that is also well suited for further quantitative analysis.

Salamuniccar G. Loncaric S.
Automated Depth/Diameter and Topographic-Cross-Profile Measurements Based on GT-57633 Catalogue of Martian Impact Craters and MOLA Data **[#1085]**
The methods for the automated depth/diameter and topographic-cross-profile measurements were applied to the newly available GT-57633 catalogue and MOLA data. The result is improved insight into the global geometric properties of martian craters.

Anderson S. W. Finnegan D.
Relationships Between Block Size Distributions and Topographic and Topographic Roughness: An Experimental Approach Using LIDAR Scanning and Variogram Analysis **[#2190]**
Block size distributions on rocky surfaces contain information regarding the lithologic material properties and the geologic processes creating the deposit. Here, we discuss experiments designed to show relationships between topographic roughness and block size.

Roark J. H.
Enhancements to Gridview: Software for Topography Data Analysis **[#1711]**
Gridview is an IDL software application designed to help users analyze, measure, and visualize gridded data. It has been used to study visible and buried basins on Mars, investigate the dichotomy boundary, and measure slope as well as volcano and crater geometry.

Clark C. S. Clark P. E.
Using Boundary-based Mapping Projections for Morphological Classification of Small Bodies **[#1133]**
We present a systematic approach to interpreting and classifying asteroids based on shape and surface morphology using Constant Scale Natural Boundary (CSNB) map projection applied to Deimos, Phobos, Eros, and Ida.

Kirk R. L. Howington-Kraus E. Rosiek M. R.
Build Your Own Topographic Model: A Photogrammetry Guest Facility for Planetary Researchers **[#1414]**
The USGS and NASA invite you to Flagstaff, where we will train you and help you collect high-resolution topographic data for your research, from spot heights to DTMs, using a state of the art stereo workstation and a wide variety of stereo images.

Walter S. H. G. Michael G. Neukum G.
Publishing Planetary Remote Sensing Data as OGC Web Services by Use of Open Source Software **[#1609]**
We will demonstrate techniques to deliver HRSC and SRC image data as well as OMEGA footprint data based on standards defined by the Open Geospatial Consortium (OGC) using open source software.

Parente M. Clark J. T. Bishop J. L. Brown A. J.
Simulating CRISM Images: A Tool for Researchers in Testing and Confirming Geologic Analyses of CRISM Images on Mars **[#2487]**
We present a system for simulating CRISM images as a tool to analyze the feasibility of mineral detections on the martian surface in different scenarios involving variable compositional,atmospheric and instrumental conditions.

Patterson G. W. Barnouin-Jha O. S. Murchie S. L. Seelos F. Ehlmann B. L. Mustard J. F.
Developing Tools to Highlight the Presence of Carbonates in CRISM Images of Mars **[#2361]**
CRISM hyperspectral images of Mars have recently been used to identify magnesium carbonate deposits. To better assess their spatial distribution and geological context, we are exploring improved techniques to identify these carbonates.

Dziková L. Dzik P. Fürstová J. Skála R.
Color of Moldavites Measured by Colorimetry **[#1720]**
Transmittance spectra of moldavites were measured to evaluate their color quantitatively. These data were converted to L*a*b* coordinates of the CIE color space. Cluster analysis was applied. The results were compared to empirical color assessment.

D'Amore M. Helbert J. Maturilli A.
Berlin Emissivity Database (BED) Archive **[#1024]**
The Berlin Emissivity Database ranges from 3 to 50 μm. BED comprises several grain-sized mineral, up to high temperature, and has a modular structure, to collect in the future Raman measurement, samples pictures, thin section images and so on.

Hare T. M. Skinner J. A. Jr. Tanaka K. L. Fortezzo C. M. Bleamaster L. F. III Sucharski R. M.
GIS-based Planetary Geologic Maps: Recommendations for Improved Preparation, Review, and Publication **[#2538]**
The PGandG funding opportunity this year will require geologic maps submitted after Jan. 2011 to be in a GIS-compatible format. To help alleviate this transition for the mapping community we have begun to implement several initiatives addressed here.

Hancher M. D. Beyer R. Broxton M. Gorelick N. Kolb E. Weiss-Malik M.
Visualizing Mars Data and Imagery with Google Earth **[#2308]**
The latest Google Earth and KML features aid in Mars data visualization, including full-resolution imagery, terrain maps, and coverage maps allowing scientists to browse satellite imagery from many instruments within a single easy-to-use interface.

Akins S. W. Gaddis L. Becker K. Barrett J. Bailen M. Hare T. Soderblom L. Raub R.
Status of the PDS Unified Planetary Coordinates Database and the Planetary Image Locator Tool (PILOT) **[#2002]**
The current status of the PDS Unified Planetary Coordinates (UPC) database and the Planetary Image Locator Tool (PILOT) web interface to search the UPC.

Wang J. Bennett K. J. Scholes D. Arvidson R. Ward J. G. Slavney S. Guinness E. A. Stein T. C. Heil-Chapdelaine V.
Planetary Data Access Through the Orbital Data Explorer from the PDS Geosciences Node **[#1193]**
An overview of Orbital Data Explorer (ODE) developed at NASA's Planetary Data System's Geosciences Node. ODE provides web-based functions to search, retrieve, and download data from multiple missions and instruments in the rapidly expanding planetary data archives.

Slavney S. Arvidson R. E. Guinness E. A. Stein T. C.
PDS Geosciences Node Data and Services **[#1303]**
The PDS Geosciences Node archives science data related to the study of the terrestrial planets. The node provides services in the form of a web site where data may be browsed and downloaded, and specialized tools for orbital and landed data sets.

Hughes J. S. Crichton D. J. Mattmann C. A.
A Framework to Manage Information Models — The Planetary Data System Case Study **[#1139]**
The Planetary Data System (PDS) information model has been captured in an ontology based tool framework. A generated specification document now provides a basis for improving the PDS standards for use both within PDS and internationally.

Henneken E. A. Accomazzi A. Grant C. S. Kurtz M. J. Thompson D. Bohlen E. Murray S. S.
The SAO/NASA Astrophysics Data System: A Gateway to the Planetary Sciences Literature **[#1873]**
The SAO/NASA Astrophysics Data System (ADS) provides various free services for finding, accessing, and managing bibliographic data, including a basic search form, the myADS notification service, and private libraries, plus access to scanned published articles.

MARS: DUNES, DUST, AND WIND
Friday, 8:30 a.m. Waterway Ballroom 1

Chairs: **Lori Fenton and Steve Metzger**

8:30 a.m. Chojnacki M. * Moersch J. E.
Valles Marineris Dune Fields: Thermophysical Properties, Morphology, and Provenance **[#2486]**
We examined 25 dune fields in Valles Marineris to identify significant trends in thermophysical properties, morphology and origin. Many dunes have high thermal inertia values (>350) implying fossilized dune surfaces or large grain sizes (1–1.7 mm).

8:45 a.m. Berman D. C. * Balme M. R. Bourke M. C. Rafkin S. Zimbelman J. R.
Transverse Aeolian Ridges on Mars: Distribution, Orientations, and Ages **[#1973]**
We have conducted a survey of all high-resolution MOC images in a pole-to-pole swath between 0° and 45°E longitude to identify and classify Transverse Aeolian Ridges (TARs) on Mars and determine their distribution, orientations and age.

9:00 a.m. Silvestro S. * Fenton L. K. Michaels T. I. Ori G. G.
Complex Dark Dune Fields in Noachis Terra, Mars. Relationship Between Morphologies and Wind Regimes **[#1862]**
We analyzed three dark dune fields in Noachis Terra. The comparison between the observed morphologies and the atmospheric models suggest that these features could be in equilibrium with present day atmospheric conditions.

9:15 a.m. Bourke M. C. * Philippoff A. Bridges N.
Studies of Dune Change on Mars Combining MOC and HiRISE Images **[#1748]**
Another example is shown where a dome dune in the North Polar region of Mars is completely eroded. This confirms that there is active sand transport on Mars. Domes dunes <30 m wide are the most likely to show change over short time periods.

9:30 a.m. Fenton L. K. *
Small Scale Features Reveal Aeolian Inactivity Poleward of 60°S in HiRISE Images of Southern Hemisphere Dune Fields on Mars **[#1425]**
HiRISE images reveal several types of small scale (2–30 m) features on southern hemisphere high-latitude dunes. The occurrence of these features indicates varying levels of aeolian activity and their spatial distribution corresponds with ground ice.

9:45 a.m. Ewing R. C. * Bourke M. Kocurek G.
Transport Conditions and Stages of Dune Development in the Olympia Undae Dune Field **[#2426]**
Dune patterns analyzed in Olympia Undae indicate two generations of dune construction and a change in wind regime. Flow fields inferred from wind ripple orientations indicate transport from the ENE, which aligns with the youngest dunes.

10:00 a.m. Bridges N. T. * Keszthelyi L. P. Thomson B. J. Wray J. J. Banks M. E. Chuang F. C. Herkenhoff K. E. Fishbaugh K. E. McEwen A. S. Michaels T. I.
Characteristics and Possible Genetic Link Between Dust Aggregate Bedforms and Yardangs as Seen by the HiRISE Camera **[#2099]**
We propose that bedforms in Tharsis are dust aggregates. These may eventually lithify into abradable yardangs and indurated surfaces, a "duststone" that appears to be a common martian rock with no known terrestrial analog.

10:15 a.m. Geissler P. E. * Arvidson R. Bell J. Bridges N. Desouza P. Golombek M. Greenberger R. Greeley R. Herkenhoff K. Lahtela H. Johnson J. R. Landis G. Li R. Moersch J. Richter L. Sims M. Soderblom J. Sullivan R. Thompson B. Verba C. Waller D. Wang A. HiRISE Team MER Team
Constraints on Aeolian Degradation Rates on Mars from Erasure of Rover Tracks **[#2257]**
Surface and orbital observations of the erasure of the wheel tracks made by the MER rovers Spirit and Opportunity provide insights into the mechanisms and timescales of aeolian degradation on Mars.

10:30 a.m. Metzger S. * Balme M. Towner M. Bos B. Pathare A.
Direct In-Situ Measurement of Natural Dust Devil Sediment Loading and Flux **[#1220]**
In situ sampling of dust devils reveals total suspended particle (TSP; 296 mgm^{-3}) and fine dust loadings (PM10; 15.1 to 43.8 mgm^{-3}), 12.3 ms^{-1} rotation and 2.7 ms^{-1} uplift, mean TSP flux of 1689 $mgm^{-3}s^{-1}$ and dust flux of ~ 1.0 to ~50.0 $mgm^{-3}s^{-1}$.

10:45 a.m. Hall N. W. * Lemmon M. T.
Mass Ejected from Martian Dust Devils as a Function of Height and Dust Devil Morphology **[#2409]**
An investigation of morphology, density, vertical velocities, and mass flux characteristics of martian dust devils observed by MER. The conservation of mass is utilized to estimate quantity and height of dust ejected into the martian atmosphere by dust devils.

11:00 a.m. Reiss D. * Lüsebrink D. Hiesinger H. Kelling T. Wurm G. Teiser J.
High Altitude Dust Devils on Arsia Mons, Mars: Testing the Greenhouse and Thermophoresis Hypothesis of Dust Lifting **[#1961]**
We investigated high altitude dust devils on Arsia Mons. Their occurrence in these low pressure (~1 mbar) environments might be possible to a Greenhouse and Thermophoresis (GT) effect which lowers the threshold for dust entrainment by wind stress.

11:15 a.m. Verba C. A. * Geissler P. E. HiRISE Team
Comparative Analysis of Martian Dust Devil Track Morphologies in Gusev and Russell Craters **[#1979]**
Seasonal variations of dust devil activity in Russell and Gusev craters are influenced by topography, sediment supply, and altitude, as well as latitudinal variations in the atmospheric dust cycle and local winds.

11:30 a.m. Masse M. * Bourgeois O. Le Mouelic S. Verpoorter C. Le Deit L. Combe J.-Ph.
Dust Deposits Within and Around the North Polar Ice Cap of Mars: What are Their Mineralogical Compositions, Their Sources and Their Accumulation Processes? **[#1841]**
We have performed an integrated morphological, structural and compositional analyses of selected areas along the contact between the North Polar Cap and the surrounding superficial sediments.

MARS: VOLCANISM
Friday, 8:30 a.m. Waterway Ballroom 4

Chairs: **Tracy Gregg and Karen Stockstill-Cahill**

8:30 a.m. Williams D. A. * Greeley R. Manfredi L. Fergason R. L. Combe J.-Ph. Poulet F. Pinet P. Rosemberg C. Clenet H. McCord T. B. Raitala J. Neukum G.
The Circum-Hellas Volcanic Province, Mars: Detailed Area-Age Estimates and Physical-Compositional Properties of the Surface **[#1401]**
We discuss new analyses for terrain in and around the Circum-Hellas Volcanic Province on Mars, providing new estimates of size and age of the province, and information on its physical-compositional properties.

8:45 a.m. Gregg T. K. P. * de Silva S.
Tyrrhena Patera and Hesperia Planum, Mars: New Insights (and Old Interpretations) from High-Resolution Imagery **[#1700]**
We present our efforts to constrain the lithologies of Tyrrhena Patera flank materials and the ridged plains of Hesperia Planum using MOC and HiRISE images.

9:00 a.m. Korteniemi J. * Raitala J. Aittola M. Ivanov M. Öhman T. Kostama V.-P. Hiesinger H.
Evidence for Dike Swarms on the Eastern Hellas Rim, Mars **[#2126]**
We present evidence for extensive dike systems on the Hadriaca Patera volcano on the east Hellas rim and in the volcanic plains south of it, near the outflow channels, and hypothesise on what controls their distribution and orientation.

9:15 a.m. Carter L. M. * Campbell B. A. Holt J. W. Phillips R. J. Putzig N. E. Okubo C. H. Seu R. Biccari D.
SHARAD Observations of Lava Flow Fields West of Ascraeus Mons **[#1954]**
SHARAD detects subsurface interfaces associated with the distal parts of smooth flows northwest of Ascraeus Mons. The dielectric properties of these flows are consistent with basaltic lavas.

9:30 a.m. Baptista A. R. * Mangold N. Zimbelman J.
Origin and Evolution of Long Lobate Lava Flows on Syria Planum, Mars **[#2090]**
We identified and described a shield volcano, Volcano A, in Syria Planum, Mars, which is the origin of long lobate lava flows placed in a complex plains-style volcanic region.

9:45 a.m. Richardson P. W. * Bleacher J. E. Glaze L. S. Baloga S. M.
The Relationship Between Lava Fans and Tubes on Olympus Mons in the Tharsis Region, Mars **[#1527]**
Lava fans and tubes were mapped on the flank of Olympus Mons. 82% of the fans were associated with lava tubes. The fan locations are not consistent with a random Poisson distribution, suggesting the possibility of more than one formation mechanism.

10:00 a.m. Kerber L. * Head J. W. III
The Age of the Medusae Fossae Formation: Reassessment Using Lava Flow Cast and Mold Contacts **[#2235]**
We reassess the age of the Medusae Fossae Formation using evidence from ancient contacts between the formation and adjacent lava flows. These relationships add stratigraphic information and suggest a Hesperian age for some parts of the formation.

10:15 a.m. Platz T. * McGuire P. C. Münn S. Cailleau B. Dumke A. Neukum G. Procter J. N.
Growth and Destruction Cycles and Eruption Styles at Tharsis Tholus, Mars **[#1522]**
In the >3.6 Gyrs of volcanic activity at Tharsis Tholus, the edifice experienced multiple volcano-tectonic events. The present-day edifice is characterised by destruction and re-growth cycles also causing the locus of activity to be shifted across the volcano.

10:30 a.m. Stockstill-Cahill K. R. * Lucey P. G. Taylor G. J. Blake D.
Thermal Emission Measurements of Foidite Rocks: Possible Martian Lithologies **[#2061]**
We collected thermal infrared spectra of the Honolulu volcanic rock suite to assess the significance and effect of unmixing spectra of silica-undersaturated rocks without feldspathoid spectra.

10:45 a.m. Poulet F. * Langevin Y. Le Roux M. Mangold N. Bibring J.-P. Gondet B.
Mars: Identification, Mapping and Modal Mineralogy of Low-Calcium Pyroxene-rich Deposits **[#1555]**
We present a systematic analysis of low calcium pyroxene-rich deposits on Mars as seen by OMEGA/MEx.

11:00 a.m. Farrand W. H. * Lane M. D. Edwards B. R.
Evidence of Mafic Volcanic Compositions Associated with Domes in Arcadia and Utopia Planitiae, Mars **[#1268]**
Domes occurring in Arcadia and Utopia Planitiae are examined with CRISM data and are found to be associated with high Ca pyroxene and are thus interpreted as basaltic volcanic domes.

11:15 a.m. Salvatore M. R. * Mustard J. F. Wyatt M. B. Murchie S. L. Barnouin-Jha O. S.
Assessing the Mineralogy of Acidalia Planitia, Mars, Using Near-Infrared Orbital Spectroscopy **[#2050]**
CRISM targeted observations of impact craters in Acidalia Planitia are examined. The identification of near-surface olivine and pyroxene supports theories that this region is primarily basaltic with limited surface alteration.

11:30 a.m. Stanley B. D. * Hirschmann M. M. Withers A. C.
CO_2 Solubility in Martian Basalts and Applications to Atmospheric Evolution **[#1952]**
We investigate the solubility of carbon dioxide in martian analogue basaltic melts at 2.0 GPa to constrain the magmatic outgassing fluxes of carbon dioxide during martian atmospheric evolution.

EARLY SOLAR SYSTEM CHRONOLOGY
Friday, 8:30 a.m. Waterway Ballroom 5

Chairs: **Gary Huss and Audrey Bouvier**

8:30 a.m. Meyer B. S. * Huss G. R.
Galactic Chemical Evolution and the Steady-State Abundances of Short-lived Radioactivities in the Interstellar Medium **[#1756]**
Simple models that treat the build up of the Galactic disk by metal-poor infall can provide useful information on the steady-state abundances of short-lived radioactivities in the interstellar medium. Details of such models are presented.

8:45 a.m. Huss G. R. * Meyer B. S.
Galactic Chemical Evolution and the Abundances of Short-lived Radionuclides Inherited by the Solar System from the Interstellar Medium **[#1957]**
We discuss the implications of a realistic model of galactic chemical evolution for the origin of the short-lived nuclides in the early solar system. A late addition of newly synthesized material, probably from a stellar source, is clearly required.

9:00 a.m. Leya I. * Schönbächler M. Halliday A. N.
Titanium Isotopes in CAIs — Heterogeneities in the Early Solar System **[#1480]**
We present Ti isotope data for CAIs from Allende and Efremovka. The new data demonstrate that n-rich isotopes, e.g., ^{50}Ti, ^{62}Ni, and ^{96}Zr, are correlated in CAIs and that the n-rich addition was heteogeneously distributed in the early solar system.

9:15 a.m. Yin Q.-Z. * Yamashita K. Yamakawa A. Tanaka R. Jacobsen B. Ebel D. Hutcheon I. D. Nakamura E.
^{53}Mn-^{53}Cr Systematics of Allende Chondrules and epsilon ^{54}Cr—Cap Delta^{17}O Correlation in Bulk Carbonaceous Chondrites **[#2006]**
New Allende chondrules ^{53}Mn-^{53}Cr date suggest they formed at 4567.5 Ma ago, removing the age gap with CAIs. Strong correlation of nuclear anomalies of ε^{54}Cr with Δ^{17}O from the same samples suggests nucleosynthetic origin of oxygen anomalies may still be viable.

9:30 a.m. Mishra R. K. Goswami J. N. * Tachibana S. Huss G. R. Rudraswami N. G.
Fe-Ni and Al-Mg Isotope Systematics in Chondrules from Unequilibrated Ordinary Chondrites **[#1689]**
Fe-Ni and Al-Mg isotope systematics study was carried out on Unequilibrated ordinary chondrites which suggest supernova as the plausible source of ^{60}Fe ejected simultaneously with ^{26}Al.

9:45 a.m. Tachibana S. * Huss G. R. Nagashima K.
Ion Microprobe Study of ^{60}Fe-^{60}Ni System in Ferromagnesian Pyroxene Chondrules in Krymka (LL3.1) by Multicollection **[#1808]**
We report our first multi-collection ion-microprobe data for the ^{60}Fe-^{60}Ni systems in ferromagnesian pyroxene-rich chondrules from Krymka (LL3.1). Three measured chondrules showed excesses of ^{60}Ni, but the ^{60}Fe-^{60}Ni systems may have been disturbed.

10:00 a.m. Connolly H. C. Jr.* Young E. D. Huss G. R. Nagashima K. McDonough W. F. Ash R. D. Beckett J. R. Tonui E. McCoy T. J.
Supra-Canonical ^{26}Al Detected by In Situ LA-MC-ICPMS and SIMS Techniques: But What Does It All Mean? **[#1993]**
We report a comprehensive study of a CAI from Allende to address the role of analytical artifacts and test interpretations of supra-canonical ^{26}Al/^{27}Al data. Agreement between LA-MC-ICPMS and SIMS techniques for the ^{26}Al-^{26}Mg system is demonstrated.

10:15 a.m. Ito M. * Messenger S.
High Precision Magnesium Isotopic Measurement of CAI Minerals with Low Al/Mg Ratio from Allende Utilizing a NanoSIMS 50L Ion Microprobe **[#1740]**
We report high-precision Mg isotopic measurements in melilite, spinel and fassaite in an Allende CAI by a NanoSIMS 50L with four Faraday cups in multidetection in order to evaluate the chronology of complex history of CAIs in the early solar system.

10:30 a.m. Wadhwa M. * Janney P. E. Krot A. N.
Evidence of Disturbance in the ^{26}Al-^{26}Mg Systematics of the Efremovka E60 CAI: Implications for the High-Resolution Chronology of the Early Solar System **[#2495]**
We report results of a laser ablation MC-ICPMS study of the Efremovka E60 CAI. Our data indicate that the ^{26}Al-^{26}Mg systematics in E60 are disturbed and we present the chronological implications of this finding.

10:45 a.m. Kleine T. * Bourdon B. Irving A. J.
Hf-W Chronology of the Angrite Parent Body: Timing of Accretion, Core Formation and Magmatism **[#2403]**
We present Hf-W isochrons for angrites and compare the Hf-W ages to those obtained from the Pb-Pb, Al-Mg and Mn-Cr chronometers. The Hf-W data are furthermore used to estimate the timescale for the accretion and earliest differentiation of the angrite parent body.

11:00 a.m. Shukolyukov A. * Lugmair G. W. Irving A. J.
Mn-Cr Isotope Systematics of Angrite Northwest Africa 4801 **[#1381]**
We studied the Mn-Cr isotope systematics of the angrite Northwest Africa and calculated a $^{53}Mn/^{55}Mn$ ratio of $(0.96 \pm 0.04) \times 10^{-6}$ at the time of isotope closure. These data combined with a precise absolute Pb-Pb age allow to use this meteorite as an absolute time marker.

11:15 a.m. Bouvier A. * Wadhwa M.
Synchronizing the Absolute and Relative Clocks: Pb-Pb and Al-Mg Systematics in CAIs from the Allende and NWA 2364 CV3 Chondrites **[#2184]**
A Pb-Pb internal isochron of a type-B CAI from the NWA 2364 CV3 chondrite gives an absolute age of 4568.6 ± 0.2 Ma which contrasts with previous internal Pb-Pb ages of CAIs from Allende and Efremovka. Al-Mg systematics are also reported for CV3 CAIs.

11:30 a.m. Qin L. * Alexander C. M. O'D. Carlson R. W. Horan M. F.
Understanding Various Contributions to the Chromium Isotopic Composition of Meteorites, and Their Implications for Mn-Cr Chronology **[#1672]**
We show here that both nucleosynthetic effects and cosmogenic effects can contribute to the variations observed in Cr isotopic composition of meteorites. These suggest caution in use of the Mn-Cr chronometer.

SEEK OUT AND EXPLORE: UPCOMING AND FUTURE MISSIONS
Friday, 8:30 a.m. Waterway Ballroom 6

Chairs: **Agustin Chicarro and Wendy Calvin**

8:30 a.m. Meyer M. *
Mars Science Laboratory in Context **[#2210]**
The Mars Science Laboratory (MSL) is considered the first astrobiology mission since Viking and represents a major step in assessing the preservation potential of martian deposits, opening the window to paleoenvironments and guiding us on what to seek on future missions.

8:45 a.m. Vasavada A. R. * MSL Science Team
Mars Science Laboratory: Looking Ahead to 2011 **[#1441]**
The Mars Science Laboratory, now scheduled for launch in late 2011, retains the next-generation scientific and technological capabilities that make it a critical element in NASA's Mars Exploration Program.

9:00 a.m. Newsom H. E. * Ollila A. M. Lanza N. L. King P. Gallegos Z. Osinski G. R. Clegg S. M. Wiens R. C. Vaniman D. Lee P. Glass B. J. Walker E. Thackrey S. Parnell J.
Simulated Rover Field Test at the Haughton-Mars Project Impact Crater Field Station **[#1446]**
Initial results from a field test for several Mars Science Laboratory instruments at the Haughton impact structure.

9:15 a.m. Chicarro A. F. *
MARS-NEXT — A Future Major Step in the European Exploration of Mars **[#1271]**
The Mars-NEXT mission represents a new concept for a three-lander network on Mars within ESA's Exploration Programme, to investigate the interior of the planet, its atmospheric dynamics, and the geology of each landing site.

9:30 a.m. Banerdt W. B. *
Cerberus: A Mars Geophysical Network Mission for New Frontiers **[#2485]**
We are developing a three-lander mission to Mars carrying geophysical instrumentation that fits within the New Frontiers guidelines. This mission will investigate the deep interior with seismometers, precision tracking and EM sounding.

9:45 a.m. Klesh A. T. *
SHOTPUT Sample Return: Examining the Compositional Gradient of Small-Body Objects **[#1223]**
A unique trajectory exists that will allow the visiting of 2001 HM10, (624) Hektor and S/2006 and 39/P Oterma. We present a mission design with triple impactors and sample return capability to establish a compositional gradient of small-body objects.

10:00 a.m. Colaprete A. Briggs G. Ennico K. Wooden D. Heldmann J. L. Sollitt L. Asphaug E. Korycansky D. Schultz P. Christensen A. Galal K. Bart G. D. LCROSS Team
An Overview of the Lunar Crater Observation and Sensing Satellite (LCROSS) Mission — An ESMD Mission to Investigate Lunar Polar Hydrogen **[#1861]**
The primary objective of the Lunar Crater Observation and Sensing Satellite (LCROSS) is to confirm the presence or absence of water ice in a permanently shadowed polar region.

10:15 a.m. Delory G. T. * Elphic R. Morgan T. Colaprete T. Horanyi M. Mahaffy P. Hine B. Boroson D.
The Lunar Atmosphere and Dust Environment Explorer (LADEE) **[#2025]**
We describe the Lunar Atmosphere and Dust Environment Explorer (LADEE) mission, designed to study the pristine lunar exosphere and dynamic dust activity.

10:30 a.m. Miller R. S. * Bonamente M. Burgess J. M. Jenke P. Lawrence D. J. O'Brien S. Orr M. R. Paciesas W. S. Young C. A.
The Lunar Occultation Observer (LOCO) — A Nuclear Astrophysics All-Sky Survey Mission Concept **[#1364]**
The Lunar Occultation Observer (LOCO) is a new ?-ray astrophysics mission concept expected to have unprecedented sensitivity in the nuclear regime. Operating in lunar orbit, LOCO will utilize lunar occultation imaging to survey and probe the cosmos.

10:45 a.m. Cohen B. A. * Bassler J. A. McDougal J. M. Harris D. W. Hill L. Hammond M. S. Morse B. J. Reed C. L. B. Kirby K. W. Morgan T. H. ILN Science Definition Team MSFC/APL ILN Engineering Team
The International Lunar Network (ILN) Anchor Nodes Mission Update **[#2021]**
The Anchor Nodes project at MSFC and APL will contribute 2–4 small geophysical stations to the ILN, improving our understanding of lunar interior structure and composition. We report our progress in pre-Phase A science and engineering activities.

11:00 a.m. Smith A. * Crawford I. A. Barber S. J. Brown P. Church P. Gao Y. Gowen R. A. Griffiths A. Hagermann A. Joy K. Pike W. T. Phipps A. Proud W. G. Sheridan S. Sims M. R. Talboys D. L. Wells N.
MoonLITE Programmatic and Technological Update **[#1508]**
MoonLITE is a proposed four penetrator lunar mission. Following a US/UK working group assessment, a science assessment and the first UK impact trials, a full mission-level phase A study has begun. A technological and programmatic update of the mission is given.

11:15 a.m. Weisbin C. R. * Clark P. Shelton K. Smith J. H. Mrozinski J. Lincoln W. Elfes A. Hua H. Adumitroaie V. Silberg R.
Formulation, Modeling and Analysis of a Mission to the Moon's Malapert Mountain **[#1054]**
This study analyzes a proposed exploration mission which takes a group of astronauts and their robotic assistants from a landing site at Shackleton Crater near the lunar south pole to Malapert Mountain, which is about 130 km away.

11:30 a.m. Lebreton J-P. * Niebur C. Cutts J. Falkner P. Greeley R. Lunine J. Blanc M. Coustenis A. Pappalardo R. Matson D. Clark K. Reh K. Stankov A. Erd C. Beauchamp P.
Joint NASA-ESA Outer Planet Mission Study Overview **[#2383]**
This presentation is an overview of the Outer Planet Mission [Europa Jupiter System Mission (EJSM) or Titan Saturn System Mission (TSSM)] selected by NASA and ESA and outlines the next steps toward implementation.

MARS: EARLY HISTORY AND IMPACT PROCESSES
Friday, 1:30 p.m. Waterway Ballroom 1

Chairs: **Shane Byrne and Lon Hood**

1:30 p.m. Frey H. V. *
New Large Late Heavy Bombardment Impact Basins on Mars Revealed in Crustal Thickness Data: Crater Retention Ages and Implications **[#1123]**
Crater retention ages for newly identified large impact basins are not significantly older than for basins already known. The large impact late heavy bombardment on Mars was a relatively brief event or the record of previous large impacts was erased.

1:45 p.m. Rodriguez J. A. P. * Kargel J. S. Tanaka K. L. Berman D. C.
Construction of a Volatile-rich Martian Upper Crust During the Impact Cataclysm **[#2347]**
We have investigated the distribution of pristine and degraded impact craters and QCDs in the plateau surfaces forming the peripheries of the chasmata, chaotic terrains and outflow channels in order to investigate the construction of a volatile-rich crust in the region.

2:00 p.m. Lillis R. J. * Halekas J. S. Louzada K. L. Stewart S. T. Manga M.
Impact Demagnetization at Mars: Using Multiple Altitude Magnetic Field Data to Constrain Properties of Crustal Magnetization **[#1444]**
We use statistical magnetization modeling and magnetic field data at two separate altitudes (185 km and ~400 km) in order to constrain crustal magnetization properties at martian impact craters. At Hellas, the demagnetization radius is 1.18 times the basin radius.

2:15 p.m. Hood L. L. * Harrison K. P. Langlais B. Lillis R. J. Poulet F. Williams D. A.
Correlations of Martian Crustal Magnetic Fields With Valley Networks, Phyllosilicate Exposures, and Volcanic Constructs: Implications for Magnetic Sources and Dynamo History **[#1747]**
We report correlations of (a) phyllosilicate exposures identified using Mars Express OMEGA data with strong crustal fields and valley networks; and (b) weaker magnetic anomalies with the Medusae Fossae Formation adjacent to Apollinaris Patera.

2:30 p.m. Loizeau D. * Bouley S. Mangold N. Meresse S. Costard F. Poulet F. Ansan V. Le Mouelic S. Bibring J.-P. Gondet B. Langevin Y.
Tyrrhena Terra: Hydrated Lobate Ejecta and Plains **[#2010]**
Hydrated minerals as phyllosilicates have been identified with OMEGA/Mars Express in Tyrrhena Terra, both on crater ejecta blankets and alluvial plains. Hypothesis are formulated about their origin and link.

2:45 p.m. Schwenzer S. P. * Kring D. A.
Impact-generated Hydrothermal Alteration on Mars: Clay Minerals, Oxides, Zeolites, and More **[#1421]**
We explore alteration mineral assemblages produced in hydrothermal systems as a function of host rock variability and thermochemical conditions and compare the results to OMEGA and CRISM data.

3:00 p.m. Barnhart C. J. * Nimmo F. Travis B. J.
Observable Effects of Post-Impact Hydrothermal Systems Incorporating Freezing **[#2013]**
We model post-impact hydrothermal systems exposed to subfreezing temperatures and quantify observable geochemical and geomorphic signatures such as discharge rate, total discharge volume, and W/R ratios.

3:15 p.m. HiRISE Team Ivanov B. A. * Melosh H. J. McEwen A. S.
Small Impact Crater Clusters in High Resolution HiRISE Images - II **[#1410]**
We present the analysis of new data on small craters and crater clusters accumulated by the HiRISE team for the first 10,000 orbits of MRO.

3:30 p.m. Burleigh K. J. * Melosh H. J. Tornabene L. L. McEwen A. S.
Small Impacts Trigger Dust Landslides on Mars **[#1431]**
Small (~10 m diameter) recent craters on Mars triggered large numbers of small dust avalanches. Mapping reveals that the trigger mechanism is airblast by the incoming bolide, not seismic shaking.

3:45 p.m. Byrne S. * Dundas C. M. Kennedy M. R. Mellon M. Shean D. Daubar I. Cull S. Seelos K. D. Murchie S. Cantor B. Arvidson R. E. Edgett K. McEwen A. Harrison T. Posiolova L. Seelos F. P. HiRISE Team CTX Team CRISM Team
Excavation of Subsurface Ice on Mars by New Impact Craters **[#1831]**
New impact craters, a few meters in size, have excavated ground ice in the martian mid-latitudes. HiRISE data show sublimation of this exposed ice over six months. We will describe this new discovery and discuss the implications of the ice-table depth.

4:00 p.m. Clevy J. R. * Kattenhorn S. A.
Localized Seasonal Variations in Water Equivalent Hydrogen on Mars and Possible Relationship to Recent Impacts **[#2265]**
Seasonal variations in water equivalent hydrogen in the eastern equatorial region of Mars, as determined from neutron spectrometer data, are considered to be a potential result of recent impacts having exposed materials rich in water ice.

4:15 p.m. Kreslavsky M. A. *
Dynamic Landscapes at High Latitudes on Mars: Constraints from Populations of Small Craters **[#2311]**
Statistical properties of populations of small impact craters at the high-latitude patterned ground on Mars indicate very quick modification and obliteration of craters and hence highly dynamic landscapes.

4:30 p.m. Hartmann W. K. * Quantin C. Werner S. C. Popova O.
Ice Flow in Debris Aprons and Central Peaks, and the Application of Crater Counts **[#1204]**
We apply studies of decameter-scale craters to studies of probable ice-flow-related features on Mars, to interpret both chronometry and geological processes among the features. We find losses of decameter-scale craters relative to nearby plains, probably due to sublimation.

MARS ANALOGS II: CHEMICAL AND SPECTRAL
Friday, 1:30 p.m. Waterway Ballroom 4

Chairs: Lindsay McHenry and Eldar Noe Dobrea

1:30 p.m. Gough R. V. * Tolbert M. A. McKay C. P. Toon O. B.
Methane Adsorption on Martian Soil Analogs: A Possible Abiogenic Explanation for Methane Variability **[#1968]**
We report laboratory results of methane adsorption onto JSC-Mars-1. Uptake coefficient values are small; however, atmospheric methane can access a large mineral surface area in the regolith. Significant methane may be temporarily lost in a season.

1:45 p.m. Pommerol A. * Schmitt B. Beck P. Brissaud O.
Water Sorption on Martian Regolith Analogs: Near-Infrared Reflectance Spectroscopy and Thermodynamics **[#1608]**
Adsorption of water by a suite of six plausible martian regolith analogs is experimentally investigated. Adsorption and desorption isotherms are measured as well as near-infrared reflectance spectra for each step of hydration/dehydration processes.

2:00 p.m. Rull F. * Sansano A. Sobron P. Lafuente B. Sarrazin P. Gailhanou M. Blake D.
Raman and XRD Field Characterisation of Sulfate Efflorescences at Rio Tinto (Spain) **[#1974]**
In this work a comparative *in situ* analysis of evaporate minerals from Rio Tinto (Spain) is undertaken using two techniques selected for Mars exploration: Raman spectrometer and CheMin XRD both selected as part of the ExoMars and MSL missions respectively.

2:15 p.m. McHenry L. J. * Chevrier V. F. Schröder C.
Jarosite in an East African Saline-Alkaline Paleolake Deposit: Implications for Mars **[#1635]**
Jarosite occurs in zeolite-dominated altered tephra from a pleistocene saline-alkaline lake deposit at Olduvai Gorge, Tanzania. This suggests that the presence of jarosite alone is insufficient evidence to demonstrate dominantly acidic conditions.

2:30 p.m. Potter S. L. * Chan M. A.
Characterization of Navajo Sandstone Concretions: Mars Comparisons and Criteria for Distinguishing Diagenetic Origins **[#2100]**
Characterization of Utah concretions and Mars spherules yields important criteria for distinguishing diagenetic origin in comparison to other models. The similarities between the two examples suggest a concretionary genesis for the Mars spherules.

2:45 p.m. McAdam A. C. * Sharp T. G. Leshin L. A. Harvey R. P. Hoffman E. J.
Antarctic Mars Analogs and Interpretation of Martian Alteration Signatures **[#1032]**
The dominant process which produced Antarctic clay-bearing soils from a Mars analog lithology was physical weathering of the deuterically altered parent rock. Lesser low temperature weathering produced salts, more Fe oxides, and minor clays minerals.

3:00 p.m. Noe Dobrea E. Z. * McKeown N. Bishop J. L. Silver E.
Terrestrial Analog Studies of Mawrth Vallis, Mars: The Painted Desert **[#2165]**
We perform airborne hyperspectral imaging studies of the Painted Desert, an analog site to Mawrth Vallis, Mars. These complement field studies of the same site.

3:15 p.m. Garvie L. A. J. * Burt D. M. Buseck P. R.
A Microscopists View of Desert Varnish from the Sonoran Desert **[#1344]**
Nanometer-scale element mapping and spectroscopy of desert varnish reveals a dynamic disequilibrium system characterized by post-depositional mineralogical, chemical, and structural changes, activated by liquid water.

3:30 p.m. Chemtob S. M. * Rossman G. R. Eiler J. M. Jolliff B. L.
Silica Coatings on the 1974 Kilauea Flow: New SEM and SIMS Results and Implications for Mars **[#2156]**
Silica and Fe-Ti oxide coatings occur on young flows in the Ka'u Desert, Hawaii, a Mars analog terrain. We present new textural, spectral and isotopic observations to determine the coating formation mechanism and apply the results to silica on Mars.

3:45 p.m. McDowell M. L. * Hamilton V. E. Cady S. L. Knauth P.
Thermal Infrared and Visible to Near-Infrared Spectral Analysis of Chert and Amorphous Silica **[#1419]**
We look in detail at the thermal infrared and visible to near-infrared spectra of various forms of chert and amorphous silica and compare the spectral variations between samples with variations in physical and chemical characteristics.

4:00 p.m. Rampe E. B. * Kraft M. D. Sharp T. G.
Chemical Weathering Trends from TIR Spectral Models: Implications for Deriving Weathering Trends from Martian Spectral Data **[#2132]**
We compare measured chemical compositions and weathering trends of terrestrial basalts to those derived from TIR spectral models. Deriving true chemistry and weathering trends from TIR models of weathered surfaces on Mars may be impractical.

4:15 p.m. Hardgrove C. J. * Moersch J. E. Whisner S. C.
Identification of Sedimentary Processes on Alluvial Fans Using Thermal Images and Ground Truth **[#1211]**
Aerial thermal images and ground based observations are used to study sedimentary processes on a wide assortment of alluvial fans in desert southwest. Thermal images reveal evidence of channelized flow, debris flows, levees and weathering processes.

4:30 p.m. Murphy N. W. * Jakosky B. M. Mellon M. T. Budd D. A.
Thermophysical Properties of Martian Duricrust Analogs **[#1420]**
We measured thermophysical properties of samples of terrestrial duricrust from a gypsum deposit in New Mexico and Lunar Lake Playa. Our results suggest that well-indurated materials may cover a significant portion of the Mars surface.

ACHONDRITES AND THEIR PARENT BODIES
Friday, 1:30 p.m. Waterway Ballroom 5

Chairs: **Gretchen Benedix and Edward Scott**

1:30 p.m. Kita N. T. * Goodrich C. A. Spicuzza M. J. Valley J. W.
Oxygen Isotopes in Ungrouped Achondrite NWA 1500 and Comparison to Brachinites **[#1393]**
NWA 1500 ungrouped achondrite may be related to brachinite based on new oxygen isotope analyses using both SIMS and laser fluorination methods. We compare NWA 1500 with brachinites and ureilites and discuss their parent body processes.

1:45 p.m. Shirai N. * Humayun M. Righter K.
Analysis of Moderately Siderophile Elements in Angrites: Implications for Core Formation of the Angrite Parent Body **[#2122]**
We determined moderately siderophile element abundances in angrites. Based on the analytical data, we discuss the core formation of the angrite parent body.

2:00 p.m. Benedix G. K. * McCoy T. J. Spratt J.
Thermodynamic Constraints on the Formation History of Lodranites **[#1494]**
We discuss closure temperatures and oxidation state of lodranites and compare to acapulcoites, winonaites and IAB irons. The effect of melting on oxidation state is elucidated by the presence of two different populations of chromite.

2:15 p.m. Gardner-Vandy K. G. * McCoy T. J. Lauretta D. S.
Formation Conditions of FeO-rich Primitive Achondrites **[#2520]**
We present a study of the fO_2 conditions under which the FeO-rich primitive achondrites (the brachinites and several ungrouped primitive achondrites) formed, and we relate these conditions to those of other primitive achondrite groups.

2:30 p.m. Huang S. * Humayun M. Downes H. Singletary S. Van Orman J. A. Jacobsen S. B.
Petrogenesis of Augite-bearing Ureilites: A LA-ICP-MS Approach **[#1330]**
Major, minor and trace elements have been determined on silicate minerals from ureilites LAR 04315, North Haig and FRO 93008 using LA-ICP-MS. The element compositions in ureilite minerals are consistent with ureilites being melting/smelting restites from a spinel peridotite.

2:45 p.m. Ash R. D. Goodrich C. A. * McDonough W. F. Van Orman J. A.
Metal in Ureilites: Siderophile Elements from LA-ICP-MS **[#1422]**
Ureilites are hard to understand. Why did God make so many ureilites? We address this question with LA-ICP-MS analyses of siderophile elements in metal, oxidized metal and silicates in ureilites.

3:00 p.m. Van Orman J. A. * Goodrich C. A. Wilson L.
Metal and Siderophile Elements in Ureilites: Reconciliation with Smelting? **[#1986]**
Ureilite bulk siderophile patterns can be reasonably modeled by batch or fractional melting in the Fe-S system, within a narrow range of starting compositions. Lack of fractionation in the Fe-C system does not contradict a smelting model.

3:15 p.m. Scott E. R. D. * Bogard D. D. Bottke W. F. Taylor G. J. Greenwood R. C. Franchi I. A. Keil K. Moskovitz N. A. Nesvorny D.
Impact Histories of Vesta and Vestoids Inferred from Howardites, Eucrites, and Diogenites **[#2295]**
Impact histories of Vesta, vestoids and other V-type asteroids are investigated using constraints from oxygen isotopic compositions and Ar-Ar ages of HEDs and ungrouped eucrites, and dynamical and astronomical studies of main belt asteroids.

3:30 p.m. Warren P. H. * Huber H. Choe W.
Siderophile and Other Geochemical Mixing Relationships Among HED-Meteoritic Breccias: Need for Recognition of Regolithic Howardite as a Distinct Subtype **[#2471]**
We report new (mainly INAA) data on the major- and trace-element bulk compositions of ~100 HEDs; these, along with noble-gas and petrographic data, show that that only a small and distinctive subset of the howardites are truly regolithic breccias.

3:45 p.m. Day J. M. D. * Walker R. J. Rumble D. III Irving A. J.
Peridotites from Another Planet? Osmium Isotope and Highly Siderophile Element Constraints on the Evolution of Diogenites and the HED Parent Body **[#1992]**
Highly siderophile element systematics of diogenites point to chondritic relative proportions of these elements in the HED parent body, providing new insight into planetary accretion processes.

4:00 p.m. Yamaguchi A. * Takeda H. Barrat J. A.
Petrology of Ferroan Diogenites, Yamato 75032 Type, Asuka 881839, and Dhofar 700 **[#1547]**
Y-75032 type, A 881839, Dho 700 are among the most ferroan diogenites, slightly more magnesian than cumulate eucrites. Minor element compositions in pyroxenes and chromite compositions indicate that Y-75032 type and the ferroan diogenites formed from different parental melts.

4:15 p.m. Isa J. * Yamaguchi A. Shinotsuka K. Ebihara M.
Northwest Africa 1109 and Camel Donga: Metal-bearing Brecciated Eucrites **[#1919]**
Two eucrites NWA1109 and Camel Donga contain significant amounts of Fe-metals. In order to better understand the origin of the Fe-metals, we performed a petrological and geochemical study of these meteorites.

4:30 p.m. Mittlefehldt D. W. * Beck A. W. Lee C.-T. A. McSween H. Y. Jr.
Chemistry of Diogenites and Evolution of Their Parent Asteroid **[#1038]**
Trace element compositions have been determined for a suite of diogenites. The results are discussed in the context of HED parent asteroid differentiations.

PLANNING FOR FUTURE EXPLORATION OF THE MOON
Friday, 1:30 p.m. Waterway Ballroom 6

Chairs: Jacob Bleacher and Noah Petro

1:30 p.m. Neal C. R. *
The Lunar Exploration Roadmap: A Progress Report from the Lunar Exploration Analysis Group (LEAG) **[#2558]**
The paper is a summary of progress to date of progress of LEAG in developing a grassroots community Lunar Exploration Roadmap.

1:45 p.m. Stubbs T. J. Glenar D. A. * Richard D. T. Colaprete A.
Predictions for the Optical Scattering at the Moon, as Observed by the LADEE UV/Vis Spectrometer **[#2348]**
Predictions are made for exospheric atomic line emissions, coronal and zodiacal light, as well as for "lunar horizon glow" produced by the forward scattering of sunlight by exospheric dust.

2:00 p.m. Halekas J. S. * Delory G. T. Stubbs T. J. Farrell W. M. Lin R. P.
Developing a Predictive Capability for Lunar Surface Charging During Solar Energetic Particle Events **[#1357]**
We investigate lunar surface charging during solar energetic particle events, with the aim of developing a predictive capability. The lunar surface can charge to kilovolt-scale negative potentials during these events, which has possible implications for lunar exploration.

2:15 p.m. Xiao Z. * Zeng Z. Xie H. Birnbaum S. J. Zhang Z.
A Preliminary Study on the Effect of Lunar-Dust Movement on the Lunar Magnetic Field **[#1227]**
Result from our model, the Electromagnetic Induction Model of Charged Active Lunar Dust, suggests the movement of lunar dust has influenced the lunar magnetic field and the influence is not negligible.

2:30 p.m. Kuhlman K. R. * Sridharan K. Garrison D. H. McKay D. S. Taylor L. A.
Decay of Reactivity Induced by Simulated Solar Wind Implantation of a Forsteritic Olivine **[#2303]**
LADTAG is studying the lifetime of reactive sites on the surfaces of irradiated lunar analogs of interest to those studying human health because of the free radicals that may be formed and not passivate when exposed to spacecraft air.

2:45 p.m. Siegler M. A. * Bills B. G. Paige D. A.
History of the Lunar Polar Cryosphere **[#2259]**
Cold traps near the lunar poles have not always existed due to changes in the lunar orbit. We examine a 4.5 Byr history of insolation in the lunar polar environment and the resulting surface and subsurface temperatures to comment on ice mobility.

3:00 p.m. Hibbitts C. A. * Dyar M. D. Orlando T. M. Grieves G. Szanyi J.
Cold Trapping of Volatiles in the Lunar Regolith **[#1926]**
Water may cold trap (cryosorb) onto non-ice materials at the lunar poles, and not exist as ice. Water can remain present, adsorbed onto the samples, at several 10s of degrees above which its ice would sublime, but not at or near room temperature.

3:15 p.m. Fouch M. J. * Garnero E. J. Robinson M. S. Yu H.
A New Paradigm for Seismic Exploration of the Moon, Mars, and Beyond **[#2233]**
In this abstract, we propose a new approach to seismic exploration of the Moon using arrays of seismic systems, which we term Small Aperture Lunar Seismic Arrays (SALSAs).

3:30 p.m. Li R. * Wu B. He S. Skopljak B. Yilmaz A. Jiang J. Banks M. S. Oman C. Bhasin K. B. Warner J. D. Knoblock E. J.
LASOIS: Enhancing the Spatial Orientation Capabilities of Astronauts on the Lunar Surface **[#1191]**
This paper presents the initial efforts in developing a Lunar Astronaut Spatial Orientation and Information System (LASOIS) to enhance the spatial-orientation capabilities of astronauts on the lunar surface to support future lunar manned missions.

3:45 p.m. Kohout T. * O'Sullivan K. Losiak A. Thaisen K. G. Weider S. Kring D. A.
Scientific Opportunities for Human Exploration of the Moon's Schrödinger Basin **[#1572]**
The Schrödinger Basin provides a diverse suite of scientific opportunities because of the superposition of several geologic processes and because of its relatively young age. Three possible landing sites were evaluated for human exploration.

4:00 p.m. Clark P. E. * Bleacher J. Mest S. Petro N. Leshin L.
Lunar Field Exploration Scenarios for a South Pole Outpost **[#1135]**
Three major 10–100's km scale field science thrusts could address high priority science objectives from the outpost: 1) SPA Basin structure (Malapert, Schrodinger); 2) Bombardment history, South Pole Highlands; 3) Volatile anomaly and inventory study.

4:15 p.m. Bleacher J. * Clark P. E. Mest S. Petro N. Leshin L.
Lunar Field Exploration Scenarios for Three Sorties **[#2148]**
We report the planning of 3 representative science objective-driven Apollo J scale (10 km radius) sortie missions to sites of potentially high science yield (Marius Hills, Olivine Hill, Nectaris Basin) to supplement outpost activity.

4:30 p.m. Yingst R. A. * Gregg T. K. P.
Lunar Geologic Mapping: A Preliminary Map of a Portion of the Marius Quadrangle **[#1319]**
As part of a new lunar mapping program, we report on a 1:2,500,000-scale preliminary map of a subset of Lunar Quadrangle 10 and discuss the first-order science results.

PRINT ONLY PRESENTATIONS

MERCURY AND VENUS

Barata M. T. Alves E. I. Vaz D.
Automatic Extraction of Wrinkle Ridges in Venus Magellan Imagery **[#1025]**
The parameters of wrinkle ridges (length, size, orientation) are determinate in a simple way if the wrinkle ridges are easily detected. This work presents the preliminary results of automatic detection of wrinkle ridges from SAR imagery at different scales.

Holin I. V.
Mercury's Core from Radar to Orbiter **[#1016]**
Messenger and BepiColombo will determine the state and size of Mercury's core to high precision. Earth-based radar can improve the final accuracies. In an intermediate state of the core additional information is desirable.

Kozlova E. A.
The Thermal Regime of "Low-Latitudinal" Cold Traps on Mercury **[#1956]**
Using the two-layer model we calculate the diurnal variance of subsurface temperatures on the depth at the different thickness of regolith layer. The calculations demonstrate that the water ice deposits can exist in such conditions during geological time.

Wieczorek M. A. Le Feuvre M. Rambaux N. Laskar J. Correia A. C. M.
Evidence for a Pre-Caloris Synchronous Rotation of Mercury **[#1276]**
The distribution of ancient impact basins on Mercury is decidedly non-uniform. Both the magnitude and direction of this asymmetry are consistent with this planet having been in a state of synchronous rotation when the ancient basins formed.

MOON

Abdrakhimov A. M.
Re-Examine Lunokhod Sites: Old and New Geochemical Data **[#2547]**
The geochemical comparing of soviet lunar rovers data and Clementine data were executed.

Evans R. Wöhler C. Lena R.
Analysis of Absorption Trough Features Using Clementine UVVIS+NIR Imagery **[#1093]**
This study explores the mapping of spectral parameters of lunar features, describing the absorption trough near 1000 nm, using the calibrated Clementine UVVIS+NIR data set covering the wavelength range between 415 and 2000 nm.

Peters S. Foing B. H. Koschny D. Grieger B. Lossett J.-L. Beauvivre S. Grande M. Huovelin J. Keller H. U. Mall U. Nathues A. Malkki A. Noci G. Sodnik Z. Kellett B. Pinet P. Chevrel S. Cerroni P. de Sanctis M. C. Barucci M. A. Erard S. Despan D. Muinonen K. Shevchenko V. Shkuratov Y. Ellouzi M. Peters S. Borst A. Bexkens F. Almeida M. Frew D. Volp J. Heather D. McMannamon P. Camino O. Racca G.
SMART-1: Review of Lunar Highlights **[#2298]**
The SMART-1 spacecraft operated from 400-3000 km for 1.5 year until impact. We shall report at LPSC2009 on SMART-1 lunar highlights relevant for science and exploration, in relation with subsequent missions Kaguya, Chang'E1 and Chandrayaan-1.

Ivatury V. McClanahan T. P.
Image Restoration of Lunar Neutron Albedo Maps for the Lunar Exploration Neutron Detector (LEND) **[#1134]**
Determine the optimal image restoration technique for restoring the hydrogen lunar albedo maps for the Lunar Exploration Neutron Detector (LEND) on the Lunar Reconnaissance Orbiter (LRO).

Khisina N. Nazarov M. Senin V. Mohov A.
Cr-Ca Symplectite Lamellea in an Olivinen Grain from the Luna-24 Regolith **[#1053]**
Lamellae of Cr-Ca symplectites consisted of spinel + diopside + ortopyroxene + larnie in the olivine grain from Luna-24 regolith were investigated using of EMPA and ASEM. The origin of the Ca-Cr symplectite lamellae is discussed.

Lena R. Wöhler C.
Effusive Lunar Domes Near Kepler and Piccolomini: Morphometry and Mode of Emplacement **[#1092]**
In this study we provide a comparative morphometric and rheologic analysis of two lunar effusive domes, located in Oceanus Procellarum to the west of the crater Kepler, and inside Rupes Altai near the crater Piccolomini, respectively.

McCallum I. S. Mullen E. K.
Mare Basalt Petrogenesis Revisited: Rb/Sr, Sm/Nd and Lu/Hf Fractionation Factors, Mantle Source Regions and Crustal Contamination **[#2380]**
Fractionation factors (Rb/Sr, Sm/Nd, Lu/Hf) of mare basalts at the time of formation constrain the mineralogy and melt fraction of mantle sources. For all but high-K basalts, mantle residues are harzburgitic. High-K basalts are KREEP contaminated.

Pugacheva S. G. Shevchenko V. V. Chikmachev V. I.
The Dependence of the Chemistry on the Depth for the South Pole-Aitken Lunar Basin **[#1109]**
The distribution of the major chemical elements (Fe and Th) depending upon the structure height levels of the South Pole-Aitken Lunar Basin, has been obtained.

Shevchenko V. El-Baz F. Gaddis L. Hiesinger H. Shkuratov Yu. Whitaker E. Wilson L. Blue J.
The IAU/WGPSN Lunar Task Group and the Status of Lunar Nomenclature **[#2016]**
This abstract summarizes the rules for naming features on planets as well as the status of nomenclature for the Moon.

Wöhler C. Lena R.
The Lunar Concentric Crater Archytas G Associated with an Intrusive Dome **[#1091]**
In this study we show that the lunar concentric crater Archytas G is associated with the intrusive dome Ar1. We estimate the morphometric parameters of Archytas G and Ar1 and discuss possible modes of formation for the concentric crater.

MARS

Bibring J-P. Poulet F. Morbidelli A.
The Martian P/T Transition: Sounding Mars Early Evolution and Habitability **[#2093]**
Mars evolution can be traced by its surface mineralogy, as inferred from orbital (OMEGA/MEX and CRISM/MRO) data. The Noachian includes a diversity of eras with distinct environments, the Phyllosian/Theikian transition ending the habitability era.

Haltigin T. W. Pollard W. H. Osinski G. R. Dutilleul P.
Polygon Morphology Within Scalloped Depressions, Utopia Planitia, Mars **[#2566]**
This paper examines possible periglacial landforms in ice-rich sediments within Utopia Planitia, Mars, using an examination of HiRISE imagery to demonstrate that polygonal terrain morphology varies with the stage of scalloped depression development.

Heet T. Arvidson R. E. Mellon M. T. Phoenix Science Team
Regional Geology and Rock Distributions of the Mars Phoenix Landing Site **[#1114]**
A geologic map of the Phoenix Mars landing site is presented. Crater counts are used to date mapped units and rock distributions provide insight into the origin and alteration of surface materials.

Maxe L. P.
Martian Dust as an End-Member of Semi-Cosmic Weathering **[#2020]**
The martian dust is a compound close to terrestrial amorphous spinel's minerals such as Hercynite, spinel ferrites. The semi-cosmic weathering affects the mineral surface by both ways: reduction (in the top layer) and oxidation (in the deeper layer).

Molina A. de Pablo M. A. Ramos M.
Study of the Surface Temperature at Nili Fossae, Mars. Preliminary Results. **[#1031]**
Here we present our preliminary analysis of surface temperature from BTR THEMIS IR data focused on the study of a possible permafrost and active layer in Nili Fossae, Mars.

Nußbaumer J. W.
Liquid Water Formed Scroll Bars in River Meanders for Decades in Elysium Planitia, Mars **[#1437]**
HiRISE images show evidence for meandering channels with scroll bars in parts of southern Elysium, Mars. The river formed meanders during a wetter climate in the past and during long term wet conditions.

Petrowsky M. J. Jones R. Coleman N. M.
Structural Deformation and Surface Properties of a Martian Crater — Insights from THEMIS Infrared Images **[#1213]**
We use THEMIS infrared images to analyze the history and surface properties of a large crater on Mars. We take advantage of a special condition — that the crater floor was offset by faulting, revealing a cross-section of underlying strata.

Sprenke K. F.
Magnetic Anomalies Within the Elliptical Borealis Basin of Mars **[#1140]**
Significant magnetic anomalies exist within the proposed elliptical Borealis Basin of Mars. These anomalies raise questions about the actual shape of the mega-impact basin as well as timing of the core field relative to the purported single impact.

Thomas C. Picaud S. Mousis O. Ballenegger V.
A Theoretical Investigation of the Influence of Clathrate Hydrates on the Atmosphere of Mars **[#1264]**
Traces of methane have recently been evidenced in the martian atmosphere. Clathrate hydrates may be at the origin of the detected CH_4, if a primitive methane-rich atmosphere has existed or if a subsurface source of CH_4 has been (or is still) present.

Tichý M.
A Creeping Soil Field on Mars **[#1190]**
A creeping soil field exists on Mars. A mass of martian soil moves along rock outcrops, which get abraded, and as a result, strands of abraded material can be observed. Previously the phenomeno was explained as the result of wind streaks.

Valenciano A. de Pablo M. A. Pacifici A.
The Role of Water on the Evolution of the Nephentes Mensae Region of Mars **[#1052]**
Here we show the repliminary results of a detailed search of water- and ice-related landforms in the Nepenthes Mensae region of Mars, what will used in the future for a wide study of the evolution of water in this martian region.

Welty C. B. Crown D. A. Balme M. R.
Morphologic Properties of Martian Gully Systems **[#2339]**
From high-resolution Mars imagery, analyses of gully morphometric parameters, locations, and settings suggest a source volume dependency over gully length and that gully formation mechanisms are likely consistent across the martian surface.

Xiao L. Smith M. Huang J. He Q. Petford N. Williams D. A. Liu J. G. Greeley R.
Volcanic Features on the Syria-Thaumasia Block, Mars: Implications for Ancient Martian Volcanology **[#1026]**
This study provides new observations of variety volcanic features in the Syria-Theumasia block. Four type volcanic feature are recoganized in the area.

de Pablo M. A. Pacifici A.
Chain of Depressions and the Watersheet Evolution in Nepenthes Mensae, Mars **[#1095]**
Our analysis of the MOLA-derived topographic map of the Nepenthes Mensae area, Mars, revealed the existence of different depressions near the highlands-lowlands boundary. We interpret the depressions such as a possible chain of lakes.

ASTROBIOLOGY

Horner J. Mousis O. Petit J.-M. Jones B. W.
Differences Between the Impact Regimes of the Terrestrial Planets **[#1179]**
We present detailed results on the similarities and differences between the impact regimes experienced by Venus, the Earth and Mars, taking into account populations of asteroidal and cometary impactors.

Ivarsson M. Lindgren P. Neubeck A. Broman C. Holm N. G. Henkel H.
Filamentous Structures in a Hydrothermal System of the Dellen Impact Structure, Sweden — Putative Microfossils? **[#1260]**
This is a report on the occurrence of putative microfossils in a hydrothermal system of the Dellen impact structure, Sweden.

Méndez A.
Standard Planetary Habitability (SPH) of Global Land Areas **[#2333]**
This work presents the Standard Planetary Habitability (SPH), a quantity that measures and compares the potential for life of global land areas for primary producers. The SPH provides a simpler and complimentary method to NDVI, faPAR, and NPP to assess the biosphere.

Thomas-Keprta K. L. Clemett S. J. McKay D. S. Gibson E. K. Wentworth S. J.
Thermal Decomposition of an Impure (Roxbury) Siderite: Relevance to the Presence of Chemically Pure Magnetite Crystals in ALH84001 Carbonate Disks **[#2116]**
Thermal decomposition of Roxbury siderite resulted in the formation of impure (Mg,Mn)-ferrites. These findings, which are supported by kinetic and thermodynamic equilibrium modeling studies, are in stark contrast to the chemically pure ALH 84001 magnetite.

METEORITES

Alexandrov A. B. Bagulya A. V. Vladimirov M. S. Goncharova L. A. Ivliev A. I. Kalinina G. V. Kashkarov L. L. Konovalova N. S. Okat'eva N. M. Polukhina N. G. Roussetski A. S. Starkov N. I. Tsarev V. A.
Super Heavy (Z>50) Galactic Cosmic Ray Nuclei Abundance on the Base of the Track Parameters Measuring in the Pallasite Olivine Crystals **[#1407]**
New results of the super-heavy cosmic ray nuclei abundance due to the track in the pallasite olivine in the frame of OLIMPIA project are presented. It was detected near 850 tracks with Z>50 and four corresponding Th-U group.

Alexeev V. A.
Ordovician Fossil Meteorites in Sweden: Numerous Meteorite Falls or Single Meteorite Shower? **[#1003]**
There is no necessity to set up a hypothesis of intensive flux of meteorites to Earth during ~1–2 Ma about 480 Ma ago.

Caporali S. Pratesi G. Moggi-Cecchi V. Franchi I. A. Greenwood R. C.
NWA 4419: A New R Chondrite from Northwest Africa **[#2488]**
NWA 4419 is an R chondrite recently found in Northwest Africa. Textural, compositional and isotopic data are presented, supporting the classification as R4 chondrite.

Dredge L. Parnell J. Lindgren P. Taylor C. Bowden S.
Elevated Flux of Mid-Ordovician Micrometeorites **[#1273]**
An elevated flux of micrometeorites is recorded from a mid-Ordovician limestone section in NW Scotland. This coincides with an elevated flux of meteorites detected previously in Sweden.

Golubeva L. F. McFadden L. A. Shestopalov D. I. Hasanova L. O.
Comparative Analysis of the Color Characteristics of Vesta's Areas and HED Meteorites **[#1064]**
From comparing the colors of the units in the northern hemisphere of Vesta and HED meteorites we inferred that Vesta units differ from HEDs in sizes of grains scattering light and in mineral compositions.

Korochantsev A. V. Lorenz C. A. Ivanova M. A. Zaytsev A. V. Kononkova N. N. Roshchina I. A. Korochantseva E. V. Sadilenko D. A. Skripnik A. Ya.
Sediment-Dispersed Extraterrestrial Chromite in Ordovician Limestone from Russia **[#1101]**
The high content of extraterrestrial chromite grains was discovered in Russian Ordovician sediments, those are coeval to Swedish limestones, bearing the fossil meteorites and extraterrestrial chromites.

Kurat G. Zinner E. Varela M. E. Ntaflos T.
SiGrMet05: A Silicate-Graphite-Metal Inclusion from the Campo del Cielo (IAB) Iron **[#1536]**
Lithologies either rich in silicates, or chromite, or graphite, form sub-units of the inclusion, which is cut by metal-graphite veins. Complex break-down reactions of exotic precursors are indicated.

Lavrentjeva Z. A.
The Formation of Pallasites **[#1042]**
Pallasites may have been formed not from core-mantle boundaries as widely inferred, but from impact-generated mixtures of core and mantle materials.

Lorenz C. A. Teplyakova S. N. Korochantsev A. V. Kononkova N. N. Roshina I. A. Sadilenko D. A.
The Structure and Composition of Large Metal Nodule from the Ghubara L5 Chondrite **[#1103]**
The large metal nodule was found in the Ghubara L5 chondrite. The metal demonstrates widmannstätten texture that is unique in chondritic metal. The nodule could be formed by the partial or complete impact melting of chondritic precursor.

Lyul A. Yu. Kolesov G. M.
Distribution of Some Elements Among Chondrules of Unequilibrated Chondrites: 1. Fe, Cr, Na, and Sc **[#1552]**
The histograms of the distribution of Fe, Cr, Na and Sc contents among chondrules of unequilibrated chondrites are presented. Effect of metamorphic processes on chemical composition of chondrules is discussed.

Marakushev A. A. Zinovieva N. G.
Liquid Immiscibility in the Parent Bodies of Ordinary Chondrites and Genetic Types of Iron Meteorites **[#1057]**
Our data on ordinary chondrites prove their genetic relations with some iron meteorites, which led us to suggest that iron and pallasite cores may occur even in planets of the most primitive (chondritic) evolutionary level.

Miyamoto M. Koizumi E. Mikouchi T.
Cooling Rates of Y 980459 and DaG 476 Shergottites on the Basis of Fe-Mg Zoning of Olivine **[#1143]**
We have developed a model to calculate the cooling rate by using the Fe-Mg zoning of olivine and applied it to martian meteorites. The results are 0.20°C/h and 0.089°C/h for Y 980459 and DaG 476 shergottites, respectively.

Moggi-Cecchi V. Pratesi G. Franchi I. A. Greenwood R. C.
Textural and Compositional Features of NWA 4222, a New Martian Meteorite **[#2387]**
Textural and compositional features of the recently discovered martian meteorite NWA 4222 are presented, focusing on differences and affinities with other desert martian meteorites.

Nazarov M. A. Ntaflos Th. Brandstaetter F. Kurat G.
FeO/MnO Ratios of Lunar Meteorite Minerals **[#1059]**
FeO/MnO ratios of lunar meteorite minerals were determined based on numerous EMP analyses. The ratio of Ca-rich pyroxene was found to be dependent on Ca content and MG#. FeO/MnO ratio of olivines and orthopyroxenes is least variable.

Papike J. J. Karner J. M. Shearer C. K. Burger P. V.
Pyroxene Mineralogy of Martian Meteorites: Major and Minor Element Systematics **[#1180]**
Chemistry of pyroxene from 19 martian meteorites.

Pizzarello S. Williams L. B.
Soluble Organic Species Released from the Insoluble Carbonaceous Material of a Pristine CR2 Meteorite **[#1369]**
The hydrothermolytic treatment of a CR2 macromolecular carbonaceous material released several aliphatic and aromatic hydrocarbons.

Pratesi G. Moggi-Cecchi V. Franchi I. A. Greenwood R. C.
NWA 4418: A New Mesosiderite from Northwest Africa **[#2430]**
NWA 4418 is a new mesosiderite recently found in Northwest Africa. Textural, compositional and isotopic data are presented, and a subclassification as 3B is proposed.

Slyuta E. N. Nikitin S. M. Korochantsev A. V. Lorents C. A. Skripnik A. Ya.
Strong Physical and Mechanical Anisotropy of Ordinary Chondrites **[#1051]**
The revealed three-dimensional distribution of compressive strength in ordinary chondrites can be approximated by prolate ellipsoid.

Wasson J. T. Choe W.-H.
The IIG Iron Meteorites: Probable Formation in the IIAB Core **[#2271]**
Because, on most element-Au diagrams, the IIG irons plot along approximate extensions of IIAB trends, we argue that these P-rich irons formed in the evolved IIAB core. Offsets on some element-Au diagrams suggest formation in pockets of P-rich magma.

IMPACTS

Ivliev A. I. Lukanin O. A. Kuyunko N. S.
The Impact Glasses Characteristics Studying by the Thermoluminescence Method **[#1058]**
In the given work new results of TL measurements in impact origins glasses are presented: in tektites from various strewn fields, in Libyan Desert glasses, and also impact glasses genetically connected with impact craters Zhamanshine and Elgygytgyn.

Lindgren P. Broman C. Holm N. G. Parnell J. Bowden S. A. Osinski G. R. Lee P.
The Raman Signature of Shocked Carbonates from the Haughton Impact Structure, Devon Island, Canada **[#1258]**
This is a study of the Raman signature of calcite and dolomite in shocked carbonate clasts within the Haughton impact melt rocks. The impact shock effects are observed with Raman analyses in dolomite, while the calcite structure remains intact.

Llorca J. Trigo-Rodriguez J. M. Docobo J. A. Neira H.
Evidence for an Atmospheric Airburst of a Huge Bolide over Spain in 939AD as Recorded in Medieval Chronicles **[#1359]**
Medieval chronicles of Spain describe the impact of a huge bolide on June 1, 939AD. The resulting airburst may be correlated with temperature variations preserved in ice cores and tree rings present in the period 930–940AD.

Misra S. Newsom H. Panda D. Sisodia M. S. Dube A.
Additional Studies of Materials from the Ramgarh Structure, India **[#1693]**
Continuing work on materials from the Ramgarh structure, India, include analysis of magnetic particles found near the structure.

Parnell J. Taylor C. W. Thackrey S. Osinski G. R. Lee P.
Permeability Data for Impact Breccias **[#1157]**
Permeability data is reported for impact breccias from the Haughton and other craters. Values are consistently low.

Povenmire H.
The First Tektites Found in Wilcox and Turner Counties, Georgia **[#1208]**
Field research describing the expansion of the Georgia tektite strewn field.

Svetsov V. V.
Impact Erosion of Water Ocean on the Early Earth with a Thin Atmosphere **[#1147]**
The work purpose was to calculate the masses of lost and retained water after the impacts of comets and asteroids on oceans of various depths. The bombardment of an atmosphereless planet by fast asteroids can wipe out the most part of an ocean.

Vishnevsky S. A. Gibsher N. A. Palchik N. A.
H_2O + Melt Jets in the Popigai Lechatelierites: Products of Shock-induced Fluid + Melt Selective Separation Derived from the Target Gneiss **[#1108]**
Lechatelierites from the Popigai suevite were intruded by jets of hot and mobile material from outside. The material was a result of early impact anatexis of target gneiss. Selective separation of Si, Na, K and H_2O vs. low mobile Al took place at this.

OUTER SOLAR SYSTEM

Mousis O. Lunine J. I. Pasek M. Cordier D. Waite J. H. Jr. Mandt K. E. Lewis W. S. Nguyen M.-J.
Is Serpentinization the Source of Titan's Atmospheric Methane? **[#1182]**
We calculate the initial D/H ratio that must be acquired by Titan's H_2O ice to be consistent with hydrothermal reactions that may produce CH_4 in the satellite's interior. If methane derives from such reactions, then the initial D/H ratio in H_2O is lower than the SMOW value.

Starodubtseva O. M. Akimov L. A.
Semiannual Variations in the North-South Asymmetry of Polarized Light of Jupiter **[#1018]**
Results of long-term polarimetric observations of Jupiter made in Kharkiv Astronomical Observatory over a 25-year period are presented. They reveal the semiannual variations in the north-south asymmetry of polarized light of Jupiter.

Ward Wm. R.
Particle Filtering by a Planetary Gap **[#1477]**
The ability of density gradients at the walls of a planetary gap to exclude particles via drag induced migration is examined. We suggest that particle diffusion and build-up at the gap edge could eventually defeat the drag barrier, enabling grain accretion by the planet.

ASTEROIDS AND COMETS

Hasegawa S. Miyasaka S. Tokimasa N. Sogame A. Ibrahimov M. A. Yoshida F. Abe M. Kuroda D.
BRz' Phase Function of Asteroid 4 Vesta During the 2006 Opposition **[#1503]**
We show BRz' phase function of asteroid 4 Vesta during the 2006 opposition.The phase function of 4 Vesta with parameters with HB = 3.93 mag and GB = 0.24, HR = 2.77 and GR = 0.21, and Hz' = 2.95 and Gz' = 0.20 were obtained.

Marboeuf U. Petit J.-M. Mousis O.
Thermodynamic Evolution of Planetesimals in the Primordial Edgeworth-Kuiper Belt Induced by Collisions **[#1568]**
We examine the implications of collisional effects on the physical and chemical differentiation of the planetesimals located in the primitive Edgeworth-Kuiper Belt. Results show changes in the initial composition only in the subsurface layers.

Rietmeijer F. J. M.
Corrected Chemical Signatures in Stardust Glass Reveal Wild 2 Particles that Resemble Matrix Grains of Aggregate IDPs **[#1189]**
Corrected for an elemental background and aerogel silica, Wild 2 chemical signatures preserved in Si-rich glass show the original petrologic grain properties.

Shevchenko V. G. Krugly Yu. N. Belskaya I. N. Chiorny V. G. Gaftonyuk N. M. Slyusarev I. G. Tereschenko I. A. Donchev Z. Ivanova V. Borisov G. Ibrahimov M. A. Marshalkina A. L. Molotov I. E.
Do Trojan Asteroids Have the Brightness Opposition Effect? **[#1391]**
Photometric observations of the Trojan asteroids 588 Achilles are presented. The rotation period and the detailed magnitude phase dependence were obtained. We have not revealed any noticeable opposition brightening down to 0.1 deg of phase angle.

Slyuta E. N.
Gravitational Deformation of Small Solar System Bodies **[#1050]**
Strength properties of small solar system bodies dependent on their composition vary within an extremely broad range – from 0.002 up to 350 MPa. There are five basic groups of objects dependent on their rheologic properties.

Tikhomirova E. N.
To the Problem of Meteor Streams and Comets Relationship **[#1087]**
The meteor streams and parent comets are suggested to identify by using the integrals of motion in frame of the averaged perturbed two-body problem. The parent comets of beta-Cancrids and lyambda-Cygnids are 3D and 73P correspondingly.

Trigo-Rodríguez J. M. Madiedo J. M. Williams I. P. Castro-Tirado A. J. Llorca J. Vítek S. Jelínek M.
A Meteorite Dropping Superbolide from the Catastrophycally Disrupted Comet C1919Q2 Metcalf: A Pathway for Meteorites from Jupiter Family Comets **[#1286]**
A meter-sized meteoroid probably produced during the disintegration of comet C1919Q2 Metcalf was observed producing a –18 magn. bolide (MNRAS, in press).The progenitor meteoroid was sufficiently large and of high enough tensile strength to produce meteorites.

PRESOLAR GRAINS AND EARLY SOLAR NEBULA

Makalkin A. B. Dorofeeva V. A.
Formation of Satellites in the Accretion Disks of Jupiter and Saturn: Comparative Modeling **[#2309]**
We present the results of comparative modeling of formation of regular satellites of Jupiter and Saturn in the accretion circumplanetary disks.

Pravdivtseva O. Meshik A. Hohenberg C. M. Kurat G.
I-Xe System in Campo del Cielo Silicates **[#1578]**
High precision I-Xe ages were determined for two distinct silicates separated from a polished section of Campo del Cielo.

Shiryaev A. A. Fisenko A. V. Krivobok V. S. Vlasov I. I. Semjonova L. F.
Nitrogen in Meteoritic Nanodiamonds: Lattice Impurity in Diamond Core or a Constituent of an Associated Carbonaceous Phases? **[#1317]**
Results of investigation of structure and of spectroscopically-active defects in nanodiamonds from Efremovka CV3 chondrite are presented. The data are discussed in comparison with known models of synthetic nanodamonds.

Simon J. I. Young E. D.
Resetting, Errorchrons and the Meaning of Canonical CAI Initial $^{26}Al/^{27}Al$ Values **[#1945]**
Here we use simple mass balance calculations to quantify the importance of open system isotopic exchange during CAI evolution and show that *in situ* supra-canonical and canonical and bulk canonical measurements can all exist for an individual CAI.

Throop H. Bally J.
UV Photolysis and Creation of Complex Organic Molecules in the Solar Nebula [#2139]
Nearby O/B stars in the Sun's birth environment can irradiate ices in the solar nebula and synthesize complex organic molecules. This process may explain the early solar system's complex organics, such as those found in chondritic meteorites.

Ustinova G. K.
On Origin of Xe-HL in Meteoritic Nanodiamonds [#1007]
The Xe-HL component is shown to be formed and captured simultaneously with the nanodiamond synthesis in the conditions of shock wave propagation from supernova explosions, and its isotopic composition is an effect of acceleration in the shock waves.

Missions and Instruments

Anderson J. A. Robinson M. S.
Challenges Utilizing Pushframe Camera Images [#1905]
Processing and analyzing images from pushframe cameras poses a difficult challenge when compared to typical frame or pushbroom instruments.

Edgett K. S. Ravine M. A. Caplinger M. A. Ghaemi F. T. Schaffner J. A. Malin M. C. Baker J. M. DiBiase D. R. Laramee J. Maki J. N. Willson R. G. Bell J. F. III Cameron J. F. Dietrich W. E. Edwards L. J. Hallet B. Herkenhoff K. E. Heydari E. Kah L. C. Lemmon M. T. Minitti M. E. Olson T. S. Parker T. J. Rowland S. K. Schieber J. Sullivan R. J. Sumner D. Y. Thomas P. C. Yingst R. A.
The Mars Science Laboratory (MSL) Mars Hand Lens Imager (MAHLI) Flight Instrument [#1197]
The MSL Mars Hand Lens Imager (MAHLI) flight instrument has been completed and delivered to JPL for installation on the rover. MAHLI is a focusable color camera that can image geologic materials at resolutions as high as 14 microns per pixel.

Malin M. C. Caplinger M. A. Edgett K. S. Ghaemi F. T. Ravine M. A. Schaffner J. A. Maki J. N. Willson R. G. Bell J. F. III Cameron J. F. Dietrich W. E. Edwards L. J. Hallet B. Herkenhoff K. E. Heydari E. Kah L. C. Lemmon M. T. Minitti M. E. Olson T. S. Parker T. J. Rowland S. K. Schieber J. Sullivan R. J. Sumner D. Y. Thomas P. C. Yingst R. A.
The Mars Science Laboratory (MSL) Mars Descent Imager (MARDI) Flight Instrument [#1199]
The MSL Mars Descent Imager (MARDI) flight instrument has been completed and installed on the rover. MARDI will provide hundreds of color images during the descent of MSL to the martian surface in 2012.

Mitrofanov I. G. Litvak M. L. Kozyrev A. S. Sanin A. B. Tretyakov V. I.
Nuclear Instruments and Methods for Space Planetology: Recent Results and New Developments [#1207]
New developments are presented of methods of nuclear physics for studies of celestial bodies. Using the heritage of instruments HEND for Mars Odyssey, LEND for LRO and DAN for MSL, the concepts of new instruments are discussed for future missions.

Zabalueva E. V. Shingareva T. V. Basilevsky A. T. Fedotov V. P. Ruzskiy E. G.
Russian "FOBOS-GRUNT" Mission. Examples of Surface Roughness Models for Phobos [#1243]
To support Russian Fobos-Grunt mission the digital model of Phobos surface was synthesized by combining the global model (P. Thomas) of the body with the geometry/abundances of typical landforms of Phobos and the Moon.

Education and Public Outreach and Data Visualization

Bérczi Sz. Boldoghy B. Cech V. Fabriczy A. Hargitai H. Hegyi S. Horváth A. Hudoba Gy. Kummert J. Nehéz I. Schiller I. Takács B. Varga T. Weidinger T.
Systems Woven by Two Flux-Subsystems: One of Them is Planetary. Concise Atlas of the Solar System (12): Space Science and Technology [#1256]
Overview from terrestrial environmental fluxes to confined fluxes in technologies at the space station help studying interrelations of various complex systems by a matrix: woven from environmental fluxes and production technologies.

Horvai F. Kereszturi A.
Geology of Mars: New University Course in Hungary **[#1673]**
The structure and characteristics of a new university course in Hungary on the geology of Mars is summarized.

Huffman J. N. Forsberg A. S. Head J. W. Dickson J. L. Fassett C. I.
Testing Geoscience Data Visualization Systems for Geological Mapping and Training **[#2086]**
We compare and describe our use of display technologies for use with planetary datasets, including a fully immersive virtual reality system, a large tiled-wall display, a stereo-capable "Practical Powerwall", and the standard computer desktop.

Lang A. Szalay K. Erdélyi S. Nickl I. Panyi T. Kiss D. Bérczi Sz.
Chemistry Experiment Measuring (pH) of the "Planetary" Soil by the Husar-5 NTX-based Rover Model of the Széchenyi István High School, Sopron, Hungary **[#1325]**
We report by a detailed description of the experiment built by students on Husar-5 rover model: how the chemical characteristics of the "planetary" soil can be measured by the indicator ribbon method, if we artificially made wet the soil.

Magyar I. Badics A. Bakonyi I. Csiszár Á. Franko M. Gyürki Á. Héricz M. Marschall B. Nagyházi Á. Varga T. N. Végh Gy. Varga T. P. Bérczi Sz.
Identification of Rocks on Planetary Surface Using Husar-9 Rover Camera: Field Work Simulations with Hunveyor-9 Space Probe Model System at Eötvös High School, Tata, Hungary **[#1120]**
We studied the rock types along the Husar-9 rover's path and identified them on the basis of their shape, color and surface textures: komatiite, basalt, granite, conglomerate, schist rock, porphyritic granite, suevite breccia, and vesicular basalt.

Simon T. Kereszturi A.
Online Astrobiology Course in Hungary **[#1048]**
We present the basic characteristics of the first online astrobiology course, specialized in planetary science in Hungary.

Sipos A. Vizi P. G.
Simulated Mars Rover Model Competition **[#2519]**
This is a competition of applied engineering sciences. The actual goal of the competition can be achieved by building a device, a rover. The track is an 8 × 8 square meter sized field of sand or special material. Competitors have to build a rover model.

** Denotes speaker*